CONDUCTIVE NANOPAPER FROM CELLULOSE NANOFIBERS AND CONDUCTIVE POLYMERS AND/OR CARBON NANOTUBES

Makara Lay

Universitat de Girona

DOCTORAL THESIS

Conductive nanopaper from cellulose nanofibers and conductive polymers and/or carbon nanotubes

Makara Lay

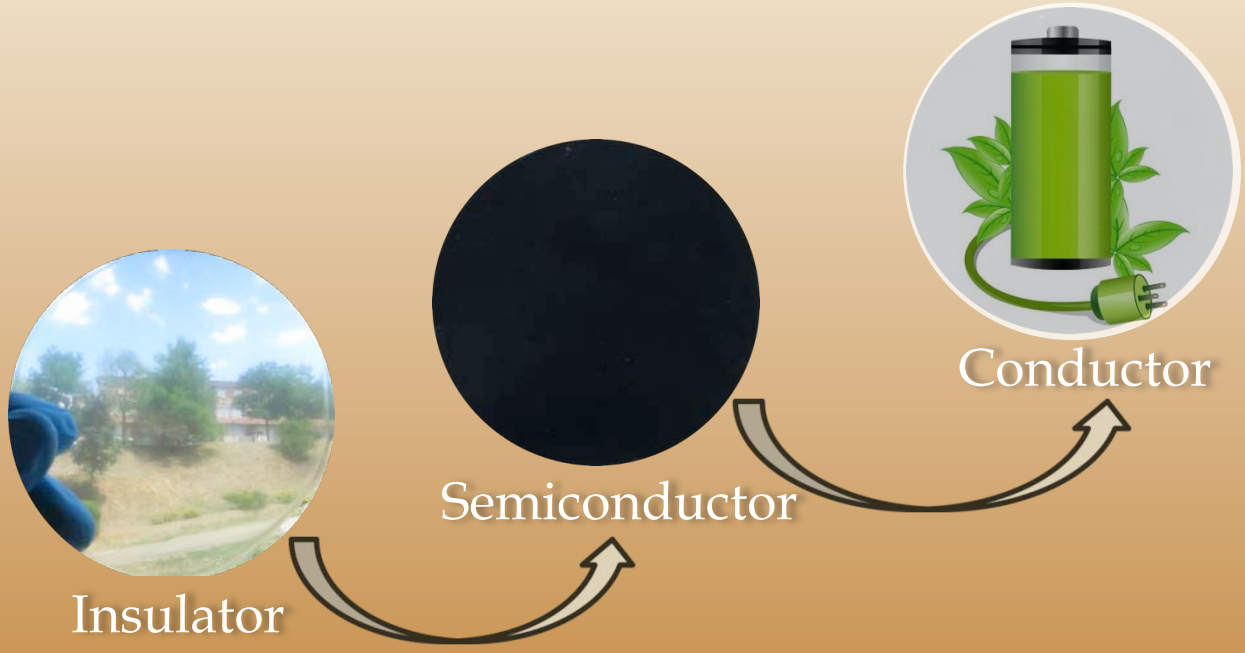

2016

Universitat de Girona

DOCTORAL THESIS

Conductive nanopaper from cellulose nanofibers and conductive polymers and/or carbon nanotubes

Makara Lay

2016

Universitat de Girona

DOCTORAL THESIS

Conductive nanopaper from cellulose nanofibers and conductive polymers and/or carbon nanotubes

Makara Lay

2016

DOCTORATE IN TECHNOLOGY

Supervised by:
Dr. Fabiola Vilaseca Morera
Dr. José Alberto Méndez González

Memory presented to obtain the Title of Doctor of Philosophy by the University of Girona

Universitat de Girona

Dr. Fabiola Vilaseca Morera and Dr. José Alberto Méndez González, professors at the Department of Chemical Engineering, Agriculture, and Food Technology of the University of Girona,

DECLARE:

That the thesis entitled "Conductive nanopaper from cellulose nanofibers and conductive polymers and/or carbon nanotubes" presented by Makara Lay has been completed under our supervision.

For all intents and purposes, we hereby sign this document.

Signature,

Dr. Fabiola Vilaseca Morera

Dr. José Alberto Méndez González

Girona, December 12th 2016

ACKNOWLEDGEMENTS

Firstly, I would like to acknowledge to my scholarship sponsor (**ERASMUS MUNDUS PROJECT TECHNO II ref. 372228-1-2012-1-FR-ERA MUNDUS-EMA21)** for its financial support during my doctoral program. I would like to thanks to Prof. Emili Garcia-Berthou, coordinator of Erasmus Mundus Project Techno II, for giving me a chance to get this scholarship.

I would like to express my sincere appreciation to my supervisors, Dr. Fabiola Vilaseca Morera and my co-supervisor Dr. José Alberto Méndez González, for the valuable guidance and advice. They inspired and motivated me greatly to contribute tremendously in this project. I would like to thank Dr. Pere Mutjé Pujol, director of LEPAMAP group for allowing me the opportunity to join his research group and to make the laboratory facilities.

Special thanks to Mr. Albert Serra and Dr. Israel González Tovar for their great assistance me in laboratory. Thanks to Mr. Daniel Reyes Bautista who helped me to do FE-SEM and Mr. Joan Pere López for helping me to do DMA and TGA experiments. And thanks to all my friends and LEPAMAP's member for the support.

Last but not least, an honorable mention goes to my beloved farther, Ly Yeaplay, my mother, Heang Saoly, my family and my relatives for their care, understanding and encouragement to me in completing this project. Without them, I won't be who I am today.

PUBLISHED AND SUBMITTED PAPERS

The present PhD thesis is based on the following publications and submitted papers.

Paper I. Lay, M., Méndez, J.A., Delgado-Aguilar, M., Bun, K.N., Vilaseca, F., 2016. Strong and electrically conductive nanopaper from cellulose nanofibers and polypyrrole. *Carbohydr. Polym*. 152, pp 331-339. DOI:10.1016/j.carbpol.2016.06.102
Journal Impact Factor 2015: 4.219 (9/85 in POLYMER SCIENCE)

Paper II. Lay, M., Méndez, J.A., Pèlach, M.A., Bun, K.N., Vilaseca, F., 2016. Combined effect of carbon nanotubes and polypyrrole on the electrical properties of cellulose-nanopaper. *Cellulose.* 23(6), 3925-3937. DOI: 10.1007/s10570-016-1060-5
Journal Impact Factor 2015: 3.195 (15/85 in POLYMER SCIENCE)

Submitted articles

Paper III. Lay, M., Pèlach, M.A., Pellicer, N., Tarrés, J.A., Bun, K.N., Vilaseca, F., 2016. Smart nanopaper based on cellulose nanofibers with hybrid PEDOT:PSS / Polypyrrole for energy storage devices. Manuscrip submitted to *Carbohydrate Polymers*.
Journal Impact Factor 2015: 4.219 (9/85 in POLYMER SCIENCE)

Paper IV. Lay, M., González, I., Tarrés J.A., Pellicer, N., Bun, K.N., Vilaseca, F., 2016. High electrical and electrochemical properties in bacterial cellulose / polypyrrole membranes. Manuscript submitted to *European Polymer Journal*.
Journal Impact Factor 2015: 3.485 (13/85 in POLYMER SCIENCE)

Summary of my contribution to the papers included in this PhD thesis:

In all papers, I have participated in the experimental planning, designed and performed all the experimental work, and written the initial version of every manuscript.

Conference contributions

1. Makara Lay, Albert Serra, Israel Gonzalez, Fabiola Vilaseca, Kim Ngun Bun, Pere Mutjé, 2014. Nanofibrillated Cellulose with conductive properties, 2014. *Oral Presentation - XIII meeting of the polymer group (GEP) of the RSEQ and RSEF, Girona, Spain.*

2. Makara Lay, Albert Serra, Israel Gonzalez, Fabiola Vilaseca, Kim Ngun Bun, and Pere Mutjé, 2014. Cellulose nanofibers films with conductive properteis. Conference. *Poster – COST FP1205 Seminar on "Ongoing Modification of Cellulose Nanofibers and their potential Applications", Madrid, SPAIN.*

3. Makara Lay, Albert Serra, Israel González, Fabiola Vilaseca, Kim Ngun Bun, Pere Mutjé., 2014. Multi-walled carbon nanotube/NFC conductive nanopaper. *Poster – The VIII IberoAmerican Congress on Pulp and Paper Research, Colombia.*

4. Makara Lay, Albert Serra, Israel González, Fabiola Vilaseca, Pere Mutjé., 2015. Cellulose Nanofibers (CNF)/Multi-Walled Carbon Nanotube (MWCNT) Conductive film. *Poster – Conference: COST FP1205, Innovative applications of regenerated wood cellulose fibres, Lasi, Romania.*

5. Makara Lay, Israel González, Fabiola Vilaseca, Pablo Ligero, Alberto Vega, Pere Mutjé., 2015. The effect of polypyrrole on the properties of cellulose nanofiber and bacterial cellulose films. *Poster – Conference: IWBLCM 2015, First International workshop on Biorefinery of Lignocellulosic Materials, Cordoba, Spain.*

LISTS OF ABBREVIATIONS

ATR	Attenuated total reflectance
BC	Bacterial cellulose
BPP	Bleached pine pulp
CNFs	Cellulose nanofibers
CNTs	Carbon nanotubes
CV	Cyclic voltammetry
DMA	Dynamic Mechanical Analysis
DP	Degree of polymerization
DTG	Derivative thermogravimetry
FESEM	Field emission scanning electron microscopy
FTIR	Fourier- transform infrared spectroscopy
HS	Herstin-Schramm nutrient
MFC	Microfibrillated cellulose
MWCNTs	Multi-walled carbon nanotubes
PEDOT:PSS	Poly(3,4-ethylenedioxythiophene)-poly(styrenesulfonate)
PPy	Polypyrrole
PTh	Polythiophene
RT	Room temperature
TEM	Transmission electron microscopy
TGA	Thermogravimetric analysis

LISTS OF CHEMICAL SYMBOLS

$FeCl_3$	Iron (III) chloride
HCl	Acid chloride
$K_2S_2O_8$	Potassium peroxodisulfate
$MgSO_47H_2O$	Magnesium sulfate heptahydrate
Na_2HPO_4	Disodium phosphate
$Na_2S_2O_8$	Sodium peroxodisulfate
NaBr	Sodium bromide
NaCl	Sodium chloride
NaOCl	Sodium hypochlorite
TEMPO	2,2,6,6-Tetramethyl-1-1-piperidinyloxy

LIST OF FIGURES

LIST OF TABLES

TABLE OF CONTENTS

ABSTRACT

Nowadays, the development of novel multi-functional nanocomposites materials has gained tremendous research interest on using low-cost and renewable raw materials, to produce sustainable, biodegradable, and eco-friendly biomaterials. Cellulose nanofibers (CNF) are a good candidate for this need. The purpose of the current work was to produce flexible, lightweight, and conductive nanocomposites by using nanocelluloses as matrix (cellulose nanofibers CNF, or bacterial cellulose BC) and conductive materials as fillers. In the current case, three different type of conductive fillers were studied, polypyrrole (PPy) and poly(3,4-ethylenedioxythiophene) : polystyrene sulfonate (PEDOT:PSS) as conductive polymers, and multi-walled carbon nanotubes (MWCNT) as conductive nanofiller. Conductive CNF-MWCNT and CNF-PEDOT:PSS nanocomposites were performed by following blending techniques, and all nanocomposites containing polypyrrole (CNF-PPy, BC-PPy, CNF-MWCNT-PPy, and CNF-PEDOT:PSS-PPy) were performed by coating the conductive polymer on the nanocelluloses surface, via in situ chemical polymerization in the presence of iron (III) chloride as oxidant agent.

Polypyrrole was chosen as conductive fillers due to its easy synthesis, good electrical conductivity and water dispersable. On the other hand, PEDOT:PSS conductive polymer has high conductivity, water dispersible, environmentally friendly and available in market (commercial product). MWCNT used in this work show high mechanical, electrical and thermal properties. In order to ensure a good dispersion, surface modification of MWCNT in acidic conditions was applied before their blending with cellulose nanofibers. The use of hybrid MWCNT-PPy or PEDOT:PSS-PPy fillers with cellulose nanofibers is proposed to achieve the electrical conductivity and specific capacitance that single fillers cannot reach.

The structure and morphology of nanocomposites were studied, as well as their thermal, mechanical, and electrical conductivity properties. The results revealed that both cellulose nanofibers and bacterial cellulose changed their nature from insulator to semiconductor, and to conductor materials after the addition or coating with conductive materials. Moreover, specific capacitances up to 300 F g^{-1} were obtained from CNF-PPy and CNF-PEDOT:PSS-PPy nanocomposites.

This work presents a trend for the application of cellulose nanofibers in the field of green and flexible electronics, biosensors, and energy storage devices such as batteries or electrochemical capacitors.

RESUMEN

Actualmente, el interés por el desarrollo de nuevos materiales compuestos multifuncionales está en auge y muestra una clara preferencia por el uso de materias primas renovables y de bajo coste, y por la preparación de materiales flexibles, ligeros, biodegradables y amigables con el medio ambiente. Las nanofibras de celulosa son un buen candidato en este sentido. En el presente estudio se persigue la fabricación de materiales nanocompuestos conductores, a la vez flexibles y ligeros, mediante el uso de nanocelulosas como matrix (nanofibras de celulosa CNF o bien celulosa bacteriana BC) y materiales conductores como carga. Se han estudiado tres tipos de cargas, el polipirrol (PPy) y el poli(3,4-etilendioxitiofeno):poliestireno sulfonato (PEDOT:PSS) como polímeros conductores, y nanotubos de carbono de pared múltiple (MWCNT) como nanocarga conductora. Los nanocompuestos conductores CNF-MWCNT y CNF-PEDOT:PSS se ha obtenido mediante técnicas de mezcla, mientras que todos los compuestos que contenían polipirrol se ha preparado por polimerización química del pirrol en la superficie de las nanofibras, en presencia de cloruro férrico como agente oxidante.

El polímero conductor polipirrol se ha escogido por ser de fácil síntesis, buen conductor y dispersable en agua. Por su parte, el poli(3,4-etilendioxitiofeno):poliestireno sulfonato es un polímero de elevada conductividad eléctrica, dispersable en agua, innocuo con el medioambientalmente y comercial. Los nanotubos de carbono de pared múltiple utilizados en este trabajo presentan elevadas propiedades mecánicas, térmicas y conductoras. En este caso, y con el fin de utilizar una buena dispersión de los nanotubos de carbono con la nanofibras de celulosa se ha llevado a cabo una modificación química superficial de los nanotubos en medio ácido. El presente estudio propone el uso de híbridos MWCNT-PPy y PEDOT:PSS-PPy como carga conductora para conseguir conductividades eléctricas y capacitancias específicas que no sería posible conseguir con las cargas conductoras individuales.

Durante el trabajo se estudia la estructura y morfología de los materiales nanocompuestos, así como sus propiedades térmicas, mecánicas y eléctricas. A partir de los resultados se deduce que las nanocelulosas pasan a ser un material aislante a un material semiconductor o conductor de la electricidad después de la adición o recubrimiento con los materiales conductores de estudio. Con ello, se han obtenido capacitancias específicas de más de 300 F g^{-1} para los nanocompouestos CNF-PPy y CNF-PEDOT:PSS-PPy. El trabajo muestra la viabilidad de aplicar nanofibras de celulosa como eco-materiales para la fabricación de productos electrónicos flexibles, biosensores, o como dispositivos de almacenamiento de energía como las baterías o los condensadores electroquímicos.

RESUM

Actualment, l'interès pel desenvolupament de nous materials compòsits multifuncionals presenta creixent considerablement i mostra una clara tendència cap a l'ús de matèries primeres renovables i de baix cost, i per la preparació de materials flexibles, lleugers, biodegradables i amigables amb el medi ambient. Les nanofibres de cel·lulosa són un bon candidat en aquest sentit. En el present treball es pretén produir materials nanocompòsits conductors, i alhora flexibles i lleugers, utilitzant nanocel·luloses com a matriu (nanofibres de cel·lulosa CNF o cel·lulosa bacteriana BC) i materials conductors com a càrrega. S'han estudiat tres tipus de càrregues, el polipirrol (PPy) i el poli(3,4-etilenedioxitiofè):poliestirè sulfonat (PEDOT:PSS) com a polímers conductors, i nanotubs de carboni de paret múltiple (MWCNT) com a nanocàrrega conductora. Els nanocompòsits conductors CNF-MWCNT i CNF-PEDOT:PSS s'han preparat a partir tècniques de mescla, mentre que tots els compòsits que contenen polipirrol s'han obtingut per polimerització química del pirrol en la superfície de les nanofibres, en presència de clorur fèrric com agent oxidant.

S'escull el polipirrol com a polímer conductor perquè és de fàcil síntesis, bon conductor elèctric i dispersable en aigua. Pel que fa al poli(3,4-etilenedioxitiofè):poliestirè sulfonat, és un polímer amb elevada conductivitat, és dispersable en aigua, innocu amb el mediambient i disponible en el mercat. Els nanotubs de carboni de paret múltiple utilitzats en aquest treball presenten elevades propietats mecàniques, tèrmiques i conductores. En aquest cas, i per tal d'assegurar una bona dispersió dels nanotubs de carboni en les nanofibres de cel·lulosa, s'ha dut a terme una modificació superficial dels nanotubs en medi àcid. El treball proposa l'ús dels híbrids MWCNT-PPy i PEDOT:PSS-PPy com a càrrega de les nanofibres de cel·lulosa per aconseguir conductivitats elèctriques i capacitàncies específiques que no es poden assolir amb materials conductors individuals.

En aquest treball s'estudien l'estructura i morfologia dels materials nanocompòsits, així com les seves propietats tèrmiques, mecàniques i elèctriques. A partir dels resultats es dedueix que tant les nanofibres de cel·lulosa com la cel·lulosa bacteriana passen de ser un material aïllant a un material semiconductor o conductor de l'electricitat després de l'addició o del revestiment amb els materials conductors d'estudi. Així, s'han obtingut capacitàncies específiques de més de 300 F g^{-1} per als nanocompòsits CNF-PPy i els CNF-PEDOT:PSS-PPy.

El treball mostra la viabilitat de l'aplicació de nanofibres de cel·lulosa com a eco-materials per a la fabricació de productes electrònics flexibles, biosensors, o com a dispositius d'emmagatzematge d'energia com les bateries o els condensadors electroquímics.

1. GENERAL INTRODUCTION

The development of nanotechnologies on portable electronic devices (such as mobile phones, notebook computers, and digital cameras) is searching for new materials that have to be multifunctional, in the trend of being small, lightweight, less expensive, sustainable energy storage devices, flexible or even rollup to meet the rapid growing modern market demands (Wang et al., 2016). One of the most significant current discussions in nanotechnology is focusing on environmental concerns as the majority of portable electronics are built on non-renewable, non-biodegradable, toxic materials, such as silicon wafers, which are highly purified, expensive and rigid substrates. Therefore, the development of sustainable materials that do not rely on fossil sources is a key of modern research. The group researchers from the University of Wisconsin-Madison (Seo et al., 2015) have come up with a new solution to alleviate the environmental burden of this discarded electronics. They have demonstrated the feasibility of making microwave biodegradable thin-film transistors from a transparent, flexible biodegradable substrate made from cellulose nanofibers (CNFs). Cellulose nanofibers films have the potential to replace silicon wafers as electronic substrates in environmental friendly, low-cost, portable gadgets or devices of the future, which will be much greener and cheaper than that of today (Seo et al., 2015). Coming from renewable and sustainable raw materials, CNFs are rapidly emerging as one of the most promising future materials. CNFs have outstanding physical, chemical, mechanical, and thermal properties, being used in bionanocomposites for lightweight products or multifunctional applications in different fields (Dufresne, 2012b). Moreover, they offer higher thermal and mechanical properties, transport barrier, and thermal resistivity in comparison with the conventional bio-composites.

1.1 Revolution from cellulose to cellulose nanofibers and its current potential research

Cellulose is the most abundant organic polymer, representing about 1.5×10^{12} tons of the total annual biomass production. It is a structural component in wood, cotton, hemp, algae, certain fungi, tunicates, and some bacteria. Thousands of years prior to the first discovery of cellulose by Payen in 1838, it has been used in the form of wood, cotton, and other plant fibers as an energy source, building materials, and clothing. In the 1920-1940s, cellulose was at the center of the pioneering research on polymer with the subsequent years being devoted to the industrial application of cellulose derivatives (Poletto, Pistor, & Zattera, 2013). The oil crisis

of the 1970s generated considerable interests in the use of cellulose as a source of biomass for the bio-production of organic chemicals. Cellulose is a fascinating polymer that has gained prominence as a nanostructured material, in the form of nanocellulose. In 1980s, the first successful production of cellulose nanofibers was found by Turbak, Snyder, & Sandberg, (1983). They studied the processing of different types of wood pulps into microfibrillated cellulose (MFC) by passing the material several times through a high-pressure homogenizer. Fifteen years later, another type of method, namely the ultrafine grinding method, was presented for the separation of CNFs (Oksman, Mathew, Pia Qvintus, Rojas, & Sain, 2014). Since then, the hug number of publication on patents, such as Nippon paper company, Tappi, and Innventia research group (Figure 1), articles, and review articles (Figure 2) about preparation of nanocelluloses in a variety of methods, such as mechanical and chemical treatments has grown, as well as their surface modification and applications.

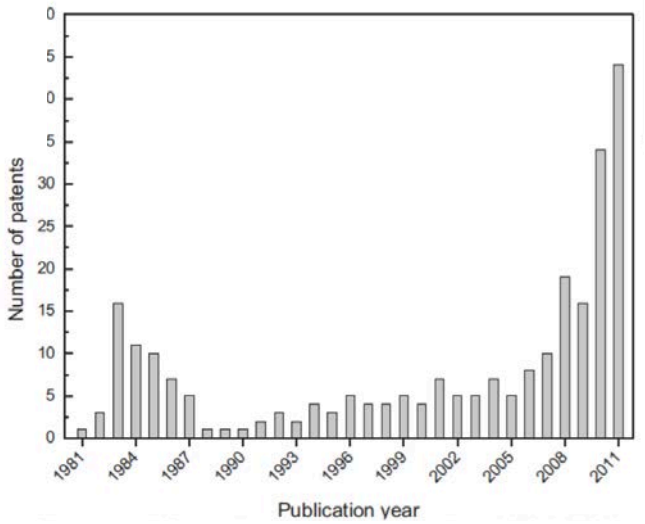

Figure 1 Number of patents on nanocellulose from 1981 until 2011.

The first book on nanocellulose entitled “Nanocellulose: From Nature to High Performance Tailored Materials” had been published by Dufresne (2012a). He described about the preparation of cellulose nanofibers (different pretreatment and mechanical treatment), characterization on physical, thermal, and mechanical properties. He also reviewed on the use of CNF as nanofillers in polymer matrix. Recently, two more books provides more in information on Nanocellulose polymer nanocomposites fundamental and applications (Asaadi

et al., 2016; Hinestroza, 2014; Kumar T, 2015). These efforts content tremendous information on cellulose nanofibers for their use in nanocomposites, application and future trends. It is addressed to scientists, universities or in industry, who wish to keep abreast of the important advances for a longstanding and reputation in this topic.

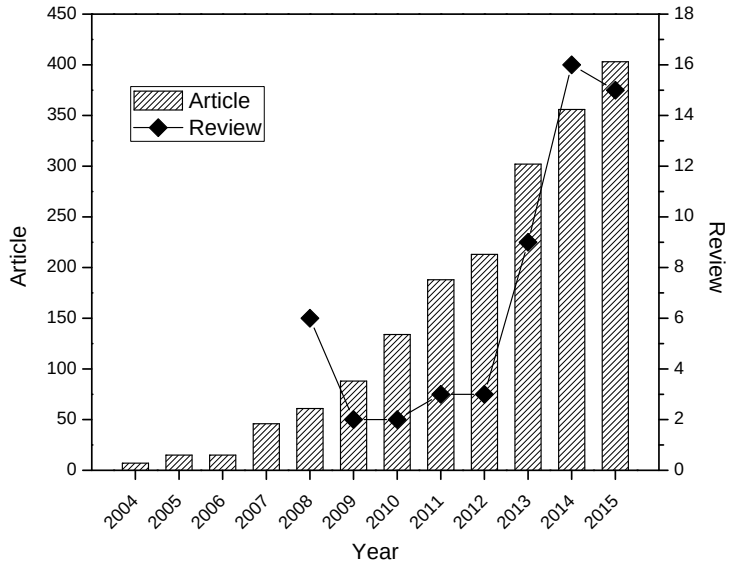

Figure 2 Publications on cellulose nanofibers (articles and reviews) from 2004 until 2015. Data analysis done on web of science website with keyword “Cellulose nanofibers”.

1.2 Cellulose nanofibers

Cellulose nanofibers (CNFs) are the smallest cellulose building the elementary fibril, made up of 36 cellulose chains, which has diameter between 5 and 50 nm (depending on cellulose source and preparation method) and length in the range of several micrometers with a high aspect ratio (Vijay & Thakur, 2015). CNF consists of repeating units of two linked D-glucose molecules with β (1–4) glycosidic bonds and composes of crystalline and amorphous regions (Figure 3). These repeating units (or called degree of polymerization, DP) depend on cellulose source, typically 300–1700 for wood based cellulose and 800–10000 for cotton and other plant fibers. CNF can be extracted from the cell wall of various raw materials mainly from trees (softwood and hardwood), plants and agriculture residual, as illustrated in Figure 4.

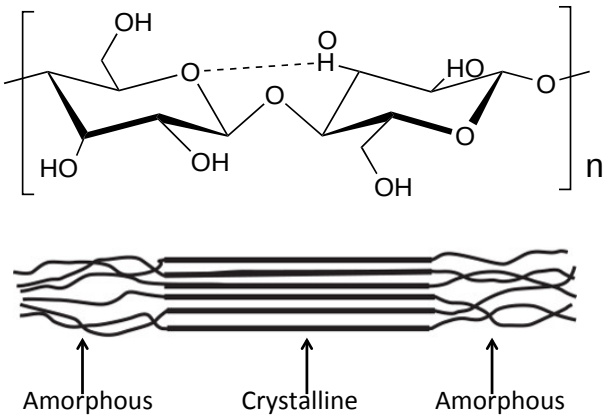

Figure 3 Chemical structure of the cellulose repeating unit (top) and their cellulose chains in amorphous and crystalline regions (bottom).

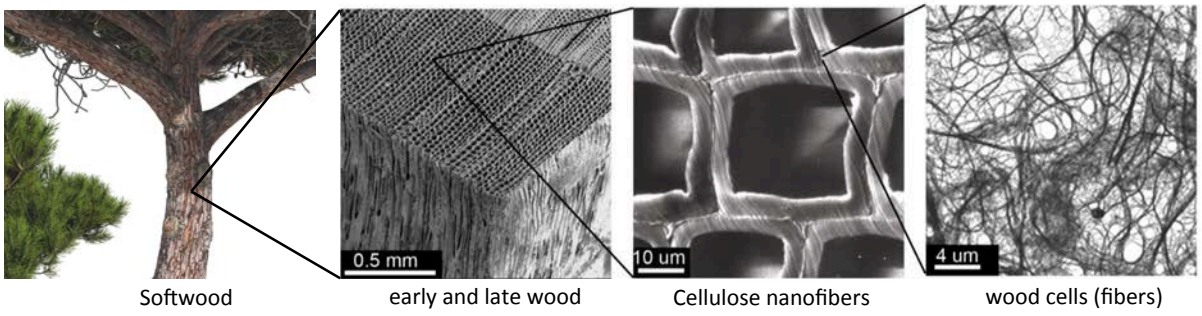

Figure 4 CNF extraction from softwood cell wall (Oksman et al. 2014).

1.2.1 Production of CNF

Since 2008, the investigations concerning CNF have focused on scaling up the nanocelluloses production. The announcement of the first commercial production of nanocelluloses, in 2012, can be considered as the starting point of CNF industrialization. Table 1 summarizes some CNF production that is available at laboratory, pilot plant, and commercial product from some companies and other organizations. The price of the raw material (around 0.5 $/kg) together with the production cost, brings the commercial product of CNF in dry state in the range between 7 to 12 $/kg. This price is around 33$/kg for a pilot plant, announced by University of Maine (Oksman et al., 2014).

Until today, there are still some issues and main challenges to overcome in the field related to the efficient separation of nanosize cellulosic materials from all natural fibers resources. According to literature review, the production of cellulose nanofibers has four main issues: 1)

the energy required to isolate nanofibrils is still high; 2) the mechanical process is still at pilot scale or commercial and yet machine was not designed for industrial scale; 3) a large variety of pretreatment and mechanical treatment increase the confusion and the grade quality (absence of standards); and 4) It is difficult to characterize the homogeneity and quality of CNF (Vijay Kumar Thakur, 2015). Besides, high energy consumption is unavoidable for the nanofibrillation of plant celluloses because it requires partial cleavage of numerous numbers of inter-fibrillar hydrogen bonds. As mentioned earlier, mechanical treatment was used to extract CNF from cellulose sources. The extraction of CNF from mechanical treatment (homogenizer) required the energy consumption from 12,000 to 70,000 kWh/t (Eriksen, 2008). In order to reduce the cost, pretreatment is applied prior mechanical treatment. Innventia isolated CNF from various fibers and different pretreatment, following by homogenization in a microfluidizer. They produced CNF from bleached sulphite pulp using enzyme pretreatment and mechanical treatment, which need lower energy consumption between 2000 and 500 kWh/t; later, by means of carboxymethylation, the energy consumption was decreased until 200 kWh/t. Therefore, the development of disintegration methods that are less energy consuming becomes a priority in securing the industrialization of CNF production. Some combinations of pre-treatments and mechanical treatments have been suggested (Lavoine, Desloges, Dufresne, & Bras, 2012).

Table 1 List of operational and announced CNF production facilities (Oksman et al. 2014).

Industry or University	Country	Production (Kg)/day	Production method	Scale of process /trade name
Borregaard	Norway	350	Enzymatic CNF	Pilot plant
UPM Kymmene Ltd.	Finland	n.a.	Enzymatic CNF with Masuko	Commercial/Biofibrils
Nippon Paper	Japan	n.a.	TEMPO-treated CNF	Commercial/CSNF Pilot scale for TEMPO treatment
Innventia	Sweden	100	Enzymatic and/or functionalized with microfluidizer or GEA	Pilot plan/R&D purpose only
University of Maine	USA	300	Mix of larger and standard CNF	Pilot plant/ Commercial grade
PFI	Norway	15	Enzymatic with Masuko grinder	Laboratory scale
LGP2/Grenouble INP	France	2	Enzymatic or TEMPO using grinder	Laboratory scale

1.2.2 Pretreatment process

The purpose of pretreatment is to obtain fiber less stiff and cohesive, which reduces energy consumption in mechanical disintegration process leading to production at the industrial level. This method make the nanofibrillation easier, mainly by shortening and loosening the cell wall structure of the cellulose fibers and limiting the hydrogen bonds, or add repulsive charge, and or decreasing the DP or the amorphous link between individual CNFs (Siró & Plackett, 2010). Three different pretreatments such as mechanically, enzymatically, and chemically are used to separation nanofibrils. Mechanical treatment such as disintegration, refining, PFI milling is used to reduce the cellulose raw material size and to open the structure for further separation. Enzymatic pretreatment is often done by using endoglucanases, as they do not attack crystalline cellulose as easily as the other types of cellulose enzymes (Henriksson, Henriksson, Berglund, & Lindström, 2007). Chemical pretreatment such as the 2,2,6,6-tetramethyl-piperidine-1-oxyl radical (TEMPO)-mediated oxidation, enzymatic, carboxymethylation, and periodate-chlorite oxidation can be used to favour the nanofibers isolation (Oksman et al., 2014). TEMPO oxidation has been more studied than other pretreatments (Figure 5). The mechanical and different pretreatments provide the CNF with different diameter and length as shown in Figure 6.

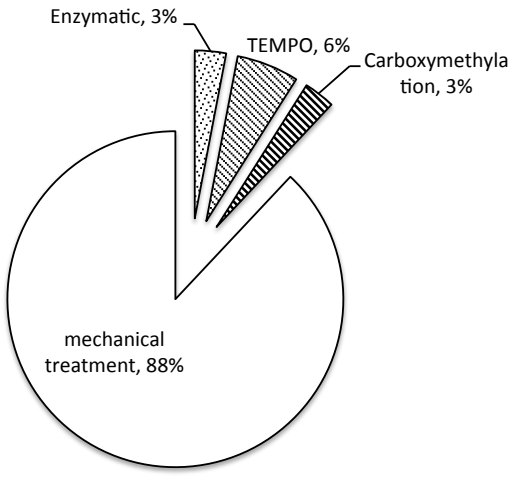

Figure 5 Quantification of the most frequently applied pretreatment used for CNF production (Lavoine et al., 2012).

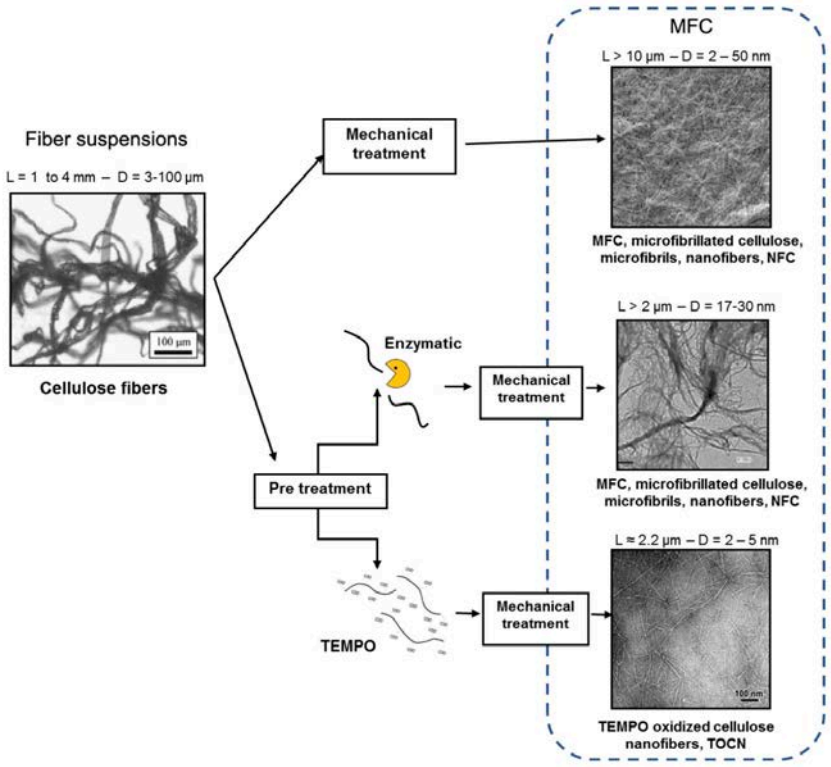

Figure 6 Different strategies for the production of CNF materials (Lavoine et al., 2012).

a) TEMPO-mediated oxidation

TEMPO-mediated oxidation is one of the advantageous and characteristic chemical reactions of native cellulose used as a pretreatment for the preparation of CNF. TEMPO has conveyed the chemistry of alcoholic hydroxyl groups to aldehydes, ketones and carboxyl groups selectively on the cellulose microfibril surfaces of wood cellulose in water under different aqueous conditions; this has reduced the energy consumption during the CNF production because the electrostatic repulsion and osmotic effect work efficiently between highly charged cellulose microfibrils during mechanical disintegration (Fukuzumi, 2012). In 1995, de Nooy et al. first applied TEMPO-mediated oxidation to water soluble polysaccharides such as starch, amylodextrin and pullulan for regioselective conversion of C6 primary hydroxyls to carboxylate groups (de Nooy, Besemer, & van Bekkum, 1995). Later, Isogai & Kata (1998) did work on TEMPO-mediated oxidation of cellulose and other polysaccharides as regioselective and effective chemical modification agent (Figure 5). They introduced TEMPO/NaBr/NaClO systems on cellulose to study the effects of oxidation conditions on chemical structures and degrees of polymerization of the products.

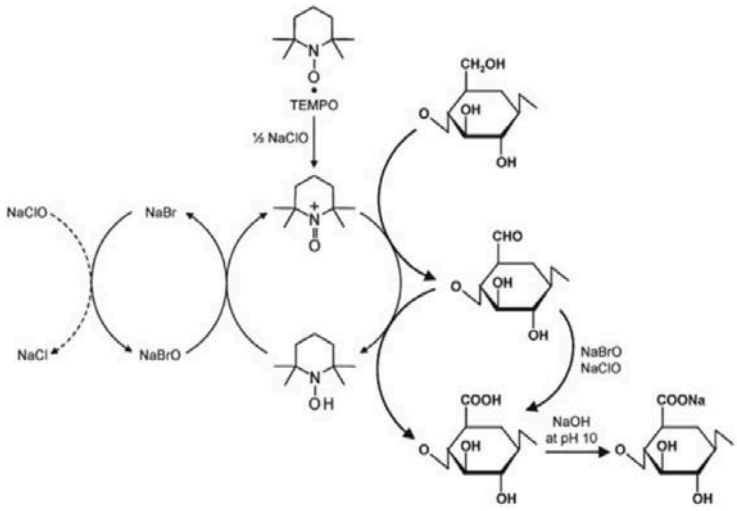

Figure 7 Regioselective oxidation of C6 primary hydroxyls of cellulose to C6 carboxylate groups by TEMPO/NaBr/NaClO oxidation in water at pH 10 (Isogai et al., 2011).

Moreover, many related studies have been extensively carried out in the last decades (Saito & Isogai, 2004; Saito, Kimura, Nishiyama, & Isogai, 2007; Saito, Nishiyama, Putaux, Vignon, & Isogai, 2006) and have been reviewed in detail (Isogai et al., 2011). Among different studies, three TEMPO-mediated oxidation systems have been reported as green chemistry: TEMPO/NaBr/NaClO at pH 10 (Saito et al., 2007), TEMPO/NaClO/$NaClO_2$ at pH 5 or 7 (Hirota, Tamura, Saito, & Isogai, 2012; Saito et al., 2007), and TEMPO electro-mediated oxidation at pH 7 or 10 (Isogai, Saito, & Isogai, 2010). Table 2 shows the impact of the different TEMPO oxidation processes on CNF from bleached softwood Kraft pulp.

Table 2 Impact of the different TEMPO oxidation processes on CNF from bleached softwood Kraft pulp (Lavoine et al., 2012).

Different TEMPO oxidation	Carboxylate content (mmol/g)	Aldehyde content (mmol/g)	Yield (%)	Degree of polymerization
TEMPO/NaBr/NaClO pH 10	1.7	<0.08	>95	600
TEMPO/NaClO/$NaClO_2$ pH 7	<1	0	–	>1000
Electro mediated oxidation TEMPO pH 10	1.01	0.29	83	520
Electro mediated oxidation 4-acetamido-TEMPO pH 6.8	0.92	0.38	93	1400
Non TEMPO treatment	0	0	–	Decrease of 30–50% of the raw materials

TEMPO/NaBr/NaClO oxidation systems is more efficient on wood cellulose without heating or sealing of the reactor compare compared to the other two oxidation systems, which need long reaction times. This is the most promising process to produce TEMPO-oxidized cellulose at the industrial level (Oksman et al., 2014). The C6 primary hydroxyl of cellulose is expected to be oxidized to C6 carboxylate groups by TEMPO/NaBr/NaClO oxidation in water at pH 10. It is possible that C6-aldehydes are oxidized to C6-carboxylates by not only N-oxoammonium cations formed in the TEMPO-mediated oxidation but also by NaClO and/or NaBrO co-existing in the system. The oxidation process can be monitored from the pattern of aqueous NaOH consumption, which is continuously added to the reaction mixture to maintain the pH at 10 during the oxidation. Figure 8 shows the carboxylate content increasing from 0.02 up to 1.7 mmol/g within 2 h by the TEMPO-mediated oxidation with NaClO of 10mmol/g-pulp with 2 h of reaction time.

CNF from TEMPO has 2–5 nm of diameter and 2.2 μm of length while CNF without pretreatment has 2–50 nm of diameter and length longer than 10 μm (Lavoine et al., 2012). However, TEMPO-oxidation will add extra material costs and also decrease thermal stability (Eyholzer et al., 2010; Fukuzumi, 2012; Fukuzumi, Saito, Iwata, Kumamoto, & Isogai, 2009).

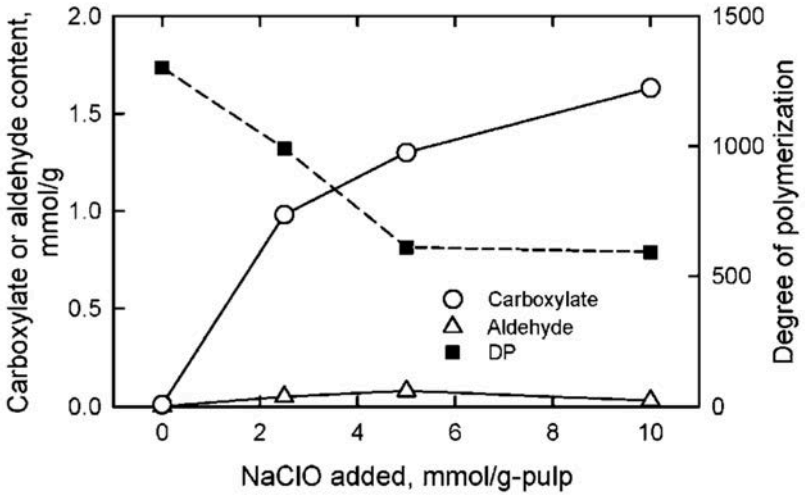

Figure 8 Relationships between carboxylate, aldehyde contents and degree of polymerization (DP) of oxidized wood celluloses with various amounts of NaClO by TEMPO/NaBr/NaClO system (Isogai et al., 2011).

1.2.3 Mechanical treatment

Mechanical treatment is applied after pretreatment process to isolate microfibrils from cell wall. In this process, different techniques had been carried out such as homogenizer, microfluidizer, grinding process, cryocrushing, electrospinning, and so on (Lavoine et al., 2012). More recently, Spence et al. (2011), conducted a very precise comparative study of the energy consumption and physical properties of CNF produced by different processing methods; homogenizer, microfluidizer, and grinder. They compared the energy consumption as a function of the mechanical treatment, the number of passes, the pressure, and the speed, as presented in Figure 9. In spite of its high-energy consumption limiting the possible scaling-up of production, homogenizer has more benefit than the others. Cellulose slurry is pumped at high pressure and fed through a spring-loaded valve assembly. The valve opens and closes in rapid succession, so the fibers are subjected to a large pressure drop under high shearing forces lead to the disruption of cell walls and their separation into nano-scale cellulose fibrils with high aspect ratio (Dinand, Chanzy, & Vignon, 1996). This combination of forces promotes a high degree of fibrillation of the cellulose fibers (Nakagaito & Yano, 2004). CNF obtained from this technique are homogenous and have uniformly sized fiber (Aulin, 2009), highest specific surface area (Spence et al., 2011), and films with the lowest water vapor transmission rate. However, films produced by a microfluidizer and a grinder presented superior physical, optical, and water interaction properties, which suggests that these materials could be produced in a more economical way interaction properties for packaging applications (Lavoine et al., 2012).

Table 3 Parameters used to produce CNF from bleached and unbleached wood pulp fibers by homogenizer, microfluidizer, and micro-grinder (Spence et al., 2011).

Processing method	Pretreatment	Pressure (MPa) or speed (rpm)	Number of passes	Total energy consumption (kWh/t)
Homogenizer	Refining	55	20	21888
Micro-grinder	None	1500 rpm	9	5580
	Refining	1500 rpm	9	1550
Microfluidizer	Refining	69 and 207	1 and 5	2939
		69	20	3119
		138	5	2550

1.3 Bacterial cellulose

1.3.1 History and production methods

Bacterial cellulose (BC) is an unbranched polysaccharide, comprising of linear chains of β-1, 4-glucopyranose residues, which is produced by microorganisms belonging to *Acetobacter xylinum*, now renamed *Gluconacetobacter xylinus* (Brown, 1886). This bacteria is found in nature on rotting fruits and a variety of niches that have fixed carbon in the form of sugars or alcohol. In the mid-20th century Hestrin, & Schramm (1954) began with the description of basic metabolic processes of this bacteria strain and ended with the development of a special culture medium for optimized production of BC on a laboratory scale, whereas D-glucose is used as a carbon source and bacto peptone as well as yeast extract as sources of nitrogen and vitamins. Both discoveries are important fundamentals for the variety of all BC production methods available today.

There are three stages of growing mechanism of bacterial cellulose. Firstly, the bacteria accept glucose into the cell. Secondly, nanocellulose that is biosynthetized on metabolic pathway by cellulose synthase is discharged outward the cell wall. Finally, the nanocellulose aggregates are settled into a pellicle (Pandey, Takagi, Kakagaito, & Kim, 2015). The cultivation can be done in the presence of molds of different sizes and shapes. A uniform surface is generated with a growth thickness of the material of 0.5–1.5 mm/day and continued to harvest between 7 and 10 days. The yield (cellulose dry weight) decreased during the 7 days of cultivation and the highest yield was obtained at day 1 because the yield was calculated only for the fructose utilization and not the small amount of glucose present in cultivation medium in the first 48 hours (Table 4). Besides, the pH also affects the cultivation of BC.

Table 4 The production of bacterial cellulose and yield present in grams of bacterial cellulose obtained per day; pH 5.5 (Gama, Gatenholm, & Klemm, 2013).

Cultivation	Yield (g/g)
Day 1	2.402
Day 2	0.541
Day 3	0.183
Day 4	0.145
Day 7	0.141

A successful proof concept by means of the experimental a pilot plant of BC (180 L of volume) generation process was constructed by subdivided into the following stages presented in figure 9 (Karlisch et al., 2011). However, there are challenges in the expansion of BC production to commercial scale (Gama et al., 2013).

1.3.2 Bacterial cellulose properties and its application

Bacterial cellulose is secreted as a ribbon-shaped fibril, less than 100 nm wide, depending on different types of nanofibers network which is composed of much finer 2–4 nm nanofibrils (Pandey et al., 2015). A unique property is its ability to be shaped into three-dimensional structures during biosynthesis (Gama et al., 2013). Another specific ultrafine network structure and superior properties such as sufficient porosity, high purity, and crystallinity of BC provides an ultimate mechanical properties, excellent biodegradability and biocompatibility (Gelin et al., 2007). BC has been used for a variety of commercial applications including textiles, cosmetics, and food products. Thanks to a unique surface chemistry, nontoxic hydrogel with good mechanical properties, BC has been extended their use in diverse fields such as biomedical electronics, paper industry, packaging, biosensors, and scaffolds for tissue engineering and organ regeneration (Czaja et al. 2007; Ul-Islam et al. 2013; Lin & Dufresne 2014; Rajwade et al. 2015). Moreover, its hydrophilic polymeric membranes have in general a high swellability, high permeability for water vapour and gases, a good fluid transport across the membrane, as well as a high selectivity for the transport of voluminous and apolar substances. These properties in combination with an adequate mechanical strength make them highly suitable for the treatment of wounds as a coverage material (Clasen, Sultanova, Wilhelms, Heisig, & Kulicke, 2006), wound healing applications (Wei, Yang, & Hong, 2011), cartilage repair (Svensson et al., 2005), bone regeneration (Zaborowska et al., 2010), and most recently, for blood vessel replacements (Wippermann et al., 2009) as shown in Figure 9.

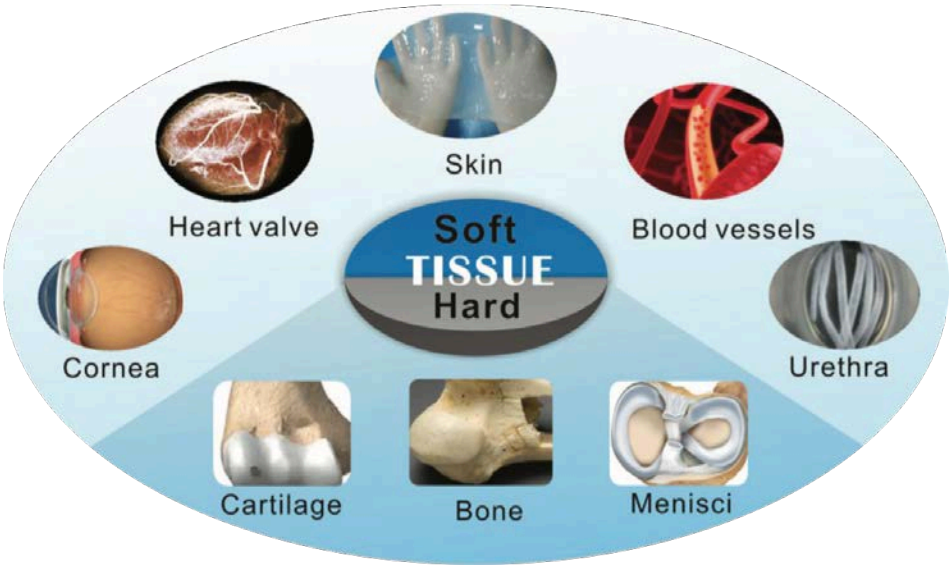

Figure 9 Prospects for the various biomedical uses of bacterial cellulose-based materials (Fu et al., 2013).

1.4 Conducting polymers

Polymers have been considered as insulators due to their insulating properties. So far, any electrical conduction in polymers is generally due to loosely bound ions was mostly regarded as an undesirable fact (Freund & Deore, 2007). There is nothing that can be novel technology without new or improved materials, and they must be synthesized. Synthesis is both a matter of creative design and experimental skill, and no target structure can prove this claim better than conjugated polymers. Conjugated polymers are fascinating species from i) a structural point of view due to the many ways of establishing an extended pi-conjugation; ii) a functional point of view due to their electronic and optical properties, which qualify them as active components of organic electronics; and iii) a research point of view due to their potential of fostering cross-disciplinary research (Müllen, Reynolds, & Masuda, 2014).

Conducting polymers (CPs) are attractive candidates because they have good intrinsic conductivity through a conjugated bond system along the polymer backbone. They are typically formed either through chemical oxidation or electrochemical oxidation of the monomer (Snook, Kao, & Best, 2011). Letheby (1862) published the synthesis of a kind of conducting polymer (polyaniline) by anodic oxidation of aniline, which was conductive and showed electrochromic behavior. In late 1970s, Alan J. Heeger, Alan G. MacDiarmid and Hideki Shirakawa discovered the large increase in the conductivity of polyacetylene after doping (Shirakawa, Louis, MacDiarmid, Chiang, & Heeger, 1977). This work is considered a

starting point for the research field of conducting polymers (Inzelt, 2012; Nystrom, 2012). Electrical conductivities of conducting polymers possess a variety depending on preparation method (chemical and electrochemical oxidation) and the process conditions of the polymer. As reported by (Snook et al., 2011) conductivities of several conducting polymer were from a few S cm^{-1} to 500 S cm^{-1} (Table 5) and were generally between semiconductor and conductor characteristics as shown in Figure 10. There are many types of conducting polymers such as polyacetylene, polypyrrole, polyphenylene vinylene, polythiophene, polyaniline, PEDOT and their derivatives (Abdelhamid et al., 2015). Their structures are listed in Figure 11.

CPs have wide applications in many fields. They can be used to produce thin-film deposition and microstructure of conducting materials (antistatic coatings, microwave absorption, microelectronics). Due to their conductivities properties and their ability to store energy, they can also be used for sensors, energy storage technologies application (Inzelt, 2012). Among them, polypyrrole (PPy), polythiophenes (PThs) and their respective derivatives are possibly more environmentally friendly and have attracted considerable attention as electrochemical supercapacitor or battery electrode in the last decade (Wang, Xu, Chen, & Du, 2007).

Table 5 Typical conductivities of various conducting polymers (Snook et al., 2011).

Conducting polymers	Conductivity (S cm^{-1})
Polyaniline	0.1 – 5
Polypyrrole	10 – 50
PEDOT	300 – 500
Polythiophene	300 – 400

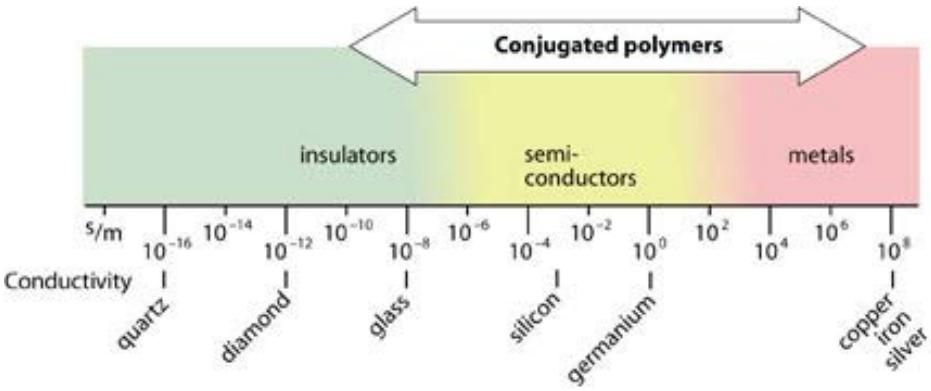

Figure 10 Classification of conductivity of insulators, semi-conductors, metals, and conjugated polymers.

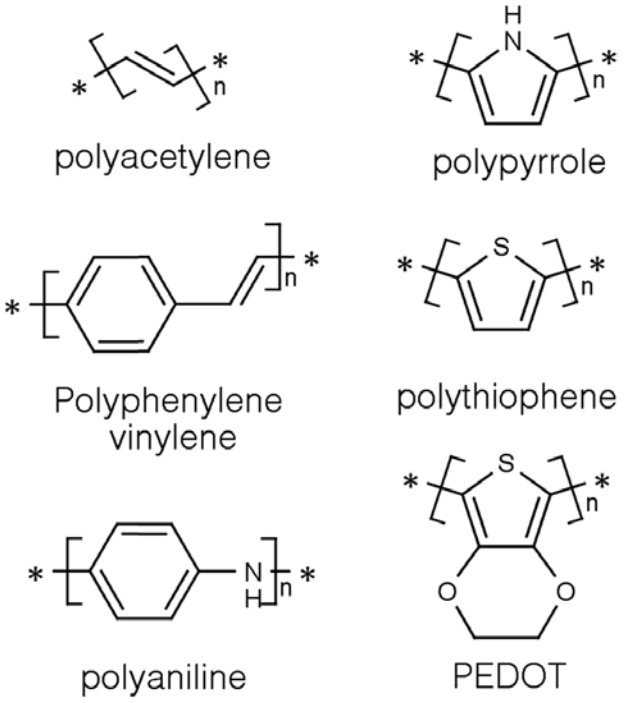

Figure 11 Structure of conducting polymers (Abdelhamid et al., 2015).

1.4.1 Polypyrrole

Polypyrrole (PPy) has an appreciable environmental stability (Buitrago-Sierra et al., 2013) and is easy to synthesize (Ansari, 2006; Eisazadeh et al., 2007; Huang et al., 2006; Trchova & Kova, 2003; Wang et al., 2001). Indeed the moderate oxidation potential of pyrrole, as well as its solubility in polar solvents including water, constitutes great advantage for this kind of synthesis (Müllen et al., 2014). Both chemical and electrochemical polymerization of pyrrole monomer are commonly used and the processes are shown in Figure 12.

Figure 13 indicates that PPy is formed by aromatic or quinoid structures along its conjugated backbone. In neutral state the polymer is not conductive and becomes conducting only when it is oxidized. The charge associated with the oxidized state is typically delocalized over several pyrrole units and can form a radical cation (polaron) or a dication (bipolaron). The physical form of polypyrrole is usually an intractable powder resulting from chemical polymerization and an insoluble film resulting from electropolymerization (Saville, 2005).

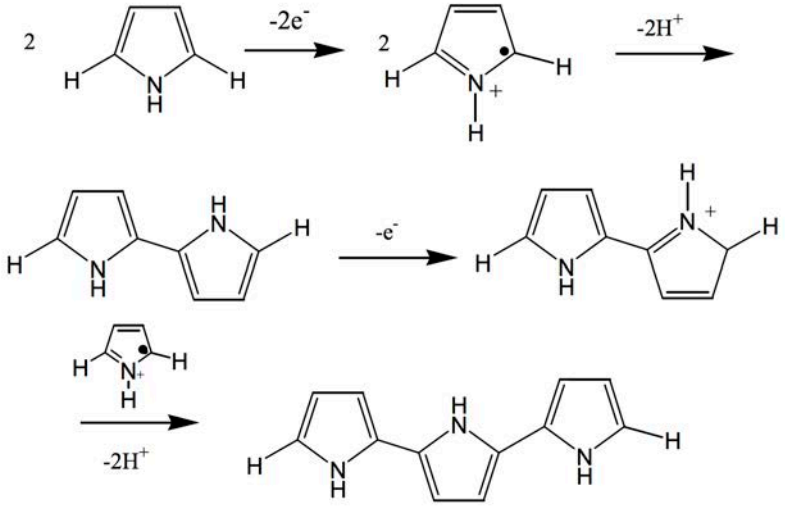

Figure 12 Polymerization process of pyrrole via one electron oxidation of pyrrole to a radical cation, which subsequently couples with another radical cation to form the 2,2'-bipyrrole. This process is then repeated to form longer chains (Saville, 2005).

Electrochemical method has been used for the synthesis of conjugated polymers since they represent an easy, clean and versatile way of obtaining the targeted materials as coatings on conductive substrates. Theoretical aspects focusing on the electrochemistry of PPy were discussed in several book chapters (Audebert & Miomadre, 2007; Müllen et al., 2014). PPy offers a greater degree of flexibility in electrochemical processing than most conducting polymers, and consequently the material has been the subject of much research as a supercapacitor or battery electrode (Snook et al., 2011). On the other hand, the chemical synthesis is described a lot in the preparation of composites, an activity that has fully emerged in the last two decades. The review by Müllen provides a couple of concrete examples of almost every type of synthesis of this outstanding polymer, which, more than any other, still triggers today a lot of active research in many application fields (Müllen et al., 2014).

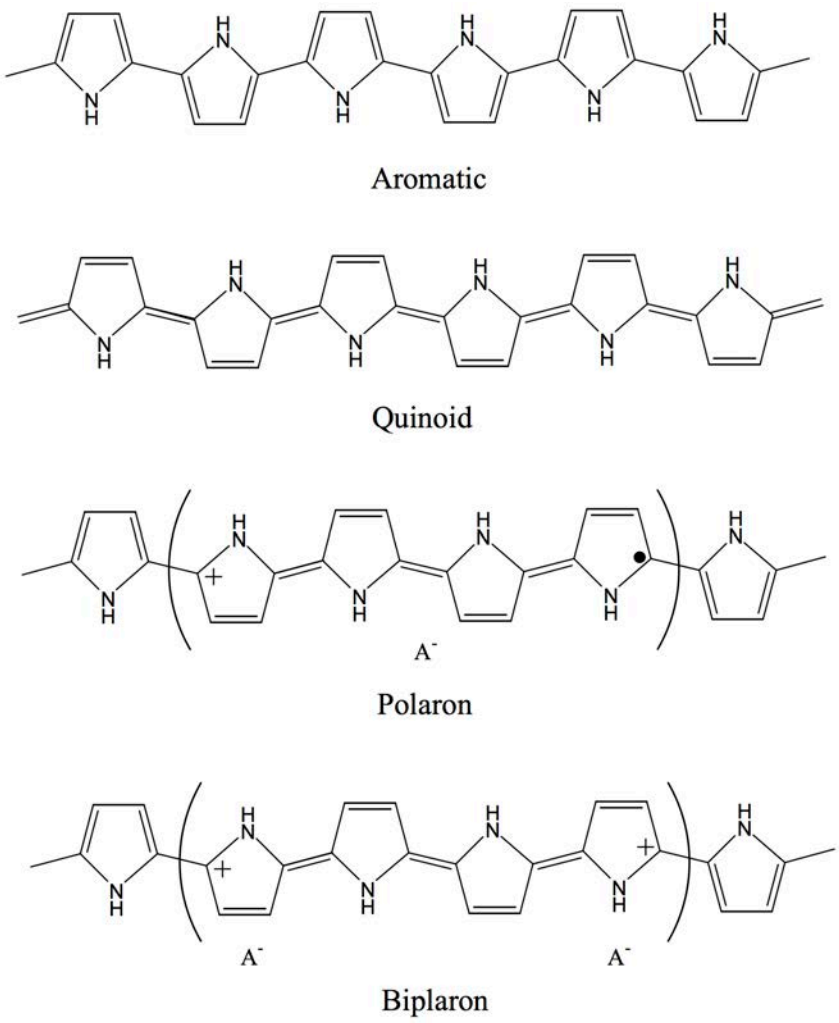

Figure 13 Chemical structure of polypyrrole in neutral aromatic and quinoid forms and in oxidized polaron and bipolaron forms.

Chemical synthesis of polypyrrole proceeds via the oxidation of pyrrole with an oxidant such as ferric chloride. The mechanism is similar to that for electropolymerisation of pyrrole and conductivities are comparable. The conductivity of polypyrrole formed from different ferric salts (effect of dopant ion) has been related to the Fe^{2+}/Fe^{3+} redox potential with strong acid anions providing the most oxidizing ferric species. Weaker acid anions typically coordinate Fe^{3+} ions more strongly, reducing its oxidizing potential (Walker, Warren, & Witucki, 1988). Various oxidants are effective to chemical polymerize of pyrrole but the preferred ones are ferric salts. Especially ferric chloride (iron (III) chloride), which is a cheap and readily available reagent, has been found to be the best chemical oxidant for chemical polymerization with respect to desirable conductivity (Ansari, 2006). Ferric perchlorate is an even more effective reagent (Audebert & Bidan, 1986) since its redox potential in acetonitrile is much

higher than ferric chloride (the reason being the stabilization of iron (III) by chloride ions), but its high price has limited its use. Therefore, no other oxidant seems to be more effective than ferric chloride, which is a technique almost universally used in recent chemical PPy syntheses, and is known to provide polymers with a high stability allied with a reasonable conductivity (1–200 S cm^{-1} according to the published works) (Machida, Miyata, & Techagumpuch, 1989). The electrical conductivity of PPy depends on the synthesis temperature and the mole ratio of oxidant and pyrrole. Synthesis of PPy at lower temperature exhibits longer conjugation length, structural order, fewer structural defects, and higher conductivity. Armes (1987) reported the optimum initial mole ratio of iron (III)/pyrrole for the polymerization at 19ºC was approximately 2.38 ± 0.04, and assuming the reaction is complete within 23 h.

1.4.2 Poly(3,4-ethylenedioxythiophene) and its derivative

Polythiophenes (PTh) have remained one of the most excellent material researched materials in the field of organic electronic. Through its good characteristics, its stability, ready availability at low costs and its lack of toxicity, in material science polythiophene is an excellent candidate. Due to the relatively facile and well-established synthetic modifications of the corresponding monomers, oligothiophene, and polythiophenes have been vastly explored in a variety of applications such as organic field effect transistor, organic photovoltaics, and sensing devices in medical and biological fields. Various synthetic methods have been used to achieve a wide variety of structural variations that showcase the attractive potential of polythiophenes (Elschner, Kirchheyer, Lovenich, Merker, & Reuter, 2011).

In 1988, researchers from Bayer AG (Leverkusen, Germany) invented a derivative of PThs, diethoxy substituted thiophene called poly(3,4-ethylenedioxythiophene) (PEDOT) also known under the trade name Baytron or Clevios (Bashir, 2013; Groenendaal, Jonas, Freitag, Pielartzik, & Reynolds, 2000). Since then, PEDOT has become one of the best conducting polymers available in terms of high conductivity, processability, and stability. Furthermore, PEDOT is the only conducting polymer that is commercially produced on a large-scale by H.C. Starck Clevios GmbH, and is used for many applications such as antistatic coatings, printed electronics, transparent transistors, organic solar cells, electronic component, and organic light-emitting diodes (OLED) displays (Li et al. 2014). In particular, widespread applications have been developed using the conducting properties of the PEDOT complex with polystyrene sulfonic acid (PEDOT:PSS, Baytron P, see Figure 14) (Skotheim &

Reynolds, 2007). The complex structure of PEDOT:PSS comes from water-borne poly(styrenesulfonic acid) and the corresponding polyanion that is able to sufficiently function as the counterion for positively charged doped PEDOT. PEDOT:PSS is also mentioned in the advanced information by the Nobel committee regarding the 2000 Chemistry Nobel Prize to Heeger, MacDiarmid, and Shirakawa. Surprisingly, due to the increasingly of the number of PEDOT patents and scientific papers published every year with more than 1000 documents, a book of only PEDOT was written by Elschner et al. (2011).

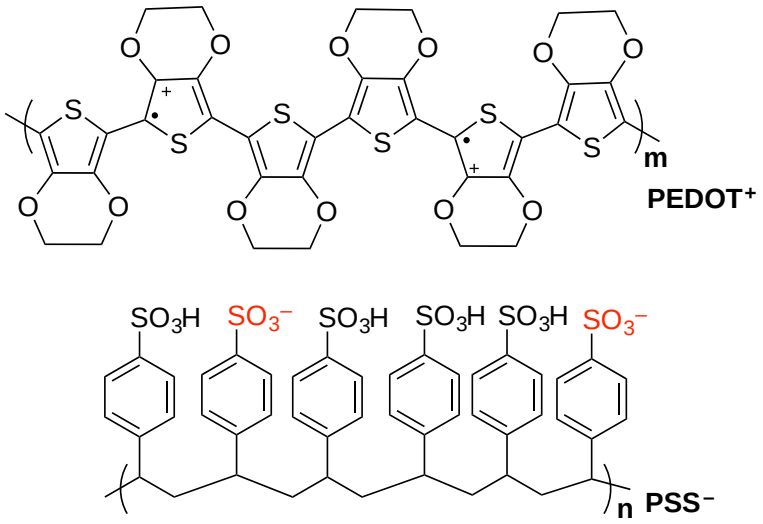

Figure 14 Chemical structure of PEDOT and PSS.

a) In situ polymerization of PEDOT:PSS and the effect of electrical conductivity

The in situ PEDOT polymers are insoluble in most solvents, which cannot be easily made into a processable, coatable solution. Polystyrene sulfonic acid (PSS) is a commercially available water-soluble polymer can serve as a good dispersant for aqueous PEDOT (Audebert & Miomadre, 2007). The solubility problem was subsequently circumvented by using a water-soluble polyelectrolyte, polystyrene sulfonic acid (PSS), as the charge-balancing dopant during polymerization to yield PEDT:PSS (Groenendaal et al., 2000). There are several available oxidants such such iron (III) chlorite ($FeCl_3$), iron (III) tosylate, potassium peroxodisulfate ($K_2S_2O_8$), and sodium peroxodisulfate ($Na_2S_2O_8$). Polymerization with the oxidant sodium peroxodisulfate ($Na_2S_2O_8$) yields a PEDT:PSS-complex in its conductive (Anna & Moos, 2012), cationic form as shown in Figure 15. The presence of PSS in the complex structure has two functions. The first is to serve as the charge-balancing counterion to the PEDOT, and the second is to disperse the PEDOT segments in the water. Without a

PSS counterion in the system, the monomolecular thiolactone oxidation product 3,4-ethylenedioxy-2(5H)-thiophenone is formed instead of the desired PEDT:PSS polymer.

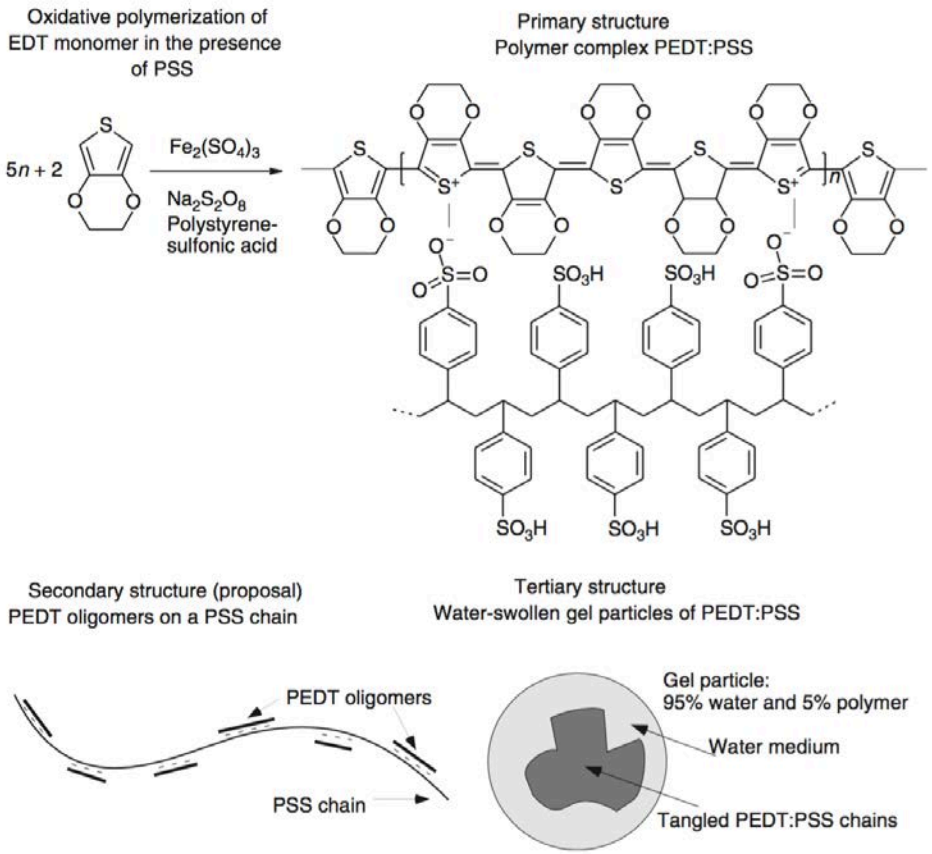

Figure 15 Synthesis, primary, secondary, and tertiary structure of PEDOT:PSS (Audebert & Miomadre, 2007).

The reaction forms a stable, easy-to-process, deep blue microdispersion of polymer gel particles. These particles consist roughly of 90-95% water. The maximum solids content achievable, while maintaining a stable dispersion, depends on the PEDOT:PSS ratio and increases with increasing PSS content. However, the PEDOT:PSS ratio affects the electrical conductivity of final product.

Table 6 summaries several typical properties of PEDOT:PSS and their applications depend on the PEDOT:PSS ratio (Audebert & Miomadre, 2007). Anna & Moos (2012) proved that the low conductivity associated with a higher PSS content precludes measurement of the seebeck coefficient due to a poor signal to noise ratio.

Table 6 Typical PEDOT:PSS grades and their characteristics.

PEDOT:PSS Ratio	Solids Content (%)	Conductivity S cm^{-1}	Typical application
1:2.5	1.3	10	Conducting coating
1:2.5	1.3	1	Antistatic
1:6	1.5	10-3	OLED
1:20	3	10-5	Passive matrix displays

1.5 Carbon nanotubes

Carbon nanotubes (CNTs) were discovered by Oberlin et al. (1976), Endo et al. (1976), without application, and then rediscovered by Iijima (1991). CNTs are allotropes of carbon with a nanostructure having a length to diameter ratio greater than 1,000 (Marquis, Guillaume, & Chivas-joly, 2005). They consist of graphite sheets seamlessly wrapped into a nano size cylindrical tube. CNTs are lattice of carbon atoms, in which each carbon is covalently bonded to three other carbon atoms and formed in three different structures such as chiral, armchair, and zigzag (Figure 16). The structure is characterized by the descriptors *n* and *m*. These structural parameters allow for a prediction of the electric conductivity. Only armchair nanotubes (*n*,*n*) and such species with *m*-*n* = 3*q* are electric conductors, and any other nanotube is semiconducting.

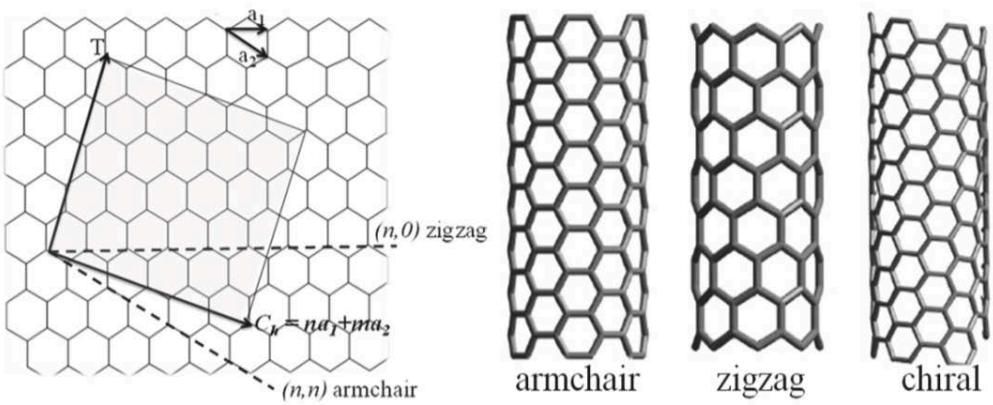

Figure 16 A sheet of graphene roll to show formation of different types of single walled carbon nanotube (Yellampalli, 2011).

These statements have been established from symmetry considerations and from determining the band structure by way of the zone-folding method. The production of single and multi-

walled nanotubes can be prepared by chemical vapor deposition (CVD), arc discharge between graphite electrodes, laser ablation or HiPCo process (Krueger, 2010).

The use of CNTs as fillers in nanocomposites has three main problems. At first, the uniform dispersion of CNTs in the host matrix materials is critical, they tend to agglomerate or bundle due to van der Waals' attraction forces between the CNTs. The second is the alignment or manipulation of the CNTs within the matrix in order to tailor the desired anisotropic properties of the composite system. The third major challenge is engineering the interface to strengthen the interaction between the CNTs and the host matrix (Šupová, Martynková, & Barabaszová, 2011).

1.5.1 Surface modification of carbon nanotubes

In order to overcome self-aggregation, surface modification of carbon nanotubes is required to improve the dispersion and the interfacial adhesion of composites (Ahmed, Haider, & Mohammad, 2013; Salajkova, Valentini, Zhou, & Berglund, 2013). Several methods for chemical modification of carbon nanotubes, such as covalent, noncovalent (Hirsch, 2002), ion adsorption, metal deposition, grafting reaction, and oxidation have been studied to oxidize carbon nanotube materials (Yu et al., 1998). Previous works (Hung, Anoshkin, Dementjev, Katorov, & Rakov, 2008; Yu et al., 1998) have suggested that heating in a mixture of concentrated acid oxidants H_2SO_4/HNO_3 in volume ratio of 3:1 (Figure 17), carbon nanotubes are very efficiently oxidized and damages to the tubular structure is prevented. In addition, the amorphous carbon and carbon nanoparticles are removed under this oxidation process. Besides, several disadvantages of surface modification like defect or deformation of outer tube during the acid treated leading to change the crystallinity and reduce the specific ratio length to outer tube (Loos, 2015).

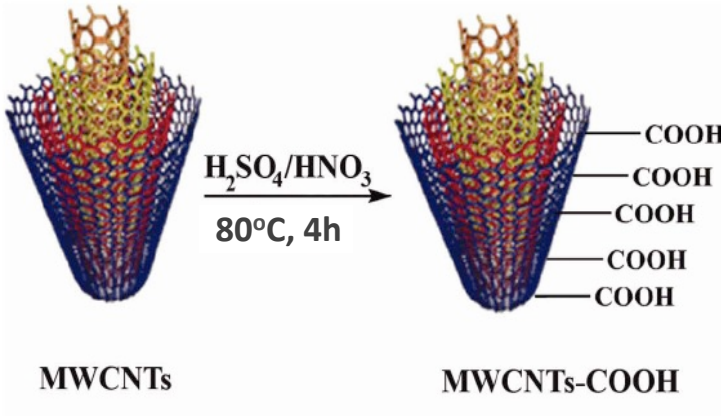

Figure 17 Scheme of the surface modification of MWCNTs (Zare, Lakouraj, Moghadam, & Azimi, 2013)

1.5.2 Properties of carbon nanotube and their applications

Carbon nanotubes (CNTs) have a length to diameter ratio that can reach of up to 28,000. Depending of their classification, carbon nanotubes (CNTs) have various outer diameter and length; length and diameter are 1–10 μm and 1–10 nm for single walled carbon nanotube, and 10 nm – 1 μm and 2–30 nm for multi-walled carbon nanotubes (Guldi & Martín, 2010; Thakur & Thakur, 2016). Thanks to their chemical and mechanical structures, carbon nanotubes are very strong and their elastic flexibility is indicated by Young's modulus, which is 10 times greater than that of steel. They withstand extreme strain and tension. Most of the materials fracture on bending because of the presence of more defects, but CNTs possess only few defects in the structure (Henrique, Camargo, Satyanarayana, & Wypych, 2009). Furthermore, the electrical properties of CNTs vary between metallic to semiconducting materials that rely on the diameter and chirality of the nanotubes. The very high electrical conductivity of CNT obtains when they have the minimum defects in the structure and they are in chiral form.

The outstanding properties of CNTs make them widely used in many applications especially in nanocomposites. In combination with water-insoluble drugs, one can obtain composites for biomedical applications such as gene delivery vectors, treatment of infectious diseases and cancer cells. Their hierarchical structure has many uses as transducers for biosensors application. They can also find use for removal of pollutants by adsorption (Thakur & Thakur, 2016). They are applied in sport equipment. For instance, the addition of CNTs in tennis rackets increases their rigidity and power, and in golf CNTs is used to increase energy transfer between golf balls and clubs. Several bicycle components are already being reinforced with CNTs to increases the resistance of handlebars and makes them lighter (Loos, 2015). In storage devices, carbon nanotubes play an important role in the battery technology because some charge carries can be successfully stored inside the nanotubes.

1.6 CNF nanocomposites and their applications

In combination with a suitable polymer matrix, cellulose nanofibers networks show considerable potential as effective reinforcement for high-quality bio-based composites. Likewise, their flexibility and high aspect ratio make CNFs outstanding materials for wide range of applications. The last decade, CNFs have been used as nanofillers to reinforce nanocomposites (Miao & Hamad, 2013; Saba et al., 2014) with thermoplastic and thermoset

polymers for packaging products, construction materials, automobiles, furniture, and pharmaceuticals (Hoenich, 2006; Ioelovich, 2008; Jeon, Yang, & Kim, 2012; Kalia et al., 2011; Zhang et al., 2013). More recently, CNFs have gained much attention for its use as biomedical material because of their exceptional surface chemistry and excellent biological properties (biocompatibility and biodegradability) (Lin & Dufresne, 2014). The application of CNF and CNF nanocomposites is presented in Figure 18.

Due to their benign nature, high available surface area, smoothness, and reduced porosity, CNF films have been reported as potential substrates for biosensors (Salas et al., 2014). However, and because of the intrinsic insulating characteristics, specific strategies need to be developed to impart electrical activity to CNF. In this sense, the combination of CNFs with conductive polymers (CPs) allows to extend the functionality of CNFs in energy storage devices, solar cells or electronic applications (Huang et al., 2013; Koga et al., 2014; Luo et al., 2014; Nyholm et al., 2011; Tammela et al., 2015; Wang et al., 2015; Zheng et al., 2013). CNF and CPs nanocomposites produce high capacitance and conductive films with the advantages of being lightweight (higher energy and power with less device mass) and flexible (Meng, Liu, Chen, Hu, & Fan, 2010). There is a large volume of published studies on CNFs/CPs in the field of biosensor, energy storage and electronic devices (Huang et al., 2013; Koga et al., 2014; Tammela et al., 2015; Zhaohui Wang et al., 2015). Because of low cost and with the capacitive response via fast redox reactions, conducting polymers have attracted extensive interest for pseudocapacitor or battery electrode application (Snook et al., 2011). Pseudocapacitors involve reversible faradaic reactions including surface adsorption/desorption of ions, redox reaction, and electrochemical doping/dedoping process between electrodes and electrolytes for energy storage.

The viability of coating PPy on CNF was demonstrated by Nyström et al., (2010). They verified the conductivity and the ion-charge capacity of cellulose nanocomposites with high amount of PPy conductive polymer.

In a further work, the authors investigated the mechanical properties of PPy-cellulose nanocomposites of different porosity (Carlsson et al., 2012). In a different study Nyström, Strømme, Sjödin, & Nyholm, (2012) improved the capacitance of this type of cellulose nanocomposites. Later, Wang et al. (2015) performed surface modification of cellulose nanofibers to produce cellulose-based supercapacitors. The coating of PPy on CNF substrate has reduced moisture content of CNF in nature and also protected against degradation, as PPy is known to be insoluble in most solutions and solvents (Sasso et al., 2010).

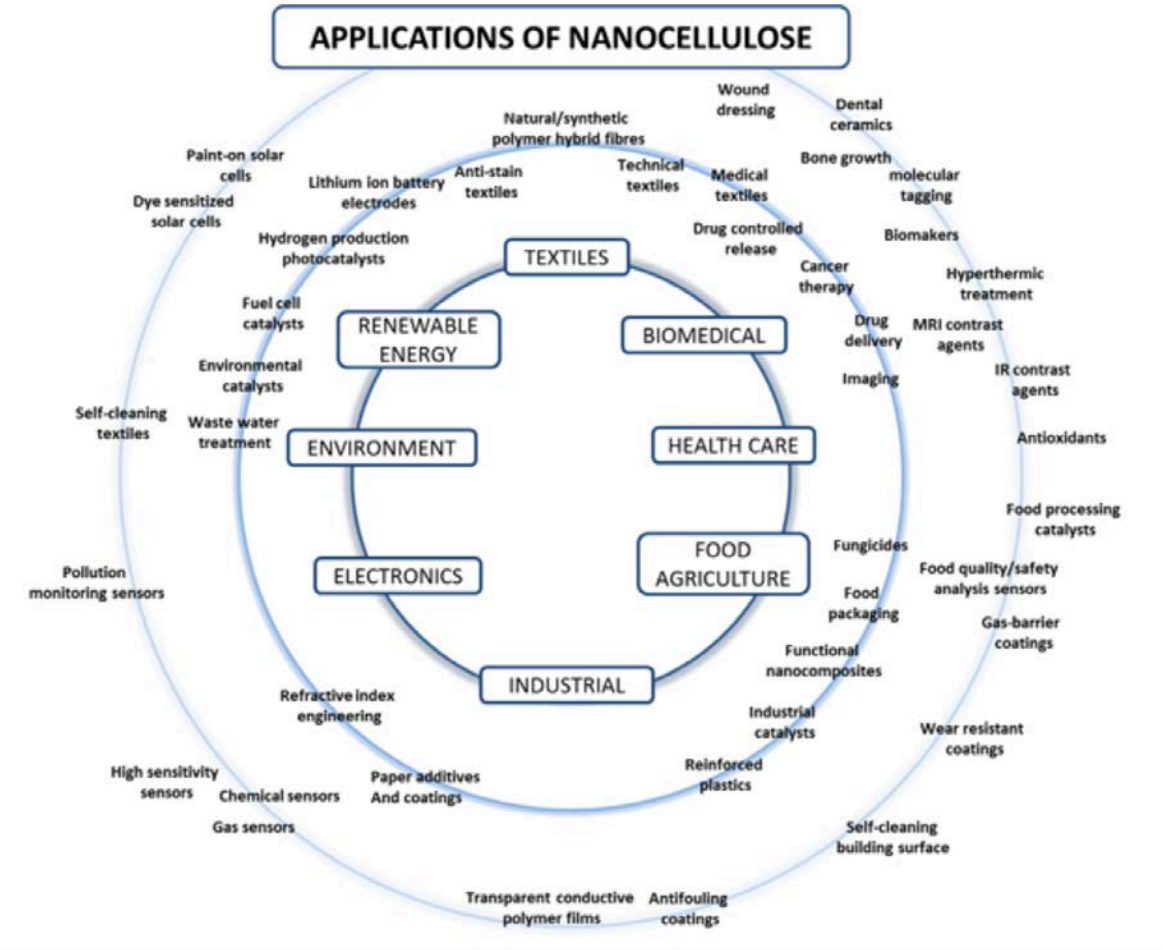

Figure 18 The application of CNF and CNF nanocomposites (Yano, 2011).

Besides that, carbon nanotubes possess outstanding mechanical properties and their carbon–carbon bonds exhibit high electrical conductivity and thermal stability (Jung et al., 2007), which have the potential to improve the electrical conductivity of CNFs. However, CNTs are intrinsically non-polar whereas CNFs are polar so that they show a poor interface interaction, and carbon nanotubes tend to agglomerate due to the establishment of van der Waals forces. In order to overcome self-aggregation, surface modification of carbon nanotubes is required to improve the dispersion and the interfacial adhesion of CNF-CNT (Ahmed et al., 2013; Salajkova et al., 2013). Several methods for chemical modification of carbon nanotubes, such as covalent, noncovalent (Hirsch, 2002), ion adsorption, metal deposition, grafting reaction, and oxidation have been studied to oxidize carbon nanotube materials (Yu et al., 1998). Previous works (Hung et al., 2008; Yu et al., 1998) have suggested that heating in a mixture of concentrated acid oxidants H_2SO_4/HNO_3 in volume ratio of 3:1, carbon nanotubes are very efficiently oxidized and damages to the tubular structure is prevented. In addition, the

amorphous carbon and carbon nanoparticles are removed under this oxidation process. Carbon nanotubes modification was used to reinforce cellulose nanofibers to obtain an electrically conductive nanopaper (Jung et al., 2007) for flexible supercapacitors (Gao et al., 2013). Several attempts have been used to perform CNF-CNT nanocomposites with different methodologies such as electrospinning (Lu & Hsieh, 2010) and mixing (Adsul, Rey, & Gokhale, 2011; Anderson et al., 2010; Salajkova et al., 2013). However, owing a difficulty for balancing between specific surface area, porosity, strength, and electronic conductivity, as well as the accessibility into internal pores, the specific capacitance of CNT can be moderate, which provides inferior performance for supercapacitor applications (Feng, 2015). In this case, the hybrid CNTs with other conjugated polymer like pyrrole is needed. (Nyholm et al. (2011) reported that the composites of PPy with CNTs have been reduced the resistance and improved specific capacitance, cycling stability, and energy/power densities of supercapacitor. Base on literature review, CNF nanocomposites seems an interesting field of research. There are still many works to be done in order to find out more materials that CNF can cooperate with and to meet the specific application of CNF nanocomposites.

2. AIMS OF THE THESIS

2.1 General objective

The overall objective of the present research is to produce lightweight, flexible, and conductive nanopapers based on cellulose nanofibers and conducting materials, aimed to be used as environmentally friendly energy storage devices.

In this work, two kinds of cellulose nanostructures (cellulose nanofibers and bacterial cellulose) and three different conductive materials are used (polypyrrole, poly(3,4-ethylenedioxythiophene):polystyrene sulfonate and multi-walled carbon nanotubes) for the preparation of conductive nanopapers or membranes.

2.2 Particular objectives

For this purpose, the specific objectives of the present work are:

- To produce strong and electrically conductive nanopaper from cellulose nanofibers (CNF) and polypyrrole (PPy) (**Paper I**).
- To study the effect of the combined multi-walled carbon nanotube/polypyrrole with cellulose nanofiber on the electrical conductivity and specific capacitance of nanopapers (**Paper II**).
- To produce conductive nanofibers based on PEDOT:PSS and hybrid PEDOT:PSS/PPy with cellulose nanofibers (**Paper III)**.
- To study the electrical conductivity and specific capacitance of bacterial cellulose/polypyrrole membranes (**Paper IV)**.

2.3 Scope of the study

The scope of this work is to characterize the mechanical properties, electrical conductivity and electrochemical properties of nanopapers from nanocelluloses with different conductive fillers. Their chemical composition, morphology, and thermal stability are investigated by FTIR, FE-SEM,TEM, and TGA; and the basic characterizations such as elemental analysis, density, and porosity of the produced nanopapers is also determined.

3. MATERIALS AND METHODS

This chapter describes the raw materials and chemical reagents used in all the experiments. It also presented the process of preparation of cellulose nanofibers, bacterial cellulose, conductive nanopapers, and their characterization.

The mechanical properties of nanopapers were investigated including, tensile test and Dynamic Mechanical Analysis (DMA). Field Emission Scanning Electron Microscopy (FESEM), Transmission Electron Microscopy (TEM) and Fourier Transform Infrared (FTIR) were carried out to determine the morphology and chemical comsition of nanopapers. Thermogravimetry Analysis (TGA) was used to determine thermal stability and thermal degradation of nanopapers. Electrical conductivity and specific capacitance were carried out by using multimeter and cyclic voltammetry.

3.1 Materials

All raw materials, chemical reagents, and their functions are listed in Table 7. Bleached pine pulp from Arauco (Chile) was used as cellulose raw material in produce cellulose nanofibers (CNF) for **Paper I-III**. 2,2,6,6-Tetramethyl-1-1-piperidinyloxy (TEMPO), sodium bromide (NaBr), sodium hypochlorite (NaOCl) were used as pre-treatment of CNF. Pyrrole (**Paper I-IV)** was supplied by Sigma Aldrich and used as received for the chemical synthesis of polypyrrole. Multi-walled carbon nanotubes (MWCNTs), **paper II**, from Sigma Aldrich containing more than 95% of carbon with an outside diameter and length of 6-9 nm x 5 μm were treated with H_2SO_4/HNO_3 (3:1) reaction mixture prior use. Aqueous solutions of 1.1 wt% of two different poly(3,4-ethylenedioxythiophene):poly(styrene sulfonates), PEDOT:PSS (Clevios PT2 and PH500), containing 1:2.5 by weight of each component were purchased from Clevios Heraeus Deutschland GmbH Co. KG (Leverkusen, Germany). These products were kept between 5 and 30 °C and remain stable for 9 months from date of production in sealed original containers (**Paper III)**. Bacterial cellulose was prepared from *Acetobacter xylinum* culture (**Paper IV)**. Glucose, yeast extract, bacto-pepton, citric acid, Na_2HPO_4, and $MgSO_4 \cdot 7H_2O$ were used to cultivate bacterial cellulose *acetobactor xylinum* culture. Silver coating 3850 was supplied by Holland shielding system BV, Holland (**Paper I-IV)**. The rest of materials, $FeCl_3$, Tween-80, HCl, NaOH, and NaCl were supplied by Sigma Aldrich and used without further purification.

Table 7 Summary of materials, chemical reagents, and their function used in this research.

Materials	Functions
Bleached pine pulped	Raw material to produce CNF and use as matrix
Herstin-Schramm nutrient (HS) medium, yest extract, bacto-pepton, critic acid, Na_2HPO_4, $MgSO_47H_2O$	Cultivation acetobater xylinum bacterial cellulose
TEMPO, NaBr, NaOCl, NaOH	Reactives for the TEMPO-oxidation: TEMPO as catalyst and NaOCl as oxidizer
Pyrrole, MWCNT, clevios PT2 &PH500	Conductive nanofillers
$FeCl_3$	Oxidant initiator
Tween80	Stabilizer
H_2SO_4 and HNO_3	Modification surface of MWCNT
HCl, NaCl, and distilled water	Reagents removal and rinsing of samples

3.2 Methods

All of the equipment to perform and characterization properties of nanopapers is shown in Table 8.

Table 8 Equipment used with their model and function to perform and characterize nanopapers.

Names	Model or Company	Function or characterization
Homogenizer	NS1001L PANDA 2K-GEA	Mechanical treatment cellulose fiber
Rapid Köthen	ISP mod. 786 FH	Drying film
Magnetic stirrer		Dispersion
Multimeter	Agilent digital 34461A	Resistant measurement
FE-SEM	HITHACHI S-4100	Microstructure analysis
Instron Universal	HOUNSFIELD from Metrotec factory	Tensile properties
FT-IR	PLATINUM-ART	Chemical composition
TGA	METTLER TOLEDO	Thermal stability and degradation
DMA	DMA/SDTA861e instrument from mettle Toledo	Thermo-mechanical analysis
Autodesk	GPSTAT302A	Cyclic voltammetry
Vacuum oven		Growing BC at 30ºC
Glass filter	HOLDER KIT MILLIPORE	Filtering samples
Sonicator	Q700	Mechanical dispersion
Nitrocellulose membrane	GSMP, 0.22 µm of pore size	Membrane during filtering
Immobilon-P transfer membrane	PVDF, pore size: 0.45 µm	Drying sample

3.3 Preparation of cellulose nanofibers (Paper I-III)

The bleached pine pulp (30 g dry weight) was dispersed in 2 L of distilled water and disintegrated at 6000 rpm for 30 min in a pulper (PAPEL QUIMIA, S.A, SPAIN). From this suspension, CNFs were extracted by means of a TEMPO-mediated oxidation followed by a mechanical homogenization (homogenizer NS1001L PANDA 2K-GEA, Italy). The TEMPO-mediated oxidation was performed at pH 10 (Fukuzumi et al., 2009) and the obtained cellulose suspension was diluted to 1wt% and passed through a high-pressure homogenizer, one time at 300 bars and three times at 600 bars of pressure. As a result, a transparent gel of cellulose nanofibers (CNF) at 1% concentration was obtained and stored at 4°C prior use.

3.4 Preparation of *Acetobacter xylinum* bacterial culture (Paper IV)

Acetobacter xylinum culture was cultivated in stationary conditions using a Herstin-Schramm nutrient (HS) medium composed of glucose – 5 w/v%, yeast extract – 0.5 w/v%, bacto-pepton – 0.5 w/v%, citric acid – 0.115 w/v%, Na_2HPO_4 – 0.27 w/v%, and $MgSO_4 \cdot 7H_2O$ –0.05 w/v% in 1 L of distilled water. The medium was mixed using mechanical stirring by dropping acetic acid to control pH 4.5. Ethanol –1 v% added after sterilization of the base for 15 min at 121ºC. 100 mL HS Medium was put in 250 mL of each flash and shook for 1 h at 300 rpm using Flash Shaker SF1. The medium solution was kept growing for 12 days in oven at 30ºC. BC membrane was taken out from the oven and heat at 60 – 70ºC in 1% of NaOH for 1 h and thoroughly washed in distilled water until neutral pH in order to remove bacteria and residues (Surma-Ślusarska, Presler, & Danielewicz, 2008). The BC membranes were soaked in distill water and kept at room temperature before use.

3.5 Functionalization of multi-walled carbon nanotubes (Paper II)

Multi-walled carbon nanotubes were submitted to surface modification prior use as shown in Figure 19. Firstly, 0.5 g of MWCNT were mixed with 100 mL of solution of 98% H_2SO_4 and 65% HNO_3 (3:1, v/v) by using ultrasonic bath at 80 ± 3°C for 4 h according to previous work (Hung et al. 2008; Wang et al. 2013). MWCNT suspension was kept cooling before centrifuging for 45 min at 10 000 rpm to remove the remaining solution of H_2SO_4/HNO_3. Later on, a solution of acetone/water (1:1, v/v) was added and centrifuged few times for 30 min and finally centrifuged one more time in distilled water. The precipitated MWCNT was

washed with 0.5 M HCl and distilled water subsequently. The filtered product was dried in a vacuum oven 100°C overnight.

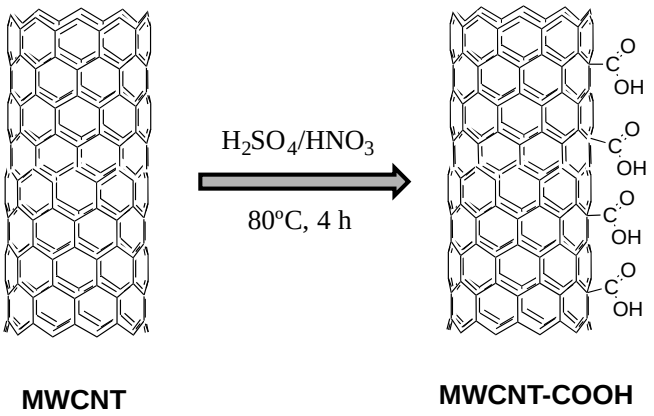

Figure 19 Functionalization of MWCNT.

3.6 Preparation of CNF and BC nanopapers, and conductive nanopapers

All nanopapers were formed using sheet dryer. The conductive nanopapers were produced by blending (CNF-MWCNT) and coating (CNF-PPy, CNF-PEDOT:PSS, CNF-MWCNT-PPy, and CNF-PEDOT:PSS-PPy).

3.6.1 CNF nanopapers (Paper I-III)

CNF gel was first diluted to 0.2% with distilled water and dispersed by using a sonicator Q700 for 10 min (5 min pulse on, 2 min pulse off, and 5 min pulse on) at 60% of amplitude. Afterwards, the CNF suspension was filtered overnight using a glass filter funnel with a nitrocellulose membrane GSWP29325 (hydrophilic) of 0.22 μm pore-size. After filtering, the nitrocellulose membrane was peeled off and the CNF cake was placed between two pieces of immobile transfer membranes of polyvinylidene fluoride (PVDF) (hydrophobic) of 0.45 μm pore-size to prevent adhesion between sample and membrane. Finally, the samples were dried using a laboratory sheet dryer at a vacuum pressure of -0.6 bar at 92 ± 3 °C for 20 min. This sheet dryer was used to dry for all nanopapers.

3.6.2 BC nanopapers (Paper IV)

Acetobacter xylinum Bacterial cellulose membrane with 7.5 cm of diameter was mechanical compressed for 10 min and dried for 25 min to form BC nanopaper.

3.6.3 CNF-PPy nanopapers (Paper I)

The preparation of CNF-PPy nanopapers the same filtering procedure was used. Firstly, a dilute suspension of CNF (0.1%, 400 mg of dry weight) was sonicated for 10 min under the same setting conditions described above. This CNF suspension will be later mixed with a solution of pyrrole. For the preparation of the pyrrole solution, 0.1 mL of pyrrole was dissolved in 15 mL of 0.5 M HCl. After stirring the mixture for 3 min using magnetic stirrer, one drop (0.05 ml) of Tween-80 was added and stirred until completely homogenous. Afterwards, the solution of pyrrole was introduced into the above CNF suspension, and the mixture was stirred for 5 min. In order to initiate the polymerization, 0.578 g of $FeCl_3$ in 15 mL of HCl 0.5 M was added drop wise into the suspension. The final mixture was stirred at room temperature for 20, 40, 60, 120, and 180 min, in independent experiments, to get the different conductive nanopapers named as CNF-PPy20, CNF-PPy40, CN-PPy60, CNF-PPy120, and CNF-PPy180, respectively. One conductive nanopaper was used 0.21 mL of pyrrole and 1.21 g of $FeCl_3$. At the end, the mixture (CNF and PPy) was filtered using a glass filter and washed subsequently with 500 mL of 0.5 M HCl, 500 mL of 0.1 M NaCl, and 500 mL of distilled water. During the last washing with distilled water, the suspension was sonicated for 2 min to remove any small gas bubbles and to allow a better organization of CNF-PPy nanostructures without undesired side effects, such as crystal structure damage (Ali et al., 2014). Thereafter, the filtration was continued for 3 more hours until there is no residual water. CNF-PPy nanopapers were formed after drying for 20 min.

3.6.4 CNF-MWCNT and CNF-MWCNT-PPy nanopapers (Paper II)

A combination of mixing/sonication method was used to produce binary CNF-MWCNT and ternary CNF-MWCNT-PPy nanopapers. First of all, the cellulose nanofibers suspension at 0.2 wt% was sonicated for 10 min. MWCNT were dispersed in distilled water (1mg/mL) using ultra-turrax (IKA, GmbH& Co. KG, Germany) for 3 min. Different amounts of MWCNT (10 to 50% with respect to CNF content) were added drop wise into the CNF suspension. The CNF-MWCNT mixture was sonicated for 2 min and stirred for 24 h at room temperature to obtain a homogenous distribution of MWCNT in the CNF network. Following similar process for making CNF nanopaper, CNF-MWCNT suspension was filtered overnight using glass filter and dried for 20 min by means of the sheet dryer.

For the preparation of ternary CNF-MWCNT-PPy nanopaper, the initial mixture of CNF and MWCNT was stirred for 24 h at room temperature. Besides, different amounts of pyrrole

monomer (0.1 to 0.5 ml) were mixed with HCl 0.5 M (1:150 v/v) and stirred for 3 min; one drop of Tween-80 was added into mixture and the magnetic stirring was kept until complete dissolution. Afterwards, the pyrrole-acid solution was added into the CNF-MWCNT suspension and stirred for another 5 min. In order to initiate the polymerization, iron (III) chloride ($FeCl_3$) in HCl 0.5 M was dropped wise into the mixture of CNF-MWCNT, with a molar proportion of 2.4 of $FeCl_3$/pyrrole. After 60 min of reaction time, the suspension was filtered and finally dried for 20 min.

3.6.5 CNF-PEDOT:PSS and CNF-PEDOT:PSS-PPy nanopapers (Paper III)

Two different types of PEDOT:PSS (PT2 and PH500) were used as conductive fillers in this work. PEDOT:PSS was first diluted to 0.5% with distilled water and stirred for 5 min using magnetic stirrer. PEDOT:PSS suspension was added into the above CNF suspension with different proportion of CNF-PEDOT:PSS (95/5, 90/10, 80/20, 70/30, 60/40, and 50/50), and the sample are labelled based on the amount of PEDOT:PSS in the nanocomposites; for instance, CNF-PT2_5, CNF-PT2_10, CNF-PT2_20, CNF-PT2_30, CNF-PT2_40, and CNF-PT2_50 for the nanocomposites with 5-50 wt% of PT2, respectively, and similarly for PH500. The mixture suspension was stirred for 24 h at room temperature and sonicated for 2 min. The mixture was filtered and dried for 20 min to obtain CNF-PEDOT:PSS nanopapers.

-PPy nanopapers were obtained via in situ chemical polymerization of polypyrrole. The mixture of pyrrole with 0.5 M HCl (1:150, v/v) together with one drop of Tween-80 were stirred for 5 min and added into CNF-PH500 suspension for another 5 min. The solution of iron (III) chloride ($FeCl_3$) with the proportion of 2.4 of $FeCl_3$/pyrrole and 0.5 M HCl was dropped wise to initial polymerization of pyrrole on the mixture of CNF-PH500. The reaction was allowed for 60 min, and the suspension was filtered and dried for 20 min.

3.6.6 BC-PPy nanopapers (Paper IV)

In situ oxidative polymerization of pyrrole was used to fabricate the BC-PPy nanopaper. BC membrane was pressed using mechanical pressing for 10 min to remove absorbed water, was immersed in the pyrrole solution with 0.5 M HCl for 5 min in order to plant the monomer of pyrrole on its surface. The mixture of $FeCl_3$ with 0.5 M HCl was added by drop-wise into BC/PPy suspension to initial the polymerization of polypyrrole. Different monomer contents

(0.1, 0.3, 0.5 and 0.7 mL) were used in this experiment, and the molar ratios of Pyrrole/0.5 M HCl, $FeCl_3$/Pyrrole and $FeCl_3$/0.5 M HCl were 0.4, 2.4 and 1, respectively. The reaction was 20, 40, and 60 min for 0.1 mL of pyrrole at 4ºC were coded as BC-PPy_1, BC-PPy_2, and BC-PPy_3, and was 60 min for 0.3, 0.5, and 0.7 mL, which were coded as BC-PPy_4, BC-PPy_5, and BC-PPy_6. The membrane turned from white to grey and finally to black within a few minute. After finishing the reaction, BC-PPy membrane was washed thoroughly with distilled water to extract the byproducts and remain reagents of the reaction. Afterwards, the mechanical pressing was applied for 5 min to remove excess water. BC-PPy nanopaper was finally obtained by drying for approximately 25 min.

3.7 Characterization of CNF, BC, and conductive nanopapers

3.7.1 Elemental analysis (Paper I-V)

Carbon, hydrogen, and nitrogen element analysis was characterized by Perkin Elmer EA2400 serie II equipment. The samples were subjected to pyrolysis in helium (He) at combustion temperature of 925–930 °C. Acetanilide powder (C_8H_9NO) was used as reference, which contents carbon (71.09%), hydrogen (6.71%), and nitrogen (10.36%). The content of carbon, hydrogen, and nitrogen were recorded for 6 min, and the PPy contents in nanopapers were calculated based on the percentage of nitrogen (N%).

3.7.2 Density and porosity of nanopaper (Paper I-III)

The density of nanopapers was calculated from the basis weight, thickness, and dimension of 1×3 cm strips. Porosity was determined from the density of the sample, of cellulose nanofibers, PH500, and from the density of polypyrrole as shown in Equation 1.

$$Porosity\ (\%) = 100 \times [1 - \frac{\rho_{sample}}{\left(w_{cell}\rho_{cell} + w_{filler}\rho_{filler}\right)}] \quad (1)$$

Where ρ_{sample} is the density of the nanopaper, ρ_{cell} the density of nanocellulose (1.5 g cm^{-3}) (Marielle Henriksson, Fogelström, Berglund, Johansson, & Hult, 2011), and the following are the density of three different fillers: ρ_{PPy} = 1.48 g cm^{-3} (Saville, 2005), ρ_{MWCNT} = 2.1 g cm^{-3} (Salajkova et al., 2013), and ρ_{PH500} = 1 g cm^{-3}, according to the

supplier. The weight fractions of nanocellulose, PPy, MWCNT, and PH500 are represented by w_{cell}, w_{PPy}, w_{MWCNT}, and w_{PH500}, respectively.

The percentages of carbon, hydrogen, and nitrogen were determined by elemental analysis by means of a Perkin Elmer EA2400 series II. The measured amount of nitrogen was used to determine the PPy content in the formulation. The samples (3 mg) were pyrolyzed in helium (He) at a combustion temperature of 925–930°C. Acetanilide powder (C_8H_9NO) was used as reference.

3.7.3 Fourier transform infrared (FTIR) (Paper I-IV)

The chemical compositions of nanopapers were characterized by Fourier transform infrared spectroscopy (FT-IR) from Bruker with a PLATINUM attenuated total reflectance mode (ART) under transmittance mode in range between 4000 cm^{-1} and 500 cm^{-1} using 24 scans at a resolution of 4 cm^{-1}.

3.7.4 Tensile properties (Paper I-IV)

Mechanical properties of nanopapers were evaluated using tensile test under control conditions of 50% relative humidity at room temperature. The rectangle specimens of nanopaper (50×5) mm with various thickness were tested using a Universal Testing Machine HOUNSFIELD, equipped with a 250 N load cell with a cross-head speed of 5 mm/min. These parameters were set according to previous work (Hamedi et al., 2014). The statistical error for each sample type was taken from at least five different specimens according to ISO 527 standard.

3.7.5 Field emission scanning electron microscopy (FE-SEM) (Paper I-IV)

The cross section surfaces of nanopapers, as well as the PPy platelet, were observed under a field emission scanning electron microscope (FE-SEM) HITACHI S-4100. The samples from tensile test were coated with gold using a sputter. The images were taken using secondary electron detector at different voltages.

3.7.6 Transmission electron microscopy (TEM) (Paper III)

Transmission electron microscopy (TEM) images of CNF, CNF-PH500_50, and CNF-PH500-PPy were recorded using a ZEISS EM-910 JEOL-2100F (1993) and an internal

charge-coupled device (CCD) camera gatan orius SC200W1. The samples were diluted to 1:50 in distilled water, and only 8 μL of each sample was drop in a cupper 400 mesh grid with formvar film for 3 min minutes. 8 μL of contrast solution uranyl acetate 1% was dropped on the solution above and kept for 3 min before testing.

3.7.7 Thermogravimetric analysis (TGA) (Paper I, III, and IV)

Thermogravimetric analysis (TGA) was used to determine the lost weight with the temperature and the degradation temperatures of nanopapers. The samples were heated from 30 to 600°C at the heating rate of 10°C min^{-1} using a METTLER TOLEDO ultra-micro balance, TGA/DSC. The purge gas was nitrogen with a flowing rate of 40 mL/min.

3.7.8 Electrical conductivity measurement (Paper I-IV)

The electrical conductivity of the obtained nanopapers was determined based on the measurement of the resistance (R) over the length of the specimens using an Agilent 34461A digital multimeter. The sample were cut were cut into (5×20) mm rectangular shape. Silver paint was applied at room temperature at the end of both sides of each sample to ensure good electrical contact with the clip probes. The measurement was done 16 h after the application of silver paint. Equation 2 calculated the conductivity:

$$\sigma' = \left(\frac{L}{R \times w \times d}\right) \qquad (2)$$

Where *L*, *w*, and *d* are length, width, and thickness of the sample, respectively.

In the cases of CNF-MWCNT and CNF-PEDOT:PSS, the prediction of percolation threshold was determined to describe the insulator-to-conductor transitions in composites made of conductive filler and an insulating matrix. Above the percolation threshold, the conductivity occurs, whereas below this concentration the composites are very resistant to electrical flow. According to Equation 3, the conductive fillers networks that follow classical geometrical percolation theory (where filler bonding occurs) obey a universal conductivity-loading relationship above the percolation threshold was carried out (Hermant, 2009; Koga et al., 2014).

$$\sigma = \sigma_0(\phi - \phi_c)^t \quad (3)$$

*W*here σ is the theoretical conductivity, σ_0 the ultimate conductivity, ϕ the volume fraction of the conductive filler, and ϕ_c is the percolation threshold. To determine the percolation threshold (ϕ_c) experimental results are fitted by plotting log σ versus log ($\phi - \phi_c$), and the value of ϕ_c was incrementally varied until the best linear fit is obtained.

3.7.9 Cyclic voltammetry measurement (Paper I-IV)

Cyclic voltammetry (CV) was carried out with a standard three-electrode electrochemical cell (working electrode), a platinum wire (counter electrode), and a 2 M NaCl-saturated Ag/AgCl electrode (reference electrode) by using a Potentistat/Galvanostat Model 273A Princeton equipment. Cyclic voltammograms were recorded in the potential window of −0.9 to +0.9 V vs Ag/AgCl at different scan rate of 5, 20, 50, 100, and 200 mV s^{-1}. CView and originPro software were used to plot the graphs. The sample dimensions were (7×15) mm. Equation 4 calculates the specific capacitance.

$$C_{sp} = i/m.v.\Delta V \quad (4)$$

Where C_{sp} (F g^{-1}) is the specific capacitance, i the integration in the CV curve, v the scan rate in V s^{-1}, m the mass (g) of the electrode material, and ΔV = 1.8 V is the potential window.

4. RESULTS AND DISCUSSION

The present work is based on the production and characterization of conductive cellulose nanopapers, or nanocomposites, with different conductive fillers. In this chapter, all the obtained results are merged and discussed, focusing on their mechanical, thermal, electrical, and electrochemical properties. FTIR and FE-SEM characterization are also presented to understand the chemical interaction between CNFs matrix and conductive fillers and their morphology. Scientific papers and manuscripts are included in the annex.

4.1 Nanopapers and conductive nanopapers

Pictures of CNF gel and the six different kinds of nanopapers prepared from cellulose nanofibers (CNF) and conductive fillers are shown in Figure 20. CNF nanopaper was flexible and had high transparency. The conductive nanopapers (CNF-PPy, CNF-MWCNT-CNF-MWCNT-PPy, CNF-PH500, and CNF-PH500-PPy) became completely black due to the presence of the black precipitated PPy, black carbon nanotube, and/or dark blue PH500 coated or dispersed on CNF surface. However, they were still very flexible.

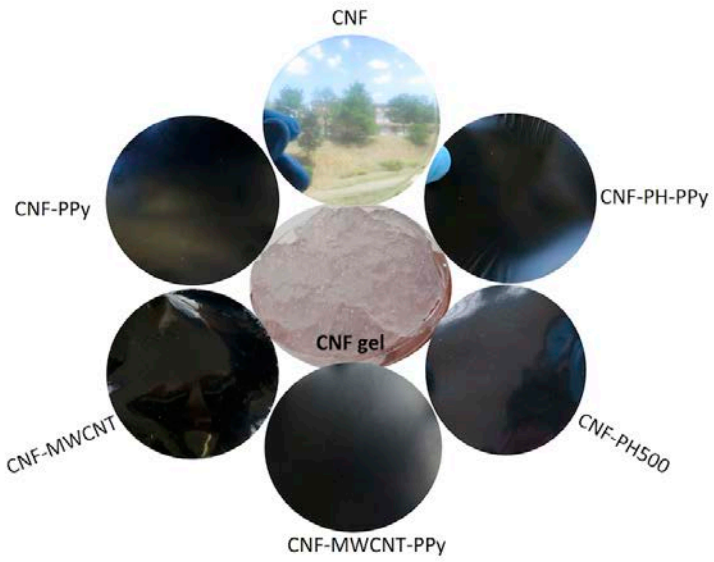

Figure 20 CNF gel, CNF nanopaper, and the conductive nanopapers based on CNF.

The BC membrane prepared in this work was also flexible but had less transparency compared to CNF nanopaper. The coating of PPy layer on the BC surface turned the membrane to black color (see Figure 21).

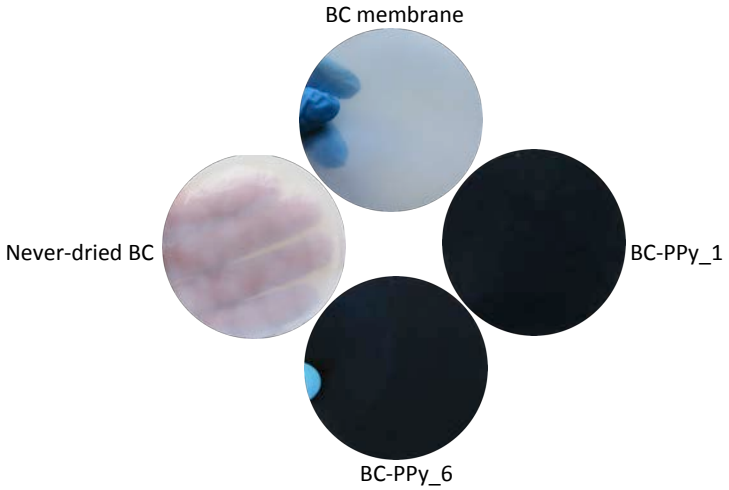

Figure 21 Never-dried BC, BC membrane and conductive membrane based on BC-PPy.

A graphical description of the interactions between components for the conductive nanopapers prepared in this work is presented in Figures 22 and 23. The chemical representation of nanocellulose chains (CNF or BC), with the hydrogen bonding with water, and the intermolecular interactions between nanocellulose chains and PPy after the in situ chemical polymerization using $FeCl_3$ is illustrated in Figure 22a, the interactions between MWCNT or MWCNT-PPy with CNF chains is outlined in Figure 22b.

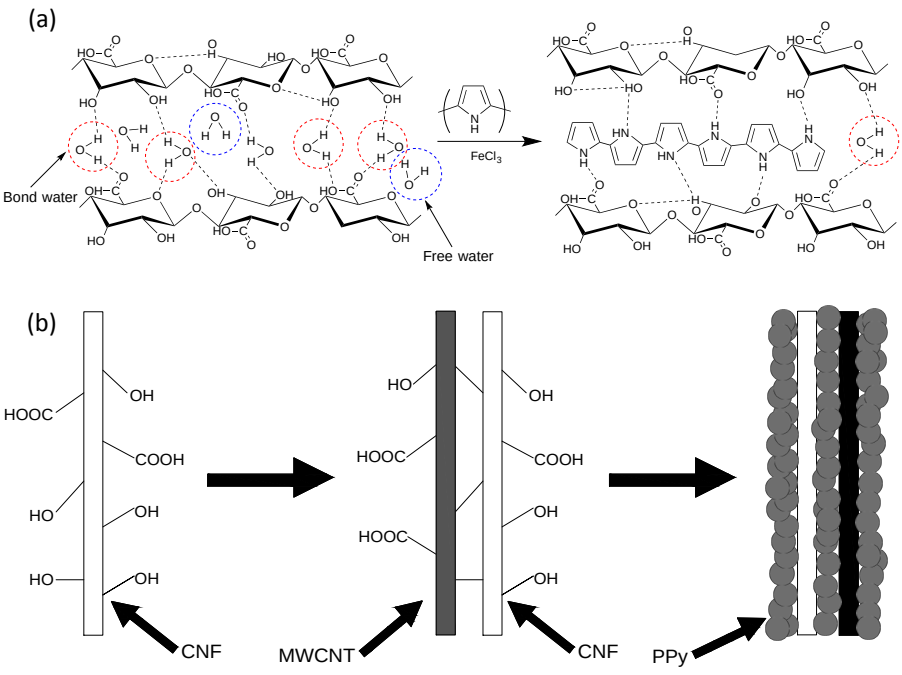

Figure 22 (a) Respresentation of the polymerization reaction of pyrrole on CNF surface; and (b) Illustration of the interaction of CNF with MWCNT and the with hybrid MWCNT/PPy.

For the nanopapers containing PEDOT:PSS or the hybrid PDETOD:PSS-PPy, the coating process is illustrated in Figure 23.

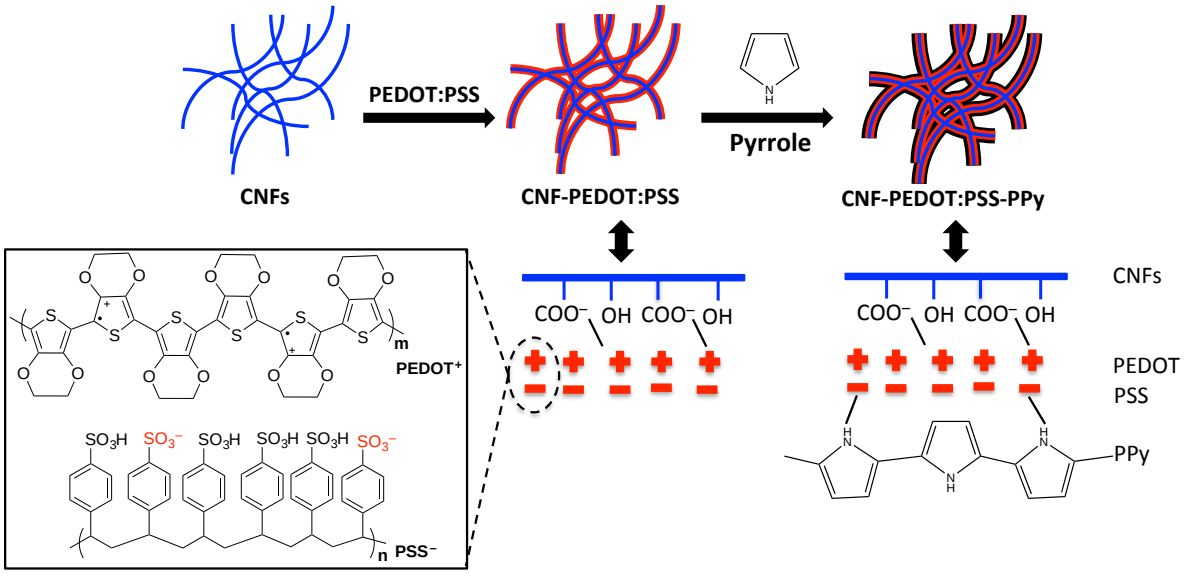

Figure 23 Scheme of CNF nanofibrils, deposition of PEDOT:PSS polymer and coating of PPy on their surface.

4.2 FTIR

The chemical composition of the different cellulose nanopapers, as well as the interactions between the functional groups, has been studied by FTIR spectroscopy. FTIR spectra of nanopapers from the combination of cellulose nanofibers (CNF), polypyrrole (PPy) and multi-walled carbon nanotubes (MWCNT) are presented in Figure 24. Figure 24a show the spectrum of pyrrole. The broad absorption band at 3393 cm^{-1} is indicative of the stretching vibration of the secondary N–H bond in the pyrrole ring, and the peak at 3105 cm^{-1} represents the stretching of the aromatic C–H bonds (Monte et al., 2014). The stretching vibration of the C=C in the aromatic ring appears at 1529 cm^{-1}, whereas at 1417 cm^{-1} the stretching (in-ring) for the single C–C links is found. The peak at 1139 cm^{-1} is assigned to the C–N bond, although it is not very intense. The absorption band at 1047 cm^{-1} is associated to the =C–H bending deformation, and the strong peak at 721 cm^{-1} corresponds to the out-of-plane bending of the three substituted C–H bonds (Lee & Boo, 1996). In the FT-IR spectrum of CNF (Figure 24b) the broadband vibration of –OH groups are found in 3334 cm^{-1}; and the stretching for

aliphatic C-H bonds of cellulose in 2898 cm^{-1}. A prominent sharp peak at 1602 cm^{-1} is attributed to the stretching of carbonyl group of TEMPO oxidized cellulose nanofibers (Soni et al., 2015). The symmetric bending of CH_2 and C–O groups of the pyranose ring of CNF are found respectively at 1416 cm^{-1} and 1314 cm^{-1} (Kargarzadeh et al., 2012). In the range of 1203 cm^{-1} and 1157 cm^{-1} the symmetric and asymmetric stretching of ether bonds (C–O–C) are assigned. Also the absorption peak at 1024 cm^{-1} corresponds to the C–O ether groups. The broad band centered at 605 cm^{-1} is assigned to the C–H bending deformation.

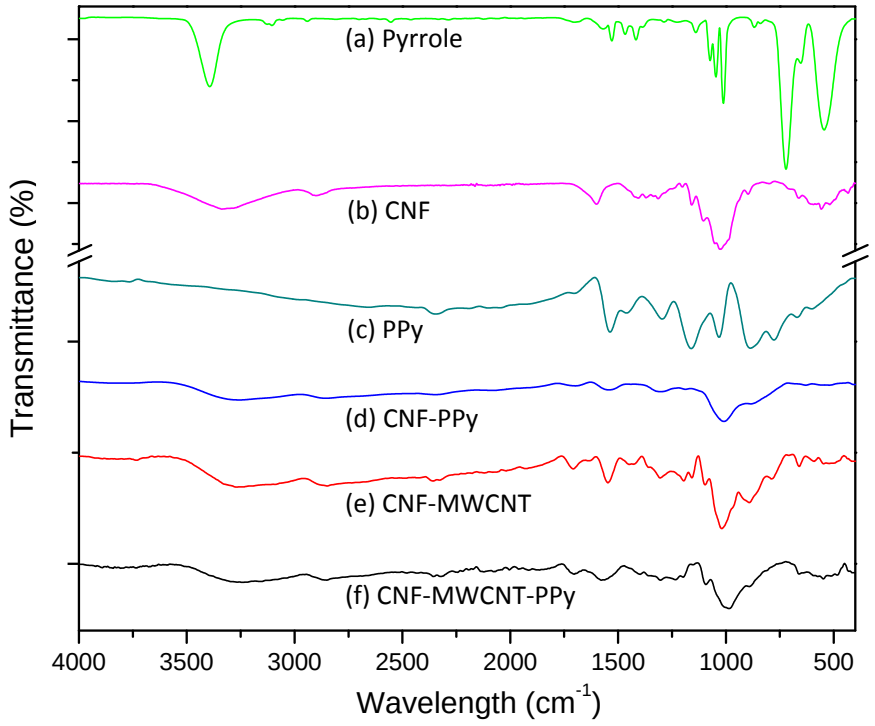

Figure 24 FTIR spectra of (a) pyrrole, (b) CNF, (c) PPy, and three different kind of conductive nanopapers; (d) CNF-PPy, (e) CNF-MWCNT, and (f) CNF-MWCNT-PPy.

Figure 24c corresponds to the FTIR spectrum of PPy. The absorption bands at 1534 cm^{-1} corresponds to the C=C stretching of the aromatic ring. The peak at 1449 cm^{-1} represents the stretching vibration of C–C and C–N links. The absorption peak at 1288 cm^{-1} is assigned to a mixed bending and stretching vibration associated to the C–N bond of the aromatic amine. At this wavelength, single C–C bonds between rings also appear; however its intensity is much lower compared to the C–N bond that has greater dipole (Saville, 2005). The C–H in-plane and out-of-plane bending deformation of PPy appears at 1160 cm^{-1} and 1036 cm^{-1},

respectively. Also centered at 1160 cm^{-1}, the stretching for the C=N link is found. Finally, the peak at 853 cm^{-1} is related to the N–H wagging of secondary amines.

CNF-PPy nanopaper (Figure 24d) has similar spectrum as polypyrrole but with all the major peaks shifted to lower wave number, which supports the existing interaction between –N–H of PPy and C–OH of CNF by means of hydrogen bonding (Firoz Babu et al., 2012). The band at 1707 cm^{-1} is assigned to the C=O bond of carboxylic acid group of CNF in the CNF-PPy nanopaper. Comparing this wavelength with the carboxyl group one of CNF (Figure 24b), the absorption peak has shifted towards higher values, which is representative of the interaction between CNF and the coating PPy. The strong band at 1546 cm^{-1} is characteristic of the C=C stretching of the aromatic ring of PPy. The absorption peaks at 1306 cm^{-1}, 1017 cm^{-1}, and 888 cm^{-1} are belong to PPy peaks, which are assigned to the C–N stretching, C–H stretching and N–H wagging.

The spectrum in Figure 24e corresponds to CNF nanopaper containing 50% of MWCNT. This spectrum has to be compared with the FTIR of modified MWCNT of Figure 25. The absorption peaks at 1706 cm^{-1} 1421 cm^{-1}, and 1017 cm^{-1}, are assigned to C=O, O–H, and C–O of carboxylic acid of MWCNT. Moreover, the change in intensity of the peak at 3250 cm^{-1} may be due to the formation of intermolecular hydrogen bonds between modified nanotubes and cellulose nanofibrils. The solubility of modified-nanotubes with nanocellulose can be due to the disruption of intramolecular hydrogen bonds in the cellulose (3340 cm^{-1}, Figure 24b) by the creation of hydroxyl groups between CNF and the modified carbon nanotubes (band of 3500 cm^{-1} in Figure 25) (Adsul et al., 2011).

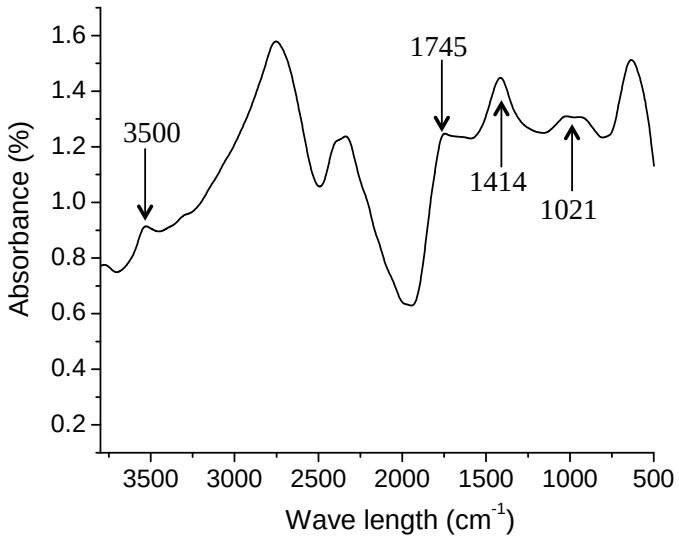

Figure 25 FTIR absorbance peaks of modified MWCNT.

The spectrum of CNF-MWCNT-PPy (Figure 24f) contains the same peaks corresponding to CNF-MWCNT, together with the peaks at 1526 cm^{-1}, 1285 cm^{-1}, 1149 cm^{-1}, 970 cm^{-1}, and 760 cm^{-1}, identified above as functional groups of PPy, confirming the presence of PPy in the sample.

FTIR results of nanopapers based on cellulose nanofibers (CNF), poly(3,4-ethylenedioxythiophene) : polystyrene sulfonate (PEDOT:PSS), and membranes from bacterial cellulose (BC) and polypyrrole (PPy) are shown in Figure 26. The spectrum of PH500 is shown in Figure 26a. In the region of 1584–1514 cm^{-1} the quinoid structure and the stretching modes of aromatic C=C (PEDOT) are found (Wang et al., 2016; Khan, Ul-Islam, Khattak, Ullah, & Park, 2015), C–C bonds at 1352 cm^{-1} and at 822 and 670 cm^{-1} the vibrations of the C–S bond of the thiophene ring. The peak at 3000 cm^{-1} is assigned to PSS chain corresponding to the stretching vibration of aromatic C–H bonds, the absorption peaks at 1158–1110 cm^{-1} are related to the asymmetric and symmetric vibrations of S–O in sulfonate groups (SO_3H and $–SO_3^-$) of PSS (Jiang et al., 2014; Zhu et al., 2015) and the peak at 1046 cm^{-1} for the S–C phenyl bonds in sulfonic acid (Khan et al., 2015). The spectrum of CNF-PH500 nanopaper (Figure 26b) has all the absorption bands of CNF and PEDOT:PSS, although some peaks of both structures are overlapping. The main bonds of thiophene backbone (C=C, C–C, and C–S) are found in the spectrum, and their intensity are higher with higher content of PEDOT:PSS in the nanopaper. Moreover, the peak of hydroxyl is broadened, indicating an increase in hydrogen-bonding interactions between the hydroxyl functionalized CNF and the electronically charged PEDOT:PSS. This indicates that PEDOT was successfully coated on the nanocellulose fibers. Figure 26c confirms that all the characteristic peaks of CNF, PH500, and polypyrrole are reflected in the spectrum of the CNF-PH500-PPy, with the shifting and changes resulting from the interactions between components (CNF-PH500, PH500-PPy): such as the increasing intensity of the band at 1530 cm^{-1} due to the presence of C=C aromatic ring of PPy and PEDOT, the overtone band at 1293 cm^{-1} combined from the absorption peak at 1288 cm^{-1} associated to the C–N bond of the aromatic amine (Lay, Méndez, Delgado-Aguilar, Bun, & Vilaseca, 2016) and the band at 1352 cm^{-1} for C-C of the thiophene ring.

Figure 26d and e show the spectra of BC and BC-PPy nanopapers. The peaks of OH stretching vibration and C–H asymmetrically stretching vibration of BC were found in the region of 3342 and 2897 cm^{-1}, respectively, as confirmed in previous work (Xu et al., 2013). The band at 1645 cm^{-1} represents O–H bending of absorbed water, and the band at 1542 cm^{-1}

associates with C=C in the aromatic ring. The peaks at 1319 cm^{-1}, 1105 cm^{-1}, and 1030 cm^{-1} indicate C–O of pyranose ring skeletal vibration, C–O–C anti-symmetric bridges stretching, and C–O of ether groups, respectively (Khan et al., 2015). The spectra of BC-PPy nanopapers have changed in the fingerprint region (1500 – 400 cm^{-1}), which belong to the characteristic tail of the electronic absorption related to electrical conductivity of PPy. The peaks shifted to higher wavelength values with an increase of PPy content (55 w%) for BC-PPy_6, for example, the peaks at 1444 cm^{-1}, 1283 cm^{-1}, 1034 cm^{-1}, 828 cm^{-1}, and 748 cm^{-1} correspond to C–C, C–N stretching aromatic amine, =C–H bending, N–H wagging, and C–H out of plane of polypyrrole ring, respectively. The blue-shift of these bands confirm that the presence of cellulose affected the delocalized π–electronics of PPy because the interactions chemical bonding between the H of the N in the pyrrole ring and the lone pairs of electrons on the O of the surface OH groups of the cellulose, and/or between the H of the OH groups of the cellulose and the lone pair of electrons on the pyrrole N were occurred (Johnston, Kelly, Moraes, Borrmann, & Flynn, 2006).

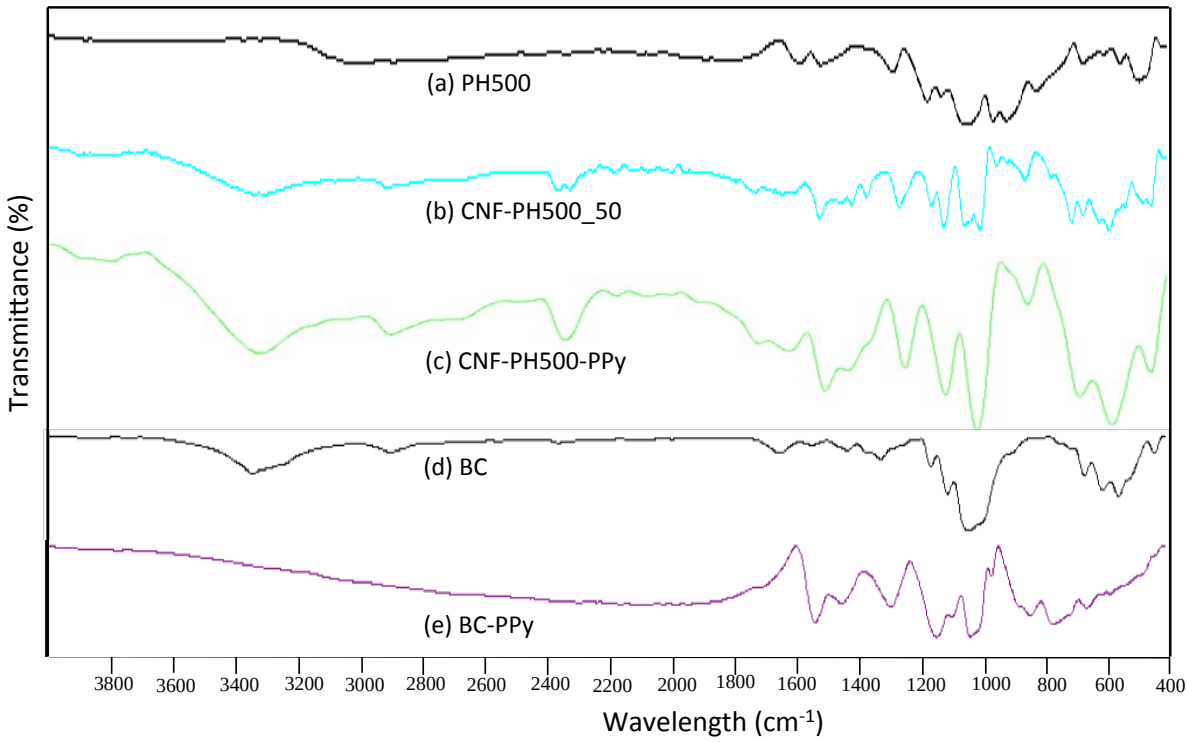

Figure 26 FTIR spectra of (a) PH500, (b) CNF-PH500_50, (c) CNF-PH500-PPy, (d) BC, and (e) BC-PPy nanopapers.

4.3 Tensile properties

Tensile properties of all samples were characterized by applying tension force. CNF nanopaper and BC membrane were used as control samples. The stress-strain curves of CNF and CNF-PPy nanopapers are presented in Figure 27. In the stress strain curve of CNF nanopaper, a linear elastic behavior corresponding to Young's modulus was found at a low strain (<0.7%). At a stress in the region of 100–130 MPa there is a knee in the stress-strain curve, followed by a linear and strong strain-hardening plastic region (Sehaqui, Allais, Zhou, & Berglund, 2011).

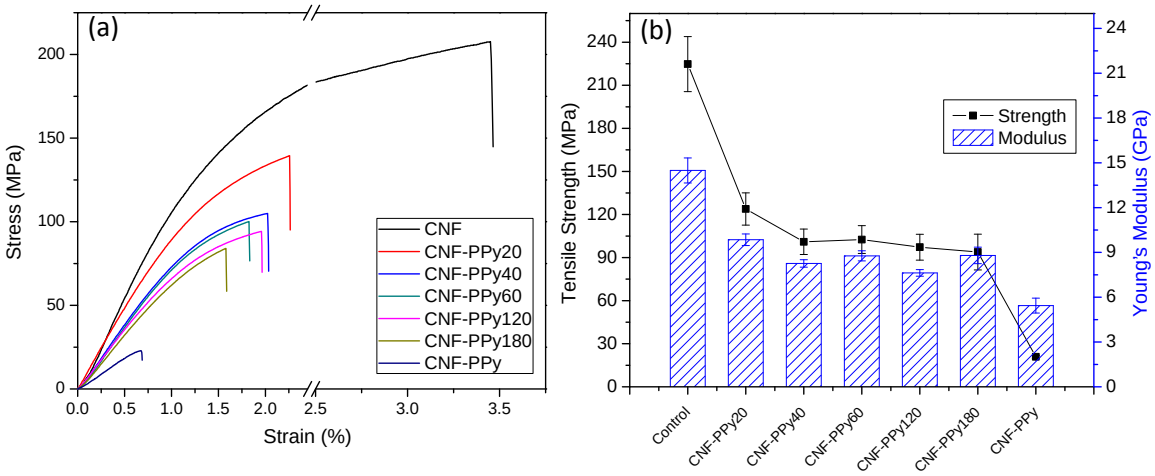

Figure 27 (a) Stress-strain curves and (b) Tensile and Young's modulus of CNF and CNF-PPy nanopapers.

CNF nanopaper exhibited outstanding tensile strength of 224 MPa and Young's modulus of 14.5 GPa (values in Table 9). The high mechanical properties are related to the strong interactions between nanofibrils and to the nanofibril entanglements (Boufi, Kaddami, & Dufresne, 2014); moreover, some nanofibrils alignment is also expected during the filtration procedure. The sonication step introduced in our methodology helped to remove the possible voids between nanofibrils and provided a homogeneous structure resulting in a low porosity of the final nanopaper (Table 9). Moreover, CNFs from TEMPO mediated oxidation show high nanofibrillation degree and unchanged original crystallinity (Isogai et al., 2011), which is responsible of the high mechanical properties of the obtained CNF nanopaper. However, the tensile strength and Young's modulus of CNF-PPy20 (with 8wt% of PPy) decreased to 124 MPa and 8.9 GPa, respectively, and continued to decrease until 20.94 MPa and 5.44 GPa,

respectively, for the CNF-PPy nanopaper, which contained 55wt% of PPy. Therefore, the incorporation of PPy in the structure produced a reduction in the mechanical properties and was more brittle than the unmodified CNF. The elongation at break also decreased with the incorporation of PPy, from 3.5% for CNF to 1.55% for CNF-PPy180 and to 0.6% for CNF-PPy nanopaper. It is expected that the PPy coating on CNF surface lessened the number of CNF inter-fibril OH interactions, as the NH group of pyrrole interacted with the hydroxyl groups of cellulose nanofibrils. The porosity is also the reason of decreasing their tensile behavior. As shown in Table 9, the coating of PPy on CNF increased the porosity from 10.45% (CNF) to 26.19% (CNF-PPy). Higher porosity caused the premature breaking of CNF-PPy nanopapers, showing a reduction in their final tensile strength. In addition, the PPy-coated CNF had fewer CNF interfibrils connections that were responsible of the diminution in the rigidity of the PPy-modified CNF nanopapers.

Table 9 Composition, thickness, density, porosity, and tensile properties of CNF and CNF-PPy nanopapers.

Sample	CNF (%)	PPy (%)	Thickness (µm)	Density (g/cm^{-3})	Porosity (%)	Strength (MPa)	Modulus (GPa)
CNF	100	0	55(3)	1.343(0.03)	10.45(0.41)	224(19)	14.5(0.8)
CNF-PPy20	92	8	70(4)	1.323(0.03)	11.74(0.99)	124(11)	9.8(0.4)
CNF-PPy40	84	16	79(3)	1.300(0.04)	13.17(1.05)	101(9)	8.2(0.3)
CNF-PPy60	82	18	84(2)	1.276(0.01)	14.74(0.55)	102(8)	8.7(0.3)
CNF-PPy120	81	19	91(3)	1.229(0.05)	17.89(1.07)	97(9)	7.7(0.2)
CNF-PPy180	80	20	94(3)	1.205(0.02)	19.45(0.83)	94(12)	8.8(0.5)
CNF-PPy	45	55	105(4)	1.092(0.01)	26.19(0.58)	20.94(1)	5.44(0.5)

The stress–strain curves in uniaxial tension, and the ultimate tensile strength and Young's modulus of CNF-MWCNT and CNF-MWCNT-PPy are shown in Figure 28. The mechanical strength diminished with the addition of MWCNT in the nanocomposites. Tensile strength and Young's modulus of CNF-MWCNT10 decreased about 30% and 38%, respectively, and the tensile strength continued to decrease 130% for the CNF-MWCNT30 nanocomposite. Instead, the Young's modulus was maintained with the incorporation of more modified MWCNT.

The increase in porosity and the lower interaction between CNF and MWCNT affected the mechanical properties of nanopapers (Salajkova et al., 2013). The negative charges of

carboxylic acid groups in TEMPO CNF and from modified MWCNT are responsible for the electrostatic repulsion between them, increasing the porosity of the nanopapers (see Table 10). The acid treatment on carbon nanotubes provoked defects and breakages that diminished their intrinsic mechanical properties. Claiming a successful preparation, controlling the microstructure of such nanocomposites system still remains a challenge due to the strong interaction forces that cause the formations of bundles and clusters, as well as the dispersion and arrangement of MWCNTs in the matrix (Yan Huang & M. Terentjev, 2012). With the addition of higher amounts of MWCNT (40–50%), however, the tensile strength started to increase 32% compared to CNF-MWCNT30. This could be a result of sufficient nanofiller-nanofiller interaction for favorable stress-transfer, which may lead to a strong matrix-nanofiller interface. It is important to notice that nanopapers maintain very good mechanical properties even at 50% of MWCNT.

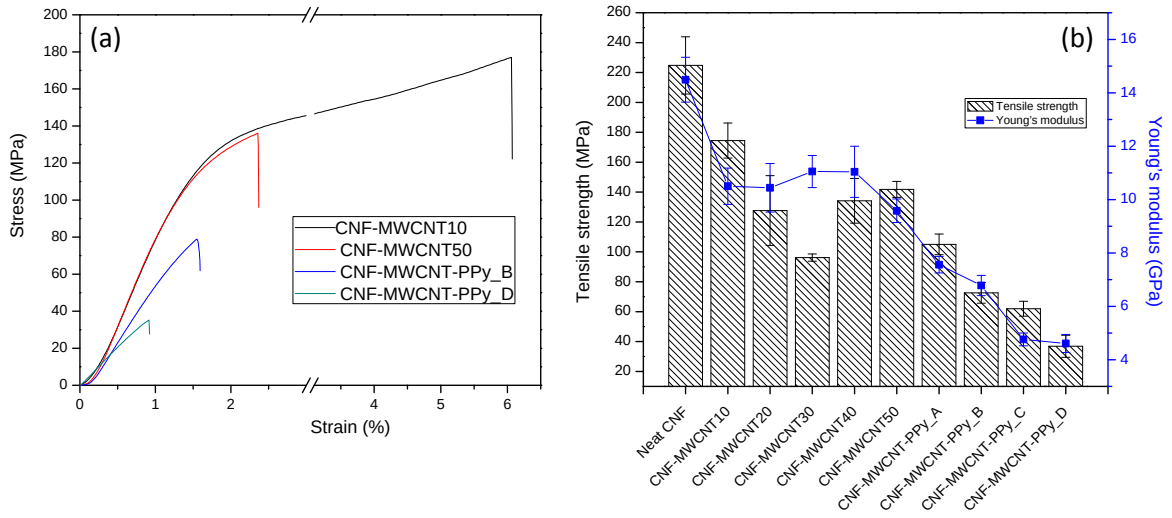

Figure 28 (a) Stress-strain curves of CNF-MWCNT and CNF-MWCNT-PPy nanopapers and (b) their tensile strength and Young's modulus.

With the polymerization of polypyrrole in CNF-MWCNT mixture, the mechanical behavior started to decrease dramatically. The weak mechanical properties is the drawback for the combination of MWCNT and conducting polymers (Baughman, Zakhidov, & de Heer, 2002). The result reveals that tensile strength decreased 4.8 times and Young's modulus decreased 2.3 times, with respect to the CNF-MWCNT10 nanopaper (Figure 28b). Moreover, they became more fragile than CNF-MWCNT nanopapers, confirmed by the diminishing of the elongation at break (Figure 28a). The addition of PPy augmented the porosity of nanopapers, which reduced the capillarity effects during drying process. Cellulose nanofibrils interact less during drying due to the presence of MWCNT and PPy, and the porosity becomes higher. It must be emphasized that the material kept its flexibility and foldability with the addition of

either 50% of MWCNT or 48% of PPy. The current mechanical properties for CNF-MWCNT are higher than those obtained in previous study by Salajkova et al. (2013), probably because of the experimental methodology that resulted in less porosity in the final nanopapers.

Table 10 Composition, density, porosity, tensile strength, and Young's modulus of CNF-MWCNT and CNF-MWCNT-PPy nanopapers.

Samples	CNF (%)	MWCNT (%)	PPy (%)	Density (g cm^{-3})	Porosity (%)	Tensile strength (MPa)	Young's modulus (GPa)
CNF-MWCNT10	90	10	-	1.305(0.048)	16.35(1.06)	174(11)	10.49(0.68)
CNF-MWCNT20	80	20	-	1.328(0.059)	18.04(1.62)	127(23)	10.44(0.91)
CNF-MWCNT30	70	30	-	1.359(0.047)	19.09(2.06)	96(02)	11.05(0.60)
CNF-MWCNT40	60	40	-	1.375(0.025)	20.99(1.06)	134(14)	11.04(0.96)
CNF-MWCNT50	50	50	-	1.436(0.042)	20.21(1.23)	141(05)	9.57(0.43)
CNF-MWCNT-PPy_A	70	10	20	1.253(0.056)	19.0891.02)	105(07)	7.55(0.30)
CNF-MWCNT-PPy_B	60	9	31	1.181(0.094)	23.07(1.32)	72(06)	6.78(0.37)
CNF-MWCNT-PPy_C	52	8	40	1.117(0.045)	26.72(1.56)	58(05)	4.61(0.24)
CNF-MWCNT-PPy_D	45	7	48	1.062(0.075)	29.81(1.97)	36(7)	4.60(0.34)

The tensile properties of CNF with PEDOT:PSS and CNF with hybrid PEDOT:PSS/PPy nanopapers are presented in Figure 29a and b (next page), and their values are summarized in Table 11. The incorporation of polythiophene derivate (PT2 or PH500) to CNFs altered the nanofibrils' connections with the presence of cationic groups in the PEDOT side. The cationic PEDOT interacted with the carboxylic group (COO^-) of CNFs, and the positive and negative charges of PEDOT:PSS were interposed between cellulose nanofibrils, thus reducing the number of intermolecular and intramolecular of hydrogen bonding in CNF (Khan et al., 2015). As a result, the mechanical properties of CNF-PT2 and CNF-PH500 nanopapers were lower compared with the unmodified CNF nanopaper. The tensile strength and Young's modulus for CNF-PH500_5 formulation was still considerable high, 194 MPa and 14.25 GPa, respectively, but had a substantial decrease for the formulation with 50wt% of PH500 (CNF-PH500_50) (Table 11). The elongation at break decreased from 5.7% to 2.5% between these two formulations. This reduction can be explained as the coating of PH500 on CNF surface lessened the number of interactions between cellulose nanofibrils, declining the number of nanofibrils' intermolecular attractions. If we compare the two kind of PEDOT:PSS used, the mechanical strength of CNF-PH500 nanopapers were superior than those of CNF-PT2

nanopapers. The different average particle size (30 nm for PH500 and 90 nm for PT2) can be the main reason for this behavior. The thinner particles of PH500, with higher surface area, formed a more homogeneous coating around the entangled cellulose nanofibrils resulting in stronger CNF-PH500 nanopaper.

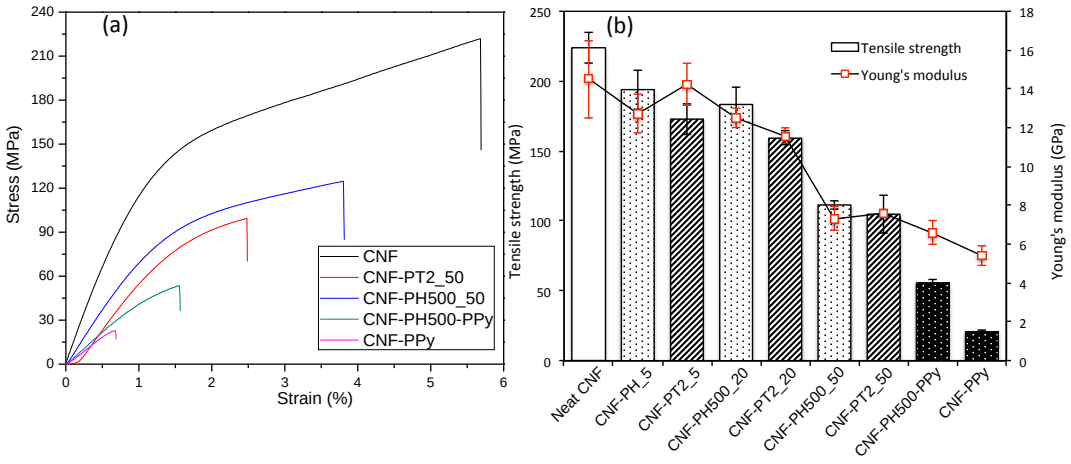

Figure 29 (a) Stress-strain curves and (b) tensile strength and Young's modulus of CNF-PT2_50, CNF-PH500_50, and CNF-PH500-PPy nanopapers.

Table 11 Composition, density, porosity, and tensile properties of CNF-PT2, CNF-PH500, and CNF-PH500-PPy nanopapers.

Sample	CNF (%)	*PT2 or PH500 (%)	PPy (%)	Density (g cm^{-1})	Porosity (%)	Tensile Strength (MPa)	Young's Modulus (GPa)
CNF-PT2_5	95	*5	-	1.322(0.027)	10.39(0.98)	172.91(14)	12.74(1)
CNF-PT2_10	90	*10	-	1.294(0.013)	10.73(0.88)	163.02(8)	11.92(0.4)
CNF-PT2_20	80	*20	-	1.242(0.013)	11.28(0.90)	159.26(12)	12.51(0.5)
CNF-PT2_30	70	*30	-	1.186(0.012)	12.13(0.92)	145.14(14)	10.48(0.2)
CNF-PT2_40	60	*40	-	1.141(0.013)	12.27(1.03)	113.98(13)	10.16(0.3)
CNF-PT2_50	50	*50	-	1.091(0.010)	12.73(0.80)	104.93(3)	7.33(0.6)
CNF-PH500_5	95	5	-	1.321(0.006)	10.46(0.39)	194.00(11)	14.25(1.1)
CNF-PH500_10	90	10	-	1.292(0.011)	10.90(0.76)	190.95(6)	11.30(0.4)
CNF-PH500_20	80	20	-	1.240(0.007)	11.46(0.80)	183.37(5)	11.60(0.4)
CNF-PH500_30	70	30	-	1.186(0.008)	12.13(0.91)	160.67(8)	10.27(0.3)
CNF-PH500_40	60	40	-	1.139(0.009)	12.40(0.56)	131.21(8)	7.75(0.4)
CNF-PH500_50	50	50	-	1.087(0.015)	13.01(1.01)	111.54(14)	7.62(0.2)
CNF-PH500-PPy	48	38	14	1.083	16.78(1.18)	55.76(3)	6.61(0.6)

Finally, the tensile properties of pure BC and BC-PPy nanopapers are shown in Figure 30, and weight percentage of PPy, thickness and tensile properties of BC-PPy nanopapers listed in Table 12.

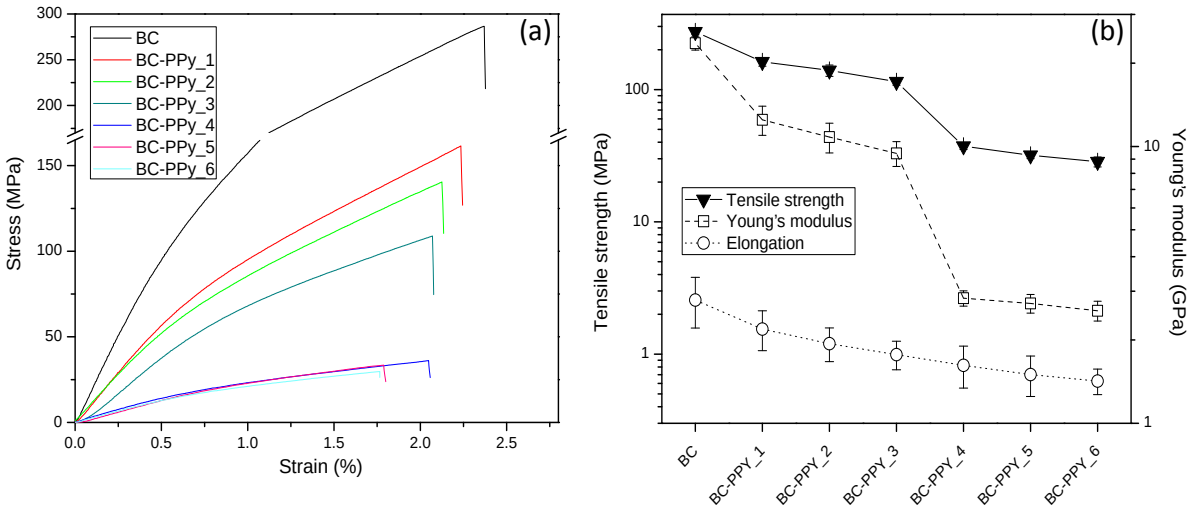

Figure 30 (a) Stress-strain curves and (b) tensile strength, Young's modulus and tensile strain of BC and BC-PPy nanopapers.

Table 12 Weight percentage of PPy, thickness, and tensile properties of BC and BC-PPy nanopapers.

Sample	PPy (%)	Thickness (μm)	Strain (%)	Tensile strength (MPa)	Young's modulus (GPa)
BC	0	43(3.8)	2.78(0.58)	273.72(13.70)	23.60(1.31)
BC-PPy_1	17	53(2.1)	2.19(0.36)	162.43(12.21)	12.48(1.51)
BC-PPy_2	21	59(1.9)	1.94(0.27)	139.59(13.69)	10.81(1.33)
BC-PPy_3	25	72(4.7)	1.77(0.21)	114.67(6.66)	9.44(0.97)
BC-PPy_4	45	102(5.0)	1.62(0.28)	37.38(2.07)	2.83(0.18)
BC-PPy_5	51	149(4.7)	1.50(0.25)	31.85(1.78)	2.71(0.21)
BC-PPy_6	55	167(6.0)	1.42(0.15)	28.49(2.45)	2.55(0.21)

The Young's modulus of BC in Figure 30a was 23.60 GPa, which is slightly superior to that from previous studies (17 – 19 GPa) (Gea et al., 2007; Gea, Bilotti, Reynolds, Soykeabkeaw, & Peijs, 2010). From the stress-strain curve, BC requires high load to elastically deform probably because of its 3-D network structure. For the high Young's modulus, and looking at

the shape of the curve at low elastic loads, one can consider BC as a very stiff material (Bäckdahl et al., 2006). On the other hand, the maximum tensile strength of BC (Figure 30b) was 273 MPa, also higher than that from some previous works (Rambo et al., 2008, Müller, Rambo, Porto, Schreiner, & Barra, 2013). These different values can be caused by the amount of sugar and the duration of cultivation of bacterium, which influence the yield and the degree of polymerization. In the present work, 5% of sugar was used and the cultivation was maintained for 12 days. The conditions bring to bacterial cellulose with polymerization degree in the range of 1700-2000, in agreement with the literature Surma-Ślusarska et al. (2008). The coating of pyrrole on the surface of BC produced the typical brittle behavior with a strain lower than 2.19 ± 0.36%. Tensile strength and Young's modulus decreased up to 162 MPa and 12.5 GPa with 17% PPy. This could be explained by the reduction of the hydrogen bonding of BC due to the presence of PPy nanoparticles adhered on the nanofibrils surfaces (Müller et al., 2013). Moreover, the fragmentation of BC occurring during the polymerization of pyrrole lead to have cracks between the BC and PPy layers. This weak interface does not favorable the stress-transfer when load was applied. On the other hand, it is important to note that the tensile properties of BC-PPy_6 were reduced 1 order of magnitude (28.5 MPa of strength and 2.55 GPa of modulus), which is related to the increasing of fibril diameter during the polymerization (50 nm for pure BC and 113 nm for BC-PPy_6). The thickness of final nanopaper increased up to 167 μm, whereas it was 43 μm for the original BC. One can say that this nanopaper was composed of about 60 μm thickness of PPy in each side, and that this thick PPy payer is the reason of the low tensile properties, because PPy themselves are mechanically weak (Pandey et al., 2015).

4.4 FE-SEM

The morphologies of CNF, BC, PPy, MWCNT surface modification (MWCNT-COOH), and conductive nanopapers were observed by FE-SEM and presented in Figure 31. The fracture surface of CNF nanopaper in Figure 31a shows a compact multilayer configuration of interconnected cellulose nanofibers. This multilayer structure and tight connection between layers contributed to the high mechanical performance of the ensuing pure CNF nanopaper.

The outstanding mechanical behavior of BC nanopapers is also related to the fibers entanglement and strong three-dimension network of BC nanofibrils, as shown in Figure 31b. PPy platelets (Figure 31c) tend to agglomerate themselves due to strong intermolecular interactions, while the microstructure surface modified MWCNTs (Figure 31d) provides some

fragments and defects, and some nanotubes shortened in length after the acid treatment process.

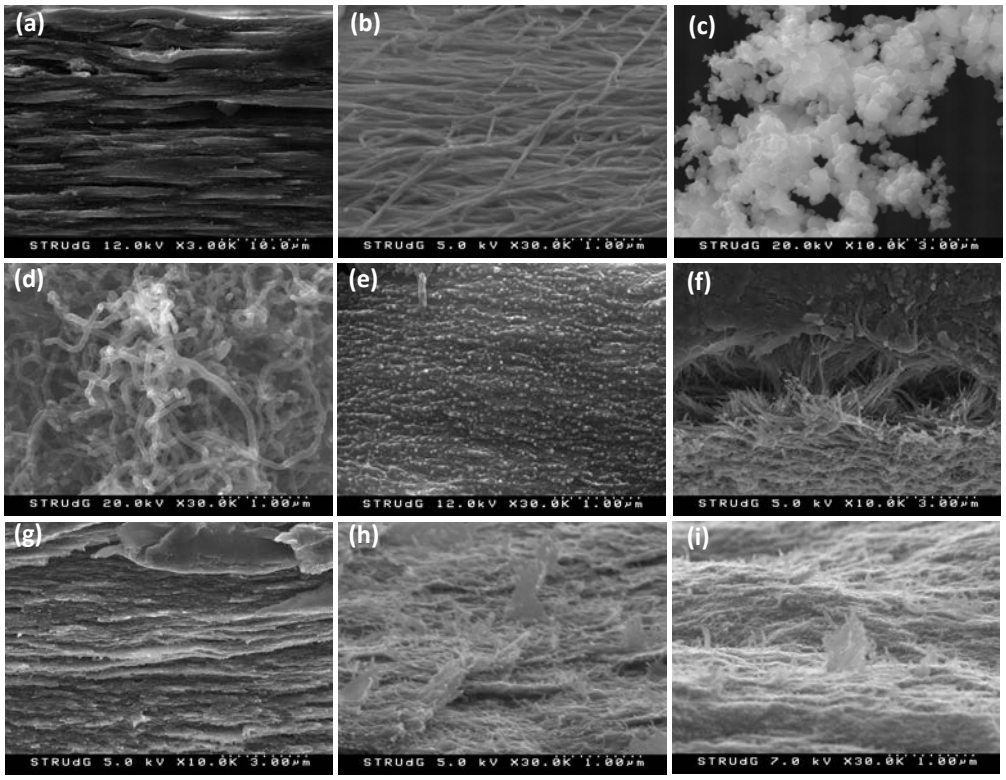

Figure 31 Microstructure surfaces of (a) CNF, (b) BC, (c) PPy, (d) MWCNT-COOH, (e) CNF-PPy20, (f), BC-PPy_3, (g) CNF-MWCNT10, (h) CNF-MWCNT-PPy_B, and (i) CNF-PH500-PPy nanopapers.

In all cases, the surface of nanocellulose became rough and brittle when they are coated with conductive filler, for example with the coating of PPy on CNF (Figure 31e) or on BC (Figure 31f). These surfaces roughness occurred since PPy platelets interpenetrated the nanofibers networks or formed core-sheath structure. On the other hand, the mixture of MWCNT and CNF, in Figure 31g, leads to less dense structure compared to neat CNF. Moreover, the CNF-MWCNT-PPy and CNF-PH500-PPy in Figure 31h and 31i have high surfaces roughness and became brittle when 20% and 14% of PPy was coated on MWCNT-CNF and on CNF-PH500 nanopapers. This is due to the intrinsically weaker PPy-PPy interactions with respect to those for cellulose-nanotube, nanotube-nanotube, cellulose-PEDOT:PSS or cellulose-cellulose connections.

4.5 Electrical Conductivity

Nanocellulose changed its electrical property from insulator to semiconductor and to conductor material by the addition of conductive fillers. Generally, the delocalized π conjugated electrons of conductive polymers induced the enhancement of electrical conductivity of nanopapers. The electrical conductivities of all conductive nanopapers are presented in Table 13. The in situ chemical polymerization of PPy on CNF substrate enhanced electrical properties of CNF. The electrical conductivities of nanopapers depend on the amount of PPy, as shown in Figure 32.

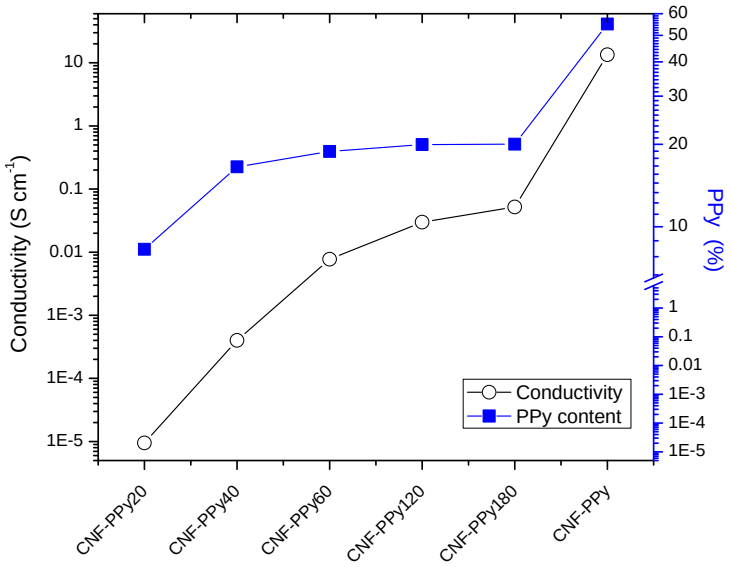

Figure 32 The correlation between conductivity and the amount of PPy in CNF-PPy nanopapers.

The amount of polypyrrole in the nanopaper steadily increased with the reaction time, and the conductivity improved substantially. From the results, the nanopaper with 8% of PPy had a conductivity of 10^{-5} S·cm^{-1}, which is similar to that of silicon (1.5 10^{-5} S·cm^{-1}), and reached up to 5.2 10^{-2} S·cm^{-1} with 20% of PPy, which is the same level of other semiconductors. Our cellulose nanopaper became conductor with 55% of PPy. The higher amount of PPy and higher porosity (26%, in Table 13) induced the facility of electron mobility and leaded to a better-bonded structure, resulting in higher electrical conductivity.

Table 13 Conductivity of the all nanopapers.

Sample	Conductivity ($S \cdot cm^{-1}$)	Sample	Conductivity ($S \cdot cm^{-1}$)	Sample	Conductivity ($S \cdot cm^{-1}$)
CNF	10^{-8}–10^{-13}	**CNF-PT2_5**	$1.02\ 10^{-5}$	**BC**	$1.8\ 10^{-13}$
CNF/PPy20	$1.0 \cdot 10^{-5}$	**CNF-PT2_10**	$7\ 10^{-4}$	**BC-PPy_1**	1.22
CNF/PPy40	$4.0 \cdot 10^{-4}$	**CNF-PT2_20**	$2.86\ 10^{-2}$	**BC-PPy_2**	1.88
CNF/PPy60	$7.7 \cdot 10^{-3}$	**CNF-PT2_30**	0.18	**BC-PPy_3**	1.94
CNF/PPy120	$3.0 \cdot 10^{-2}$	**CNF-PT2_40**	0.59	**BC-PPy_4**	2.66
CNF/PPy180	$5.2 \cdot 10^{-2}$	**CNF-PT2_50**	0.65	**BC-PPy_5**	3.22
CNF-PPy	13.45	**CNF-PH500_5**	$5\ 10^{-5}$	**BC-PPy_6**	3.39
CNF-MWCNT10	$0.02\ 10^{-2}$	**CNF-PH500_10**	$1.87\ 10^{-3}$		
CNF-MWCNT20	$2.35\ 10^{-2}$	**CNF-PH500_20**	$3.30\ 10^{-2}$		
CNF-MWCNT30	0.26	**CNF-PH500_30**	0.70		
CNF-MWCNT40	0.44	**CNF-PH500_40**	1.69		
CNF-MWCNT50	0.78	**CNF-PH500_50**	2.58		
CNF-MWCNT-PPy_A	0.049	**CNF-PH500-PPy**	10.55		
CNF-MWCNT-PPy_B	0.42				
CNF-MWCNT-PPy_C	1.43				
CNF-MWCNT-PPy_D	2.41				

The blending of modified MWCNT with CNF also changed the electrical properties of nanopapers (Table 13). Conductive filler networks that follow classical geometrical percolation theory (where filler bonding occurs) obey a universal conductivity-loading relationship above the percolation threshold (Hermant, 2009), according to the Equation 3 (see page 41).

To determine the percolation threshold (Φ_c) experimental results are fitted by plotting log σ versus log $(\Phi - \Phi_c)$, and the value of Φ_c is incrementally varied until the best linear fit is obtained. Percolation thresholds have been reported in the range from 0.001 wt% to more than 10wt% depending on the matrix, the processing technique, and the type of conductive filler (Koga et al., 2013). In the present case, the percolation thresholds of MWCNT and MWCNT-PPy in cellulose nanopapers were found to be 0.06 and 0.2 respectively. A formulation with a volume fraction of conductive filler below the percolation threshold would not show any electrical conductivity. For the case of MWCNT, the formulation with 10wt% corresponded to a volume fraction of 0.074, above the 0.06 percolation threshold. Therefore, and based on the percolation threshold result, CNF turned into conductive network at lower filler contents than CNF-MWCNT and CNF-MWCNT-PPy nanopapers. For each value of

Φ_c, the value of *t* has been determined from the slope of the linear relation of log σ and log $(\Phi - \Phi_c)$, and this linear correlation was plotted in the inset of Figure 33. For the formulations of CNF-MWCNT and CNF-MWCNT-PPy, the experimental conductivity and their predicted values with respect the volume fraction are presented in Figure 33a. In both nanopapers, the critical exponent *t* was 2.62 and 2.76. Many conductive fillers networks, including carbon nanotube in polymeric composites, exhibit a non-universal value for *t*. This has been linked to the fact that the electrical percolation networks in these systems are not geometrical and tunneling between nearest-neighbors governs the conduction mechanism.

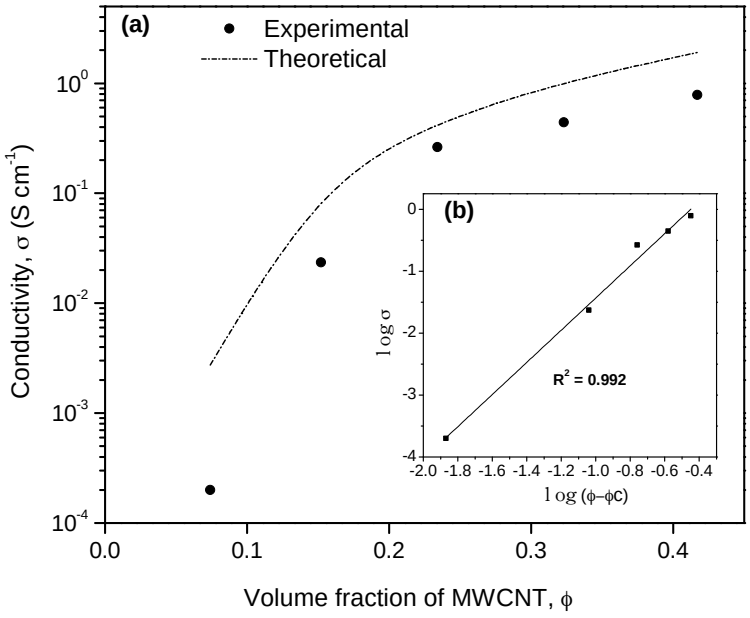

Figure 33 (a) Experimental and predicted electrical conductivities of CNF-MWCNT (square) and CNF-MWCNT-PPy (circle) nanopapers with the volume fraction of conductive fillers and (b) Linear correlation between log σ and log $(\Phi - \Phi_c)$ and predicted *t* values for Equation 3.

The conductivity of nanopaper with 50% of MWCNT reached 0.78 S cm^{-1} because the MWCNTs within the CNFs network created a conductive pathway. However, this value is still low considering the electrical conductivity of pristine MWCNT that is in the range of the metallic materials. One can say that the acid modification of MWCNT provoked defects on MWCNT sidewall, by forming carboxylic and other oxygen-containing groups on their surface, reducing the electric conductivity of MWCNT (Li & Zhitomirsky, 2013). Moreover, the modified carbon nanotubes consisted of negative charges of carboxylic acid leading to an

increase of the porosity of nanopapers, as shown in previous works (Salajkova et al., 2013). However, formulations of CNF-MWCNT containing PPy showed a significant improve on the electrical conductivity as shown in Table 13. In CNF-MWCNT-PPy_B nanopaper, containing only 9% of MWCNT and by adding 31% of PPy, the conductivity was similar to that of nanopapers with 40wt% of MWCNT. Moreover, the conductivity increased with the PPy content; PPy chains build a good conductive network by wrapping on both cellulose nanofibrils and MWCNTs, which favored the electron transport through the sample.

The percolation thresholds of nanopapers made from CNF-PT2 and CNF-PH500 were found to be 0.036 and 0.002, respectively (Figure 34). This difference is related to several factors such as the ultimate conductivities (80 S cm^{-1} and 300 S cm^{-1}), particle size (90 and 30 nm), and viscosity (80 and 25 mPa s), respectively for each PT2 and PH500. The ultra-low percolation threshold for CNF-PH500 nanopaper is due to the higher surface area of PH500, uniformly distributed, aligned (uniform in one direction) and disentangled in the nanopaper.

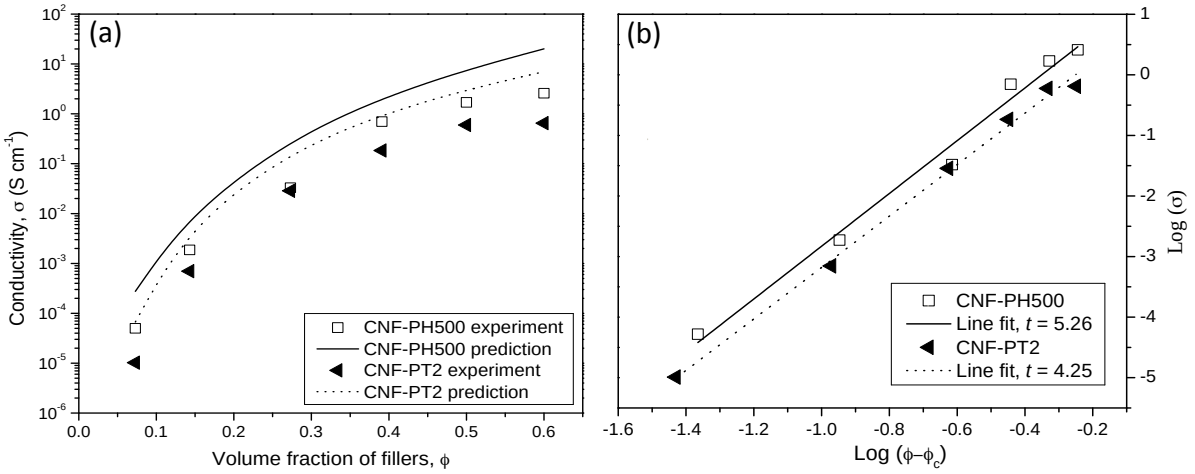

Figure 34 (a) Experimental and predicted electrical conductivities of CNF-PT2 (triangle) and CNF-PH500 (rectangle) nanopapers with the volume fraction of conductive fillers and (b) linear correlation between log σ and log $(\Phi - \Phi c)$ and predicted *t* values for Equation 3.

The conductivity of CNF-PT2_5 nanopaper was five times lower compared with CNF-PH500_5 nanopaper. High electrical conductivity is ensued when the volume fraction of conductive filler is up to 0.5 (1.6 S cm^{-1}) or 0.6 (2.5 S cm^{-1}). In addition, the polymerization of 14% of PPy into the CNF-PH500 suspension gave a CNF-PH500-PPy nanopaper with a dramatically increased conductivity of 10.55 S cm^{-1}. This enhancement probably attributes to

increase porous structure of nanocomposite (Table 13) and also due to a bridging of the highly conducting domains by the PPy. As the results, CNF-PPy (45:55, wt%) nanopaper had conductivity of 13.45 S cm^{-1}.

The linear fit in Figure 34b is plotted to determine the critical exponents (*t*) from Equation 3. Then, the theoretical conductivity can be calculated considering the ultimate conductivity (σ_o) of each filler. With the filler volume fraction from 0.1 to 0.6 (Figure 34a), the experimental conductivity was lower than the predicted conductivity between five to ten times. The lower experimental results, especially at high filler loading, can be related to low disentanglement of PEDOT:PSS chains (agglomerates), or the non-uniform distribution of individual PEDOT:PSS on microscopic scale (Li. J et al., 2007).

Figure 35 depicts the electrical conductivity of BC-PPy nanopapers. In the case of BC-PPy nanopaper, the percolation threshold (Figure 36) was found at 0.155.

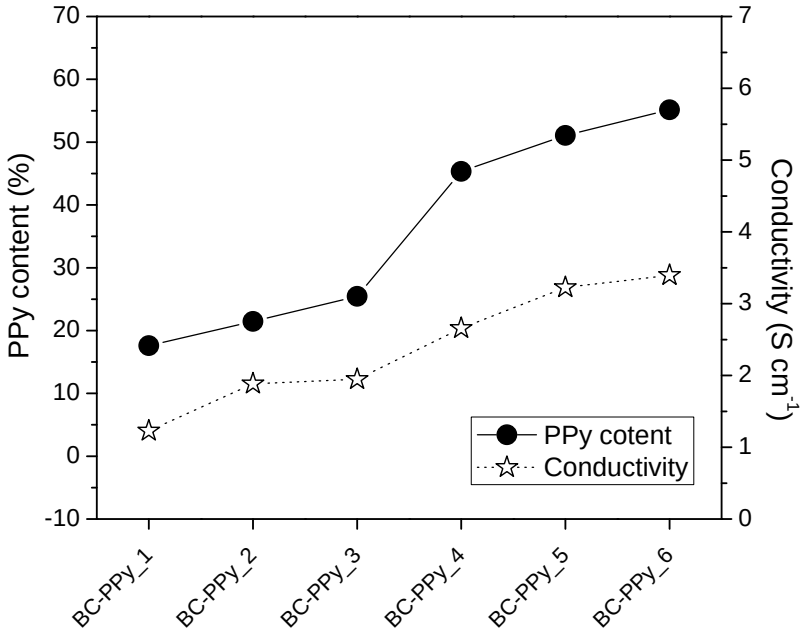

Figure 35 The PPy content and electrical conductivity of BC-PPy nanopapers.

The graph shows that conductive properties significantly increased in the same trend of log10 with the amount of PPy in nanopaper. The conductivity of nanopapers with 17–55 w% of PPy (Table 13) were in the range of 1.22–3.39 S cm^{-1}, which is 13 orders of magnitude higher than that of pure BC (1.8 10^{-13} S cm^{-1}). This property is comparable to the value of BC-PPy from the previous report of Xu et al. (2013) or even higher than that of Müller et al. (2013) and Tang, Han, Jiang, Chen, & Wang (2015). The conductivity of the BC-PPy nanopaper is

higher than that of our CNF-PPy nanopaper Lay et al. (2016) or the one from Nyström et al. (2010). From our results, BC worked as a good template for the polymerization of pyrrole to produce a highly conductive nanopaper.

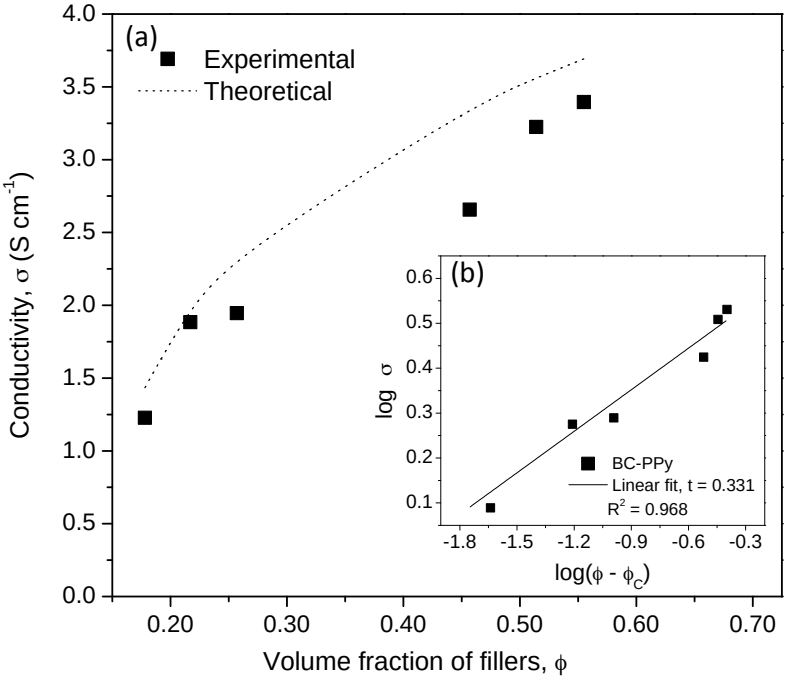

Figure 36 (a) Experimental and predicted electrical conductivities of BC-PPy nanopapers with the volume fraction of conductive fillers and (b) Linear correlation between log σ and log $(\Phi - \Phi_c)$ and predicted *t* values for Equation 3.

4.6 Cyclic voltammetry

The specific capacitances of the conductive nanopapers were determined by cyclic voltammetry (CV) in 2 M NaCl electrolyte. Cyclic voltammograms of conductive nanopapers were plotted from the potential window between –0.9 and +0.9 V at various scan rate of 5, 20, 50, 100, and 200 mV s^{-1} as presented in Figures 37–39. From theses cyclic voltammograms, the specific capacitances we calculated according to Equation 4 (see page 42), and their values can be seen in Table 14 (see page 65). Nanopapers consisting of high amount of PPy, for instance CNF-PPy, CNF-MWCNT-PPy, and CNF-PH500-PPy, the oxidation peaks were around +0.2 V and the reduction peaks at around -0.4 V vs Ag/AgCl. This oxidation-reduction peaks belong to the characteristic redox behavior of PPy (Nyström et al., 2010). Figure 37 depicts the cyclic voltammograms of CNF-PPy180 (20wt% of PPy) and CNF-PPy (55wt% of PPy) nanopapers at different scan rate of 5, 20, 50, 100, and 200 mV s^{-1} in the

potential window between -0.9 and +0.9 V (vs. Ag/AgCl). All curves are elliptical with increased current upon increasing the scan rate. At small amount of PPy (20%), the oxidation and reduction peaks seem did not appear. The specific capacitance of CNF-PPy180 at 5 mV s^{-1} was 7.40 F g^{-1}, which decreased to 0.35 F g^{-1} at the highest scan rate of 200 mV s^{-1}. The decrement of this value has been related to the sample compression during the sheet drying, which reduced the porosity. When the porosity is decreased the ion mass transport is too slow to allow for full utilization of the inherent charge storage capacity for scan rates above 5mV s^{-1} (Wang, Tammela, Zhang, Stromme, & Nyholm, 2014). As mentioned by Carlsson et al., (2012), porous samples allow fast transport of anions throughout the electro-active material. They found that the capacity of compact samples decreased with increasing scan rate while the porous samples showed a slight increase in capacity. Therefore, a more porous structure enhances the rate of ionic mass transport (Wang et al., 2007). In the voltammogram for CNF-PPy, Figure 37b, the oxidation-reduction peaks appear more clearly (especially in Figure 37c). As the result, when 55% of PPy was added, CNF-PPy increased porosity to 26.19%, and its specific capacitance was increased up to 300.18 F g^{-1}. This high value is also related to the sufficient amount of PPy platelets coating on CNF.

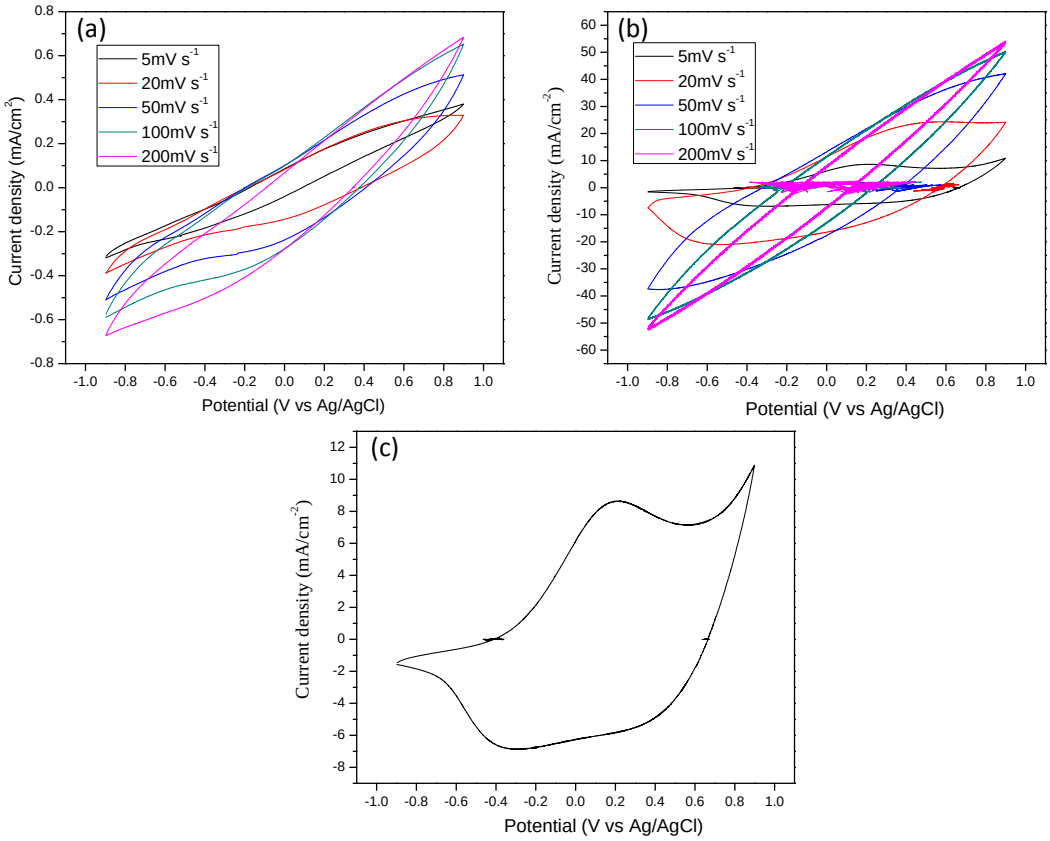

Figure 37 Cyclic voltammograms of (a) CNF-PPy180, (b) CNF-PPy at different scan rate of 5, 20, 50, 100, and 200 mV s^{-1}, (c) cyclc voltammogram of CNF-PPy at 5 mV s^{-1}.

Table 14 Specific capacitance of CNF-PPy nanopaper at different scan rate (mV s^{-1}).

Sample	Specific capacitance (F g^{-1}) at different scan rate (mV s^{-1})				
	5	20	50	100	200
CNF-PPy180	7.40	1.86	1.05	0.63	0.35
CNF-PPy	300.18	215.93	140.68	83.69	49.05
CNF-MWCNT20	1.38	0.57	0.33	0.22	0.14
CNF-MWCNT50	16.40	6.53	3.29		1.31
CNF-MWCNT-PPy_B	53.17	18.88	8.81	4.79	2.54
CNF-MWCNT-PPy_D	113.08	44.21	23.15	13.69	7.87
CNF-PT2_50	7.86	2.59	1.44	1.23	0.87
CNF-PH500_50	6.21	2.79			
CNF-PH500-PPy	315.53	224.57			
BC-PPy_3	19.68	12.30	7.38	4.1	2.06
BC-PPy_5	191.94	64.79	29.41	19.09	9.59

On the other hand, from cyclic voltammograms in Figure 38, the specific capacitances of CNF-MWCNT20 and CNF-MWCNT50 at 5 mv s^{-1} were 1.38 F g^{-1} and 16.4 F g^{-1}, respectively. Carbon nanotubes can be employed as high energy density electrode materials because of their good conductivity, however, as a consequence of the lack of micropores for ions accumulation, it is difficult to obtain a high capacitance over a pure carbon nanotube based electrode (Xiong, Zhu, & Wang, 2015). Zhang et al. (2009) explained that although MWCNTs has high specific surface area (>1000 m^2/g), the specific capacitance is usually smaller than 100 F g^{-1} because not all of the internal surface, such as those of the wall of micro-pores, can be accessed by ions in the activated carbon for charge storage. Peng et al. (2007) also found that the untreated carbon nanotubes had a specific capacitance about 10 F g^{-1}, and this property improved five times after acid treatment (50 F g^{-1}). The surface modified MWCNTs helped to improve the specific capacitance due to the functional groups (carboxylic, hydroxyl) formed during the acid treatment, that are known to act as redox active centers (Peng et al., 2007). The ternary formulation with 48% of PPy content (CNF-MWCNT-PPy_D) had a capacitance of 113 F g^{-1}, around seven times higher than the one of binary formulation with 50% MWCNT (CNF-MWCNT50). This high specific capacitance can be explained by the direct interaction between the delocalized electrons on polymer chains and the MWCNT. It was mentioned that PPy has capability to provide the capacitive response via fast redox reactions of the conjugated area in polymer networks (Xiong et al., 2015). Moreover, the coating of PPy on the outer surface of the nanotube enhanced the

faradaic charge transfer reaction providing a high specific capacitance (Fu, Du, Zou, Li, & Zhang, 2013; G. Yu, Xie, Pan, Bao, & Cui, 2013).

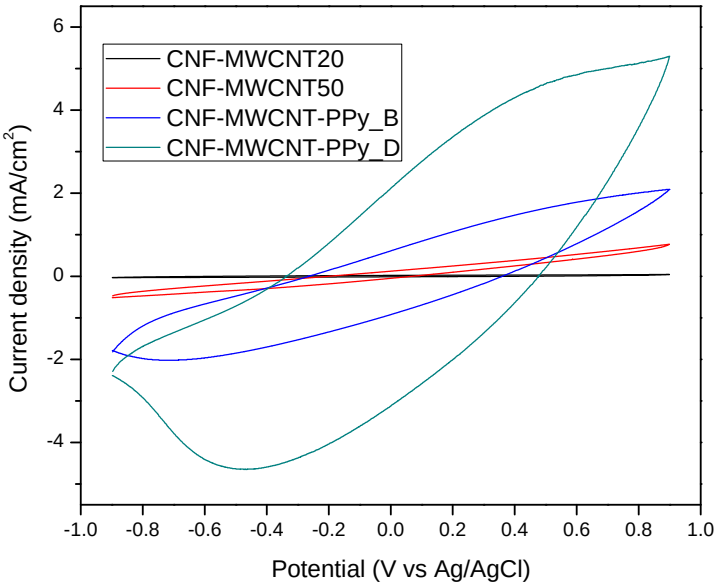

Figure 38 Cyclic voltammograms of CNF-MWCNT20, CNF-MWCNT50, CNF-MWCNT-PPy_B, and CNF-MWCNT-PPy_D at scan rate of 5 mV s^{-1}.

The cyclic voltammograms of CNF-PT2_50, CNF-PH500_50, CNF-PH500-PPy, and BC-PPy nanopapers are shown in Figure 39, and Table 14 presents their specific capacitances. The oxidation reduction peaks of nanopapers containing polypyrrole (CNF-PH500-PPy) are more pronounced than those of CNF nanopapers with only PEDOT:PSS as shown Figure 39a and b. In this case, the specific capacitances of all nanopapers decreased with increasing the scan rates. Explicitly, the specific capacitances of CNF-PT2_50, CNF-PH500_50, and CNF-PH500-PPy nanopapers at 5mV s^{-1} of scan rate were 7.86, 6.21, and 315.6 F g^{-1}, respectively (Table 14). The very high capacitance of CNF-PH500-PPy is related to the more porous structure and especially to a synergistic effect between the two conductive fillers, PPy and PH500. Regarding the synergy phenomenon, it is plausible that the successive coating procedure allowed the sequential interactions, first between oxidized-cellulose nanofibers and cation in the PEDOT chains, and next between anion PSS chains and polypyrrole backbone. The synergistic effect between PEDOT:PSS and PPy on cellulose nanofibers plays an important role to facilitate counter ions and electrons transport in the nanocomposites (Zhaohui Wang et al., 2014).

The CV curves of both CNF-PT2_50 and CNF-PH500_50 nanopapers in Figure 39c exhibit a distorted elliptical shape at low scan rate and become deformed when scan rate reach 100 mV s^{-1} for BC-PPy_3 and 50 mV s^{-1} for BC-PPy_5. The oxidation-reduction peaks of BC-PPy_5 are found at +0.6 V and –0.6 V vs Ag/AgCl, which demonstrates the retention of the important redox feature of conducting polymer in the BC-PPy nanopaper (Wang, Bian, Zhou, Tang, & Tang, 2012). However, these peaks did not appear at low amount of PPy (25wt%) for BC-PPy_3, as well as 18% of PPy for CNF-PPy180 nanopaper. Table 14 indicates that BC-PPy_5 has the specific capacitance of 191.94 F g^{-1} at 5 mV s^{-1}, which is ten times higher than the BC-PPy_3 nanopaper (19.68 F g^{-1}). The increasing thickness (~100 μm) of PPy around the BC nanofibrils could provide a larger specific surface area of the electrode/electrolyte interface (Xu et al., 2013).

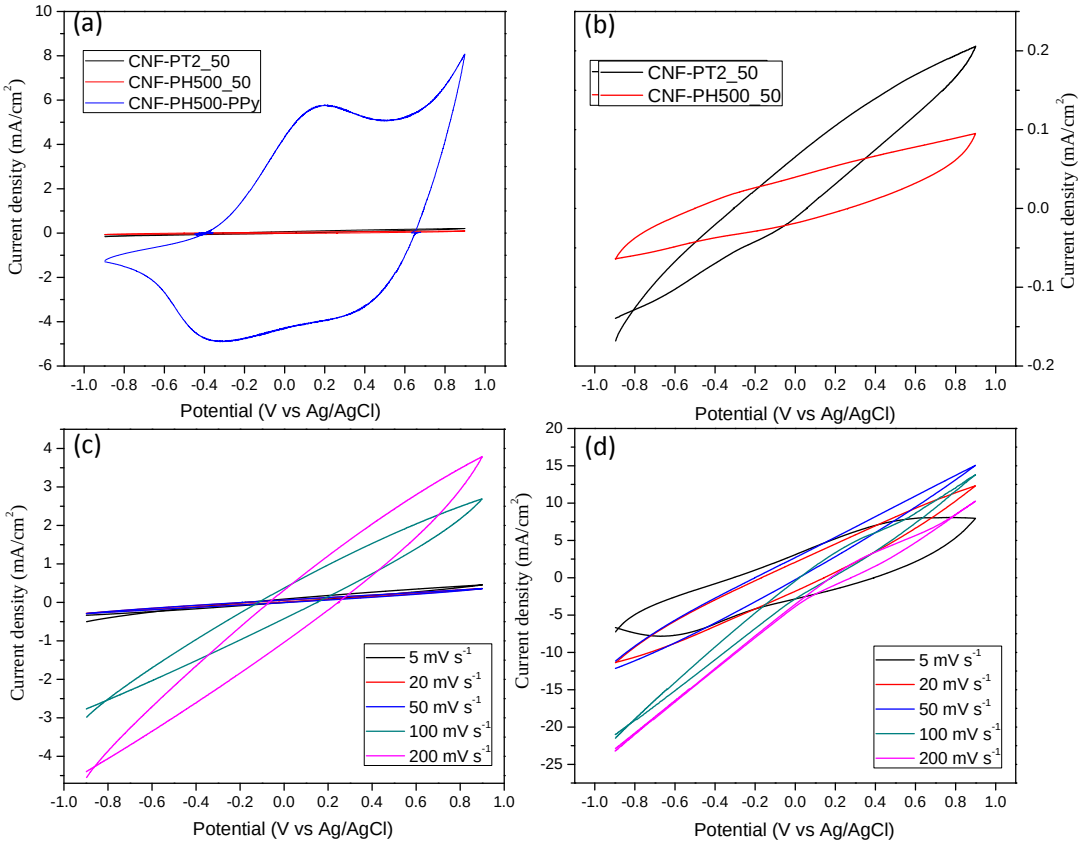

Figure 39 Cyclic voltammograms of (a) CNF-PT2_50, CNF-PH500_50, and CNF-PH500-PPy; (b) enlarged CNF-PT2_50 and CNF-PH500_50 at 5mV s^{-1} scan rate; (c) BC-PPy_3, and (d) BC-PPy_5 at scan rate of 5, 20, 50, 100, and 200 mV s^{-1}.

4.7 Thermogravimetric analysis

The weight loss with temperature and the maximum degradation temperatures of CNF, BC, PPy, PH500, CNF-PPy180, CNF-PH500_50, CNF-PH500-PPy, and BC-PPy_6 nanopapers were studied by thermogravimetric analysis and are shown in Figure 40. The maximum degradation temperatures can be determined from the derivative thermogravimetric curves (Figure 40b).

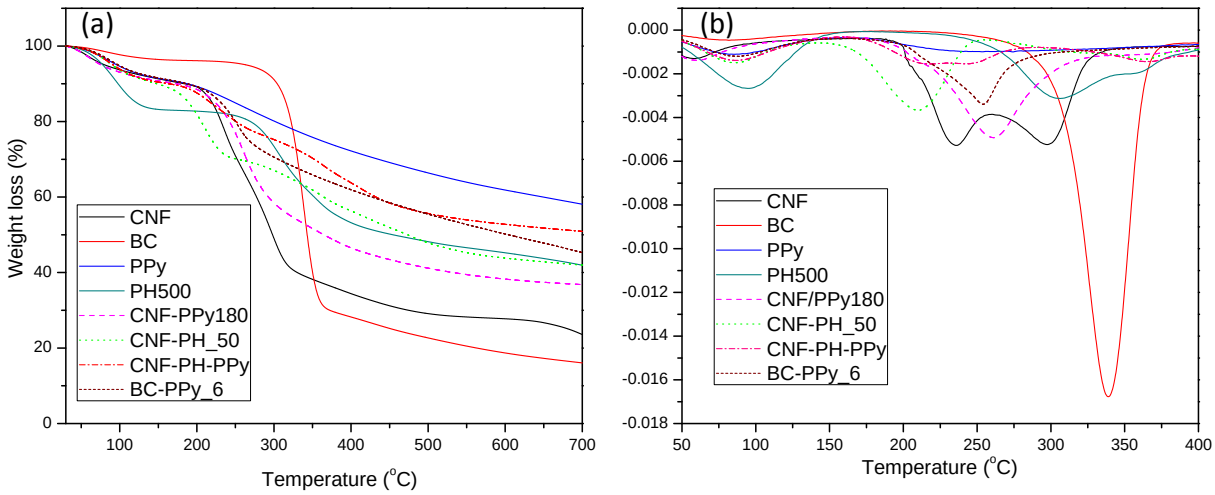

Figure 40 (a) TGA and (b) DTG of CNF, BC, PPy, PH500, and different conductive nanopapers (CNF-PPy180, CNF-PH500_50, CNF-PH500-PPy, and BC-PPy_6).

The values of initial weight loss, the maximum degradation temperatures, and total weight loss at 700ºC are listed in Table 15.

Table 15 The initial weight loss, maximum degradation and total weight loss of samples.

Samples	Initial weight loss (%) around 100 °C	Maximum degradation temperature (ºC)	Total weight loss at 700ºC (%)
CNF	7	232 and 296	76
BC	2.32	334	84
PPy	7	230	42
PH500	8	298	52
CNF-PPy	7	257	64
CNF-PH500_50	7	210	57
CNF-PH500-PPy	7	224	49
BC-PPy	7	249	55

The initial weight loss (Figure 40a) of all samples around 100ºC was about 7%, which relates to residual moisture present in the samples (Lee et al., 2012). For CNF nanopaper, cellulose pyrolysis started at 201ºC and continued until around 330ºC leading to depolymerization of solid cellulose to form active cellulose and thereafter various anhydro-monosaccharides, retroaldol, dehydrated species, carbon oxides, and char (Lin et al., 2009; Nyström et al., 2010). The weight loss for CNF nanopaper was of 61.5% at 330°C and of 76% at 700°C, similar to the values found in previous studies (Nyström et al., 2010). In Figure 40b, the thermal degradation of CNF from TEMPO-oxidation was broad and consisted of mainly two peaks around 232°C and 296°C, both below the degradation point of original cellulose (~310°C). This confirms the formation of sodium carboxylate groups at the C_6 primary hydroxyls of cellulose. According to literature (Fukuzumi, 2012), the first degradation peak corresponds to the degradation of sodium anhydroglucuronate units, and the second relates to the degradation of cellulose chains containing more unstable anhydroglucuronate units in the crystal surface.

With respect to BC, the TGA graph shows a weak loss of weight (2.32%) due to the evaporation of water and a quick drop in weight beginning at a temperature of 280°C up to 380ºC, resulting a maximum degradation temperature of 334ºC, presented in the DTG curve (Figure 40b); in previous work this was found around 350–370ºC (Surma-Ślusarska et al., 2008).

In the case of CNF-PPy180 nanopaper, the weight loss between 230°C and 350°C was of 31% and of 64% at 700°C. For this nanopaper, the loss was not only a result of the degradation process of the cellulose but also partly because of the thermal degradation of the polymer backbone in polypyrrole. For the polymer itself (PPy), the total weight loss at 700°C was 42%, following a slow degradation mechanism. The degradation kinetics of PPy is much slower than the degradation of CNF. It is known that PPy degrades in two steps, a degradation process involving the counterions first and the polymer backbone degradation afterwards. The process during which the counterion is expelled occurs before the polymer backbone degradation in PPy and is probably responsible for shifting the main degradation of CNF/PPy to have its maximum degradation temperature at a lower temperature than the one for CNF (Nyström et al., 2010).

Regarding the nanopapers from PEDOT:PSS, the maximum degradation temperature of CNF-PH500_50 nanopaper was 210ºC. The coating of PH500 on cellulose nanofibers prevented the char formulation at high temperature, which reduced the total weight loss at 700ºC (57%). Since PPy was thermally more stable, the total weight loss of CNF-PH500-PPy was lower

than those of CNF, CNF-PH500, and CNF-PPy nanopapers (see Table 15). From the TGA/DTG result, one can say that the coating of cellulose nanofibers with a conductive polymer like PPy, PH500 or PH500/PPy gave a more thermally stable nanopaper.

5. CONCLUSIONS AND FUTURE WORK

5.1 General conclusions

In this investigation, conductive nanopapers or nanocomposites were produced from cellulose nanofibers (CNF from TEMPO-oxidized bleached softwood) or bacterial cellulose (BC from *Acetobacter Xylinum* bacterial culture) combined with conducting materials, such as polypyrrole (PPy), poly(3,4-ethylenedioxythiophene):polystyrene sulfonate (PEDOT:PSS) and multi-walled carbon nanotubes (MWCNT). Different electrically conductive nanopapers were successfully prepared by *in-situ* polymerization of pyrrole in the presence of CNF or BC, and by blending techniques that allow a homogeneous distribution of the conducting filler in the nanocellulose matrix. The experimental approach is a simple and environmentally friendly method based on mixing/sonication/filtering/drying process.

In general, and with respect to mechanical behavior, the tensile strength of BC nanopaper was higher than CNF nanopaper. The incorporation of any conductive nanofiller reduced the mechanical performance of the ensuing nanocomposite, however, among them, the addition of MWCNT or PEDOT:PSS resulted in nanopapers of better mechanical properties compared with those imparted by the use of PPy or the hybrid fillers containing PPy (MWCNT:PPy or PEDOT:PSS-PPy). Regarding the electrical properties, the insulator nature of cellulose nanofibers turned to be semiconductor or fully conductive after coating or mixing with conducting materials. The unique architecture and high-performance capacitance of nanopapers, together with their low-cost, lightweight, flexible, abundant, and environment-friendly materials offers a great promise for their use in the next generation of small green electronics and energy storage devices such as batteries or electrochemical capacitors.

5.2 Main specific findings

- BC membrane showed a tensile strength and Young's modulus of 273 MPa and 23.6 GPa, respectively; whereas these properties were 224 MPa and 14.5 GPa, respectively, for the CNF nanopaper. By the addition of 50 wt% of MWCNT or PEDOT:PSS, the tensile strength was reduced up to 141 MP and 111 MPa respectively; and the Young's modulus diminished until 9.57 GPa and 7.62 GPa for the same materials.
- CNF nanopapers showed semiconductor properties (electrical conductivity of 5.2 10^{-2} S cm^{-1}) after coating with 20% of PPy on CNF surface, and turned to conductor with 55% of PPy (electrical conductivity of 13.45 S cm^{-1}).

- In combination with MWCNT, CNF acted as strong and though matrix assisting the formation of nanostructured and nanodispersed CNF-MWCNT nanocomposites. The binary formulation, CNF-MWCNT (50:50), had an electrical conductivity of 0.78 S cm^{-1} while it was 2.41 S cm^{-1} for the ternary formulation CNF-MWCNT-PPy (45:7:48). The use of hybrid MWCNT-PPy is then a more economic and effective conductive nanofiller.
- The coating of the hybrid PEDOT:PSS-PPy on CNF surface provided electrical conductivity of 10.55 S cm^{-1}.
- The specific capacitances, in crescent order, of the conductive nanocomposites in the present work were: 6.21, 7.40, 16.40, 113.08, 191.94, and 315 F g^{-1}, respectively for CNF-PH500_50, CNF-PPy180, CNF-MWCNT_50, CNF-MWCNT-PPy, BC-PPy_5, and CNF-PH500-PPy, measured at 5 mV s^{-1} of scan rate.
- The current findings add to a growing body of literature on searching eco-friendly biomaterials to be used in the field of electronic or energy storage devices.

5.3 Future work

In this thesis, several conductive materials coated on nanocellulose are presented to change the electrical conductivity of cellulose nanofibers and bacterial cellulose. However, still a lot of work needs to be completed. Membranes made of BC-PEDOT:PSS nanopaper have also been performed, not included in this work, and will be fully characterized. Several keys are suggested for future work:

- To better understand the use of cellulose nanofibers nanopaper in energy storage device, for instance as supercapacitor or batteries, charge-discharge and cycling stability should be performed.
- In low porosity nanopapers, the ion mass transport is too slow to allow full utilization of the inherent charge storage capacity, so that, drying under ambient temperature or supercritical CO_2 drying methodologies should be used to compare with current method.
- It would be interesting to combine other carbon-based and conducting polymer-based materials with cellulose nanofibers for hybrid capacitor applications. Carbon materials could provide long cycle stability while conducting polymer offers high energy density.

6. REFERENCES

Abdelhamid, M. E., O'Mullane, A. P., Snook, G. A., Wu, H., Yu, G., Pan, L., Katashinskii, A. S. (2015). Storing energy in plastics: a review on conducting polymers & their role in electrochemical energy storage. *RSC Adv.*, *5*(15), 11611–11626.

Adsul, M. G., Rey, D. A., & Gokhale, D. V. (2011). Combined Strategy for the Dispersion/Dissolution of Single Walled Carbon Nanotubes and Cellulose in Water. *The Journal of Physical Chemistry*, *21*, 2054–2056.

Ahmed, D. S., Haider, A. J., & Mohammad, M. R. (2013). Comparesion of functionalization of multi-walled carbon nanotubes treated by oil olive and nitric acid and their characterization. *Energy Procedia*, *36*, 1111–1118.

Ali, F., Reinert, L., Levêque, J.-M., Duclaux, L., Muller, F., Saeed, S., & Shah, S. S. (2014). Effect of sonication conditions: Solvent, time, temperature and reactor type on the preparation of micron sized vermiculite particles. *Ultrasonics Sonochemistry*, *21*(3), 1002–1009.

Anderson, R. E., Guan, J., Ricard, M., Dubey, G., Su, J., Lopinski, G., Simard, B. (2010). Multifunctional single-walled carbon nanotube–cellulose composite paper. *Journal of Materials Chemistry*, *20*(12), 2400–2407.

Anna, K., & Moos, R. (2012). Why Does the Electrical Conductivity in PEDOT : PSS Decrease with PSS Content ? A Study Combining Thermoelectric Measurements with Impedance Spectroscopy. *Polymer Science*, 976–983.

Ansari, R. (2006). Polypyrrole Conducting Electroactive Polymers: Synthesis and Stability Studies. *E-Journal of Chemistry*, *3*(4), 186–201.

Armes, S. P. (1987). Optimum reaction conditions for the polymerization. *Synthetic Metals*, *20*, 365–371.

Asaadi, S., Belgacem, M. N., Dazen, K., Fritz, C., Gandini, A., Gonzalez, R., Xweckmair, T. (2016). *Cellulose Chemistry and Properteis: Fibers Nanocelluloses and Advanced Materials*. (O. J. Rojas, Ed.). London: Springer.

Audebert, P., & Bidan, G. (1986). Comparison of carbon paste electrochemistry of polypyrroles prepared by chemical and electrochemical oxidation paths. Some characteristics of the chemically prepared polyhalopyrroles. *Journal of Chemical Information and Modeling*, *14*(1–2), 71–80.

Audebert, P., & Miomadre, F. (2007). Handbook of Conducting Polymers: Conjugated Polymers Processing and Applications. (Skotheim, T. A. & Reynolds, J. R., Eds.)*Chemistry &* (third). London New York: CRC Press.

Bäckdahl, H., Helenius, G., Bodin, A., Nannmark, U., Johansson, B. R., Risberg, B., & Gatenholm, P. (2006). Mechanical properties of bacterial cellulose and interactions with smooth muscle cells. *Biomaterials*, *27*(9), 2141–2149.

Bashir, T. (2013). *Conjugated Polymer-based Conductive Fibers for Smart Textile Applications*. University of Boras, Sweden.

Baughman, R. H., Zakhidov, A. a, & de Heer, W. A. (2002). Carbon nanotubes – the route toward applications. *Science*, *297*(5582), 787–92.

Boufi, S., Kaddami, H., & Dufresne, A. (2014). Mechanical Performance and Transparency of Nanocellulose Reinforced Polymer Nanocomposites. *Macromolecular Materials and Engineering*, *299*(5), 560–568.

Brown, A. J. (1886). On an acetic ferment which forms cellulose. *J. Chem. Soc., Trans.*, *49*(0), 432–439.

Buitrago-Sierra, R., García-Fernández, M. J., Pastor-Blas, M. M., & Sepúlveda-Escribano, A. (2013). Environmentally friendly reduction of a platinum catalyst precursor supported on polypyrrole. *Green Chemistry*, *15*(7), 1981–1990.

Carlsson, D. O., Nyström, G., Zhou, Q., Berglund, L. A., Nyholm, L., & Strømme, M. (2012).

Electroactive nanofibrillated cellulose aerogel composites with tunable structural and electrochemical properties. *Journal of Materials Chemistry*, *22*(36), 19014–19024.

Clasen, C., Sultanova, B., Wilhelms, T., Heisig, P., & Kulicke, W. M. (2006). Effects of different drying processes on the material properties of bacterial cellulose membranes. *Macromolecular Symposia*, *244*, 48–58.

Czaja, W. K., Young, D. J., Kawecki, M., & Brown, R. M. (2007). The future prospects of microbial cellulose in biomedical applications. *Biomacromolecules*, *8*(1), 1–12.

de Nooy, A. E. J., Besemer, A. C., & van Bekkum, H. (1995). Highly selective nitroxyl radical-mediated oxidation of primary alcohol groups in water-soluble glucans. *Carbohydrate Research*, *269*(1), 89–98.

Dinand, E., Chanzy, E., & Vignon, M. R. (1996). Parenchymal cell cellulose from sugar beet pulp: preparation and properties. *Cellulose*, *3*, 183–188.

Dufresne, A. (2012a). *Nanocellulose: From Nature to High Performance Tailored Materials*. Berlin, Germany: Walter de Gruyter GmbH.

Dufresne, A. (2012b). Nanocellulose: Potential Reinforcement in Composites. In M. J. John & T. Sabu (Eds.), *Natural Polymers : Volume 2: Nanocomposites* (Vol. 2, pp. 1–32). RSC Green Chemistry.

Eisazadeh, H., Engineering, C., & Box, P. O. (2007). Studying the Characteristics of Polypyrrole and its Composites. *World Journal of Chemistry*, *2*(2), 67–74.

Elschner, A., Kirchheyer, S., Lovenich, W., Merker, U., & Reuter, K. (2011). *PEDOT Principles and Applications of an Intrinsically Conductive Polymer*. New York: CRC Press.

Elschner, A., Kirchheyer, S., Lovenich, W., Merker, U., & Reuter, K. (2013). *PEDOT Principles and Applications of an Intrinsically Conductive Polymer* (Vol. 53). New York: CRC Press.

Eriksen, Ø. (2008). The use of microfibrillated cellulose produced from kraft pulp as strength enhancer in TMP paper. *Nordic Pulp and Paper Research Journal*, *23*(3), 299–304.

Eyholzer, C., Bordeanu, N., Lopez-Suevos, F., Rentsch, D., Zimmermann, T., & Oksman, K. (2010). Preparation and characterization of water-redispersible nanofibrillated cellulose in powder form. *Cellulose*, *17*(1), 19–30.

Feng, X. (2015). Nanocarbons for advanced Energy Storage (Vol. 1). Weinheim, Germany: Wiley-VCH.

Firoz Babu, K., Dhandapani, P., Maruthamuthu, S., & Anbu Kulandainathan, M. (2012). One pot synthesis of polypyrrole silver nanocomposite on cotton fabrics for multifunctional property. *Carbohydrate Polymers*, *90*(4), 1557–1563.

Freund, M. S., & Deore, B. (2007). Self-doped conducting polymers. John Wiley & Sons.

Fu, H., Du, Z., Zou, W., Li, H., & Zhang, C. (2013). Carbon nanotube reinforced polypyrrole nanowire network as a high-performance supercapacitor electrode. *Journal of Materials Chemistry A*, *1*(47), 14943–14950.

Fu, L., Zhang, J., & Yang, G. (2013). Present status and applications of bacterial cellulose-based materials for skin tissue repair. *Carbohydrate Polymers*, *92*(2), 1432–1442.

Fukuzumi, H. (2012). *Studies on structures and properties of TEMPO-oxidized cellulose nanofibril films*. University of Tokyo, Japan.

Fukuzumi, H., Saito, T., Iwata, T., Kumamoto, Y., & Isogai, A. (2009). Transparent and high gas barrier films of cellulose nanofibers prepared by TEMPO-mediated oxidation. *Biomacromolecules*, *10*(1), 162–165.

Gama, M., Gatenholm, P., & Klemm, D. (2013). *Bacterial NanoCellulose*. New York: CRC Press.

Gao, K., Shao, Z., Wang, X., Zhang, Y., Wang, W., & Wang, F. (2013). Cellulose nanofibers/multi-walled carbon nanotube nanohybrid aerogel for all-solid-state flexible supercapacitors. *RSC Advances*, *3*(35), 15058–15064.

Gea, S., Bilotti, E., Reynolds, C. T., Soykeabkeaw, N., & Peijs, T. (2010). Bacterial cellulose-poly(vinyl alcohol) nanocomposites prepared by an in-situ process. *Materials Letters*, *64*(8), 901–904.

Gea, S., Torres, F. G., Troncoso, O. P., Reynolds, C. T., Vilasecca, F., Iguchi, M., & Peijs, T. (2007). Biocomposites based on bacterial cellulose and apple and radish pulp. *International Polymer Processing*, *22*(5), 497–501.

Gelin, K., Bodin, A., Gatenholm, P., Mihranyan, A., Edwards, K., & Strømme, M. (2007). Characterization of water in bacterial cellulose using dielectric spectroscopy and electron microscopy. *Polymer*, *48*(26), 7623–7631.

Groenendaal, B. L. B., Jonas, F., Freitag, D., Pielartzik, H., & Reynolds, J. R. (2000). Poly(3,4-ethylenedioxythiophene) and Its Derivatives : Past , Present , and Future. *Advanced Materials*, *12*, 481–494.

Guldi, D. M., & Martín, N. (2010). *Carbon Nanotubes and Related Structures: Synthesis, Characterization, Functionalization, and Applications*. Weinheim, Germany: Wiley-VCH.

Hamedi, M. M., Hajian, A., Fall, A. B., Hkansson, K., Salajkova, M., Lundell, F., Berglund, L. a. (2014). Highly conducting, strong nanocomposites based on nanocellulose-assisted aqueous dispersions of single-wall carbon nanotubes. *ACS Nano*, *8*(3), 2467–2476.

Henriksson, M., Fogelström, L., Berglund, L. A., Johansson, M., & Hult, A. (2011). Novel nanocomposite concept based on cross-linking of hyperbranched polymers in reactive cellulose nanopaper templates. *Composites Science and Technology*, *71*(1), 13–17.

Henriksson, M., Henriksson, G., Berglund, L. a., & Lindström, T. (2007). An environmentally friendly method for enzyme-assisted preparation of microfibrillated cellulose (MFC) nanofibers. *European Polymer Journal*, *43*(8), 3434–3441.

Henrique, P., Camargo, C., Satyanarayana, K. G., & Wypych, F. (2009). Nanocomposites : Synthesis , Structure , Properties and New Application Opportunities. *Material Research*, *12*(1), 1–39.

Hermant, M. C. (2009). Manipulating the Percolation Threshold of Carbon Nanotubes in Polymeric Comosites. Eindhoven University of Technology, Netherland.

Hestrin, S., & Schramm, M. (1954). Synthesis of cellulose by Acetobacter xylinum. II. Preparation of freeze-dried cells capable of polymerizing glucose to cellulose. *The Biochemical Journal*, *58*(2), 345–52.

Hinestroza, J. (2014). Cellulose Based Composites New Green Nanomaterials. Wiley-VCH.

Hirota, M., Tamura, N., Saito, T., & Isogai, A. (2012). Cellulose II nanoelements prepared from fully mercerized,.pdf. *Cellulose*, *19*, 435–442.

Hirsch, A. (2002). Functionalization of single-walled carbon nanotubes. *Angewandte Chemie - International Edition*, *41*(11), 1853–1859.

Hoenich, N. (2006). Cellulose for medical applications: past, present, and future. *BioResources*, *1*(2), 270–280.

Huang, B., Kang, G. J., & Ni, Y. (2006). Preparation of conductive paper by in-situ polymerization of pyrrole in a pulp fibre system. *Conductive Papers*, *2*, 38–42.

Huang, J., Zhu, H., Chen, Y., Preston, C., Rohrbach, K., Cumings, J., & Hu, L. (2013). Highly transparent and flexible nanopaper transistors. *ACS Nano*, *7*(3), 2106–2113.

Hung, N. T., Anoshkin, I. V., Dementjev, a. P., Katorov, D. V., & Rakov, E. G. (2008). Functionalization and solubilization of thin multiwalled carbon nanotubes. *Inorganic Materials*, *44*(3), 219–223.

Inzelt, G. (2012). Conducting Polymers A New Era in Electrochemistry. (F. Scholz, Ed.) (second). Berlin, Germany: Springer.

Ioelovich, M. (2008). Cellulose as a nanostructured polymer: A short review. *BioResources*, *3*(4), 1403–1418.

Isogai, A., & Kata, Y. (1998). Preparation of polyuronic acid from cellulose by TEMPO-

mediated oxidation. *Cellulose*, *6*, 153–164.
Isogai, A., Saito, T., & Fukuzumi, H. (2011). TEMPO-oxidized cellulose nanofibers. *Nanoscale*, *3*(1), 71–85.
Isogai, T., Saito, T., & Isogai, A. (2010). TEMPO electromediated oxidation of some polysaccharides including regenerated cellulose fiber. *Biomacromolecules*, *11*(6), 1593–9.
Jeon, G., Yang, S. Y., & Kim, J. K. (2012). Functional nanoporous membranes for drug delivery. *Journal of Materials Chemistry*, *22*, 14814–14834.
Jiang, Q., Liu, C., Song, H., Xu, J., Mo, D., Shi, H., Zhu, Z. (2014). Free-standing PEDOT: PSS film as electrode for the electrodeposition of bismuth telluride and its thermoelectric performance. *International Journal of Electrochemical Science*, *9*(12), 7540–7551.
Johnston, J. H., Kelly, F. M., Moraes, J., Borrmann, T., & Flynn, D. (2006). Conducting polymer composites with cellulose and protein fibres. *Current Applied Physics*, *6*(3), 587–590.
Jung, R., Kim, H. S., Kim, Y., Kwon, S. M., Lee, H. S., & Jin, H. J. (2007). Electrically Conductive Transparent Paper Using Multiwalled Carbon Nanotubes. *Journal of Polymer Science Part B: Polymer Physics*, *46*, 1235–1242.
Kalia, S., Dufresne, A., Cherian, B. M., Kaith, B. S., Avérous, L., Njuguna, J., & Nassiopoulos, E. (2011). Cellulose-based bio- and nanocomposites: A review. *International Journal of Polymer Science*, *2011*, 1–35.
Kargarzadeh, H., Ahmad, I., Abdullah, I., Dufresne, A., Zainudin, S. Y., & Sheltami, R. M. (2012). Effects of hydrolysis conditions on the morphology, crystallinity, and thermal stability of cellulose nanocrystals extracted from kenaf bast fibers. *Cellulose*, *19*(3), 855–866.
Karlisch, D., Hessler, N., Sultanova, B., Klemm, D., Erdmann, R., Schmidt, W., Mueller, F. (2011). HoLiR: Continuous generation of planar bacteria-produced nanocellulose. *Am. Chem. Soc*.
Khan, S., Ul-Islam, M., Khattak, W. A., Ullah, M. W., & Park, J. K. (2015). Bacterial cellulose-poly(3,4-ethylenedioxythiophene)-poly(styrenesulfonate) composites for optoelectronic applications. *Carbohydrate Polymers*, *127*, 86–93.
Koga, H., Nogi, M., Komoda, N., Nge, T. T., Sugahara, T., & Suganuma, K. (2014). Uniformly connected conductive networks on cellulose nanofiber paper for transparent paper electronics. *NPG Asia Materials*, *6*, 1–8.
Koga, H., Saito, T., Kitaoka, T., Nogi, M., Suganuma, K., & Isogai, A. (2013). Transparent, conductive, and printable composites consisting of TEMPO-oxidized nanocellulose and carbon nanotube. *Biomacromolecules*, *14*(4), 1160–1165.
Krueger, A. (2010). Carbon Materials and Nanotechnology. Weinheim: Wiley-VCH.
Kumar T, V. (2015). Nanocellulose polymer nanocomposites: funadamentals and applications, Wiley.
Lavoine, N., Desloges, I., Dufresne, A., & Bras, J. (2012). Microfibrillated cellulose – Its barrier properties and applications in cellulosic materials: A review. *Carbohydrate Polymers*, *90*(2), 735–764.
Lay, M., Méndez, J. A., Delgado-Aguilar, M., Bun, K. N., & Vilaseca, F. (2016). Strong and electrically conductive nanopaper from cellulose nanofibers and polypyrrole. *Carbohydrate Polymers*.
Lee, K. Y., Tammelin, T., Schulfter, K., Kiiskinen, H., Samela, J., & Bismarck, A. (2012). High performance cellulose nanocomposites: Comparing the reinforcing ability of bacterial cellulose and nanofibrillated cellulose. *ACS Applied Materials and Interfaces*, *4*(8), 4078–4086.
Lee, S. Y., & Boo, B. H. (1996). Molecular Structures and Vibrational Spectra of Pyrrole and Carbazole by Density Functional Theory and Conventional ab Initio Calculations. *The*

Journal of Physical Chemistry, *100*(37), 15073–15078.
Letheby, H. (1862). On the production of a blue substance by the electrolysis of sulphate of aniline. *J. Chem. Soc.*, *15*, 161–163.
Li, J., Ma, P. C., Chow, W. S., To, C. K., Tang, B. Z., & Kim, J. K. (2007). Correlations between percolation threshold, dispersion state, and aspect ratio of carbon nanotubes. *Advanced Functional Materials*, *17*(16), 3207–3215.
Li, X., & Zhitomirsky, I. (2013). Electrodeposition of polypyrrole-carbon nanotube composites for electrochemical supercapacitors. *Journal of Power Sources*, *221*, 49–56.
Li, Y., Hu, X., Zhou, S., Yang, L., Yan, J., Sun, C., & Chen, P. (2014). A facile process to produce highly conductive poly(3,4-ethylenedioxythiophene) films for ITO-free flexible OLED devices. *J. Mater. Chem. C*, *2*(5), 916–924.
Lin, N., & Dufresne, A. (2014). Nanocellulose in biomedicine : Current status and future prospect. *European Polymer Journal*, *59*, 302–325.
Lin, Y., Cho, J., Tompsett, G. a, Westmoreland, P. R., & Huber, G. W. (2009). Kinetics and Mechanism of Cellulose Pyrolysis. *Physical Chemistry*, *113*(January), 20097–20107.
Loos, M. (2015). *Carbon Nanotube Reinforced Composites*. MA: Elsevier.
Lu, P., & Hsieh, Y.-L. (2010). Multiwalled Carbon Nanotube (MWCNT) Reinforced Cellulose Fibers by Electrospinning. *ACS Applied Materials & Interfaces*, *2*(8), 2413–2420.
Luo, Y., Zhang, J., Li, X., Liao, C., & Li, X. (2014). The Cellulose Nanofibers for Optoelectronic Conversion and Energy Storage. *Journal of Nanomaterials*, *2014*, 1–13.
Machida, S., Miyata, S., & Techagumpuch, A. (1989). Chemical synthesis of highly electrically conductive polypyrrole. *Synthetic Metals*, *31*(3), 311–318.
Marquis, D. M., Guillaume, É., & Chivas-joly, C. (2005). Properties of Nano fillers in Polymer. In *Nanocomposites and polymers with analytical method*, INTECH.
Meng, C., Liu, C., Chen, L., Hu, C., & Fan, S. (2010). Highly flexible and all-solid-state paperlike polymer supercapacitors. *Nano Letters*, *10*(10), 4025–4031.
Miao, C., & Hamad, W. Y. (2013). Cellulose reinforced polymer composites and nanocomposites : a critical review. *Cellulose*, *20*, 2221–2262.
Monte, R. S., Kotzebue, L. R. V., Alexandre, D. L., Furtado, R. F., Santos, J. A. C., Dantas, J. D. P., & Alves, C. R. (2014). Morphological and Electrochemical Characteristics of Electrosynthesized PPy/CD Composite. *Journal of the Brazilian Chemical Society*, *25*(3), 597–601.
Müllen, K., Reynolds, J. R., & Masuda, T. (2014). Conjugated Polymers A Practical Guide to Synthesis. UK: Royal Society of Chemistry.
Müller, D., Rambo, C. R., Porto, L. M., Schreiner, W. H., & Barra, G. M. O. (2013). Structure and properties of polypyrrole/bacterial cellulose nanocomposites. *Carbohydrate Polymers*, *94*(1), 655–662.
Nakagaito, a. N., & Yano, H. (2004). The effect of morphological changes from pulp fiber towards nano-scale fibrillated cellulose on the mechanical properties of high-strength plant fiber based composites. *Applied Physics A: Materials Science & Processing*, *78*(4), 547–552.
Nyholm, L., Nyström, G., Mihranyan, A., & Strømme, M. (2011). Toward Flexible Polymer and Paper-Based Energy Storage Devices. *Advanced Materials*, *23*, 3751–3769.
Nystrom, G. (2012). *Nanocellulose and Polypyrrole Composites for Electrical Energy Storage*. Uppsala University.
Nyström, G., Mihranyan, A., Razaq, A., Lindström, T., Nyholm, L., & Strømme, M. (2010). A nanocellulose polypyrrole composite based on microfibrillated cellulose from wood. *The Journal of Physical Chemistry. B*, *114*(12), 4178–4182.
Nyström, G., Strømme, M., Sjödin, M., & Nyholm, L. (2012). Rapid potential step charging of paper-based polypyrrole energy storage devices. *Electrochimica Acta*, *70*, 91–97.

Oksman, K., Mathew, A. P., Pia Qvintus, A. B., Rojas, O., & Sain, M. (2014). Handbook of Green Materials, Bionanomaterials*: separation processes, characterization and properties Vol.5*. World Scienctific.

Pandey, J. K., Takagi, H., Kakagaito, A. N., & Kim, H. (Eds.). (2015). Handbook of Polymer Nanocomposites. *Processing, Performance and Application* (first edit, Vol. C: Polymer). New York: Springer.

Peng, C., Jin, J., & Chen, G. Z. (2007). A comparative study on electrochemical co-deposition and capacitance of composite films of conducting polymers and carbon nanotubes. *Electrochimica Acta*, *53*(2), 525–537.

Poletto, M., Pistor, V., & Zattera, A. J. (2013). Structural Characteristics and Thermal Properties of Native Cellulose. *Cellulose – Fundamental Aspects*, 45–68.

Rajwade, J. M., Paknikar, K. M., & Kumbhar, J. V. (2015). Applications of bacterial cellulose and its composites in biomedicine. *Applied Microbiology and Biotechnology*, ASAP.

Rambo, C. R., Recouvreux, D. O. S., Carminatti, C. A., Pitlovanciv, A. K., Antônio, R. V., & Porto, L. M. (2008). Template assisted synthesis of porous nanofibrous cellulose membranes for tissue engineering. *Materials Science and Engineering C*, *28*(4), 549–554.

Saba, N., Tahir, P., & Jawaid, M. (2014). A Review on Potentiality of Nano Filler/Natural Fiber Filled Polymer Hybrid Composites. *Polymers*, *6*, 2247–2273.

Saito, T., & Isogai, A. (2004). TEMPO-mediated oxidation of native cellulose. The effect of oxidation conditions on chemical and crystal structures of the water-insoluble fractions. *Biomacromolecules*, *5*(5), 1983–1989.

Saito, T., Kimura, S., Nishiyama, Y., & Isogai, A. (2007). Cellulose nanofibers prepared by TEMPO-mediated oxidation of native cellulose. *Biomacromolecules*, *8*(8), 2485–2491.

Saito, T., Nishiyama, Y., Putaux, J.-L., Vignon, M., & Isogai, A. (2006). Homogeneous suspensions of individualized microfibrils from TEMPO-catalyzed oxidation of native cellulose. *Biomacromolecules*, *7*(6), 1687–91.

Salajkova, M., Valentini, L., Zhou, Q., & Berglund, L. A. (2013). Tough nanopaper structures based on cellulose nanofibers and carbon nanotubes. *Composites Science and Technology*, *87*, 103–110.

Salas, C., Nypelö, T., Rodriguez-Abreu, C., Carrillo, C., & Rojas, O. J. (2014). Nanocellulose properties and applications in colloids and interfaces. *Current Opinion in Colloid and Interface Science*, *19*(5), 383–396.

Sasso, C., Zeno, E., Petit-Conil, M., Chaussy, D., Belgacem, M. N., Tapin-Lingua, S., & Beneventi, D. (2010). Highly Conducting Polypyrrole/Cellulose Nanocomposite Films with Enhanced Mechanical Properties. *Macromolecular Materials and Engineering*, *295*(10), 934–941.

Saville, P. (2005). *Polypyrrole Formation and Use*. *DRDC Atlantic TM, Canada* (Vol. 4).

Sehaqui, H., Allais, M., Zhou, Q., & Berglund, L. a. (2011). Wood cellulose biocomposites with fibrous structures at micro- and nanoscale. *Composites Science and Technology*, *71*(3), 382–387.

Seo, J.-H., Chang, T.-H., Lee, J., Sabo, R., Zhou, W., Cai, Z., Ma, Z. (2015). Microwave flexible transistors on cellulose nanofibrillated fiber substrates. *Applied Physics Letters*, *106*, 262101.

Shirakawa, H., Louis, E. J., MacDiarmid, A. G., Chiang, C. K., & Heeger, A. J. (1977). Synthesis of electrically conducting organic polymers: halogen derivatives of polyacetylene, (CH)x. *Journal of the Chemical Society, Chemical Communications*, (16), 578.

Siró, I., & Plackett, D. (2010). Microfibrillated cellulose and new nanocomposite materials: a review. *Cellulose*, *17*(3), 459–494.

Skotheim, T. A., & Reynolds, J. R. (Eds.). (2007). Handbook of Conducting Polymers

Conjugated polymers: *Theory, Synthesis, Properties, and Characterization* (third). New york: CRC Press.

Snook, G. a., Kao, P., & Best, A. S. (2011). Conducting-polymer-based supercapacitor devices and electrodes. *Journal of Power Sources*, *196*(1), 1–12.

Soni, B., Hassan, E. B., & Mahmoud, B. (2015). Chemical isolation and characterization of different cellulose nanofibers from cotton stalks. *Carbohydrate Polymers*, *134*, 581–589.

Spence, K. L., Venditti, R. a., Rojas, O. J., Habibi, Y., & Pawlak, J. J. (2011). A comparative study of energy consumption and physical properties of microfibrillated cellulose produced by different processing methods. *Cellulose*, *18*(4), 1097–1111.

Šupová, M., Martynková, G. S., & Barabaszová, K. (2011). Effect of Nanofillers Dispersion in Polymer Matrices: A Review. *Science of Advanced Materials*, *3*(1), 1–25.

Surma-Ślusarska, B., Presler, S., & Danielewicz, D. (2008). Characteristics of bacterial cellulose obtained from Acetobacter Xylinum culture for application in papermaking. *Fibres and Textiles in Eastern Europe*, *16*(4), 108–111.

Svensson, A., Nicklasson, E., Harrah, T., Panilaitis, B., Kaplan, D. L., Brittberg, M., & Gatenholm, P. (2005). Bacterial cellulose as a potential scaffold for tissue engineering of cartilage. *Biomaterials*, *26*(4), 419–431.

Tammela, P., Wang, Z., Frykstrand, S., Zhang, P., Sintorn, I.-M., Nyholm, L., & Strømme, M. (2015). Asymmetric supercapacitors based on carbon nanofibre and polypyrrole/nanocellulose composite electrodes. *RSC Adv.*, *5*(21), 16405–16413.

Tang, L., Han, J., Jiang, Z., Chen, S., & Wang, H. (2015). Flexible conductive polypyrrole nanocomposite membranes based on bacterial cellulose with amphiphobicity. *Carbohydrate Polymers*, *117*, 230–235.

Thakur, V. K., & Thakur, M. K. (2016). Chemical functionalization of carbon nanomaterials chemistry and applications. New York: CRC Press.

Trchova, M., & Kova, J. (2003). Synthesis and structural study of polypyrroles prepared in the presence of surfactants. *Synthetic Metals*, *138*, 447–455.

Turbak, A. F., Snyder, F. W., & Sandberg, K. R. (1983). Microfibrillated cellulose, a new cellulose product: properties, uses, and commercial potential. *J. Appl. Polym. Sci.: Appl. Polym. Symp.; 37 (*United States*)*.

Ul-Islam, M., Khattak, W. A., Kang, M., Kim, S. M., Khan, T., & Park, J. K. (2013). Effect of post-synthetic processing conditions on structural variations and applications of bacterial cellulose. *Cellulose*, *20*(1), 253–263.

Vijay, K. T., & Thakur, M. K. (2015). Eco-friendly polymer nanocomposites. Vol 75 *Advanced Structured Materials*, Springer.

Vijay Kumar Thakur. (2015). *Nanocellulose Polymer Nanocomposites: Fundamentals and Applications*. MA: Wiley.

Walker, J. A., Warren, L. F., & Witucki, E. F. (1988). New chemically prepared conducting "pyrrole blacks." *Journal of Polymer Science Part A: Polymer Chemistry*, *26*(5), 1285–1294.

Wang, H., Bian, L., Zhou, P., Tang, J., & Tang, W. (2012). Core–sheath structured bacterial cellulose/polypyrrole nanocomposites with excellent conductivity as supercapacitors. *Journal of Materials Chemistry A*, *1*(3), 578–584.

Wang, J., Xu, Y., Chen, X., & Du, X. (2007). Electrochemical supercapacitor electrode material based on poly(3,4-ethylenedioxythiophene)/polypyrrole composite. *Journal of Power Sources*, *163*(2), 1120–1125.

Wang, L.-X., Li, X.-G., & Yang, Y.-L. (2001). Preparation, properties and applications of polypyrroles. *Reactive and Functional Polymers*, *47*, 125–139.

Wang, M., Anoshkin, I. V., Nasibulin, A. G., Korhonen, J. T., Seitsonen, J., Pere, J., Ikkala, O. (2013). Modifying Native Nanocellulose Aerogels with Carbon Nanotubes for Mechanoresponsive Conductivity and Pressure Sensing. *Advanced Materials*, *25*(17),

2428–2432.
Wang, Z., Carlsson, D. O., Tammela, P., Hua, K., Zhang, P., Nyholm, L., & Strømme, M. (2015). Surface Modified Nanocellulose Fibers Yield Conducting Polymer-Based Flexible Supercapacitors with Enhanced Capacitances. *ACS Nano*, *9*(7), 7563–7571.
Wang, Z. H., Tammela, P., Zhang, P., Stromme, M., & Nyholm, L. (2014). Efficient high active mass paper-based energy-storage devices containing free-standing additive-less polypyrrole-nanocellulose electrodes. *Journal of Materials Chemistry A*, *2*, 7711–7716.
Wang, Z., Tammela, P., Huo, J., Zhang, P., Stromme, M., & Nyholm, L. (2016). Solution-processed poly(3,4-ethylenedioxythiophene) nanocomposite paper electrodes for high-capacitance flexible supercapacitors. *J. Mater. Chem. A*, *4*(5), 1714–1722.
Wang, Z., Tammela, P., Zhang, P., Strømme, M., & Nyholm, L. (2014). Efficient high active mass paper-based energy-storage devices containing free-standing additive-less polypyrrole–nanocellulose electrodes. *Journal of Materials Chemistry A*, *2*(21), 7711.
Wei, B., Yang, G., & Hong, F. (2011). Preparation and evaluation of a kind of bacterial cellulose dry films with antibacterial properties. *Carbohydrate Polymers*, *84*(1), 533–538.
Wippermann, J., Schumann, D., Klemm, D., Kosmehl, H., Salehi-Gelani, S., & Wahlers, T. (2009). Preliminary Results of Small Arterial Substitute Performed with a New Cylindrical Biomaterial Composed of Bacterial Cellulose. *European Journal of Vascular and Endovascular Surgery*, *37*(5), 592–596.
Xiong, P., Zhu, J., & Wang, X. (2015). Recent advances on multi-component hybrid nanostructures for electrochemical capacitors. *Journal of Power Sources*, *294*, 31–50.
Xu, J., Zhu, L., Bai, Z., Liang, G., Liu, L., Fang, D., & Xu, W. (2013). Conductive polypyrrole-bacterial cellulose nanocomposite membranes as flexible supercapacitor electrode. *Organic Electronics: Physics, Materials, Applications*, *14*(12), 711–718.
Yan Huang, Y., & M. Terentjev, E. (2012). Dispersion of Carbon Nanotubes: Mixing, Sonication, Stabilization, and Composite Properties. *Polymers*, *4*, 275–295.
Yano, H. (2011). The cellulose sub-elementary fibril in plants is the most abundant nanomaterial on Earth. Kyoto University, Japan. http://people.forestry.oregonstate.edu/john-simonsen/research-areas
Yellampalli, S. (2011). Carbon nanotubes – polymer nanocomposites. Rijeka, Croatia: INTECH.
Yu, G., Xie, X., Pan, L., Bao, Z., & Cui, Y. (2013). Hybrid nanostructured materials for high-performance electrochemical capacitors. *Nano Energy*, *2*(2), 213–234.
Yu, R., Chen, L., Liu, Q., Lin, J., Tan, K. L., Ng, S. C., Andy, H. T. S. (1998). Platinum Deposition on Carbon Nanotubes via Chemical Modifica tion. *American Chemical Society*, *10*(3), 718–722.
Zaborowska, M., Bodin, A., Bäckdahl, H., Popp, J., Goldstein, A., & Gatenholm, P. (2010). Microporous bacterial cellulose as a potential scaffold for bone regeneration. *Acta Biomaterialia*, *6*(7), 2540–2547.
Zare, E. N., Lakouraj, M. M., Moghadam, P. N., & Azimi, R. (2013). Novel Polyfuran/ Functionalized Multiwalled Carbon Nanotubes Composites With Improved Conductivity : Chemical Synthesis , Characterization , and Antioxidant Activity. *Polymer Composites*, *34*(5), 732–739.
Zhang, H., Cao, G., & Yang, Y. (2009). Carbon nanotube arrays and their composites for electrochemical capacitors and lithium-ion batteries. *Energy & Environmental Science*, *2*, 932–943.
Zhang, Y., Nypelö, T., Salas, C., Arboleda, J., Hoeger, I. C., & Rojas, O. J. (2013). Cellulose Nanofibrils: From Strong Materials to Bioactive Surfaces. *Journal of Renewable Materials*, *1*(3), 195–211.
Zheng, G., Cui, Y., Karabulut, E., Wågberg, L., Zhu, H., & Hu, L. (2013). Nanostructured

paper for flexible energy and electronic devices. *MRS Bulletin*, *38*(4), 320–325.
Zhu, Z., Song, H., Xu, J., Liu, C., Jiang, Q., & Shi, H. (2015). Significant conductivity enhancement of PEDOT:PSS films treated with lithium salt solutions. *Journal of Materials Science: Materials in Electronics*, *26*(1), 429–434.

7. ANNEX: PUBLICATIONS AND MANUSCRIPTS

PAPER I

Strong and electrically conductive nanopaper from cellulose nanofibers and polypyrrole

Makara Lay, J. Alberto Méndez, Marc Delgado-Aguilar, Kim Ngun Bun, Fabiola Vilaseca

Carbohydrate Polymers 152 (2016) 361–369

Carbohydrate Polymers 152 (2016) 361–369

Contents lists available at ScienceDirect

Carbohydrate Polymers

journal homepage: www.elsevier.com/locate/carbpol

Strong and electrically conductive nanopaper from cellulose nanofibers and polypyrrole

Makara Lay[a,b], J. Alberto Méndez[a], Marc Delgado-Aguilar[a], Kim Ngun Bun[b], Fabiola Vilaseca[a,*]

[a] LEPAMAP Group, Dept. of Chemical Engineering, Agricultural and Food Technology, University of Girona, C/Maria Aurèlia Capmany 61, 17071 Girona, Spain
[b] Dept. of Geo-resources and Geotechnical Engineering, Institute of Technology of Cambodia, PP Box 86, Russian Conf. Blvd. Phnom Penh, Cambodia

ARTICLE INFO

Article history:
Received 17 May 2016
Accepted 27 June 2016
Available online 11 July 2016

Keywords:
Cellulose nanofibers
Polypyrrole
Conductive nanopaper
Mechanical properties
Electrical conductivity

ABSTRACT

In this work, we prepare cellulose nanopapers of high mechanical performance and with the electrical conductivity of a semiconductor. Cellulose nanofibers (CNF) from bleached softwood pulp were coated with polypyrrole (PPy) via in situ chemical polymerization, in presence of iron chloride (III) as oxidant agent. The structure and morphology of nanopapers were studied, as well as their thermal, mechanical and conductive properties. Nanopaper from pure CNF exhibited a very high tensile response (224 MPa tensile strength and 14.5 GPa elastic modulus). The addition of up to maximum 20% of polypyrrole gave CNF/PPy nanopapers of high flexibility and still good mechanical properties (94 MPa strength and 8.8 GPa modulus). The electrical conductivity of the resulting CNF/PPy nanopaper was of 5.2 10^{-2} S cm^{-1}, with a specific capacitance of 7.4 F g^{-1}. The final materials are strong and conductive nanopapers that can find application as biodegradable flexible thin-film transistor (TFT) or as flexible biosensor.

1. Introduction

The recent development of nanotechnology, together with the global concern for environment, is focusing on the use of bio-resources as alternative to mineral or non-renewable ones (Thakur, 2015). Nowadays, one exciting research area is the isolation and use of nanocelluloses. Cellulose is the most abundant biological raw material that can self-assemble into well-defined architectures at micro and nano scale. Therefore, from their origin, cellulose nanofibers are renewable, inexpensive, and non-toxic. In addition, and due to their chemical structure and high crystallinity, nanocelluloses have and remarkable physical, thermal, and mechanical properties, such as high specific surface area and high elastic modulus (Lavoine, Desloges, Dufresne, & Bras, 2012; Siró & Plackett, 2010). Among the different nanocelluloses, cellulose nanofibers (CNFs) consist of a long web-like structure with micrometer length and 10–100 nm in diameter that imparts unique properties. The isolation of CNFs can be performed by a wide variety of mechanical techniques such as refining, grinding, high pressure homogenization or cryocrushing (Wang, Sain, & Oksman, 2007). Different pre-treatments can also be applied to reduce the energy consumption as well as to modify the surface energy of CNFs (Jonoobi et al., 2015).

In combination with a suitable polymer matrix, cellulose nanofibers networks show considerable potential as effective reinforcement for high-quality bio-based composites. Likewise, their flexibility and high aspect ratio make CNFs outstanding materials for wide range of applications. The last decade, CNFs have been used as nanofillers to reinforce nanocomposites (Miao & Hamad, 2013; Saba, Tahir, & Jawaid, 2014) with thermoplastic and thermoset polymers for packaging products, construction materials, automobiles, furniture, and pharmaceuticals (Hoenich, 2006; Ioelovich, 2008; Jeon, Yang, & Kim, 2012; Kalia et al., 2011; Zhang, Nypelö et al., 2013; Zhang, Zhang et al., 2013). More recently, CNFs have gained much attention for its use as biomedical material because of their exceptional surface chemistry and excellent biological properties (biocompatibility and biodegradability) (Lin & Dufresne, 2014).

Due to their benign nature, high available surface area, smoothness, and reduced porosity, CNF films have been reported as potential substrates for biosensors (Salas, Nypelö, Rodriguez-Abreu, Carrillo, & Rojas, 2014). However, and because of the intrinsic insulating characteristics, specific strategies need to be developed to impart electrical activity to CNF. In this sense, the combination of CNFs with conductive polymers (CPs) allows to extend the functionality of CNFs in energy storage devices, solar

* Corresponding author.
E-mail address: fabiola.vilaseca@udg.edu (F. Vilaseca).

http://dx.doi.org/10.1016/j.carbpol.2016.06.102
0144-8617/

cells or electronic applications (Huang et al., 2013; Koga et al., 2014; Luo, Zhang, Li, Liao, & Li, 2014; Nyholm, Nyström, Mihranyan, & Strømme, 2011; Tammela et al., 2015; Wang et al., 2015; Zheng et al., 2013).

Conducting polymers are attractive candidates because they have good intrinsic conductivity, from a few to 500 S cm^{-1}. CPs are rendered conductive through a conjugated bond system along the polymer backbone. They are typically formed either through chemical oxidation or electrochemical oxidation of the monomer (Snook, Kao, & Best, 2011). In the chemical oxidation process, for example with iron chloride, the molecular weight and structural features of the resulting polymer are feasible to control. Among conducting polymers, polypyrrole (PPy) has an appreciable environmental stability (Buitrago-Sierra, García-Fernández, Pastor-Blas, & Sepúlveda-Escribano, 2013) and is easy to synthesize (Ansari, 2006; Eisazadeh, Engineering, & Box, 2007; Huang, Kang, & Ni, 2006; Trchova & Kova, 2003; Wang, Li, & Yang, 2001). PPy offers a greater degree of flexibility in electrochemical processing than most conducting polymers, and consequently the material has been the subject of much research as a supercapacitor or battery electrode (Snook et al., 2011). In 2006, Huang et al. investigated the in-situ polymerization of pyrrole on different pulp systems demonstrating the good adhesion between the conductive polymer and the fibers (Huang et al., 2006). The specific parameters and the sequence for the polymerization reaction, and their effect on the fiber degradation have also been studied (Beneventi, Alila, Boufi, Chaussy, & Nortier, 2006). Other authors have performed a soaking-polymerization procedure on printing paper (Yuan et al., 2013). In this case, the conductive polymer remained mainly at the surface of the printing paper showing high value of surface electrical conductivity. The viability of coating PPy on CNF was demonstrated by Nyström et al. (2010). They verified the conductivity and the ion-charge capacity of a cellulose nanocomposite with high amount of PPy conductive polymer. In a further work, the authors investigated the mechanical properties of PPy-cellulose nancomposites of different porosity (Carlsson et al., 2012). In a different study (Nyström, Strømme, Sjödin, & Nyholm, 2012), they improved the capacitance of this type of cellulose nanocomposites. Later, Wang et al. (2015) performed surface modification of cellulose nanofibers to produce cellulose-based supercapacitors. The coating of PPy on CNF substrate has reduced moisture content of CNF in nature and also protected against degradation, as PPy is known to be insoluble in most solutions and solvents (Sasso et al., 2010). Carlsson, Mihranyan, Strømme, and Nyholm (2014) found that the individual nanocellulose fibrils should be coated by a thin layer of PPy less than 50 nm of thickness to avoid the problems associated with the low redox reaction rates and poor mechanical properties of nanocomposites.

In the present work, cellulose nanofibers are coated with polypyrrole using $FeCl_3$ as oxidant agent. In previous studies, large amounts of polypyrrole were used to obtain a substantial increase of the electrical activity of cellulose nanofibers. However, as consequence, brittle cellulose-nanocomposites were obtained. In this study, pyrrole was polymerized on cellulose nanofiber surface at certain reaction times to obtain very flexible and strong structures with electrical conductive capacity. The obtained CNF/PPy nanopapers were characterized considering their morphology and their mechanical, thermal and electrical response.

2. Materials and methods

2.1. Materials

Bleached pine pulp from Arauco (Chile) was used as cellulose raw material. The cellulose content of the pulp was 95%. Pyrrole was supplied by Sigma Aldrich and used as received for the chemical synthesis of polypyrrole. The rest of materials, $FeCl_3$, Tween-80, 2,2,6,6-tetramethyl-1-1-piperidinyloxy (TEMPO), sodium bromide (NaBr), sodium hypochlorite (NaOCl), HCl, NaOH, and NaCl were also supplied by Sigma Aldrich and used without further purification. Silver coating 3850 was supplied by Holland shielding system BV, Holland.

2.2. Preparation of CNF suspension

The bleached pine pulp (30 g dry weight) was dispersed in 2 L of distilled water and disintegrated at 6000 rpm for 30 min in a pulper (PAPEL QUIMIA, S.A, SPAIN). From this suspension, CNFs were extracted by means of a TEMPO-mediated oxidation followed by a mechanical homogenization (homogenizer NS1001L PANDA 2K-GEA, Italy). The TEMPO-mediated oxidation was performed at pH 10 (Fukuzumi, Saito, Iwata, Kumamoto, & Isogai, 2009) and the obtained cellulose suspension was diluted to 1 wt% and passed through a high-pressure homogenizer, one time at 300 bar and three times at 600 bar of pressure. As a result, a transparent gel of cellulose nanofibers (CNF) at 1% concentration was obtained and stored at 4 °C prior use.

2.3. Preparation of CNF and CNF/PPy nanopapers

CNF gel was first diluted to 0.2% with distilled water and dispersed by using a sonicator Q700 for 10 min (5 min pulse on, 2 min pulse off, and 5 min pulse on) at 60% of amplitude. Afterwards, the CNF suspension was filtered overnight using a glass filter funnel with a nitrocellulose membrane GSWP29325 (hydrophilic) of 0.22 μm pore-size. After filtering, the nitrocellulose membrane was peeled off and the CNF cake was placed between two pieces of immobile transfer membranes of polyvinylidene fluoride (PVDF) (hydrophobic) of 0.45 μm pore-size to prevent adhesion between sample and membrane. Finally, the samples were dried using a laboratory sheet dryer at a vacuum pressure of −0.6 bar at 92 ± 3 °C for 20 min.

For the preparation of CNF/PPy nanopapers the same filtering procedure was used. Firstly, a dilute suspension of CNF (0.1%, 400 mg of dry weight) was sonicated for 10 min under the same setting conditions described above. This CNF suspension will be later mixed with a solution of pyrrole. For the preparation of the pyrrole solution, 0.1 mL of pyrrole was dissolved in 15 mL of 0.5 M HCl. After stirring the mixture for 3 min using magnetic stirrer, one drop (0.05 mL) of Tween-80 was added and stirred until completely homogenous. Afterwards, the solution of pyrrole was introduced into the above CNF suspension, and the mixture was stirred for 5 min. In order to initiate the polymerization, 0.578 g of $FeCl_3$ in 15 mL of HCl 0.5 M was added drop wise into the suspension. The final mixture was stirred at room temperature for 20, 40, 60, 120, and 180 min, in independent experiments, to get the different conductive nanopapers named as CNF/PPy20, CNF/PPy40, CNF/PPy60, CNF/PPy120, and CNF/PPy180, respectively. At the end, the mixture (CNF and PPy) was filtered using a glass filter and washed subsequently with 500 mL of 0.5 M HCl, 500 mL of 0.1 M NaCl, and 500 mL of distilled water. During the last washing with distilled water, the suspension was sonicated for 2 min to remove any small gas bubbles and to allow a better organization of CNF/PPy nanostructures without undesired side effects, such as crystal structure damage (Ali et al., 2014). Thereafter, the filtration was continued for 3 more hours until there is no residual water. The obtained CNF/PPy was finally dried in sheet dryer for 20 min.

2.4. Characterization of CNF and CNF/PPy nanopapers

The percentages of carbon, hydrogen, and nitrogen were determined by elemental analysis by means of a Perkin Elmer EA2400 series II. The measured amount of nitrogen was used to determine the PPy content in the formulation. The samples (3 mg) were pyrolyzed in helium (He) at a combustion temperature of 925–930 °C. Acetanilide powder (C_8H_9NO) was used as reference.

The FTIR spectrum of CNF/PPy nanopaper was obtain to characterize the absorption peaks of nanopapers after the chemical polymerization. For comparative purpose, FTIR spectra of pyrrole, cellulose nanofibers (CNF) and polypyrrole (PPy) were also recorded. The FTIR was performed using an ALPHA-FTIR spectrometer from Bruker, in the transmission mode in the range of 4000–500 cm^{-1} using 24 scans.

Mechanical properties of nanocomposites were evaluated using tensile test under control conditions of 50% relative humidity at room temperature. The rectangle specimens of CNF nanopaper $(50 \times 5 \times 0.055)$mm and CNF/PPy nanopapers $(50 \times 5 \times (0.07 \pm 0.015))$mm were tested using a Universal Testing Machine HOUNSFIELD, equipped with a 250 N load cell with a crosshead speed of 5 mm/min. These parameters were set according to previous work (Hamedi et al., 2014). Data of at least five specimens were collected to obtain the statistical standard deviation for each sample.

The cross section surfaces of CNF and CNF/PPy nanopapers, as well as the PPy platelet, were observed under a field emission scanning electron microscope (FE-SEM) HITACHI S-4100. The samples from tensile test were coated with gold using a sputter. The images were taken using secondary electron detector at 20 kV accelerating voltage for PPy powder and 12 kV for CNF and CNF/PPy nanopapers to prevent burning the samples.

Dynamic mechanical analysis (DMA) was employed to study the viscoelastic behaviour of CNF and CNF/PPy nanopapers with the changing of temperature, using a DMA/SDTA861e instrument from Mettler Toledo, operating in 3 point bending mode. The isochronal scans were recorded from −100 to 200 °C at a heating rate of 5 °C min^{-1}, at 1 Hz of frequency and 15 μm of amplitude. The sample dimensions were $(5 \times 20 \times (0.07 \pm 0.015))$mm. A reducing force mode was engaged by regulating the static force during the test to minimize creep. The experiment was performed under dry nitrogen (N_2) flow to limit water sorption during experiment.

Thermogravimetric analysis (TGA) was used to determine the lost weight with the temperature and the degradation temperatures of CNF/PPy nanopapers. The samples were heated from 30 to 600 °C at the heating rate of 10 °C min^{-1} using a METTLER TOLEDO ultra micro balance, TGA/DSC. The purge gas was nitrogen with a flowing rate of 40 mL/min.

The electrical conductivity of the obtained nanopapers was determined based on the measurement of the resistance (R) over the length of the specimens using an Agilent 34461A digital multimeter. All CNF/PPy nanopapers were cut into $(5 \times 20 \times (0.075 \pm 0.015))$mm stripes. Silver paint was applied at room temperature at the end of both sides of each sample to ensure good electrical contact with the clip probes. The measurement was done 16 h after the application of silver paint. The conductivity was calculated by equation: $\sigma = (L/R \times w \times d)$, where L, w, and d are length, width, and thickness of the sample, respectively.

Cyclic voltammetry (CV) was carried out with a standard three-electrode electrochemical cell (working electrode), a platinum wire (counter electrode), and a 2 M NaCl-saturated Ag/AgCl electrode (reference electrode) by using a Potentistat/Galvanostat Model 273A Princeton equipment. Cyclic voltammograms were recorded in the potential window of −0.9 to +0.9 V vs Ag/AgCl at different scan rate of 5, 20, 50, 100, and 200 mV s−1. CView and originPro software were used to plot the graphs. The sample dimensions were $(7 \times 15 \times (0.075 \pm 0.015))$mm. The capacitance and specific capacitance were calculated by $C_{sp} = i/(m.v.\Delta V)$, where C_{sp} (F g^{-1}) is the specific capacitance, i is the integration in CV curve, v is the scan rate in mV s^{-1}, m is the mass (g) of electrode material, and ΔV is the potential difference window $\Delta V = 1.8$ V.

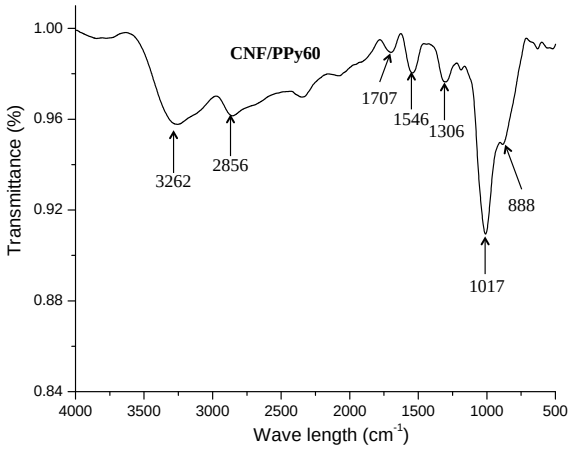

Fig. 1. FT-IR spectrum CNF/PPy60 nanopaper.

3. Results and discussion

Scheme 1 illustrates the intermolecular interaction between CNF chains, and the interaction mechanism between CNF and PPy after the in situ chemical polymerization using $FeCl_3$ as oxidant agent; pictures of CNF gel (Sc. 1a), high transparent CNF nanopaper (Sc. 1b), CNF/PPy nanopaper (Sc. 1c), as well as the high flexibility of CNF/PPy nanopapers (Sc. 1d) are also depicted in Scheme 1. The obtained CNF/PPy nanopapers were flexible black films due to the presence of black precipitated PPy on CNF surface. The yield of PPy (%) at each reaction time is presented in the Supplementary information S1. Likewise, the thickness, density and porosity of each sample are listed in S3.

The FTIR absorption spectrum of CNF/PPy nanopaper is shown in Fig. 1. For comparison, FTIR spectra of cellulose nanofibers (CNF), pyrrole, and polypyrrole are presented in S4. CNF/PPy60 nanopaper exhibited similar spectrum as polypyrrole but with all the major peaks shifted to lower wave number, which supports the existing interaction between —N—H of PPy and C—OH of CNF by means of hydrogen bonding (Firoz Babu, Dhandapani, Maruthamuthu, & Anbu Kulandainathan, 2012). The band at 1707 cm^{-1} is assigned to the C═O bond of carboxylic acid group of CNF in the CNF/PPy nanopaper. Comparing this wavelength with the carboxyl group one of CNF (S4b), the absorption peak has shifted towards higher values, which is representative of the interaction between CNF and the coating PPy. The strong band at 1546 cm^{-1} is characteristic of the C═C stretching of the aromatic ring of PPy. The absorption peaks at 1306 cm^{-1}, 1017 cm^{-1}, and 888 cm^{-1} are assigned to the C – N stretching, C – H stretching and N—H wagging of the polypyrrole ring, respectively. In the region 1300–800 cm^{-1} the absorption peaks corresponding to C—H bending and C—O ethers links for the CNF are also found (see S4).

The stress-strain curves, tensile strength and Young's modulus of neat CNF and CNF/PPy nanopapers are presented in Fig. 2. CNF nanopaper exhibited outstanding tensile strength of 224 MPa and Young's modulus of 14.5 GPa. These values are higher than previous works (González et al., 2014; Sehaqui, Liu, Zhou, & Berglund, 2010), where the nanopapers were produced by means of Rapid

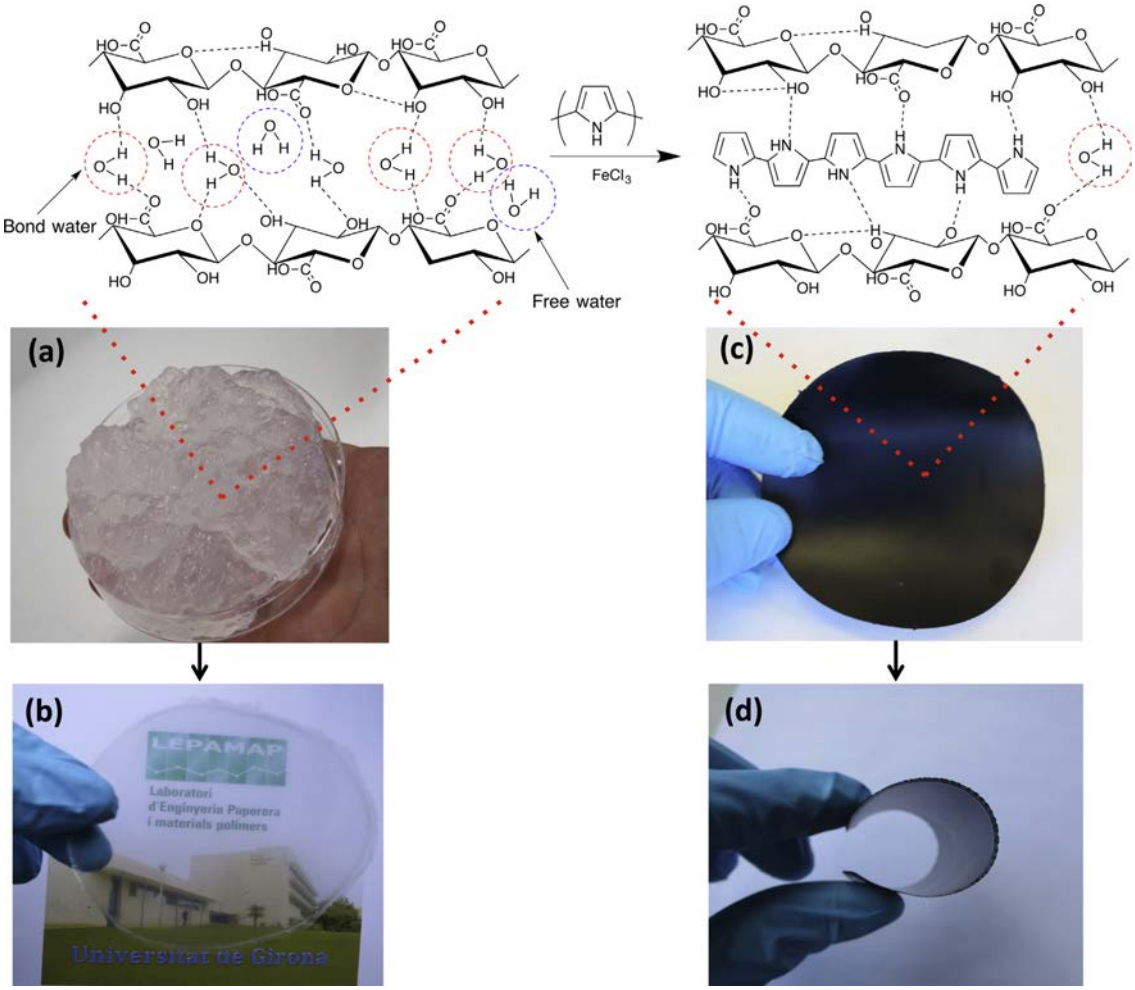

Scheme 1. Interaction between CNF and PPy, and photographs of CNF gel (a), CNF nanopaper (b), CNF/PPy (c), and flexible CNF/PPy nanopaper (d).

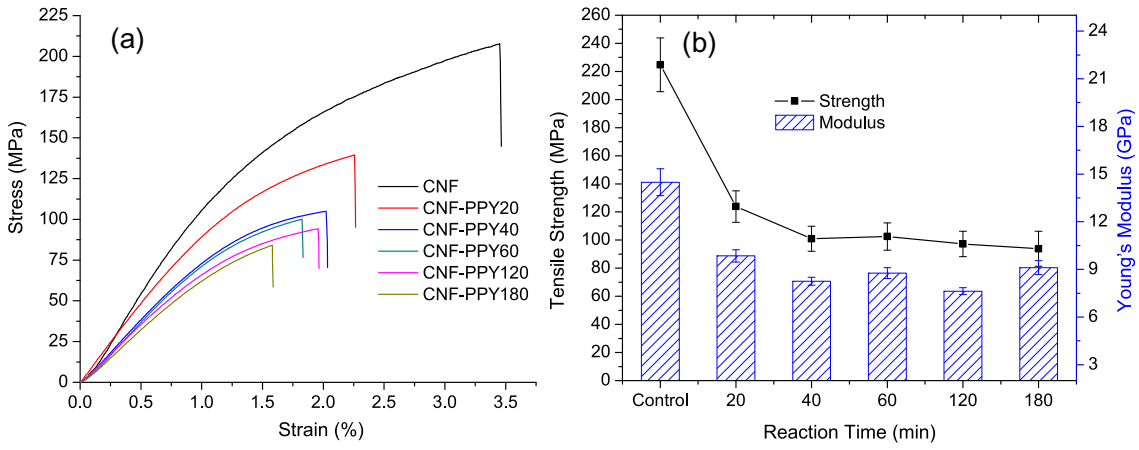

Fig. 2. (a) Stress – strain curves and (b) Tensile strength and Young's modulus of CNF and CNF/PPy nanopapers at different reaction times.

Köthen (sheet dryer). These high mechanical properties are related to the strong interactions between nanofibrils and to the nanofibril entanglements (Boufi, Kaddami, & Dufresne, 2014); some nanofibrils alignment is also expected during the filtration procedure. The sonication step introduced in our methodology helped to remove the possible voids between nanofibrils and provided a homogeneous structure resulting in a low porosity of the final nanopaper, as presented in S2 and S3. Moreover, CNFs from TEMPO mediated oxidation show high nanofibrillation degree and unchanged original crystallinity (Isogai, Saito, & Fukuzumi, 2011), which is responsible of the high mechanical properties of the obtained CNF nanopaper. However, the tensile strength and Young's modulus of CNF/PPy20 decreased to 124 MPa and 8.9 GPa, respectively, and continued to decrease until 94 MPa and 8.8 GPa, respectively, for the CNF/PPy180 nanopaper. Therefore, the incorporation of PPy in the structure produced a reduction in the mechanical properties of the unmodified CNF, with a maximum decrease of 58% for the tensile strength and of 39% for the Young's modulus (CNF/PPy180). As a result, CNF/PPy nanopapers were more brittle than neat CNF nanopaper. The elongation at break also decreased with the incorporation of PPy, from 3.5% for CNF to 1.55% for CNF/PPy180. It is expected that the PPy coated on CNF surface lessened the number of CNF inter-fibril —OH interactions, as the —NH group of pyrrole interacted with the hydroxyl groups of cellulose nanofibrils. The coating of CNF with PPy increased the porosity from 10.45% (CNF) to 19.45% (CNF/PPy180) as shown in S3. The higher porosity caused the premature breaking point of the CNF/PPy nanopapers, showing the decrease in their final tensile strength. In addition, the PPy-coated CNF had fewer CNF interfibrils connections that were responsible of the diminution in the rigidity of the PPy-modified CNF nanopapers. However, CNF/PPy nanopapers still showed considerably high mechanical properties. Moreover, after certain level of PPy coating (after 40 min of reaction time), the strength and the modulus were not very much reduced. Instead, higher content of PPy kept lessening the toughness of the resulting CNF/PPy nanopaper. It is worth mentioning, however, that all CNF/PPy nanopaper showed great flexibility (Sc. 1d) together with these remarkable mechanical properties. The values of the mechanical properties with the thickness, density and porosity of each nanopaper are presented in S3.

To support this, the fracture surfaces of CNF and CNF/PPy nanopapers were observed by FE-SEM (Fig. 3). FE-SEM microph-

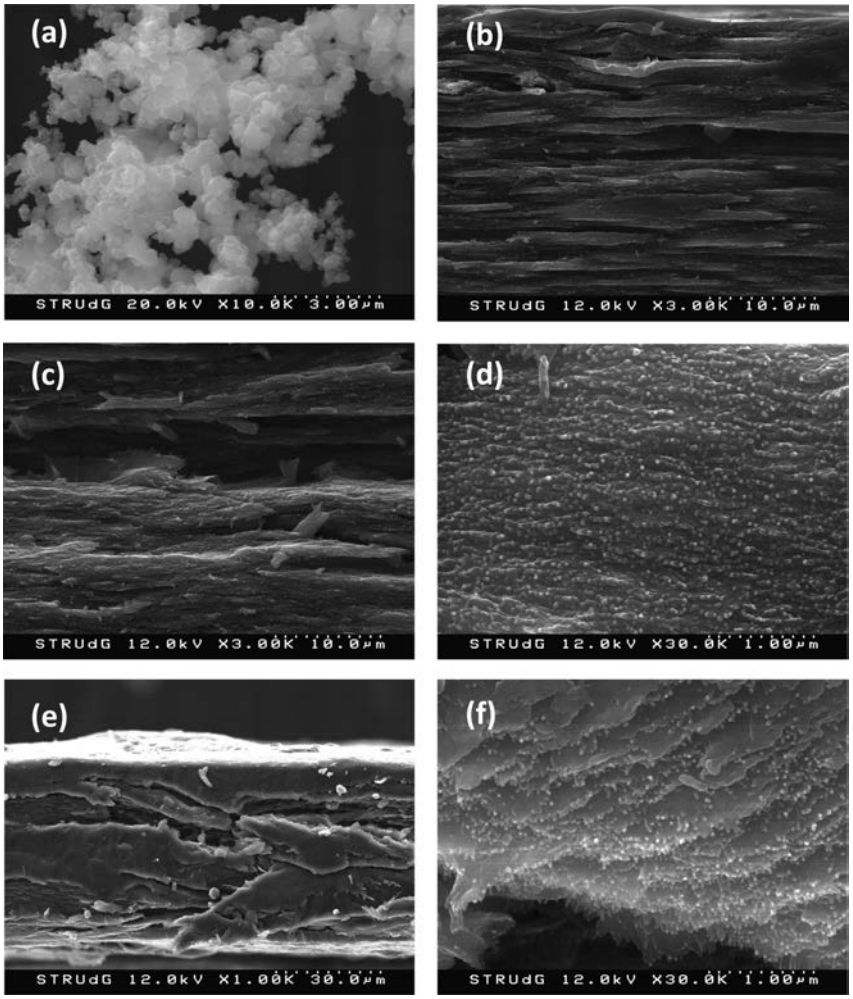

Fig. 3. FE-SEM of (a) PPy platelet; (b) cross-sectional surface of CNF nanopaper; (c and d) CNF/PPy20 nanopaper at magnification of 3000× and 30 000× and (e and f) CNF/PPy120 nanopaper at 1000× and 30 000×.

tograph of PPy platelet is shown in Fig. 3a. PPy tends to agglomerate itself due to strong intermolecular interactions. CNF nanopaper showed a compact multilayer configuration of interconnected cellulose nanofibers (Fig. 3b). This multilayer structure and tight connection between layers contributed to the high mechanical performance of the ensuing pure CNF nanopaper. The multilayer structure was conserved for the PPy-coated CNF nanopaper (Fig. 3c). With the addition of PPy the surface roughness of CNF/PPy nanopaper increased, as the PPy platelets interpenetrated the cellulose nanofibers network. The perfect distribution of PPy within the cellulose nanofiber network is evidenced in Fig. 3d. However, the coating of excess PPy on the CNF surface induced higher roughness, as shown in Fig. 3e. This leaded to a diminish in the mechanical properties because PPy—PPy-bonds has low mechanical properties and the PPy coating reduced the number of CNF—CNF strong bonds (Nyström et al., 2010).

The PPy–PPy interactions are intrinsically weaker than cellulose–cellulose ones (Zhang, Nypelö et al., 2013; Zhang, Zhang et al., 2013) and PPy itself possesses scarce mechanical properties (Sasso et al., 2010). Moreover, the tensile force was applied to parallel layers of CNFs and PPy, resulting in a more brittle nanopaper than the neat CNF nanopaper (Sasso et al., 2010). The microstructure of CNFs (Fig. 3b) shows their fibrils alignment and smoothness at the breaking point. The fibrils were bonded together leading to a strong interface that undergoes to CNF nanopaper with very high mechanical strength. With an excess of polypyrrole on CNF surface (Fig. 3f) all CNFs chains were coated and residual PPy platelet was found, confirming that during the polymerization reaction, not all polypyrrole (—NH) interacted with cellulose nanofibers (—OH).

The thermal mechanical properties of three materials namely neat CNF nanopaper, CNF/PPy20 and CNF/PPy120 nanopapers were studied by DMA. In the test, an oscillating force is applied to a sample and the material's response is analysed. The data presented in Fig. 4 corresponds to the complex modulus ($E^* = E' + iE''$). The complex modulus is composed of real and imaginary terms, equivalent to the storage modulus (E') and loss modulus (E''), respectively. The materials obtained in the present study exhibited mainly an elastic behaviour, with values for storage modulus much higher than the ones for loss modulus ($E' \gg E''$), so then the complex modulus is very similar to the storage modulus ($E^* \approx E'$) (S5). The dynamo-mechanic test started at −100 °C of temperature. Under conditions of low molecular mobility, cellulose composites can be very stiff (Sehaqui, Allais, Zhou, & Berglund, 2011) and, as expected, the modulus decreases with increasing temperature. The complex modulus of our pure CNF nanopaper, at this low temperature, was above 25 GPa and decreased with temperature. The value of the storage modulus indicates how elastic the material is, and ideally would be equivalent to Young's modulus at room temperature. In our case, the complex modulus at 23 °C for CNF, CNF/PPy20, and CNF/PPy120 nanopapers were 15.3, 10.9, and 7.8 GPa, while the Young's modulus from tensile test were 14.5, 9.8, and 8.8 GPa, respectively. This difference can be explained for the experimental methods in determining each value. Young's modulus is calculated from the slope of a line over a range of stresses and strains, whereas the complex modulus (or storage modulus) comes from what can be considered a point on the line. Moreover, the tests methods are very different as one material is constantly stretched in the stress-strain tests, whereas it is oscillated under bending conditions in the dynamic test (Int, 2008). For CNF nanopaper, molecules of cellulose are tightly compressed at −77 °C temperature and at −60 °C temperature for CNF/PPy, which define the solid-state transition in each case (Int, 2008). When the materials are heated up, localized movements and solid chain movements occurred. This represents the gamma transition (Tγ) that involves association with water as cellulose contains some moisture (Int, 2008; Sehaqui et al., 2011). As heating continued, a glass transition was not found for all samples; the native CNFs has no glass transition because of its high degree of crystallinity (Rastogi, Stanssens, & Samyn, 2014). The complex modulus of CNF nanopaper steady diminished with the temperature between 40 °C and 160 °C due to a slippage of crystallites between one another. Conversely, the presence of PPy on CNF surface hindered chain movements making CNF/PPy slowly changed from glassy to rubbery state compared to CNF nanopaper. At the temperature between 40 and 110 °C, CNF/PPy showed the region of rubbery plateau, which is related to physical and chemical cross-link between PPy and CNF chains (Henriksson, Fogelström, Berglund, Johansson, & Hult, 2011). Moreover, above 160 °C, PPy-modified nanopapers showed higher complex modulus than pure CNF nanopaper, telling that PPy improved thermal stability of nanopapers.

The degradation temperatures of CNF, PPy, and CNF/PPy nanopapers were studied by thermogravimetric analysis (Fig. 5a). The initial weight loss of about 7% in the range of 50–105 °C was due to residual moisture present in the samples (Lee et al., 2012). In CNF nanopaper, cellulose pyrolysis started at 201 °C and continued until around 330 °C leading to depolymerization of solid cellulose to form

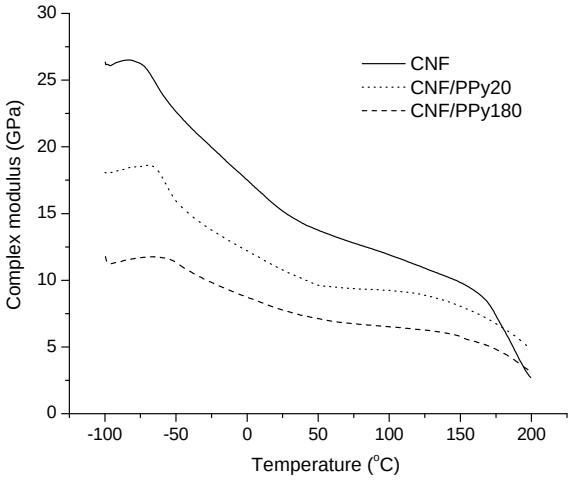

Fig. 4. Complex modulus of CNF and CNF/PPy nanopapers at frequency of 1 Hz.

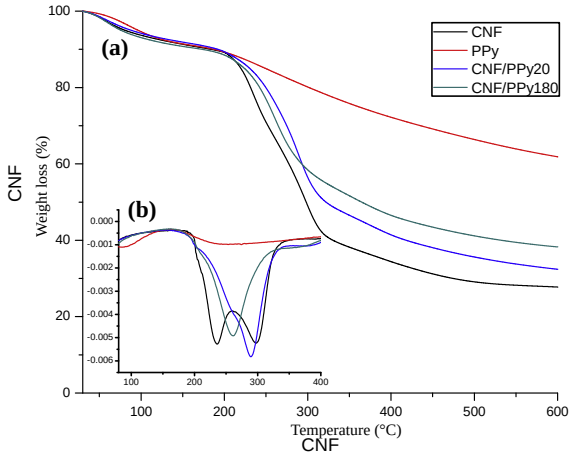

Fig. 5. TGA (a) and DTG (b) of pure CNF nanopaper and CNF/PPy nanopapers as a function of temperature.

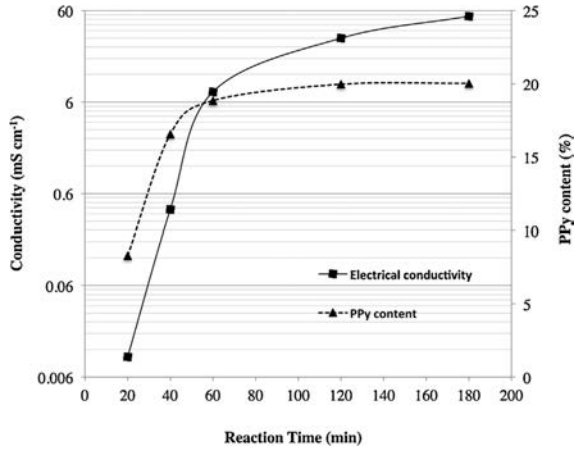

Fig. 6. Electrical conductivity and PPy content in CNF/PPy nanopapers with the different reaction time.

active cellulose and thereafter various anhydro-monosaccharides, retroaldol, dehydrated species, carbon oxides, and char (Lin, Cho, Tompsett, Westmoreland, & Huber, 2009; Nyström et al., 2010). The weight loss for CNF nanopaper was of 61.5% at 330 °C and of 73% at 600 °C, similar to the values found in previous studies (Nyström et al., 2010). In the case of CNF/PPy180 nanopaper, the weight loss between 230 °C and 350 °C was of 31% and of 61.5% at 600 °C. For this nanopaper, the loss was not only a result of the degradation process of the cellulose but also partly because of the thermal degradation of the polymer backbone in polypyrrole. For the polymer itself (PPy), the total weight loss at 600 °C was 42%, following a slow degradation mechanism. One can say that the degradation kinetics of PPy is much slower than the degradation of CNF. PPy degrades in two steps, a degradation process involving the counterions first and the polymer backbone degradation afterwards. The process during which the counterion is expelled occurs before the polymer backbone degradation in PPy and is probably responsible for shifting the main degradation of CNF/PPy to have its maximum degradation temperature at a lower temperature than the one for CNF (Nyström et al., 2010). The values of the maximum degradation temperatures can be seen from the derivative thermogravimetric curves (Fig. 5b). The thermal degradation of CNF from TEMPO-oxidation was broad and consisted of mainly two peaks around 232 °C and 296 °C, both below the degradation point of original cellulose (~310 °C). This confirms the formation of sodium carboxylate groups at the C_6 primary hydroxyls of cellulose. According to literature (Fukuzumi, 2012), the first degradation peak corresponds to the degradation of sodium anhydroglucuronate units, and the second relates to the degradation of cellulose chains containing more unstable anhydroglucuronate units in the crystal surface. The decomposition of PPy was found at 230 °C; therefore, CNF nanopaper with higher amount of PPy showed a decrease in the degradation temperature of the CNF/PPy nanopaper (decomposition temperature of 286 °C for CNF/PPy20 and of 257 °C for CNF/PPy180) (Fig. 5b). The morphology and stability of PPy depend on its composition. Conducting films made with ferric chloride have chloride counterions (dopant), which has a higher mobility than other counterions (Saville, 2005). From the TGA/DTG analysis, it is important to note that PPy coated on cellulose nanofibers decreased the maximum degradation temperature and it slowed the kinetics of the degradation mechanism of the resulting CNF/PPy nanopaper.

The electrical conductivities, together with the results of elemental analysis, are shown in Fig. 6. In situ chemical polymerization of PPy on CNF substrate enhanced electrical properties of CNF. Elemental analysis confirmed the higher amount of PPy on

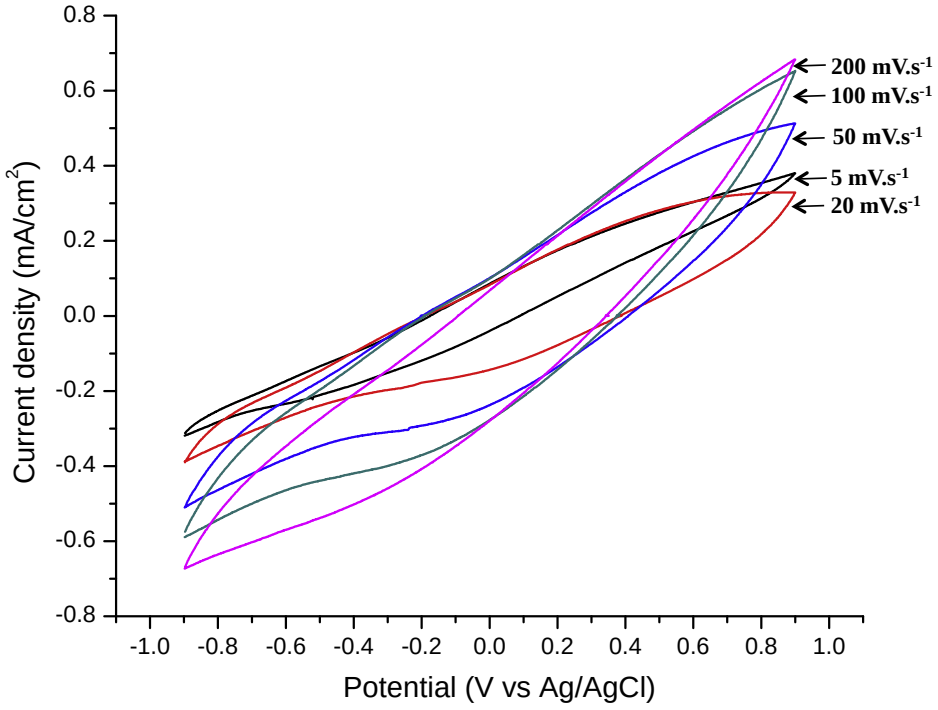

Fig. 7. Cyclic voltammograms of CNF/PPy180 at different scan rate of 5, 20, 50, 100, and 200 mV s^{-1}.

CNF nanofibers with increasing the reaction time. The electrical conductivities of nanopapers depend on the amount of coated PPy. From the results, the electrical conductivity of CNF/PPy20 was 10^{-5} S cm^{-1}, which is already similar to that of silicon ($1.5\ 10^{-5}$ S cm^{-1}), and reached up to $5.2\ 10^{-2}$ S cm^{-1} for the CNF/PPy180 nanopaper, at the level of other semiconductors. Considering the insulating property of cellulose nanofibers (between 10^{-13}–10^{-8} S cm^{-1}, depending on moisture content), the addition of a very low content of PPy filler (only 8%) turned the PPy-modified CNF nanopapers in a semi-conductor material, thanks to the uniformly connected conductive networks on cellulose nanofibers surface during the filtering and drying process (Koga et al., 2014). The amount of polypyrrole in the nanopaper steadily increased with the reaction, whereas the conductivity improved dramatically. The electrical conductivity was enlarged 2 orders of magnitude with only 18% of PPy, and one more order of magnitude above with only 20% PPy. The increase in porosity leads to a better-bonded structure, resulting in higher electrical conductivity (S3).

The electrochemical properties of the conducting CNF/PPy180 were determined by cyclic voltammetry in 2 M NaCl electrolyte. Fig. 7 depicts different scan rate of 5, 20, 50, 100, and 200 mV s^{-1} of CNF/PPy180 in the potential window between −0.9 and +0.9 V (vs. Ag/AgCl). All the curves are elliptical, with increased current upon increasing the scan rate. The oxidation and reduction peaks did not appear due to the relatively small amount of pyrrole (20%) in the nanopapers. The specific capacitance found for CNF/PPy180 at 5 mV s^{-1} was 7.40 F g^{-1}, which decreased to 0.35 F g^{-1} at the highest scan rate of 200 mV s^{-1}. The dramatic decrement of specific capacitance has been related to the sample compression during the sheet drying, which reduced the porosity. When the porosity is decreased the ion mass transport is too slow to allow for full utilization of the inherent charge storage capacity for scan rates above 5 mV s^{-1} (Wang, Tammela, Zhang, Strømme, & Nyholm, 2014). As mentioned by Carlsson et al. (2012), porous samples allow fast transport of anions throughout the electro-active material. They found that the capacity of compact samples decreased with increasing scan rate while the porous samples showed a slight increase in capacity.

4. Conclusions

A strong and electrically conductive nanopaper was obtained by coating softwood cellulose nanofibers with polypyrrole. The structure of PPy modified nanopapers were composed of multilayers of CNF with PPy chains interpenetrating the cellulose nanofiber network. The obtained pure CNF nanopaper had very high tensile properties, with 224 MPa of strength and 14.5 GPa of elastic modulus. On the other hand, nanopapers containing up to 20% of PPy showed lower but still good mechanical properties (94 MPa strength and 8.8 GPa modulus), with an electrical conductivity of $5.2\ 10^{-2}$ S cm^{-1}. In fact, the conductivity of this PPy-modified CNF nanopaper was three orders of magnitude above the one of typical semiconductor like silicon ($1.5\ 10^{-5}$ S cm^{-1}). This modification changed the nature of CNF nanopaper from insulator to semiconductor material, after coating with polypyrrole polymer. Compared to previous results in the literature, the proposed methods and products provided strong and flexible cellulose nanopapers of high mechanical properties and the electrical conductivity in the range of semiconductors. With these results, new applications can be expected for cellulose nanofibers as biodegradable thin-film transistors or as biosensors. This work opens the door to use cellulose nanofibers in green, low-cost, and portable electronic devices in the future.

Acknowledgement

The authors want to thank the financial support of the European Commission (Erasmus Mundus Project Techno II, ref. 372228-1-2012-1-FR-ERA MUNDUS-EMA21).

Appendix A. Supplementary data

Supplementary data associated with this article can be found, in the online version, at http://dx.doi.org/10.1016/j.carbpol.2016.06.102.

References

Ali, F., Reinert, L., Levêque, J.-M., Duclaux, L., Muller, F., Saeed, S., & Shah, S. S. (2014). Effect of sonication conditions: Solvent, time, temperature and reactor type on the preparation of micron sized vermiculite particles. *Ultrasonics Sonochemistry*, *21*(3), 1002–1009.

Ansari, R. (2006). Polypyrrole conducting electroactive polymers: Synthesis and stability studies. *E-Journal of Chemistry*, *3*(4), 186–201.

Beneventi, D., Alila, S., Boufi, S., Chaussy, D., & Nortier, P. (2006). Polymerization of pyrrole on cellulose fibres using a FeCl3 impregnation- pyrrole polymerization sequence. *Cellulose*, *13*(6), 725–734.

Boufi, S., Kaddami, H., & Dufresne, A. (2014). Mechanical performance and transparency of nanocellulose reinforced polymer nanocomposites. *Macromolecular Materials and Engineering*, *299*(5), 560–568.

Buitrago-Sierra, R., García-Fernández, M. J., Pastor-Blas, M. M., & Sepúlveda-Escribano, A. (2013). Environmentally friendly reduction of a platinum catalyst precursor supported on polypyrrole. *Green Chemistry*, *15*(7), 1981–1990.

Carlsson, D. O., Nyström, G., Zhou, Q., Berglund, L. A., Nyholm, L., & Strømme, M. (2012). Electroactive nanofibrillated cellulose aerogel composites with tunable structural and electrochemical properties. *Journal of Materials Chemistry*, *22*(36), 19014–19024.

Carlsson, D. O., Mihranyan, A., Strømme, M., & Nyholm, L. (2014). Tailoring porosities and electrochemical properties of composites composed of microfibrillated cellulose and polypyrrole. *RSC Advances*, *4*(17), 8489–8497.

Eisazadeh, H., Engineering, C., & Box, P. O. (2007). Studying the characteristics of polypyrrole and its composites. *World Journal of Chemistry*, *2*(2), 67–74.

Firoz Babu, K., Dhandapani, P., Maruthamuthu, S., & Anbu Kulandainathan, M. (2012). One pot synthesis of polypyrrole silver nanocomposite on cotton fabrics for multifunctional property. *Carbohydrate Polymers*, *90*(4), 1557–1563.

Fukuzumi, H., Saito, T., Iwata, T., Kumamoto, Y., & Isogai, A. (2009). Transparent and high gas barrier films of cellulose nanofibers prepared by TEMPO-mediated oxidation. *Biomacromolecules*, *10*(1), 162–165.

Fukuzumi, H. (2012). *Studies on structures and properties of TEMPO-oxidized cellulose nanofibril films*. University of Tokyo: Japan.

González, I., Alcalà, M., Chinga-Carrasco, G., Vilaseca, F., Boufi, S., & Mutjé, P. (2014). From paper to nanopaper: Evolution of mechanical and physical properties. *Cellulose*, *21*(4), 2599–2609.

Hamedi, M. M., Hajian, A., Fall, A. B., Hkansson, K., Salajkova, M., Lundell, F., . . . & Berglund, L. A. (2014). Highly conducting, strong nanocomposites based on nanocellulose-assisted aqueous dispersions of single-wall carbon nanotubes. *ACS Nano*, *8*(3), 2467–2476.

Henriksson, M., Fogelström, L., Berglund, L. A., Johansson, M., & Hult, A. (2011). Novel nanocomposite concept based on cross-linking of hyperbranched polymers in reactive cellulose nanopaper templates. *Composites Science and Technology*, *71*(1), 13–17.

Hoenich, N. (2006). Cellulose for medical applications: Past, present, and future. *BioResources*, *1*(2), 270–280.

Huang, B., Kang, G. J., & Ni, Y. (2006). Preparation of conductive paper by in-situ polymerization of pyrrole in a pulp fibre system. *Conductive Papers*, *2*, 38–42.

Huang, J., Zhu, H., Chen, Y., Preston, C., Rohrbach, K., Cumings, J., & Hu, L. (2013). Highly transparent and flexible nanopaper transistors. *ACS Nano*, *7*(3), 2106–2113.

Int, H. P. M. (2008). *Dynamic mechanical analysis: A practical introduction. textbook*. CRC Press: New york.

Ioelovich, M. (2008). Cellulose as a nanostructured polymer: A short review. *BioResources*, *3*(4), 1403–1418.

Isogai, A., Saito, T., & Fukuzumi, H. (2011). TEMPO-oxidized cellulose nanofibers. *Nanoscale*, *3*(1), 71–85.

Jeon, G., Yang, S. Y., & Kim, J. K. (2012). Functional nanoporous membranes for drug delivery. *Journal of Materials Chemistry*, *22*, 14814–14834.

Jonoobi, M., Oladi, R., Davoudpour, Y., Oksman, K., Dufresne, A., Hamzeh, Y., & Davoodi, R. (2015). Different preparation methods and properties of nanostructured cellulose from various natural resources and residues: A review. *Cellulose*, *22*(2), 935–969.

Kalia, S., Dufresne, A., Cherian, B. M., Kaith, B. S., Avérous, L., Njuguna, J., & Nassiopoulos, E. (2011). Cellulose-based bio- and nanocomposites: A review. *International Journal of Polymer Science*, *2011*, 1–35.

Koga, H., Nogi, M., Komoda, N., Nge, T. T., Sugahara, T., & Suganuma, K. (2014). Uniformly connected conductive networks on cellulose nanofiber paper for transparent paper electronics. *NPG Asia Materials*, *6*, 1–8.
Lavoine, N., Desloges, I., Dufresne, A., & Bras, J. (2012). Microfibrillated cellulose—Its barrier properties and applications in cellulosic materials: A review. *Carbohydrate Polymers*, *90*(2), 735–764.
Lee, K. Y., Tammelin, T., Schulfter, K., Kiiskinen, H., Samela, J., & Bismarck, A. (2012). High performance cellulose nanocomposites: Comparing the reinforcing ability of bacterial cellulose and nanofibrillated cellulose. *ACS Applied Materials and Interfaces*, *4*(8), 4078–4086.
Lin, N., & Dufresne, A. (2014). Nanocellulose in biomedicine: Current status and future prospect. *European Polymer Journal*, *59*, 302–325.
Lin, Y., Cho, J., Tompsett, G. A., Westmoreland, P. R., & Huber, G. W. (2009). Kinetics and mechanism of cellulose pyrolysis. *Physical Chemistry*, *113*(January), 20097–20107.
Luo, Y., Zhang, J., Li, X., Liao, C., & Li, X. (2014). The cellulose nanofibers for optoelectronic conversion and energy storage. *Journal of Nanomaterials*, *2014*, 1–13.
Miao, C., & Hamad, W. Y. (2013). Cellulose reinforced polymer composites and nanocomposites: A critical review. *Cellulose*, *20*, 2221–2262.
Nyholm, L., Nyström, G., Mihranyan, A., & Strømme, M. (2011). Toward flexible polymer and paper-based energy storage devices. *Advanced Materials*, *23*, 3751–3769.
Nyström, G., Mihranyan, A., Razaq, A., Lindström, T., Nyholm, L., & Strømme, M. (2010). A nanocellulose polypyrrole composite based on microfibrillated cellulose from wood. *The Journal of Physical Chemistry B*, *114*(12), 4178–4182.
Nyström, G., Strømme, M., Sjödin, M., & Nyholm, L. (2012). Rapid potential step charging of paper-based polypyrrole energy storage devices. *Electrochimica Acta*, *70*, 91–97.
Rastogi, V., Stanssens, D., & Samyn, P. (2014). Mechanism for tuning the hydrophobicity of microfibrillated cellulose films by controlled thermal release of encapsulated wax. *Materials*, *7*(11), 7196–7216.
Saba, N., Tahir, P., & Jawaid, M. (2014). A review on potentiality of nano filler/natural fiber filled polymer hybrid composites. *Polymers*, *6*, 2247–2273.
Salas, C., Nypelö, T., Rodriguez-Abreu, C., Carrillo, C., & Rojas, O. J. (2014). Nanocellulose properties and applications in colloids and interfaces. *Current Opinion in Colloid and Interface Science*, *19*(5), 383–396.
Sasso, C., Zeno, E., Petit-Conil, M., Chaussy, D., Belgacem, M. N., Tapin-Lingua, S., & Beneventi, D. (2010). Highly conducting polypyrrole/cellulose nanocomposite films with enhanced mechanical properties. *Macromolecular Materials and Engineering*, *295*(10), 934–941.
Saville, P. (2005). . *Polypyrrole formation and use* (Vol. 004) Canada: DRDC Atlantic TM.
Sehaqui, H., Liu, A., Zhou, Q., & Berglund, L. A. (2010). Fast preparation procedure for large, flat cellulose and cellulose/inorganic nanopaper structures. *Biomacromolecules*, *11*(9), 2195–2198.
Sehaqui, H., Allais, M., Zhou, Q., & Berglund, L. A. (2011). Wood cellulose biocomposites with fibrous structures at micro- and nanoscale. *Composites Science and Technology*, *71*(3), 382–387.
Siró, I., & Plackett, D. (2010). Microfibrillated cellulose and new nanocomposite materials: A review. *Cellulose*, *17*(3), 459–494.
Snook, G. A., Kao, P., & Best, A. S. (2011). Conducting-polymer-based supercapacitor devices and electrodes. *Journal of Power Sources*, *196*(1), 1–12.
Tammela, P., Wang, Z., Frykstrand, S., Zhang, P., Sintorn, I.-M., Nyholm, L., & Strømme, M. (2015). Asymmetric supercapacitors based on carbon nanofibre and polypyrrole/nanocellulose composite electrodes. *RSC Advance*, *5*(21), 16405–16413.
Thakur, V. K. (2015). *Nanocellulose polymer nanocomposites: fundamentals and applications*. MA: Wiley.
Trchova, M., & Kova, J. (2003). Synthesis and structural study of polypyrroles prepared in the presence of surfactants. *Synthetic Metals*, *138*, 447–455.
Wang, L.-X., Li, X.-G., & Yang, Y.-L. (2001). Preparation, properties and applications of polypyrroles. *Reactive and Functional Polymers*, *47*, 125–139.
Wang, B., Sain, M., & Oksman, K. (2007). Study of structural morphology of hemp fiber from the micro to the nanoscale. *Applied Composite Materials*, *14*(2), 89–103.
Wang, Z., Tammela, P., Zhang, P., Strømme, M., & Nyholm, L. (2014). Efficient high active mass paper-based energy-storage devices containing free-standing additive-less polypyrrole–nanocellulose electrodes. *Journal of Materials Chemistry A*, *2*(21), 7711.
Wang, Z., Carlsson, D. O., Tammela, P., Hua, K., Zhang, P., Nyholm, L., & Strømme, M. (2015). Surface modified nanocellulose fibers yield conducting polymer-based flexible supercapacitors with enhanced capacitances. *ACS Nano*, *9*(7), 7563–7571.
Yuan, L., Yao, B., Hu, B., Huo, K., Chen, W., & Zhou, J. (2013). Polypyrrole-coated paper for flexible solid-state energy storage. *Energy & Environmental Science*, *6*(2), 470–476.
Zhang, Y., Nypelö, T., Salas, C., Arboleda, J., Hoeger, I. C., & Rojas, O. J. (2013). Cellulose nanofibrils: From strong materials to bioactive surfaces. *Journal of Renewable Materials*, *1*(3), 195–211.
Zhang, D., Zhang, Q., Gao, X., & Piao, G. (2013). A nanocellulose polypyrrole composite based on tunicate cellulose. *International Journal of Polymer Science*, *2013*, 6 pp
Zheng, G., Cui, Y., Karabulut, E., Wågberg, L., Zhu, H., & Hu, L. (2013). Nanostructured paper for flexible energy and electronic devices. *MRS Bulletin*, *38*(04), 320–325.

Strong and electrically conductive nanopaper from cellulose nanofibers and polypyrrole

Makara Lay, J. Alberto Méndez, Marc Delgado-Aguilar, Kim Ngun Bun, Fabiola Vilaseca*

*fabiola.vilaseca@udg.edu

The polymerization of pyrrole was carried out by chemical oxidation at different reaction times: 20, 40, 60, and 180 minutes. The yield of PPy increased from 68% to 88% with increasing of reaction time from 20 to 180 minutes, as shown in **S1**. The inset (**S1b**) shows a photograph of the black PPy platelet.

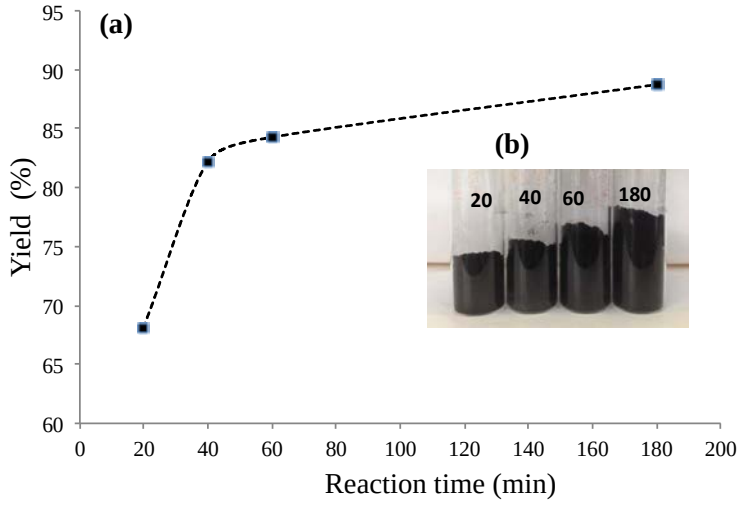

S1 In situ polymerization of polypyrrole at different reaction times: 20, 40, 60, and 180 minutes; (a) yield of PPy and (b) PPy platelet.

The density was calculated from the basis weight, thickness, and dimension of 1 × 3 cm strips. Porosity was determined from the density of the sample, the density of pure cellulose, and the density of pure polypyrrole (**S2**).

$$Porosity\ (\%) = 100 \times [1 - \rho_{sample}/(w_{cell} \times \rho_{cell} + w_{PPy} \times \rho_{PPy})] \qquad \boldsymbol{S2}$$

Where ρ_{sample} is the density of the nanopaper and ρ_{cell} and ρ_{PPy} are the density of nanocellulose and polypyrrole, assumed to be 1.5g cm^{-3} (Henriksson et al., 2011) and 1.48 g cm^{-3} (Saville, 2005), respectively. The weight fractions of nanocellulose and polypyrrole are represented by w_{cell} and w_{PPy}.

The final values for the thickness, density and porosity of the samples are included in **S3**, together with the tensile strength, elastic modulus and electrical conductivity**.**

S3. Composition, thickness, density, porosity, tensile strength, elastic modulus and electrical conductivity of the obtained nanopapers

Sample	**Reaction time (min)**	**CNF (%)**	**PPy (%)**	**Thickness (μm)**	**Density (g/cm^{-3})**	**Porosity (%)**	**Strength (MPa)**	**Modulus (GPa)**	**Conductivity ($S \cdot cm^{-1}$)**
CNF		100	0	55	1.34	10.45	224(19)	14.5(0.8)	insulator
CNF/PPy20	20	92	8	70	1.32	11.74	124(11)	9.8(0.4)	$1.0 \cdot 10^{-5}$
CNF/PPy40	40	84	16	79	1.30	13.17	101(9)	8.2(0.3)	$4.0 \cdot 10^{-4}$
CNF/PPy60	60	82	18	84	1.28	14.74	102(8)	8.7(0.3)	$7.7 \cdot 10^{-3}$
CNF/PPy120	120	81	19	91	1.23	17.89	97(9)	7.7(0.2)	$3.0 \cdot 10^{-2}$
CNF/PPy180	180	80	20	94	1.21	19.45	94(12)	8.8(0.5)	$5.2 \cdot 10^{-2}$

The FT-IR spectra of pyrrole, cellulose nanofibers (CNF) and polypyrrole (PPy) are shown in **S4**.

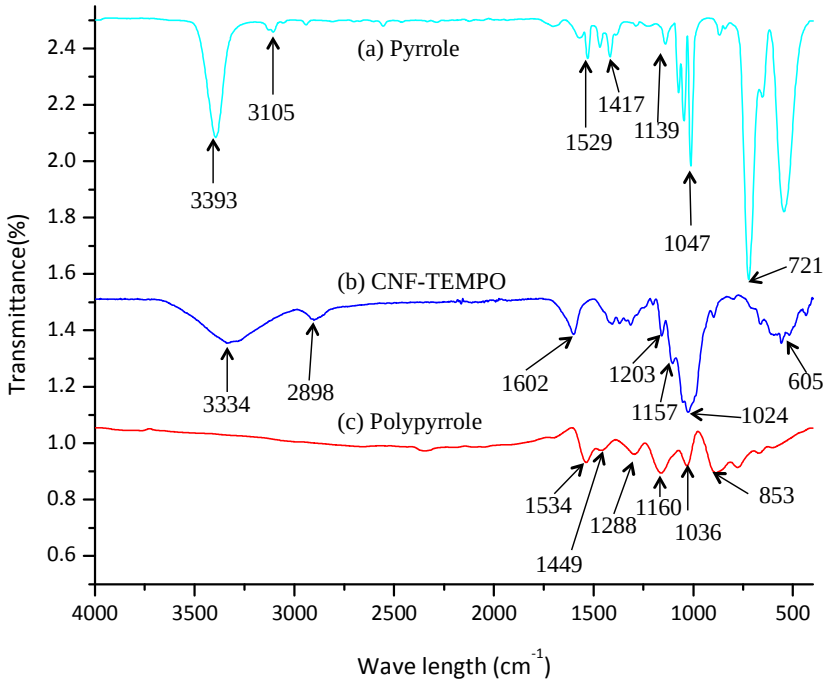

S4. FT-IR spectra of (a) pyrrole, (b) CNF nanopaper and (c) polypyrrole (PPy).

The broad absorption band at 3393 cm^{-1} (**S4.a**) is indicative of the stretching vibration of the secondary N–H bond in the pyrrole ring, and the peak at 3105 cm^{-1} represents the stretching of the aromatic C–H bonds (Monte et al., 2014). The stretching vibration of the C=C in the aromatic ring appears at 1529 cm^{-1}, whereas at 1417 cm^{-1} the stretching (in-ring) for the single C–C links is found. The peak at 1139 cm^{-1} is assigned to the C–N bond, although it is not very intense. The absorption band at 1047 cm^{-1} is associated to the =C–H bending deformation, and the strong peak at 721 cm^{-1} corresponds to the out-of-plane bending of the three substituted C–H bonds (Lee & Boo, 1996).

In the FT-IR spectrum of CNF (**S4.b**) the broad band vibration of –OH groups are found in 3334 cm^{-1}; and the stretching for aliphatic C-H bonds of cellulose in 2898 cm^{-1}. A prominent sharp peak at 1602 cm^{-1} is attributed to the stretching of carbonyl group of TEMPO oxidized cellulose nanofibers (Soni et al., 2015). The symmetric bending of CH_2 and C–O groups of the pyranose ring of CNF are found respectively at 1416 cm^{-1} and 1314 cm^{-1} (Kargarzadeh et al., 2012). In the range of 1203 cm^{-1} and 1157 cm^{-1} the symmetric and asymmetric stretching of ether bonds (C–O–C) are assigned. Also the absorption peak at 1024 cm^{-1} corresponds to the C–O ether groups. The broad band centred at 605 cm^{-1} is assigned to the C–H bending deformation.

S4.c corresponds to the FTIR spectrum of PPy. The absorption bands at 1534 cm^{-1} corresponds to the C=C stretching of the aromatic ring. The peak at 1449 cm^{-1} is assigned to the stretching vibration of C–C and C–N links. The absorption peak at 1288 cm^{-1} is assigned to a mixed bending and stretching vibration associated to the C–N bond of the aromatic amine. At this wavelength, single C–C bonds between rings also appear; however its intensity is much lower compared to the C–N bond that has greater dipole (Saville, 2005). The C–H in-plane and out-of-plane bending deformation of PPy appears at 1160 cm^{-1} and 1036 cm^{-1}, respectively. Also centred at 1160 cm^{-1}, the stretching for the C=N link is found. Finally, the peak at 853 cm^{-1} is related to the N–H wagging of secondary amines.

An example of the characteristic DMA curves (complex modulus E*, storage modulus E’ and loss modulus E’’), for a specific formulation, is shown in S5.

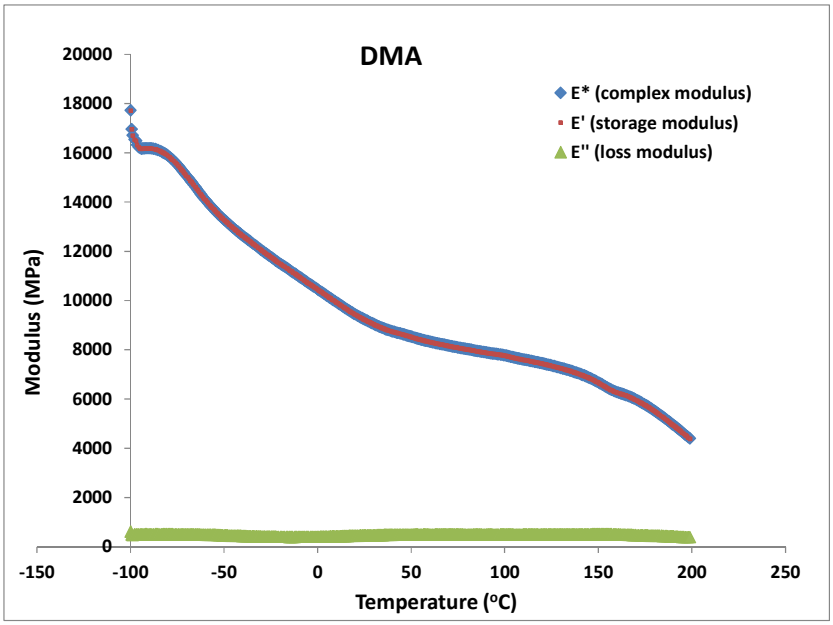

S5. Complex modulus (E*), elastic modulus (E') and loss modulus (E'') with increasing temperature for the CNF/PPy60 nanopaper.

References

Henriksson, M., Fogelström, L., Berglund, L. a., Johansson, M., & Hult, A. (2011). Novel nanocomposite concept based on cross-linking of hyperbranched polymers in reactive cellulose nanopaper templates. *Composites Science and Technology*, *71*(1), 13–17.

Kargarzadeh, H., Ahmad, I., Abdullah, I., Dufresne, A., Zainudin, S. Y., & Sheltami, R. M. (2012). Effects of hydrolysis conditions on the morphology, crystallinity, and thermal stability of cellulose nanocrystals extracted from kenaf bast fibers. *Cellulose*, *19*(3), 855–866.

Lee, S. Y., & Boo, B. H. (1996). Molecular Structures and Vibrational Spectra of Pyrrole and Carbazole by Density Functional Theory and Conventional ab Initio Calculations. *The Journal of Physical Chemistry*, *100*(37), 15073–15078.

Monte, R. S., Kotzebue, L. R. V., Alexandre, D. L., Furtado, R. F., Santos, J. A. C., Dantas, J. D. P., & Alves, C. R. (2014). Morphological and Electrochemical Characteristics of Electrosynthesized PPy/CD Composite. *Journal of the Brazilian Chemical Society*, *25*(3), 597–601.

Saville, P. (2005). *Polypyrrole Formation and Use*. *DRDC Atlantic TM, Canada* (Vol. 004).

Soni, B., Hassan, E. B., & Mahmoud, B. (2015). Chemical isolation and characterization of different cellulose nanofibers from cotton stalks. *Carbohydrate Polymers*, *134*(February 2016), 581–589.

PAPER II

Combined effect of carbon nanotubes and polypyrrole on the electrical properties of cellulose-nanopaper

Makara Lay, José Alberto Méndez, M. Àngels Pèlach, Kim Ngun Bun, Fabiola Vilaseca

Cellulose 2016, 23(6), 3925-3937

Lay, M., Méndez, J.A., Pèlach, M.A., Bun, K.N., Vilaseca, F. "Combined effect of carbon nanotubes and polypyrrole on the electrical properties of cellulosenanopaper". *Cellulose*. Vol. 23, Issue 6 (2016) : 3925-3937

http://dx.doi.org/10.1007/s10570-016-1060-5

https://link.springer.com/article/10.1007%2Fs10570-016-1060-5

Received: 16 June 2016 / Accepted: 29 August 2016 / Published online: 19 September 2016

Abstract

In the present study, 2,2,6,6,-tetramethylpiperidine-1-oxyl (TEMPO)-oxidized cellulose nanofibers (CNF) were combined with multi-walled carbon nanotubes (MWCNTs) and with hybrid MWCNT/polypyrrole to produce a variety of binary and ternary formulations of conductive nanopapers. By following a simple mixing/sonication/filtering process, a homogeneous and well-distributed CNF-MWCNT nanostructure was formed, resulting in a nanopaper of strong mechanical properties (141 MPa tensile strength and 9.41 GPa Young's modulus) and good electrical conductivity (0.78 S cm^{-1}), for the formulation with 50 wt% of MWCNT. The subsequent in situ polymerization of pyrrole in CNF-MWCNT mixtures produced ternary multiphase CNF-MWCNT-PPy nanopapers with much improved electrical conductivity (2.41 S cm^{-1}) and electrochemical properties (113 F g^{-1} specific capacitance), even using little amounts of MWCNTs. With these materials, improved hybrid capacitors can be designed. The article presents a trend for the application of cellulose nanofibers in the field of green and flexible electronics.

Keywords

Conductive nanopaper; Multi-walled carbon nanotube; Polypyrrole; Mechanical properties; Conductivity; Electrochemical properties

PAPER III

Smart nanopaper based on cellulose nanofibers with hybrid PEDOT:PSS/Polypyrrole for energy storage devices

Makara Lay, M. Àngels Pèlach, Neus Pellicer, Joaquim A. Tarrés, Kim Ngun Bun, Fabiola Vilaseca

Carbohydrate Polymers (submitted and revised manuscript)

Smart nanopaper based on cellulose nanofibers with hybrid PEDOT:PSS/Polypyrrole for energy storage devices

Makara Lay,[a,b] M. Àngels Pèlach,[a] Neus Pellicer,[a] Joaquim A. Tarrés,[a] Kim Ngun Bun[b], Fabiola Vilaseca [a *]

a. Dept. of Chemical Engineering, Agricultural and Food Technology, Universitat de Girona, C/Maria Aurèlia Capmany 61, 17071 Girona, Spain.

b. Dept. of Geotechnic and Georesources Engineering, Institute of Technology of Cambodia, PP Box 86, Russian conf. Blvd. Phnom Penh, Cambodia.

*corresponding author: fabiola.vilaseca@udg.edu

Abstract

In the current work, flexible, lightweight, and strong conductive nanopapers based on cellulose nanofibers (CNFs) with poly(3,4-ethylenedioxythiophene):polystyrene sulfonate (PEDOT:PSS) and/or polypyrrole (PPy) were prepared by following a mixing and in situ polymerization method. A successful homogeneous coating of PEDOT:PSS on cellulose nanofibers occurred by means of interactions between PEDOT chains and the hydroxyl and carboxylic groups of cellulose nanofibers, as shown by FTIR spectra. The electrical conductivity and the specific capacitance of CNF-PEDOT:PSS nanopapers were 2.58 S cm^{-1} and 6.21 F g^{-1}, respectively. Further coating of PPy produced a substantial improvement on the electrical conductivity (10.55 S cm^{-1}) and the specific capacitance (315.5 F g^{-1}) of the resulting CNF-PEDOT:PSS-PPy nanopaper. A synergistic phenomenon between both conductive polymers supported the high

electrical conductivity and specific capacitance of the ternary formulation. Moreover, CNF-PEDOT:PSS-PPy nanopaper showed higher mechanical properties and it was more flexible than the nanopaper containing only polypyrrole conducting polymer (CNF-PPy). It is concluded that the good mechanical, electrical and electrochemical properties of the ternary formulation can apply for the next generation of flexible electronics and energy storage devices.

Keywords: cellulose nanofibers; PEDOT:PSS; polypyrrole; electrical conductivity; specific capacitance; green electronics

Graphical abstract

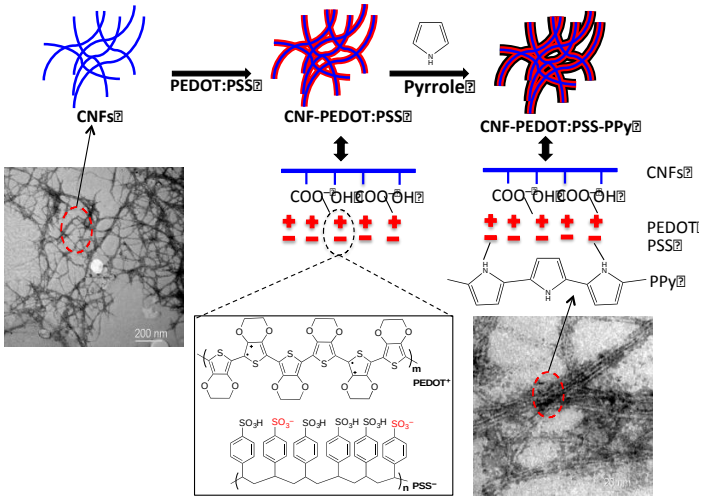

1. Introduction

The majority of portable electronics devices such as mobile phones, transistors, notebook computers, and digital cameras are built on non-renewable, non-biodegradable, toxic materials, such as silicon wafers, which are highly purified, expensive and rigid substrates. This is why the

development of nanotechnologies is focused on using environmentally friendly materials made from renewable sources. One example is the group of researchers from the University of Wisconsin-Madison (Seo et al., 2015) that have come up with a new solution to alleviate the environmental burden of these discarded electronics. They have demonstrated the feasibility of making microwave biodegradable thin-film transistors from a transparent, flexible biodegradable substrate made from cellulose nanofibers (CNFs). These CNFs films have the potential to replace silicon wafers as electronic substrates in environmental friendly, low-cost, portable gadgets or devices of the future, which will be much greener and cheaper than it is today (Seo et al., 2015). Coming from renewable and sustainable raw materials, cellulose nanofibers are strong, flexible, transparent, and exhibit low thermal expansion coefficient, which means that the material will not change shape as the temperature variations. Moreover, the combination of CNFs with conducting polymers (CPs) produces high capacitance and conductive films with the advantages of being lightweight (higher energy and power with less device mass) and flexible (Meng, Liu, Chen, Hu, & Fan, 2010). There are several published studies on CNFs/CPs in the field of biosensor, energy storage and electronic devices (Huang et al., 2013; Koga et al., 2014; Tammela et al., 2015; Wang et al., 2015). Due to low cost and with the capacitive response, conducting polymers have attracted extensive interest in the pseudocapacitors application. Among them, polypyrrole (PPy), polythiophenes (PThs) and their respective derivatives are possibly more environmentally friendly and have attracted considerable attention in the last decade (Wang, Xu, Chen, & Du, 2007). Already in 1988, researchers from Bayer AG (Leverkusen, Germany) invented a derivative of PThs, diethoxy substituted thiophene called poly(3,4-ethylenedioxythiophene) (PEDOT) also known under the trade name Clevios (Bashir, 2013; Groenendaal, Jonas, Freitag, Pielartzik, & Reynolds, 2000). Since then, PEDOT has become one

of the best conducting polymers available in terms of conductivity, processability and stability. Furthermore, PEDOT is the only conducting polymer that is commercially produced on a large-scale by H.C. Starck Clevios, and is used for many applications such as antistatic coatings, printed electronics, transparent transistors, organic solar cells, and organic light-emitting diodes (OLED) displays (Elschner, Kirchheyer, Lovenich, Merker, & Reuter, 2013; Li et al., 2014).

In this work we report a simple methodology to produce flexible, lightweight, and strong nanopaper from cellulose nanofibers and poly(3,4-ethylenedioxythiophene) : poly(styrene sulfonate) (CNF-PEDOT:PSS). PEDOT:PSS consists of a conductive polythiophene derivate that is electrostatically bounded to a PSS polyanion (Suchand Sangeeth, Jaiswal, & Menon, 2009). The presence of PSS converts PEDOT:PSS into water soluble polymer, and this may help to improve the dispersion of the conductive polymer with the cellulose nanofibers in the CNF-PEDOT:PSS nanocomposites. We report as well a novel design of nanopapers based on cellulose nanofibers with hybrid PEDOT:PSS-PPy not yet been investigated up to date, to the best of our knowledge. The combination of PEDOT:PSS and polypyrrole conducting polymers in CNF nanopapers aims to enhance the electrical conductivity and specific capacitance that each component could not reach individually. PEDOT:PSS-PPy nanopaper is also compared with CNF-PPy nanopapers in terms of mechanical, electrical and electrochemical properties.

2. Materials and Methods

2.1 Materials

Bleached Softwood Kraft Pulp from Arauco (Chile) was used as cellulose raw material. Pyrrole from Sigma Aldrich with 98% of purity was used for the chemical synthesis of polypyrrole, used as conductive polymer. Two different types of poly(3,4-

ethylenedioxythiophene):poly(styrene sulfonates), PEDOT:PSS, were also used in this work as conductive polymers. Aqueous solutions of 1.1wt% of the two different PEDOT:PSS (Clevios PT2 and PH500), containing 1:2.5 by weight of each component were purchased from Clevios Heraeus Deutschland (Leverkusen, Germany). These products are kept between 5 and 30 °C and remain stable for 9 months from the date of production, in the sealed original containers. Silver coating 3850 was supplied by Holland shielding system BV (Dordrecht, Holland). The rest of materials such as iron (III) chloride ($FeCl_3$), Tween-80, 2,2,6,6-tetramethyl-1-1-piperidinyloxy (TEMPO), sodium bromide (NaBr), sodium hypochlorite (NaClO), HCl, NaOH, and NaCl were supplied by Sigma Aldrich and used without further purification.

2.2 Preparation of cellulose nanofibers, CNF nanopaper, and of CNF-PT2, CNF-PH500, CNF-PPy and CNF-PH500-PPy nanopapers

Scheme 1 shows the nanopapers produced in this work, namely CNF, CNF-PT2, CNF-PH500, CNF-PPy, and CNF-PH500-PPy nanopapers. The preparation of cellulose nanofibers followed the TEMPO-mediated oxidation described in previous work (Fukuzumi, Saito, Iwata, Kumamoto, & Isogai, 2009) using 10 mmol of NaClO at pH 10. After TEMPO-oxidation, the cellulose suspension was filtered thoroughly with distilled water to remove all non-reacted reagents and free ions. Thereafter, the cellulose suspension at 1wt% concentration was passed three times through a high-pressure homogenizer (NS1001L PANDA 2K-GEA) at pressure of 600 bars. Finally, a transparent CNF gel-like was obtained and stored at 4°C before use.

Scheme 1 Preparation of different types of nanopapers (A) CNF, (B) CNF-PPy, (C) CNF-PH500-PPy, (D) CNF-PH500, and (E) CNF-PT2.

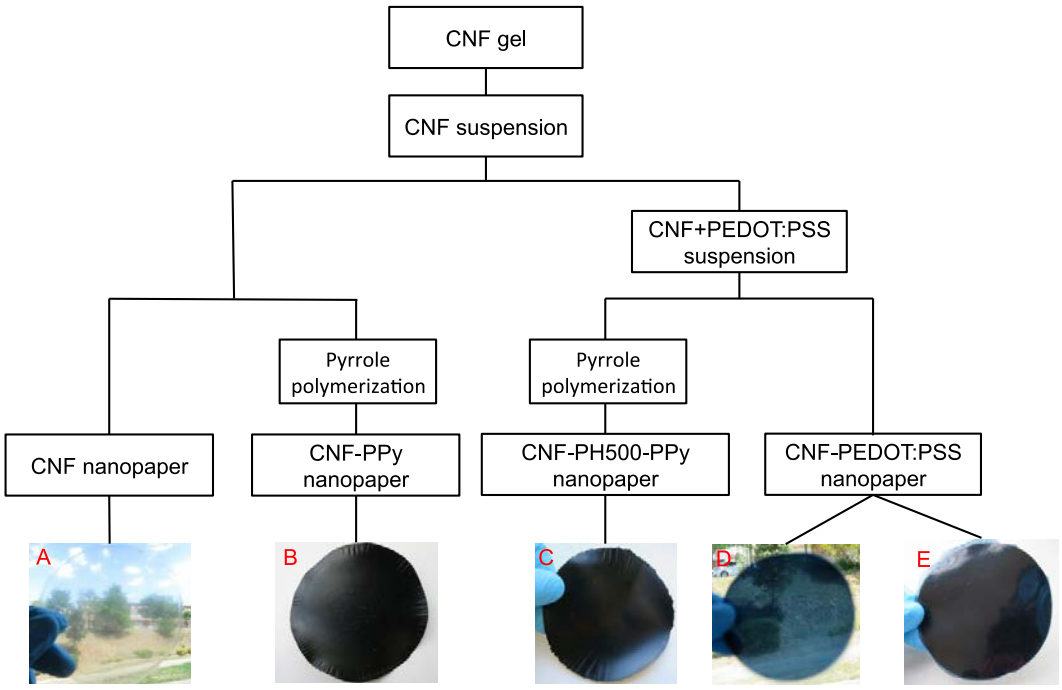

For the preparation of CNF nanopaper, CNF gel was diluted to 0.2% with distilled water and the suspension was dispersed and sonicated for 10 min (5 min pulse on, 2 min pulse off, and 5 min pulse on) at 60% of amplitude setting using a Q700 sonicator. Afterwards, the CNF suspension was filtered overnight using glass filter (HOLDER KIT MILLIPORE) with a nitrocellulose membrane GSWP2935 (hydrophilic membrane) of 0.22 μm pore-size. After that, this membrane was carefully peeled off, and two pieces of polyvinilydene fluoride (PVDF) immobile transfer membranes of 0.45 μm pore-size were placed at each side of the sample to prevent its adhesion onto the membranes during the next drying process. The sample was dried

for 20 min at a vacuum pressure of -0.6 to -0.8 bar and 92 ± 3°C temperature in a laboratory sheet dryer.

In this work, two different types of PEDOT:PSS (PT2 and PH500) were used as conductive fillers. PEDOT:PSS was first diluted to 0.5% with distilled water and stirred for 5 min using magnetic stirrer. PEDOT:PSS suspension was added into the above CNF suspension with different proportion of CNF-PEDOT:PSS (95/5, 90/10, 80/20, 70/30, 60/40, and 50/50), and the sample are labelled based on the amount of PEDOT:PSS in the nanocomposites; for instance, CNF-PT2_5, CNF-PT2_10, CNF-PT2_20, CNF-PT2_30, CNF-PT2_40, and CNF-PT2_50 for the nanocomposites with 5-50 wt% of PT2, respectively, and similarly for PH500. The mixture suspension was stirred for 24 h at room temperature and after that it was sonicated for 2 min. Finally, it was filtered and dried for 20 min to obtain CNF-PEDOT:PSS nanopapers.

For the preparation of CNF-PPy nanopapers, a dilute suspension of CNF (0.1%, 200 mg of dry weight) was sonicated for 10 min under the same setting conditions described above. 0.21 mL of pyrrole was dissolved in 30 mL of 0.5 M HCl. After stirring the mixture for 3 min using magnetic stirrer, one drop (0.05 ml) of Tween-80 was added and stirred until completely homogenous dispersion. Afterwards, the solution of pyrrole was introduced into the above CNF suspension, and the mixture was stirred for 5 min. In order to initiate the polymerization, 1.21 g of $FeCl_3$ in 30 mL of HCl 0.5 M was added drop wise into the suspension. The final mixture was stirred at room temperature for 60 min. At the end, the mixture CNF-PPy was filtered using a glass filter and washed subsequently with 500 mL of 0.5 M HCl, 500 mL of 0.1 M NaCl, and 500 mL of distilled water. During the last washing with distilled water, the suspension was sonicated for 2 min to remove any small gas bubbles and to allow a better organization of CNF/PPy nanocomposite without undesired side effects, like any crystal structure damage (Ali et

al., 2014). Thereafter, the filtration was continued for 3 more hours until no residual water was left. The obtained CNF/PPy was finally dried in the sheet dryer for 20 min, following the same vacuum and temperature conditions.

CNF-PH500-PPy nanopapers were obtained via in situ chemical polymerization of pyrrole. The mixture of pyrrole with 0.5 M HCl (1:150, v/v) together with one drop of Tween-80 were stirred for 5 min and added into CNF-PH500 suspension for another 5 min. The solution of iron (III) chloride ($FeCl_3$) with the proportion of 2.4 of $FeCl_3$/pyrrole and 0.5 M HCl was drop-wise to initial polymerization of pyrrole on the mixture of CNF-PH500. The reaction was allowed for 60 min, and the suspension was filtered and dried for 20 min.

2.3 Characterization of nanopapers

Carbon, hydrogen, and nitrogen element analysis was characterized by Perkin Elmer EA2400 serie II equipment. The samples were subjected to pyrolysis in helium (He) at combustion temperature of 925–930°C. Acetanilide powder (C_8H_9NO) was used as reference, which contents carbon (71.09%), hydrogen (6.71%), and nitrogen (10.36%). The content of carbon, hydrogen, and nitrogen were recorded for 6 min, and the PPy contents in CNF-PPy and CNF-PH500-PPy nanopapers were calculated base on the percentage of nitrogen (N%).

The density of nanopapers was calculated from the basis weight, thickness, and dimension of 1×3 cm strips. Porosity was determined from the density of the sample, of cellulose nanofibers, PH500, and from the density of polypyrrole as shown in Equation 1.

$$Porosity\ (\%) = 100 \times \left[1 - \frac{\rho_{sample}}{\left(w_{cell}\rho_{cell} + w_{PH500}\rho_{PH500} + w_{PPy}\rho_{PPy}\right)}\right] \quad (1)$$

Where ρ_{sample} is the density of the nanopaper and ρ_{cell}, ρ_{PH500}, and ρ_{PPy} are the densities of nanocellulose, PH500, and polypyrrole, assumed to be 1.5 g cm^{-3} (Henriksson, Fogelström,

Berglund, Johansson, & Hult, 2011), 1 g cm^{-3} (according to supplier), and 1.48 g cm^{-3} (Saville, 2005), respectively. The weight fractions of nanocellulose, PH500, and polypyrrole are represented by w_{cell}, w_{PH500}, and w_{PPy}.

The chemical compositions of CNF, PH500, CNF-PH500, and CNF-PH500-PPy nanopapers were characterized by an ATR ALPHA FT-IR under transmittance mode in range between 500 cm^{-1} and 4000 cm^{-1} using 24 scans at resolution of 4 cm^{-1}.

Mechanical properties of all samples were evaluated using a Universal Testing Machine HOUNSFIELD, equipped with a 250 N load cell with crosshead speed of 5 mm/min. The rectangle specimens were cut into (50×5×(0.060 ± 0.005)) mm of dimension and kept under control condition of 50% relative humidity at room temperature. These parameters were set according to previous work (Hamedi et al., 2014). The results were obtained from at least five different specimens, in agreement with the ISO 527 standard.

The cross section surfaces of CNF-PT2, CNF-PH500, and CNF-PH500-PPy were observed using FE-SEM (HITACHI S-4100). The samples were coated with gold using a sputter.

Transmission electron microscopy (TEM) images of CNF, CNF-PH500_50, and CNF-PH500-PPy were recorded using a ZEISS EM-910 JEOL-2100F (1993) and an internal charge-coupled device (CCD) camera Gatan Orius SC200W1. The samples were diluted to 1:50 in distilled water, and only 8 μL of each sample was drop in a cupper 400 mesh grid with formvar film for 3 min minutes. 8 μL of contrast solution uranyl acetate 1% was dropped on the solution above and kept for 3 min before testing.

Thermogravimetric analysis was used to characterize their thermal stabilities, especially when 3,4-ethylenedioxythiophene): poly(styrene sulfonate) (PEDOT:PSS) or hybrid clevios PH500-PPy was coated on CNF substrate. The samples were heated from 30 to 700°C at a heating rate

of 10°C min^{-1} using a METTLER TOLEDO ultra-micro balance, TGA/DSC. The purge gas was nitrogen with a flowing rate of 40 mL/min, and the sample holder were pans made of alumina.

Silver paint was applied at the end of both sides of each sample and kept 16 h at room temperature to ensure a good electrical contact with the clip probes. Agilent 34461A digital multimeter was used to measure the resistance (*R*) over the length of the stripes of the specimens. The conductivity (σ') was calculated by $\sigma' = L/(R \times w \times d)$, where *L*, *w*, and *d* are the length, width, and thickness of the sample, respectively. *R* is the resistance (Ω) and was measured from the multimeter (Agilent 34461A). In this section, the prediction of percolation threshold was determined to describe the insulator-to-conductor transitions in composites made of conductive filler and an insulating matrix. Above the percolation threshold, the conductivity occurs, whereas below this concentration the composites are very resistant to electrical flow. The prediction of electrical conductivity nanopapers was calculated according to Equation 2 (Hermant, 2009; Koga et al., 2014).

$$\sigma = \sigma_0(\phi - \phi_c)^t \qquad (2)$$

*W*here σ is the theoretical conductivity, σ_0 the ultimate conductivity, ϕ the volume fraction of the conductive filler, and ϕ_c is the percolation threshold. To determine the percolation threshold (ϕ_c) experimental results are fitted by plotting log σ versus log ($\phi - \phi_c$), and the value of ϕ_c was incrementally varied until the best linear fit is obtained for *t* the critical exponent.

A Potentistat/Galvanostat Model 273A Princeton with a three-electrode electrochemical system consisting of the sample as working electrode, a platinum wire as counter electrode, and a solution of electrolyte 2 M NaCl-saturated Ag/AgCl as reference electrode was used to measure the electrochemical properties of the conductive nanopapers. The data were recorded in the

potential window of -0.9 to +0.9 V vs Ag/AgCl with different scan rate between 5 and 200 mV s^{-1}. CView and originPro softwares were used to plot cyclic voltammograms, and the specific capacitance was obtained following by Equation 3:

$$C_{sp} = i/m.v.\Delta V \quad (3)$$

Where C_{sp} (F g^{-1}) is the specific capacitance, i the integration in the CV curve, v the scan rate in V s^{-1}, m the mass (g) of the electrode material, and ΔV = 1.8 V is the potential window.

3. Results and discussion

Conductive nanopapers based on cellulose nanofibers (CNF), polythiophene derivate (PEDOT:PSS) and polypyrrole (PPy) as conductive polymers were prepared and their final compositions were characterized by Fourier-transform infrared spectroscopy (FTIR). The spectra of CNF, PH500, CNF-PH500, and CNF-PH500-PPy nanopaper are shown in Figure 1.

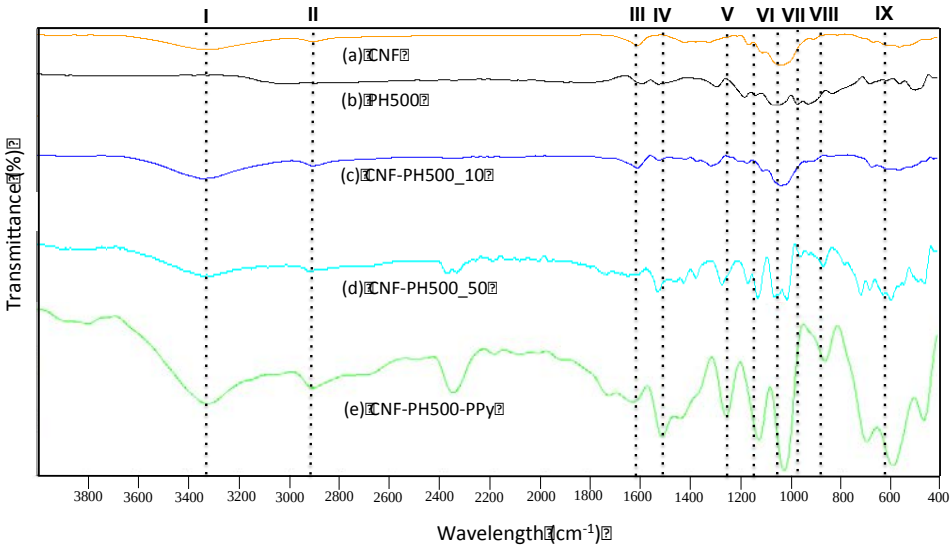

Figure 1 FTIR spectra of cellulose nanopaper and the conductive nanopapers.

The CNF nanopaper (Figure 1a) exhibits absorption peaks at 3334, 2988, 1602, 1416, 1314, and 1157 cm^{-1}, attributed to –OH group, aliphatic C–H bond of cellulose, stretching of carbonyl group from TEMPO oxidized cellulose, symmetric bending of CH_2 and C–O bonds of pyranose rings, and the asymmetric stretching of C–O–C groups, respectively. Figure 1b shows the spectrum of PH500 (PEDOT:PSS). The quinoid structure and the stretching modes of aromatic C=C (PEDOT) are found in the region of 1584–1514 cm^{-1}(Khan, Ul-Islam, Khattak, Ullah, & Park, 2015; Z Wang et al., 2016), while the C–C bonds and the vibrations of the C–S bond of the thiophene ring are presented at 1352 cm^{-1} and 822 cm^{-1}, 670 cm^{-1}, respectively. The peak at 3000 cm^{-1} corresponds to the stretching vibration of aromatic C–H bonds of PSS, the peak at 1046 cm^{-1} corresponds to the S–C phenyl bonds in sulfonic acid (Khan et al., 2015), and the absorption peaks at 1158–1110 cm^{-1} are related to the asymmetric and symmetric vibrations of S–O in sulfonate groups (SO_3H and $–SO_3^-$) of PSS chains (Jiang et al., 2014)(Zhu et al., 2015).The spectrum of CNF-PH500 nanopaper (Figure 1c and d) has all the absorption bands of CNF and PEDOT:PSS, although some peaks of both structures are overlapping. The main bonds of polythiophene backbone (C=C, C–C, and C–S) are found in the spectrum, and their intensity is higher with the greater amount of PEDOT:PSS in the nanopaper. Moreover, the peak at zone I (hydroxyl group) is broadening with the PEDOT:PSS content, indicating an increase in hydrogen-bonding interactions between the hydroxyl functionalized CNF and the electronically charged PEDOT:PSS. This indicates that PEDOT really interacting with CNF and successfully coated on the nanocellulose fibers. Figure 1e shows the spectrum for CNF-PH500-PPy nanopaper. It is confirmed that all the characteristic peaks of CNF, PH500, and polypyrrole (Lay, Méndez, Delgado-Aguilar, Bun, & Vilaseca, 2016) are reflected in the spectrum of the CNF-PH500-PPy, with the shifting and changes resulting from the interactions between components

(CNF-PH500, PH500-PPy): such as the increasing intensity of the band at 1530 cm^{-1} due to the presence of C=C aromatic ring of PPy and PEDOT, the overtone band at 1293 cm^{-1} combined from the absorption peak at 1288 cm^{-1} associated to the C–N bond of the aromatic amine (Lay et al., 2016) and the band at 1352 cm^{-1} for C-C of the thiophene ring.

By following the described methodology, our CNF nanopaper showed very high mechanical response, with a tensile strength of 224 MPa and Young's modulus of 14.5 GPa. These properties are higher than the ones reported in previous works (González et al., 2014; Sehaqui, Liu, Zhou, & Berglund, 2010) also produced by means of sheet forming equipment. The stress-strain curves and tensile properties of some nanopapers are shown in Figure 2 (a), with the ultimate tensile strength and Young's modulus represented in Figure 2 (b), and all the values listed in Table 1.

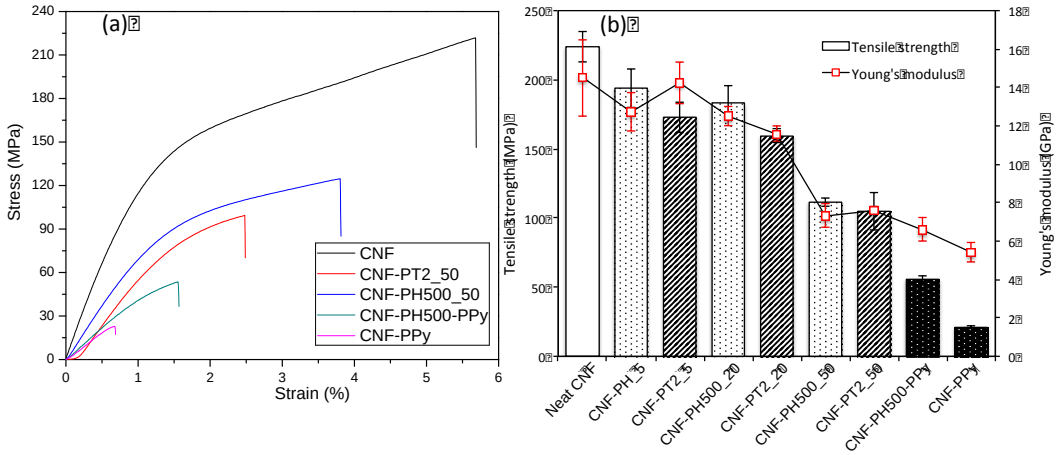

Figure 2 (a) Stress-strain curves of CNF nanopaper and CNF conductive nanopapers and (b) their ultimate tensile strength and Young's modulus.

Table 1 Composition, density, porosity, tensile strength, Young's modulus, and conductivity of the nanopapers (standard deviations in parenthesis).

Sample	CNF (%)	*PT2 or PH500 (%)	PPy (%)	Density (g cm^{-1})	Porosity (%)	Tensile Strength (MPa)	Young's Modulus (GPa)	Conductivity (S cm^{-1})
CNF	100	0	-	1.326	11.60	224.12(11)	14.50(2)	10^{-8} - 10^{-13}
CNF-PT2_5	95	*5	-	1.322	10.39	172.91(14)	12.74(1)	1.02 10^{-5}
CNF-PT2_10	90	*10	-	1.294	10.73	163.02(8)	11.92(0.4)	7 10^{-4}
CNF-PT2_20	80	*20	-	1.242	11.28	159.26(12)	12.51(0.5)	2.86 10^{-2}
CNF-PT2_30	70	*30	-	1.186	12.13	145.14(14)	10.48(0.2)	0.18
CNF-PT2_40	60	*40	-	1.141	12.27	113.98(13)	10.16(0.3)	0.59
CNF-PT2_50	50	*50	-	1.091	12.73	104.93(3)	7.33(0.6)	0.65
CNF-PH500_5	95	5	-	1.321	10.46	194.00(11)	14.25(1.1)	5 10^{-5}
CNF-PH500_10	90	10	-	1.292	10.90	190.95(6)	11.30(0.4)	1.87 10^{-3}
CNF-PH500_20	80	20	-	1.240	11.46	183.37(5)	11.60(0.4)	3.30 10^{-2}
CNF-PH500_30	70	30	-	1.186	12.13	160.67(8)	10.27(0.3)	0.70
CNF-PH500_40	60	40	-	1.139	12.40	131.21(8)	7.75(0.4)	1.69
CNF-PH500_50	50	50	-	1.087	13.01	111.54(14)	7.62(0.2)	2.58
CNF-PH500-PPy	48	38	14	1.083	16.78	55.76(3)	6.61(0.6)	10.55
CNF-PPy	45	0	55	1.034	26.19	20.94(1)	5.42(0.5)	13.45

The outstanding mechanical properties of our CNF nanopaper is associated with the good cellulose nanofiber individualization during the processing and strong interactions between nanofibrils, and for the nanofibrils entanglements (Boufi, Kaddami, & Dufresne, 2014), as shown in the images from transmission electron microscopy (Figure 3a). It is believed that the sonication step removed all possible air in nanofibrils' suspension, and that the filtration promoted some nanofibrils' alignment. This process provided a homogeneous structure resulting in a low porosity final nanopaper, responsible of the high mechanical properties of the obtained CNF nanopaper. However, the addition of the conductive polymers in the nanocellulose network disrupted the CNF interfibril entanglement (Figure 3b). The incorporation PT2 or PH500 to CNFs altered the nanofibrils' connections. Very likely, hydrogen bonds can be formed between

CNF and PEDOT chains and also the cationic PEDOT chain may interact with the carboxylic group (COO^-) of CNFs. Moreover, the negatively charged chains of PSS (SO_3^-) may interpose between cellulose nanofibrils thus reducing the number of intermolecular and intramolecular of hydrogen bonding in CNF (Khan et al., 2015). As a result, the mechanical properties of CNF-PT2 and CNF-PH500 nanopapers were lower compared with the unmodified CNF nanopaper. The further coating of PPy created a quite uniform layer of polypyrrole around the system of CNF and the polythiophene polymer (Figure 3c and 3d). The coating of an excess of PPy on the interpenetrated CNF-PH500 network created PPy-PPy weak bonds, that induced low mechanical properties of the final nanopapers (Nyström et al., 2010).

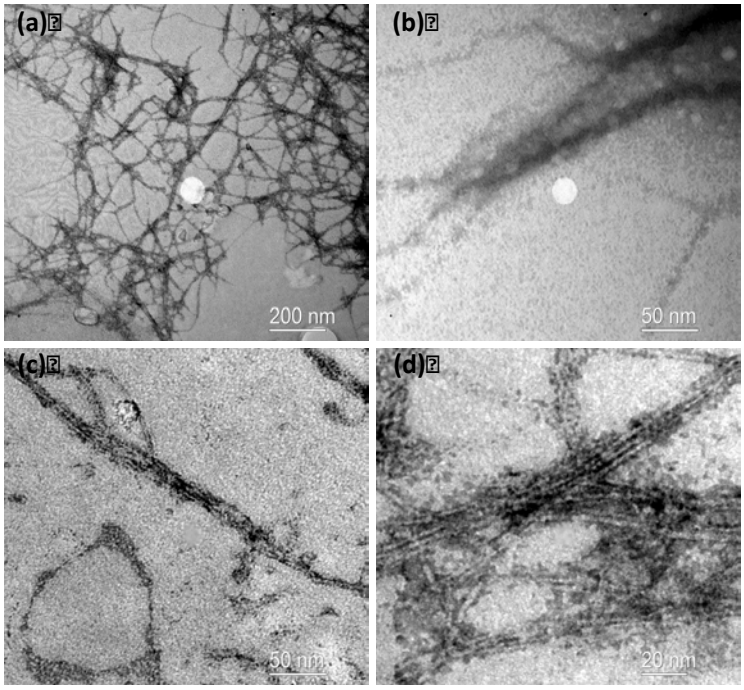

Figure 3 TEM images of (a) CNF hydrogel at 50 nm scale, (b) CNF-PH500_50 at 50 nm scale, and (c-d) CNF-PH500-PPy at 50 nm and 20 nm scales.

If we compare the two polythiophenes used in this work, the mechanical properties of CNF-PH500 nanopapers were superior to those from CNF-PT2. The different average particle size, 30 nm for PH500 and 90 nm for PT2, is found as the main reason for this behavior. The thinner particles of PH500, with higher surface area, form a more homogeneous coating around the entangled cellulose nanofibrils resulting in stronger CNF-PH500 nanopaper. The microstructures observed with SEM microscopy (Figure 4) helps to support this hypothesis. The surface of CNF-PH500 (Figure 4c and 4d) is more smooth than the surface of CNF-PT2 (Figure 4a and 4b). Therefore, the existence of polythiophene polymer diminished the tensile mechanical response of nanopapers, that experienced a substantial decrease for the formulations wit 50wt%. The coating of polythiophene on CNF surface lessened the number of interactions between cellulose nanofibrils, decreasing the number of nanofibrils' intermolecular attractions. The further polymerization of pyrrole produced a significant reduction on the mechanical properties of the nanopaper. Just a 14wt% of polypyrrole reduced up to 56 MPa and 6.6 GPa the strength and modulus of CNF-PH500-PPy nanopaper. The lower tensile strength of CNF-PPy is due to the high porosity that causes a premature breaking point of the nanopaper. Moreover, the coating of PPy on CNF surface limits the number of CNF inter-fibril –OH interactions (Nyström et al., 2010). The microstructures shown in Figure 4e and f) evidence the unevenness and the surface roughness and less compact structure of the nanocomposite with PPy, especially clear at 600 nm of scale.

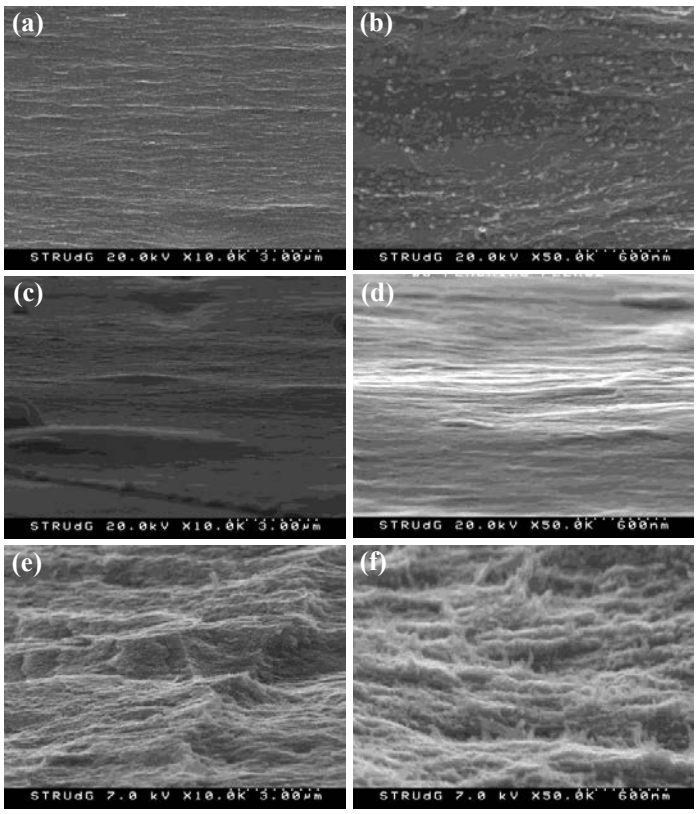

Figure FE-SEM cross-section surfaces of CNF-PT2 nanopapers (a–b), CNF-PH500 nanopapers (c-d) and CNF-PH500-PPy nanopapers (e-f); scales at 3 μm and 600 nm in each case.

The degradation temperatures and the maximum weight loss of CNF, PPy, CNF-PT2_50, CNF-PH500_50, and CNF-PH500-PPy nanopapers were studied by thermogravimetric analysis, shown in Figure 5a. The initial weight loss of about 7% in the temperature range of 50–105°C, was related to the presence of residual moisture in samples (Fox et al., 2012). For CNF nanopaper, cellulose pyrolysis started at 201°C and continued until around 330°C leading to depolymerization of solid cellulose to form active cellulose and thereafter various anhydro-

monosaccharides, retroaldol, dehydrated species, carbon oxides, and finally char (Lin, Cho, Tompsett, Westmoreland, & Huber, 2009; Nyström et al., 2010). The weight loss in this range was of 54.5%. The thermal degradation of CNF from TEMPO-oxidation was broad and consisted of mainly two peaks around 232°C and 296°C (Figure 5b), both below the degradation point of original cellulose (~310°C), similar to the values found in previous studies (Lay et al., 2016; Nyström et al., 2010). The total weight loss for CNF nanopaper at 700°C was about 76%. The degradation temperatures for nanopapers containing PEDOT:PSS (CNF-PT2_50 and CNF-PH500_50) were similar with a maximum degradation temperature around 210°C, bellow the degradation temperature of CNF. For these polythiophene nanopapers, the weight loss at 700°C was about 57%. Their inferior total weight loss compared to CNF nanopaper is probably because PEDOT:PSS coating on cellulose nanofibers prevented the char formation at higher temperatures. Since PPy was thermally more stable, the total weight loss for CNF-PH500-PPy nanopaper was still lower than the other nanopapers. Hence, at 350°C, the weight loss of CNF-PH500-PPy nanopaper was only 30% because of the partial degradation process of the cellulose and PH500. The 14% of PPy in the CNF-PH500-PPy formulation resulted in a thermally more stable conductive nanopaper. It is important to note that the degradation kinetics of PPy is much slower than the degradation of CNF and PEDOT:PSS. PPy degrades in two steps (after water leave the sample at 105°C), which are degradation process involving the counterions (105–315°C) and the degradation of the polymer backbone (315–600°C). The maximum degradation of PPy backbone in the CNF-PH500-PPy nanopaper is shifted bellow the maximum degradation of CNF degradation process, in agreement with literature results (Lay et al., 2016; Nyström et al., 2010).

The electrical conductivities of the nanopapers were measured and compared to theoretical values (Figure 5c). Depending on the matrix, the processing technique, and the type of conductive filler, percolation thresholds has been reported in the range from 0.001 wt% to more than 10 wt%(Koga et al., 2013). In our case, the percolation thresholds for CNF-PT2 and CNF-PH500 nanopapers were found to be 0.036 and 0.002 wt%. This difference is related to several factors such as the ultimate conductivities (80 S cm^{-1} and 300 S cm^{-1}), particle size (90 and 30 nm), and viscosity (80 and 25 mPa s) respectively for each PT2 and PH500. The ultra-low percolation threshold for CNF-PH500 nanopaper is due to the higher surface area of PH500, uniformly distributed, aligned (uniform in one direction) and disentangled in the nanopaper. Based on the percolation threshold result, cellulose nanofibers turned into conductive network at low filler contents. The result indicates that the conductivity of CNF-PT2_5 nanopaper was five times lower compared with CNF-PH500_5 nanopaper (Table 1). High electrical conductivity is ensued when the volume fraction of conductive filler is up to 0.5 (1.6 S cm^{-1}) or 0.6 (2.5 S cm^{-1}). In addition, the polymerization of 14% of PPy into the CNF-PH500 suspension gave a CNF-PH500-PPy nanopaper with a dramatically increased conductivity of 10.55 S cm^{-1}. This enhancement is probably attributed to the increased porous structure of nanocomposite (Table 1) and also to the bridging of the highly conducting domains of PPy. From the results, CNF-PPy (45:55, wt%) nanopaper had a conductivity of 13.45 S cm^{-1}, higher than the conductive paper from cellulose nanofibers and PPy from other authors (Sasso et al., 2010; Nyström et al., 2010).

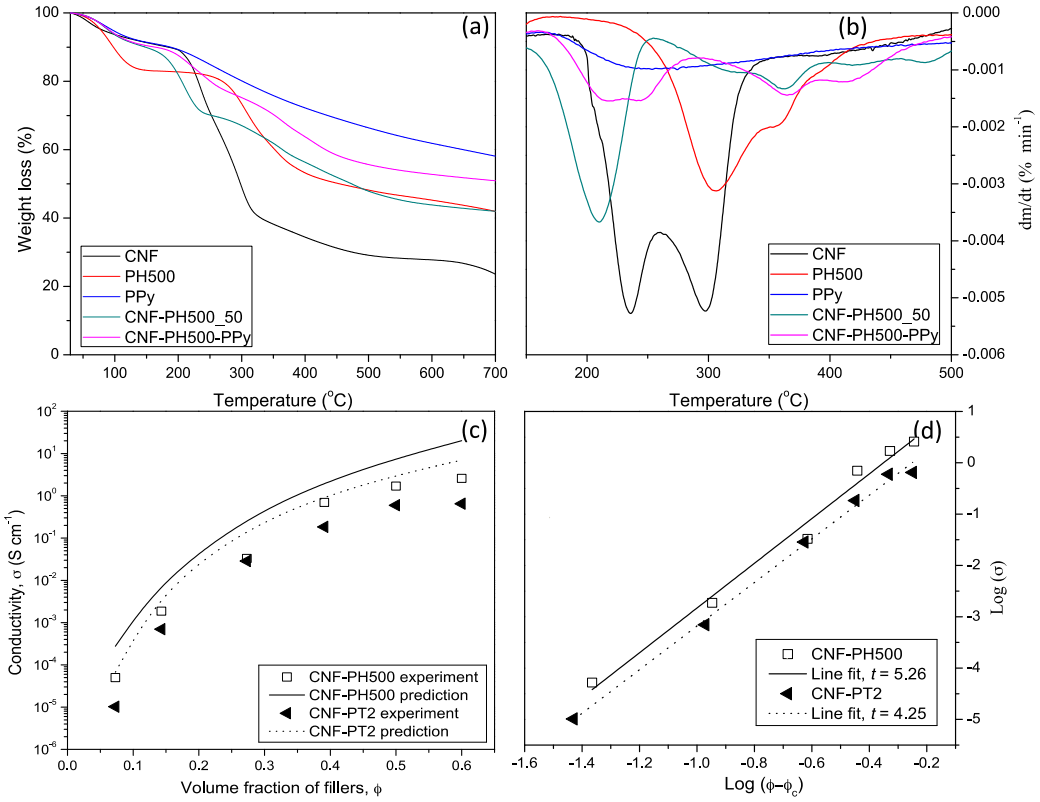

Figure 5 (a) TGA and (b) DTG of nanopapers; (c) Experimental and predicted electrical conductivities of CNF-PT2 (triangle) and CNF-PH500 (rectangle) nanopapers with the volume fraction of conductive fillers and (d) Linear correlation between log σ and log (Φ – Φc) and predicted *t* values for Equation 2.

The linear fit in Figure 5d is plotted to determine the critical exponents (*t*) for Equation 2. The theoretical conductivity can be calculated considering the ultimate conductivity (σ_o) for each filler. With the volume fraction from 0.1 to 0.6 (Figure 5c), the experimental conductivity was five to ten times lower than the predicted conductivity. The lower experimental results, especially at high filler loading, can be related to the low disentanglement of PEDOT:PSS chains (agglomerates), or the non-uniform distribution of individual PEDOT:PSS on microscopic scale

438 (Li et al., 2007). Besides, Malti et al. (2016) studied how to improve the conductivity of CNF-
439 PEDOT:PSS films. They used solvents like glycerol or dimethysulfoxide (DMSO) to allow ions
440 to move much easier in the composite network and to increase the electronic conductivity of
441 PEDOT:PSS. In our case, however, a solvent-free process was chosen.
442 Cyclic voltammetry is a commonly used method to determine electrochemical properties, like
443 the specific capacitance. The cyclic voltammograms of CNF-PT2_50, CNF-PH500_50, CNF-
444 PPy, and CNF-PH500-PPy nanopapers are shown in Figure 6a. The oxidation reduction peak of
445 CNF-PH500-PPy nanopaper is more pronounced than that of CNF-PT2_50, CNF-PH500_50,
446 and CNF-PPy nanopapers as shown in Figure 6b. Explicitly, the specific capacitances of CNF-
447 PT2_50, CNF-PH500_50, and CNF-PH500-PPy nanopapers at 5mV s^{-1} of scan rate were 7.86,
448 6.21, and 315.5 F g^{-1}, respectively (Figure 6c). The very high capacitance of CNF-PH500-PPy
449 relates to the electrochemically active phase of PPy and PEDOT:PSS. In this case, PPy plays as a
450 bridge between polythiophene regions and the PEDOT:PSS phase allows one to fully utilize the
451 capacity of the PPy. The good interaction of PPy with the polythiophene and PSS counterions
452 leads to lower interfacial charge-transfer resistance at the interface between the PEDOT:PSS and
453 PPy on CNF surface. Yue et al. (2012) explained that interfacial charge-transfer is much smaller
454 on the PEDOT:PSS/PPy electrode than that of the PPy and PEDOT:PSS. However, their specific
455 capacitances decreased with increasing the scan rates (Figure 6d). The sample compression
456 during the sheet drying provides nanopapers of very low porosity, and then, the ion mass
457 transport is too slow to allow for full utilization of the inherent charge storage capacity at scan
458 rates above 5mV s^{-1} (Wang, Tammela, Zhang, Strømme, & Nyholm, 2014b).
459
460

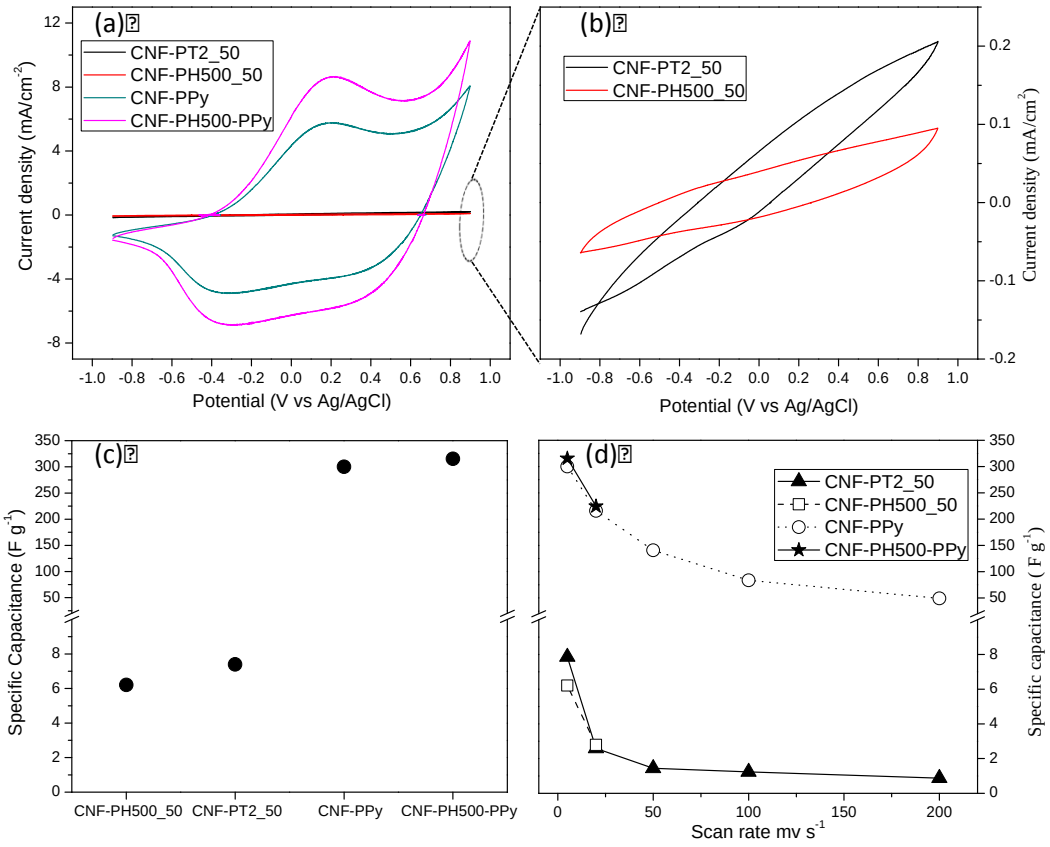

Figure 6 Cyclic voltammograms of (a) CNF-PT2, CNF-PH500_50, CNF-PPy, and CNF-PH500-PPy at 5 mV s^{-1}; (b) CNF-PT2_50 and CNF-PH500_50; (c) specific capacitance at 5 mV s^{-1} and (d) specific capacitance at all scan rates 5, 20, 50, 100, and 200 mV s^{-1}.

On the other hand, CNF-PPy nanopaper showed a lower specific capacitance of 300.2 F g^{-1} at 5 mV s^{-1}, compared to CNF-PH500-PPy, probably because the molar mass of the pyrrole unit is lower than that of 3,4-ethylenedioxythiophene (EDOT) (Lota, Khomenko, & Frackowiak, 2004). The oxidation peaks at +0.2 V and the reduction peaks at -0.4 V vs Ag/AgCl found for CNF-PH500-PPy and CNF-PPy nanopapers (Figure 6a) have the characteristic redox behavior of PPy

(Nyström et al., 2010). The synergistic effect between PEDOT:PSS and PPy on cellulose nanofibers plays an important role to facilitate electrons transport in the nanocomposites (Wang, Tammela, Zhang, Strømme, & Nyholm, 2014a). The specific capacitances of other cellulose-based conductive nanopapers found in the literature are gathered in Table 2 and compared with the values from current work. The ternary formulation in our work (CNF-PH500-PPy) has specific capacitance similar to that shown by other ternary hybrid structures, or by nanocomposites based on cellulose nanocrystals. As shown in Table 2, Yang et al. (2015) performed flexible CNF/MWCNT/PANI aerogel by freeze-drying process with a high specific capacitance of 530 F g^{-1}. The high porosity of the aerogel facilitated the electron and ion transport along the structure. However, when the same formulation was compressed, the specific capacitance diminished to 235 F g^{-1}. One can emphasize as well that polyaniline (PANI) is less environmentally friendly than polypyrrole and PEDOT:PSS polymers. Therefore, in terms of materials used, preparation method and results, the current work provides a formulation with very high specific capacitance by using both environmentally friendly materials and methods.

Table 2. Comparison between specific capacitances measured by cyclic voltammetry from cellulose nanopapers found in literature and from the cellulose nanopapers in the current work.

Material	Specific Capacitance (F g^{-1})	Testing conditions	Reference
CNF/MWCNT/PANI aerogel	530	CV, 5 mV s^{-1}, in range of -0.2 to +0.8 V	(Yang et al., 2015)
CNF/MWCNT/PANI	235	CV, 5 mV s^{-1}, in range of -0.2 to +0.8 V	(Yang et al., 2015)
MWCNT/Cellulose acetate	145	Electrodes at current density of 10 A g^{-1}	(Deng et al., 2013)
PPy/Cellulose nanocrystal (CNC)	238.8	CV, -0.6 to 0.4 V (vs Ag/AgCl), 10 mV s^{-1}	(Wu, Tang, Duan, Yu, & Berry, 2014)
PPy/PVP/CNC	322.6	CV, -0.6 to 0.4 V (vs Ag/AgCl), 10 mV s^{-1}	(Wu et al., 2014)
CNF/MWCNT aerogel	178	CV, 0–1V (vs Ag/AgCl), 5 mV s^{-1}	(Gao et al., 2013)
CNF-PPy (80:20)	7.40	CV, 2M, -0.9 to +0.9 v (vs Ag/AgCl), 5 mV s^{-1}	(Lay et al., 2016)

CNF-PPy (45:55)	300.2	CV, 2M, -0.9 to +0.9 v (vs Ag/AgCl), 5 mV s-1	Current work
CNF-PH500 (50:50)	6.21		
CNF-PH500-PPy (48:36:14)	315.5		

501

502

503 **4. Conclusions**

504 This study sets out the production of highly conductive nanopaper structures from cellulose
505 nanofibers (CNFs), PEDOT:PSS and PPy by a simple and environmentally friendly method.
506 FTIR spectra revealed that PEDOT:PSS was successfully coated on CNFs. The good cooperation
507 between PEDOT:PSS and PPy improved the thermal stability, electrical conductivity and
508 electrochemical properties of CNF-PEDOT:PSS-PPy nanopaper. Two different PEDOT:PSS
509 polymers were tested (PT2 and PH500) and the morphological characterization showed a
510 homogeneous coating of the conductive polymer on cellulose nanofibers. The percolation
511 thresholds were found to be 0.036 and 0.002wt%, respectively for PT2 and PH500. The coating
512 of PEDOT:PSS polymer augmented by 8 to 13 orders of magnitude the electrical conductivity of
513 neat CNF nanopaper, and the addition of PPy on CNF and CNF-PH500 formulation significantly
514 improved both the electrical conductivities (13.45 and 10.55 S cm^{-1}) and the specific
515 capacitances (300.2 and 315.5 F g^{-1}) for CNF-PPy and CNF-PH500-PPy, respectively. The
516 unique architecture and high-performance capacitance of these nanopapers, together with their
517 low-cost, lightweight, flexibility, abundance of stocks and environment-friendly materials offers
518 a great promise for their use in the next generation of small green electronics, and energy storage
519 devices such as batteries or electrochemical capacitors.

520

521

522

Acknowledgement

The authors want to thank the financial support of the European Commission (Erasmus Mundus project Techno II, ref. 372228-1-2012-1-FR-ERA MUNDUS-EMA21).

References

Ali, F., Reinert, L., Levêque, J.-M., Duclaux, L., Muller, F., Saeed, S., & Shah, S. S. (2014). Effect of sonication conditions: Solvent, time, temperature and reactor type on the preparation of micron sized vermiculite particles. *Ultrasonics Sonochemistry*, *21*(3), 1002–1009.

Bashir, T. (2013). *Conjugated Polymer-based Conductive Fibers for Smart Textile Applications*. University of Boras, Sweden.

Boufi, S., Kaddami, H., & Dufresne, A. (2014). Mechanical Performance and Transparency of Nanocellulose Reinforced Polymer Nanocomposites. *Macromolecular Materials and Engineering*, *299*(5), 560–568.

Deng, L., Young, R. J., Kinloch, I. A., Abdelkader, A. M., Holmes, S. M., De Haro-Del Rio, D. A., & Eichhorn, S. J. (2013). Supercapacitance from cellulose and carbon nanotube nanocomposite fibers. *ACS Applied Materials and Interfaces*, *5*(20), 9983–9990. h

Elschner, A., Kirchheyer, S., Lovenich, W., Merker, U., & Reuter, K. (2013). *PEDOT Principles and Applications of an Intrinsically Conductive Polymer* (Vol. 53). New York: CRC Press.

Fox, D. M., Lee, J., Zammarano, M., Katsoulis, D., Eldred, D. V., Haverhals, L. M., Gilman, J. W. (2012). Char-forming behavior of nanofibrillated cellulose treated with glycidyl phenyl POSS. *Carbohydrate Polymers*, *88*(3), 847–858.

Fukuzumi, H., Saito, T., Iwata, T., Kumamoto, Y., & Isogai, A. (2009). Transparent and high gas barrier films of cellulose nanofibers prepared by TEMPO-mediated oxidation. *Biomacromolecules*, *10*(1), 162–165. http://doi.org/10.1021/bm801065u

Gao, K., Shao, Z., Wang, X., Zhang, Y., Wang, W., & Wang, F. (2013). Cellulose nanofibers/multi-walled carbon nanotube nanohybrid aerogel for all-solid-state flexible supercapacitors. *RSC Adv.*, *3*(35), 15058–15064.

González, I., Alcalà, M., Chinga-Carrasco, G., Vilaseca, F., Boufi, S., & Mutjé, P. (2014). From paper to nanopaper: Evolution of mechanical and physical properties. *Cellulose*, *21*(4), 2599–2609.

Groenendaal, B. L. B., Jonas, F., Freitag, D., Pielartzik, H., & Reynolds, J. R. (2000). Poly(3,4-ethylenedioxythiophene) and Its Derivatives : Past , Present , and Future. *Advanced Materials*, *12*, 481–494.

557 Hamedi, M. M., Hajian, A., Fall, A. B., Hkansson, K., Salajkova, M., Lundell, F., Berglund, L. a.
558 (2014). Highly conducting, strong nanocomposites based on nanocellulose-assisted aqueous
559 dispersions of single-wall carbon nanotubes. *ACS Nano*, *8*(3), 2467–2476.

560 Henriksson, M., Fogelström, L., Berglund, L. A., Johansson, M., & Hult, A. (2011). Novel
561 nanocomposite concept based on cross-linking of hyperbranched polymers in reactive
562 cellulose nanopaper templates. *Composites Science and Technology*, *71*(1), 13–17.

563 Hermant, M. C. (2009). *Manipulating the Percolation Threshold of Carbon Nanotubes in*
564 *Polymeric Comosites*. Eindhoven University of Technology, Netherland.

565 Hou, Y., Cheng, Y., Hobson, T., & Liu, J. (2010). Design and synthesis of hierarchical MnO2
566 nanospheres/carbon nanotubes/conducting polymer ternary composite for high performance
567 electrochemical electrodes. *Nano Letters*, *10*(7), 2727–2733.

568 Huang, J., Zhu, H., Chen, Y., Preston, C., Rohrbach, K., Cumings, J., & Hu, L. (2013). Highly
569 transparent and flexible nanopaper transistors. *ACS Nano*, *7*(3), 2106–2113.

570 Jiang, Q., Liu, C., Song, H., Xu, J., Mo, D., Shi, H., Zhu, Z. (2014). Free-standing PEDOT: PSS
571 film as electrode for the electrodeposition of bismuth telluride and its thermoelectric
572 performance. *International Journal of Electrochemical Science*, *9*(12), 7540–7551.

573 Khan, S., Ul-Islam, M., Khattak, W. A., Ullah, M. W., & Park, J. K. (2015). Bacterial cellulose-
574 poly(3,4-ethylenedioxythiophene)-poly(styrenesulfonate) composites for optoelectronic
575 applications. *Carbohydrate Polymers*, *127*, 86–93.

576 Koga, H., Nogi, M., Komoda, N., Nge, T. T., Sugahara, T., & Suganuma, K. (2014). Uniformly
577 connected conductive networks on cellulose nanofiber paper for transparent paper
578 electronics. *NPG Asia Materials*, *6*, 1–8.

579 Koga, H., Saito, T., Kitaoka, T., Nogi, M., Suganuma, K., & Isogai, A. (2013). Transparent,
580 conductive, and printable composites consisting of TEMPO-oxidized nanocellulose and
581 carbon nanotube. *Biomacromolecules*, *14*(4), 1160–1165.

582 Lay, M., Méndez, J. A., Delgado-Aguilar, M., Bun, K. N., & Vilaseca, F. (2016). Strong and
583 electrically conductive nanopaper from cellulose nanofibers and polypyrrole. *Carbohydrate*
584 *Polymers*.

585 Li, J., Ma, P. C., Chow, W. S., To, C. K., Tang, B. Z., & Kim, J. K. (2007). Correlations between
586 percolation threshold, dispersion state, and aspect ratio of carbon nanotubes. *Advanced*
587 *Functional Materials*, *17*(16), 3207–3215.

588 Li, Y., Hu, X., Zhou, S., Yang, L., Yan, J., Sun, C., & Chen, P. (2014). A facile process to
589 produce highly conductive poly(3,4-ethylenedioxythiophene) films for ITO-free flexible
590 OLED devices. *J. Mater. Chem. C*, *2*(5), 916–924.

591 Lin, Y., Cho, J., Tompsett, G. a, Westmoreland, P. R., & Huber, G. W. (2009). Kinetics and
592 Mechanism of Cellulose Pyrolysis. *Physical Chemistry*, *113*, 20097–20107.

593 Lota, K., Khomenko, V., & Frackowiak, E. (2004). Capacitance properties of poly(3,4-

ethylenedioxythiophene)/carbon nanotubes composites. *Journal of Physics and Chemistry of Solids*, *65*(2–3), 295–301.

Malti, A., Edberg, J., Granberg, H., Khan, Z. U., Andreasen, J. W., Liu, X., Berggren, M. (2016). An Organic Mixed Ion-Electron Conductor for Power Electronics. *Advanced Science*, *3*, 1500305.

Meng, C., Liu, C., Chen, L., Hu, C., & Fan, S. (2010). Highly flexible and all-solid-state paperlike polymer supercapacitors. *Nano Letters*, *10*(10), 4025–4031.

Nyström, G., Mihranyan, A., Razaq, A., Lindström, T., Nyholm, L., & Strømme, M. (2010). A nanocellulose polypyrrole composite based on microfibrillated cellulose from wood. *The Journal of Physical Chemistry. B*, *114*(12), 4178–4182.

Sasso, C., Zeno, E., Petit-Conil, M., Chaussy, D., Belgacem, M. N., Tapin-Lingua, S., & Beneventi, D. (2010). Highly conducting polypyrrole/cellulose nanocomposite films with enhanced mechanical properties. *Macromolecular Materials and Engineering*, *295*(10), 934–941.

Saville, P. (2005). *Polypyrrole Formation and Use*. *DRDC Atlantic TM*, Canada.

Sehaqui, H., Liu, A., Zhou, Q., & Berglund, L. A. (2010). Fast preparation procedure for large, flat cellulose and cellulose/inorganic nanopaper structures. *Biomacromolecules*, *11*(9), 2195–2198.

Seo, J.-H., Chang, T.-H., Lee, J., Sabo, R., Zhou, W., Cai, Z., Ma, Z. (2015). Microwave flexible transistors on cellulose nanofibrillated fiber substrates. *Applied Physics Letters*, *106*, 262101.

Suchand Sangeeth, C. S., Jaiswal, M., & Menon, R. (2009). Correlation of morphology and charge transport in poly(3,4-ethylenedioxythiophene)-polystyrenesulfonic acid (PEDOT-PSS) films. *Journal of Physics. Condensed Matter*, *21*(7), 72101.

Tammela, P., Wang, Z., Frykstrand, S., Zhang, P., Sintorn, I.-M., Nyholm, L., & Strømme, M. (2015). Asymmetric supercapacitors based on carbon nanofibre and polypyrrole/nanocellulose composite electrodes. *RSC Adv.*, *5*(21), 16405–16413.

Wang, J., Xu, Y., Chen, X., & Du, X. (2007). Electrochemical supercapacitor electrode material based on poly(3,4-ethylenedioxythiophene)/polypyrrole composite. *Journal of Power Sources*, *163*(2), 1120–1125.

Wang, Z., Carlsson, D. O., Tammela, P., Hua, K., Zhang, P., Nyholm, L., & Strømme, M. (2015). Surface Modified Nanocellulose Fibers Yield Conducting Polymer-Based Flexible Supercapacitors with Enhanced Capacitances. *ACS Nano*, *9*(7), 7563–7571.

Wang, Z., Tammela, P., Huo, J., Zhang, P., Stromme, M., & Nyholm, L. (2016). Solution-processed poly(3,4-ethylenedioxythiophene) nanocomposite paper electrodes for high-capacitance flexible supercapacitors. *J. Mater. Chem. A*, *4*(5), 1714–1722.

Wang, Z., Tammela, P., Zhang, P., Strømme, M., & Nyholm, L. (2014a). Efficient high active

mass paper-based energy-storage devices containing free-standing additive-less polypyrrole–nanocellulose electrodes. *Journal of Materials Chemistry A*, *2*(21), 7711.

Wang, Z., Tammela, P., Zhang, P., Strømme, M., & Nyholm, L. (2014b). High areal and volumetric capacity sustainable all-polymer paper-based supercapacitors. *Journal of Materials Chemistry A: Materials for Energy and Sustainability*, *2*, 16761–16769.

Wu, X., Tang, J., Duan, Y., Yu, A., & Berry, M. (2014). Conductive cellulose nanocrystals with high cycling stability for supercapacitor applications†. *Journal of Materials Chemistry A: Materials for Energy and Sustainability*, *2*, 19268–19274.

Yang, C., Chen, C., Pan, Y., Li, S., Wang, F., Li, J., Li, D. (2015). Flexible highly specific capacitance aerogel electrodes based on cellulose nanofibers, carbon nanotubes and polyaniline. *Electrochimica Acta*, *182*, 264–271.

Yue, G., Wu, J., Xiao, Y., Lin, J., Huang, M., & Lan, Z. (2012). Application of Poly(3,4-ethylenedioxythiophene):Polystyrenesulfonate/Polypyrrole Counter Electrode for Dye-Sensitized Solar Cells. *The Journal of Physical Chemistry C*, *116*, 18057–18063.

Zhu, Z., Song, H., Xu, J., Liu, C., Jiang, Q., & Shi, H. (2015). Significant conductivity enhancement of PEDOT:PSS films treated with lithium salt solutions. *Journal of Materials Science: Materials in Electronics*, *26*(1), 429–434.

PAPER IV

High electrical and electrochemical properties in bacterial cellulose / polypyrrole membranes

Makara Lay, Israel González, Joaquim A. Tarrés, Neus Pellicer, Kim Ngun Bun, Fabiola Vilaseca

European Polymer Journal (submitted manuscript)

High electrical and electrochemical properties in bacterial cellulose / polypyrrole membranes

Makara Lay[a,b], Israel González[a], Joaquim A. Tarrés[a], Neus Pellicer[a], Kim Ngun Bun[b], Fabiola Vilaseca[a*]

[a]*LEPAMAP GROUP, Dept. of Chemical Engineering, Universitat de Girona, 17071 Girona, Spain.*

[b]*Dept. of Geo-resources and Geotechnical Engineering, Institute of Technology of Cambodia, PP Box 86, Russian conf. Blvd. Phnom Penh, Cambodia.*

Corresponding author:

Fabiola Vilaseca

Dept. of Chemical Engineering, Universitat de Girona,

C/ Maria Aurèlia Capmany, 61, Girona 17071, Spain.

Tel: +34 667 29 2597

Email: fabiola.vilaseca@udg.edu

Abstract

The purpose of the current work was to produce conducting electroactive membranes from bacterial cellulose (BC) coated with polypyrrole (PPy) via in situ chemical polymerization of pyrrole at 4ºC using $FeCl_3$ as oxidant agent. The electrical conductivity, tensile, thermal and electrochemical properties of BC/PPy membranes were investigated. The results revealed that the uniformly coating of PPy nanoparticles on the surface of BC template achieved high electrical conductivity of 3.39 S cm^{-1} and a

specific capacitance of 191.94 F g^{-1} at 5 mv s^{-1} scan rate. The high conductivity and specific capacitance of the present BC-PPy membranes opens new potential applications for BC in various fields as biosensors, flexible electronics, or energy storage devices.

Keyword: Bacterial cellulose, Polypyrrole, Surface coating, Electrical conductivity, Specific capacitance, Biosensors.

1. Introduction

The development of novel multi-functional nanocomposites has gained tremendous research interest during the last decade. In this direction, low cost resources, with renewable and biodegradable characteristics, are aimed for light weight, flexible and eco-friendly biomaterials intended to wearable electronics, biosensors or energy storage devices [1,2]. With this purpose, the combination of nanocelluloses with conducting electroactive polymers is been studied. Thanks to their high electrical conductivity, good environmental stability, fast oxidation/reduction reaction, facile synthesis and availability at industrial scale [3,4], polymers such as polypyrrole (PPy), polythiophene, and their derivatives, have been chosen as candidates for coating nanocellulose [5–7].

A special kind of nanocellulose, bacterial cellulose (BC) is an unbranched polysaccharide, comprising linear chains of β-1,4-glucopyranose residues, which is produced by microorganisms belonging to *Acetobacter xylinum*, now renamed *Gluconacetobacter xylinus*. BC has diameters between 20 to 100 nm depending on the type of nanofibers network formed [8]. The specific ultrafine network structure and other superior properties, such as sufficient porosity, high purity, and crystallinity of BC develop into membranes of high ultimate mechanical properties, excellent

biodegradability and biocompatibility [1]. BC has been used for a variety of commercial applications including textiles, cosmetics, and food products. Thanks to a unique surface chemistry, nontoxic hydrogel with good mechanical properties, BC has extended its use in other fields such as medicine, electronics, paper industry, packaging, biosensors, biomedical devices and scaffolds for tissue engineering and organ regeneration [9–11].

All these features make BC a good candidate for the preparation of multi-functional nanocomposites. More specifically, the excellent physical-mechanical properties of BC matrix (insulating polymer) combined with conducting electroactive polymers (poor mechanical properties) are expected to provide nanocomposites with the electrical, thermal, and mechanical characteristics that could not be reached by the single materials.

Several studies in the literature show the preparation of BC/PPy composites via in situ oxidative polymerization of PPy on BC membrane to be used as flexible supercapacitor [12–15]. It has also been reported the use of polyaniline (BC/PAni) [16–18] and polythiophenes (BC/PEDOT:PSS) [19,20] for the production of electroactive films.

Wang and co-workers used the freeze-drying methodology in the process to obtain PAni/BC [21] and PPy/BC [12] nanocomposites. In 2013, Müller et al. [14] performed PPy/BC through oxidative polymerization of pyrrole by using different oxidant agent ($Fe_3Cl.6H_2O$ and ammonium persulfate APS). They obtained a PPy/BC nanocomposite with 2.7 S cm^{-1} of conductivity and 4.1 MPa of tensile strength when $Fe_3Cl.6H_2O$ was used as oxidant agent. However, although there are some works studying the electrical conductivity of BC/PPy nanocomposite, few reports have considered the supercapacitor performance of these nanocomposites, and the mechanical behavior has only been

characterized in one case.

The purpose of the present work is to form flexible conducting electroactive membranes of very good mechanical properties from BC and PPy via in situ chemical polymerization of pyrrole in aqueous solution. Different amounts of PPy will be deposited on a BC film and the effects on the mechanical, thermal, electrical conductivity, and electrochemical properties will be investigated.

2. Material and methods

2.1 Materials

Bacterial cellulose was prepared from *Acetobacter xylinum* culture. Pyrrole (Aldrich), 98% of purity, was used for the chemical synthesis of polypyrrole (PPy). Silver coating 3850 was supplied by Holland shielding system BV, Holland. The rest of materials such as $FeCl_3$, tween-80, 2,2,6,6-tetramethyl-1-1-piperidinyloxy (TEMPO), sodium bromide (NaBr), sodium hypochlorite (NaOCl), glucose, yeast extract, bacto-pepton, citric acid, Na_2HPO_4, $MgSO_4 \cdot 7H_2O$, HCl, NaOH, and NaCl were supplied by Sigma Aldrich and used without further purification.

2.2 Acetobacter xylinum bacterial culture

Acetobacter xylinum culture was cultivated in stationary conditions using a Herstin-Schramm nutrient (HS) medium composed of glucose – 5 w/v%, yeast extract – 0.5 w/v%, bacto-pepton – 0.5 w/v%, citric acid – 0.115 w/v%, Na_2HPO_4 – 0.27 w/v%, and $MgSO_4 \cdot 7H_2O$ –0.05 w/v% in 1 L of distilled water. The medium was mixed using mechanical stirring by dropping acetic acid to control pH 4.5. Ethanol –1 v% added after sterilization of the base for 15 min at 121ºC. 100 mL of HS Medium was put in 250 mL of each flash and shook for 1 h at 300 rpm using Flash Shaker SF1. The medium solution was kept growing for 12 days in an oven at 30ºC. BC wet membrane

was removed from the oven and heated at 60 – 70ºC in 1% of NaOH for 1 h, and later thoroughly washed in distilled water until neutral pH in order to remove all the bacteria and residues [22]. The BC membranes were soaked in distilled water and kept at room temperature before use.

2.3 Preparation of BC and BC-PPy membranes

Acetobacter xylinum Bacterial cellulose membrane of 7.5 cm diameter was dried for 25 min at 80ºC temperature in a sheet drying to form BC membrane. In situ oxidative polymerization of pyrrole was used to fabricate the BC-PPy membrane. BC membrane was pressed using mechanical pressing for 10 min to remove absorbed water, and immersed in the pyrrole solution in 0.5 M HCl for 5 min in order to plant the monomer of pyrrole on its surface. The mixture of $FeCl_3$ with 0.5 M HCl was added dropwise into BC/PPy suspension to initiate the polymerization of polypyrrole. Different monomer contents (0.1, 0.3, 0.5 and 0.7 mL) were used in this experiment, and the molar ratios of pyrrole/0.5 M HCl, $FeCl_3$/Pyrrole and $FeCl_3$/0.5 M HCl were 0.4, 2.4 and 1, respectively. The reaction times were 20, 40, and 60 min for 0.1 mL of pyrrole at 4ºC, coded as BC-PPy_1, BC-PPy_2, and BC-PPy_3, and it was only 60 min for the proportions with 0.3, 0.5, and 0.7 mL of pyrrole, which were coded as BC-PPy_4, BC-PPy_5, and BC-PPy_6. The BC membrane turned from white to grey and finally to black within few minutes. After the polymerization reaction, the BC-PPy membrane was washed thoroughly with distilled water to extract the byproducts and the remaining reagents of the reaction. Thereafter, mechanical pressing was applied for 5 min to remove the excess of water. The BC-PPy membrane was finally obtained by drying in a sheet dryer for approximately 25 min at 80ºC.

2.3 Characterization

The degree of polymerization (DP) of bacterial cellulose was determined from intrinsic viscosity data, using the equation $\eta = K \cdot DP^a$, with K = 1.87±0.22 and a = 0.771±0.016 [23]. The intrinsic viscosity measurements were performed according to UNE 57039 (which is equivalent to ISO 5351:2010) using cupriethylendiamine as solvent. The elemental analysis was performed by using a Perkin Elmer EA2400 serie II equipment. The samples were pyrolyzed in helium (He) at a combustion temperature of 925–930 °C. Acetanilide powder (C_8H_9NO) was used as reference. The chemical compositions of membranes were characterized by Fourier transform infrared spectroscopy (FT-IR), using a Bruker equipment with a PLATINUM attenuated total reflectance method (ART) under transmittance mode in range the between 4000 cm^{-1} and 500 cm^{-1} using 24 scans at a resolution of 4 cm^{-1}. The cross section surfaces of bacterial cellulose (BC) and BC-PPy membranes were observed by FE-SEM (HITACHI S-4100). The samples were gold coated using a sputter type EMITECH K550. The images were taken using secondary electron detector at accelerating voltage of 5 kV, following our previous study [24]. The tensile properties were evaluated using a Universal Testing Machine HOUNSFIELD, equipped with a 250 N load cell with a crosshead speed of 5 mm/min. Specimens were cut in rectangular shape of (50×5) mm and kept under controlled conditions of 50% relative humidity at room temperature. The statistical error for each formulation was taken from at least five different specimens [25]. In order to measure the electrical conductivity of the samples, silver paint was applied at the edge of both sides of each sample and kept 16 h at room temperature to ensure good electrical contact with the clip probes. Agilent 34461A digital multimeter was used to measure the resistance (R) over the length of the stripes of the specimens

[24]. The conductivity was calculated from Equation 1, where σ, L, w, and d are conductivity, length, width, and thickness of the sample, respectively. R is the resistance (Ω) measured from the multimeter.

$$\sigma = L/(R \times w \times d) \quad (1)$$

A Potentiostat/Gavanostat Model 273A Princeton with a three-electrode electrochemical system consisting of the sample as working electrode, a platinum wire as counter electrode, and a 2 M NaCl-saturated Ag/AgCl electrode as reference electrode was used for the electrochemical measurement of the conductive membranes. The data were recorded in the potential window of -0.9 to +0.9 V vs Ag/AgCl at different scan rate at 5, 20, 50, 100, and 200 mV s^{-1}. The specific capacitance was calculated according to previous work [24]. Thermogravimetric analysis (TGA) was used to determine the loss weight with the temperature and the degradation temperatures of membranes. The samples were heated from 30 to 600°C at the heating rate of 10°C min^{-1} using a METTLER TOLEDO ultra micro balance, TGA/DSC. The purge gas was nitrogen with a flowing rate of 40 mL/min.

3. Results and discussion

An example of the never-dried bacterial cellulose hydrogel from the present study, the ensuing BC membrane, and the following electroactive BC-PPy membranes are shown in Figure 1. The translucent BC membrane turned to black after coating with polypyrrole (PPy) via in situ polymerization of pyrrole, and the thickness of the resulting BC-PPy nanocomposites (Table 1) augmented with the reaction time, as well as with an increase of the starting PPy content.

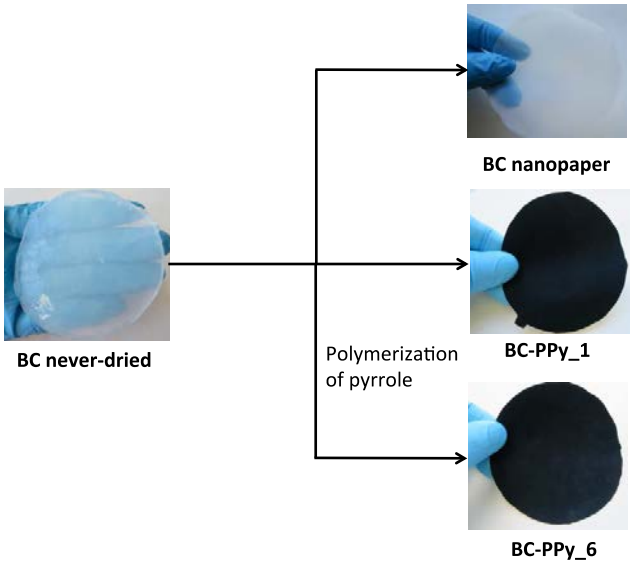

Figure 1 Schematic of preparation BC and conductive BC-PPy membranes.

Table 1 PPy content, thickness, elongation at break, tensile strength, Young's modulus, and conductivity of BC and BC-PPy membranes.

Sample	PPy	Thickness	Strain at break	Tensile Strength	Young's Modulus	Conductivity
	(%)	(μm)	(%)	(MPa)	(GPa)	S cm^{-1}
BC	0	43±3.8	2.78±0.58	273.72±13.70	23.60±1.31	1.8 10^{-13}
BC-PPy_1	17	53±2.1	2.19±0.36	162.43±12.21	12.48±1.51	1.22
BC-PPy_2	21	59±1.9	1.94±0.27	139.59±13.69	10.81±1.33	1.88
BC-PPy_3	25	72±4.7	1.77±0.21	114.67±6.66	9.44±0.97	1.94
BC-PPy_4	45	102±5.0	1.62±0.28	37.38±2.07	2.83±0.18	2.66
BC-PPy_5	51	149±4.7	1.50±0.25	31.85±1.78	2.71±0.21	3.22
BC-PPy_6	55	167±6.0	1.42±0.15	28.49±2.45	2.55±0.21	3.39

Fourier transform infrared spectroscopy was performed to understand the chemical composition of the samples, especially when PPy was coated on the BC membrane. Figure 2 shows the spectra of BC and BC-PPy membranes. The peaks of OH stretching vibration and C–H asymmetrically stretching vibration of BC were found in the region of 3342 and 2897 cm^{-1}, respectively, as confirmed in previous work [13]. The band at

1645 cm^{-1} represents O–H bending of absorbed water. The peaks at 1319 cm^{-1}, 1105 cm^{-1}, and 1030 cm^{-1} indicate C–O of pyranose ring skeletal vibration, C–O–C anti-symmetric bridges stretching, and C–O of ether groups, respectively [20]. The spectra of BC-PPy membranes have changed in the fingerprint region (1550 – 400 cm^{-1}), which belongs to the characteristic tail of the electronic absorption related to PPy [24]. The peak at 1542 cm^{-1} is ascribed to C=C in the aromatic ring of polypyrrole. The peaks shifted to higher wavelength values with an increase of PPy content. In the BC-PPy_6 (55 wt% of PPy), for instance, the peaks at 1444 cm^{-1}, 1283 cm^{-1}, 1034 cm^{-1}, 828 cm^{-1}, and 748 cm^{-1} correspond to C–C, C–N stretching aromatic amine, =C–H bending, N–H wagging, and C–H out of plane of polypyrrole ring, respectively. The blue-shift of these bands confirms that the presence of cellulose affected the delocalized π–electrons of PPy, because of the chemical interactions between the H of the nitrogen in the pyrrole ring and the lone pairs of electrons on the oxygen of the surface OH groups of the cellulose, and/or between the H of the OH groups of the cellulose and the lone pair of electrons on the nitrogen of pyrrole ring occurred [26].

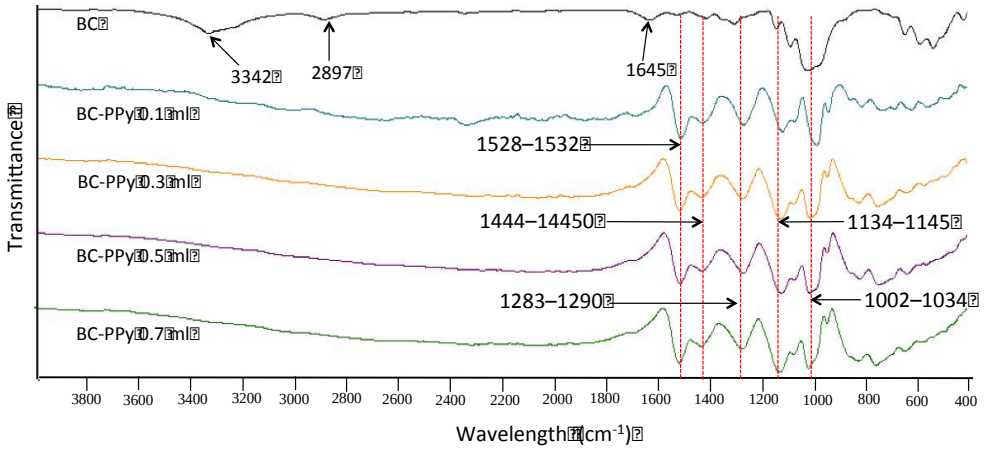

Figure 2 FT-IR spectra BC and BC-PPy membranes.

The cross-section surfaces of pure BC, BC-PPy_3, and BC-PPy_6 nanocomposites were investigated by FE-SEM, as shown in Figure 3. BC membrane with 50 ± 6 nm of diameter shows the fibers' entanglement and forms a strong three-dimensional network and textile structure (Figure 3a–c). After the addition of 25 % PPy, the diameter of nanofibrils were changed to 78 ± 13 nm (Figure 3d–f). This obvious change is due to the PPy deposited on the surface of BC forming a core-shell structure. Moreover, the coating of 55% of PPy forms a continue assembly along the nanofibers, which is the reason of increasing diameter up to 113 ± 17 nm (Figure 3g–i). The interaction between hydrogen bonds of BC and –NH of pyrrole ring helps to prevent self-aggregation of PPy nanoparticles, turning BC in a good polymerization template.

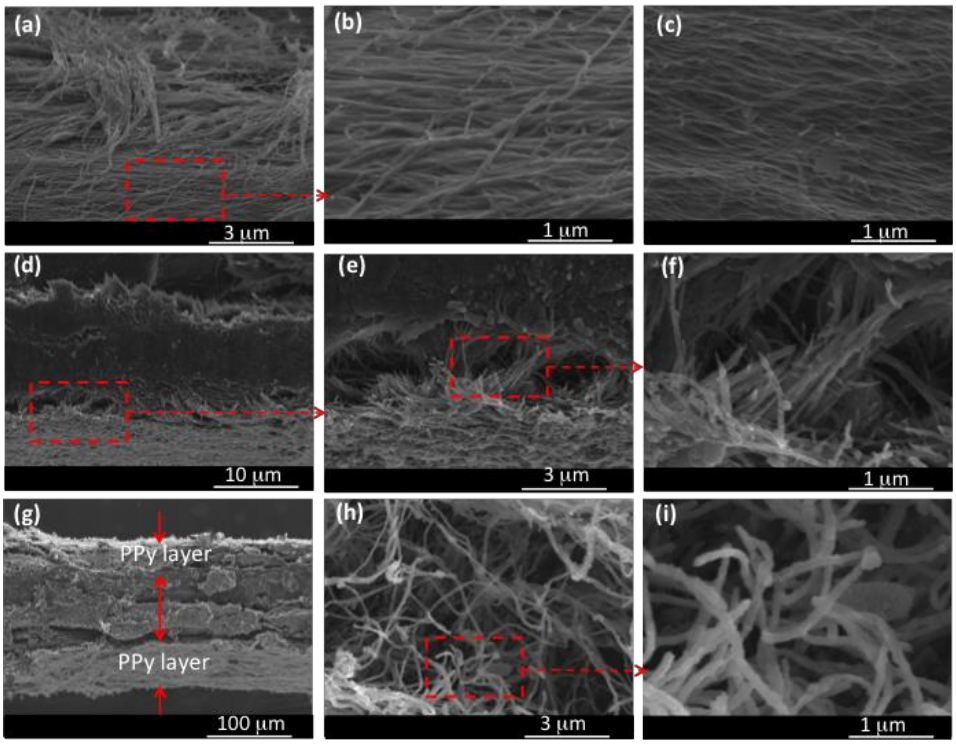

Figure 3 FE-SEM of cross-section surface fractures (a–c) pure BC, (d–f) BC-PPy_3, and (g–i) BC-PPy_6 membranes.

The typical stress-strain curves and the evolution of the ultimate tensile strength, elastic modulus and strain at break for the pure BC membrane and each BC-PPy formulation are found in Figure 4, with the numerical values listed in Table 1. The Young's modulus was calculated from the stress-strain ratio at the linear elastic behavior (linear slope), and it was 23.60 GPa for pure BC, which is above the value described in previous studies (17 – 19 GPa) [27,28]. BC requires high loads to elastically deform probably because of its 3-D network structure. On the other hand, the tensile strength for pure BC was 273 MPa (Figure 4b) also higher than the one found in previous works [29],[14]. This different value can be caused by the amount of sugar and the duration of cultivation of bacterium, which influence the yield and the degree of polymerization. In the present work, 5% of sugar was used and the cultivation was maintained for 12 days. These conditions brings to bacterial cellulose with polymerization degree in the range of 1700-2000, in agreement with the literature [22]. The coating of pyrrole on the surface of BC resulted in a brittle behavior with a value of strain below $2.19 \pm 0.36\%$. Tensile strength and Young's modulus decreased to 162 MPa and 12.5 GPa respectively with 17% content of PPy. The lessening of hydrogen bonding between BC fibrils due to the presence of PPy nanoparticles adhered on nanofibers surfaces [14] can explain this fact. Moreover, the BC fragmentation occurred during the polymerization of pyrrole leads to have more cracks between the BC and PPy layers. This weak interface does not favor the stress-transfer when load was applied on the BC-PPy membrane. It is worth noticing the tensile properties of BC-PPy_6 that were reduced 1 order of magnitude (28.5 MPa of strength and 2.55 GPa of modulus). On the other hand, the fiber diameter was enlarged from 50 nm for pure BC to 113 nm for BC-PPy_6. The PPy coating, therefore, affected the thickness of the final membrane that moved from 43 μm for pure BC up to

167 μm for BC-PPy. The appearance of BC and PPy coated-BC is shown in figure 3. From the smooth, clean and well-ordered bacterial cellulose fibrils, a more disordered and thick filaments are obtained after the polymerization of pyrrole on the BC surface. For the membrane with highest PPy content (Figure 3g) one can affirm that the BC-PPy membrane was composed of about 60 μm layer of PPy in both sides; and this is the reason for the lower tensile properties for this membrane, since PPy chains themselves show weak mechanical properties [8].

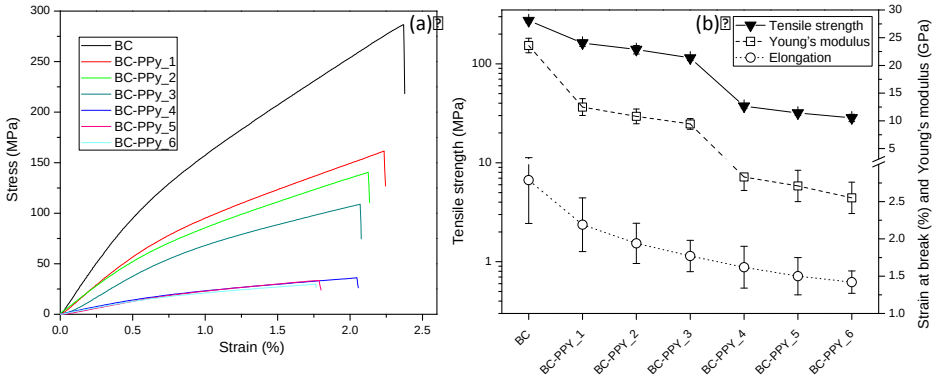

Figure 4 (a) Stress-strain curves and (b) Tensile strength, Young's modulus, and elongation at break of BC and BC-PPy membrane.

The delocalized π conjugated electrons induced the enhancement of the electrical conductivity of membranes. The conductivity of membranes with 17–55 w% of PPy (Table 1) were in the range of 1.22–3.39 S cm^{-1}, which is 13 orders of magnitude higher than that of pure BC (1.8 10^{-13} S cm^{-1}). This property is comparable value of BC-PPy from the previous report of Xu et al. [13] or even higher than that of previous authors [14-15]. It is also higher than the conductive paper from cellulose nanofibers (CNF) and PPy [5]. This proves that BC worked as a good template for the polymerization of pyrrole for highly conductive membrane. Figure 5 shows the comparison between the

predicted and the experimental values of electrical conductivities according to equation 2 [30].

$$\sigma = \sigma_0(\phi - \phi_c)^t \quad (2)$$

*W*here σ is the theoretical conductivity, σ_0 the ultimate conductivity, ϕ the volume fraction of the conductive filler, and ϕ_c is the percolation threshold. To determine the percolation threshold (ϕ_c) experimental results are fitted by plotting log σ versus log ($\phi - \phi_c$), and the value of ϕ_c was incrementally varied until the best linear fit is obtained. In this case, the percolation threshold for BC-PPy membrane was found to be 0.155 wt%. This value is useful to predict the electrical conductivity of PPy reinforced BC membrane.

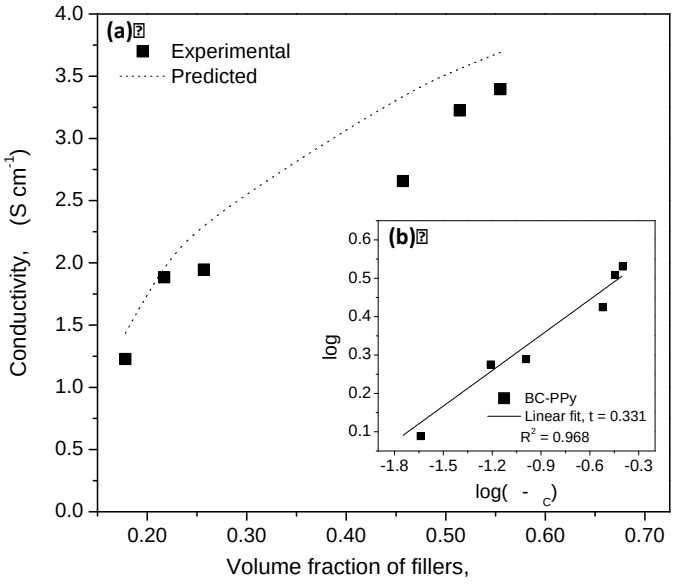

Figure 5 (a) Experimental and predicted electrical conductivities of BC-PPy membrane with the volume fraction of conductive fillers and (b) Linear correlation between log σ and log Φ -Φ_c, and predicted t value for equation 2.

To understand the electrochemical properties of conducting BC-PPy membrane, cyclic voltammetry (CV) was performed in 2 M NaCl electrolyte (Figure 6). Cyclic voltammograms of BC-PPy_3 and BC-PPy_5 membranes were plotted from potential window between –0.9 and +0.9 V at various scan rate of 5, 20, 50, 100, and 200 mV s^{-1}, as shown in Figure 6a and 6b, respectively. Figure 6c indicates enlargement of BC-PPy_3 and BC-PPy_5 at 5 mV s^{-1}, while Figure 6d shows their specific capacitances, calculated from cyclic voltammograms. The CV curves of both membranes exhibited a distorted elliptical shape at low scan rate and became deformed when scan rate reach 100 mV s^{-1} for BC-PPy_3 and 50 mV s^{-1} for BC-PPy_5. The oxidation-reduction peaks of BC-PPy_5 are found at +0.6 V and –0.6 V vs Ag/AgCl, which demonstrates the retention of the important redox feature of conducting polymer in the BC-PPy membrane [12].

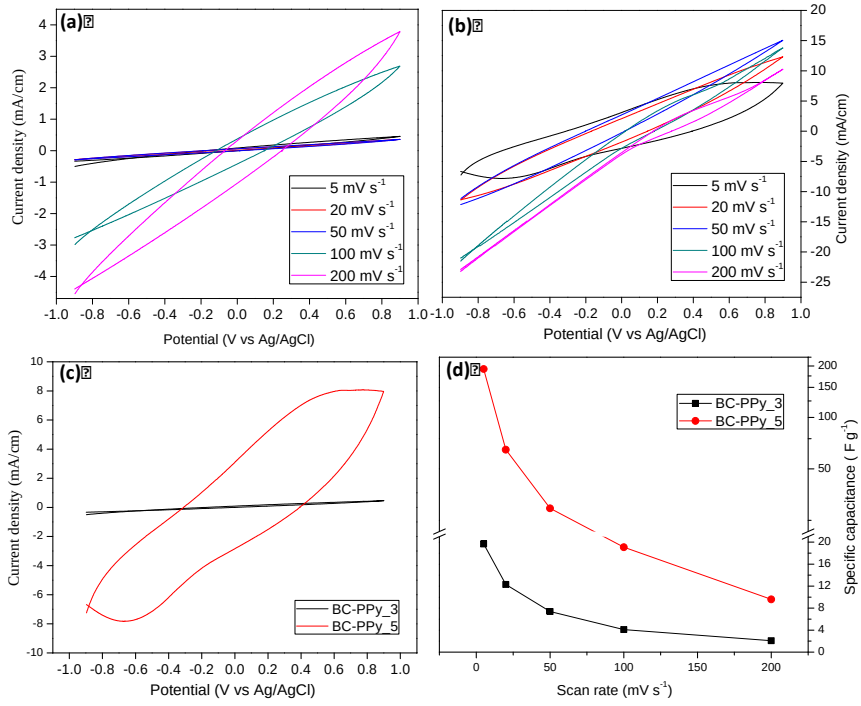

Figure 6 Cyclic voltammograms (a) BC-PPy_3 and (b) BC-PPy_5 at different scan rate between 5 and 200 mV s^{-1}, (c) at 5 mV s^{-1}, and (d) their specific capacitance.

However, this peak did not appear for BC-PPy_3, due to the low amount of PPy (25wt%). From figure 6d, the specific capacitance of BC-PPy_5 is of 191.94 F g^{-1} at 5 mV s^{-1}, which is ten times higher than the BC-PPy_3 membrane (19.68 F g^{-1}). This is due to the increasing of PPy layer (~100 μm) between BC fibrils and the increasing thickness of PPy wrapped around the BC nanofibrils, which could provide a larger specific surface area of electrode/electrolyte interface [13].

The total weight loss and the maximum degradation of BC, PPy, and BC-PPy_6 membranes were estimated by gravimetric analysis (Figure 7). At temperature of 100ºC, the initial weight loss was 2.32% for pure BC membrane in (Figure 7a), which is related to the loss of water bond to the fiber surface, and the dramatically weight loss was found from 280ºC up to 380ºC confirming by the maximum degradation at 335ºC, as shown in Figure 7b. BC/PPy_6 membrane had maximum thermal degradation temperature at 249ºC, which was lower than that of pure BC. It was associated with the loss of intermolecular hydrogen bonds of cellulose chains with the presence of the PPy deposited on nanofibers [18], and is also mainly because the crystal structure of BC was partly destroyed during the polymerization process [15]. On the other hand, it is also involved with the degradation of counterion process of PPy at temperature of between 105 and 315ºC [24].

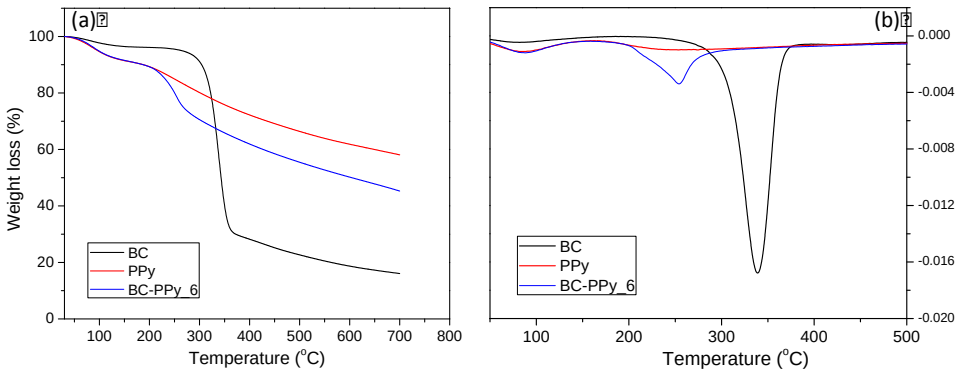

Figure 7 (a) TGA and (b) derivative thermogravimetry of BC, PPy, and BC-PPy_6.

4. Conclusions

In this investigation, conductive membranes from bacterial cellulose (*Acetobacter Xylinum* bacterial culture) with polypyrrole by in situ oxidative polymerization at 4ºC were performed. It was found that the PPy nanoparticles interacted with BC nanofibers and were deposited along their surface. With a 17% of PPy content, flexible BC-PPy membranes had conductivity of 1.22 S cm^{-1} and specific capacitance of 19.68 F g^{-1}, which is adequate for flexible electronic application such as organic light-emitting diode (OLED). Later on, an addition of 50% of PPy on BC template provided the BC-PPy membrane with highest conductivity (3.39 S cm^{-1}) and specific capacitance (191.94 F g^{-1}), which are values comparable to those of nanopapers from cellulose nanofibers with conducting polymers. With these characteristics, the current BC-PPy membranes can be used for biosensor or as energy storage devices, such as supercapacitors and batteries. The current findings add to a growing body of literature on searching for eco-friendly and biomaterial for energy and environmental sustainability sources.

Acknowledgement

This work was supported by Erasmus Mundus project Techno II (Grant No. 372228-1-2012-1-FR-ERA MUNDUS-EMA21). The authors also wish to thank to the Spanish Ministry of Economy and Competitiveness for the funded research project CTM2011-28506.

References

[1] K. Gelin, A. Bodin, P. Gatenholm, A. Mihranyan, K. Edwards, M. Strømme, Characterization of water in bacterial cellulose using dielectric spectroscopy and electron microscopy, Polymer (Guildf). 48 (2007) 7623–7631. doi:10.1016/j.polymer.2007.10.039.

[2] T. Janoschka, M.D. Hager, U.S. Schubert, Powering up the future: Radical

polymers for battery applications, Adv. Mater. 24 (2012) 6397–6409. doi:10.1002/adma.201203119.

[3] R. Ansari, Polypyrrole Conducting Electroactive Polymers: Synthesis and Stability Studies, E-Journal Chem. 3 (2006) 186–201.

[4] A. Elschner, S. Kirchheyer, W. Lovenich, U. Merker, K. Reuter, PEDOT Principles and Applications of an Intrinsically Conductive Polymer, CRC Press, New York, 2013. doi:10.1017/CBO9781107415324.004.

[5] G. Nyström, A. Mihranyan, A. Razaq, T. Lindström, L. Nyholm, M. Strømme, A nanocellulose polypyrrole composite based on microfibrillated cellulose from wood., J. Phys. Chem. B. 114 (2010) 4178–4182. doi:10.1021/jp911272m.

[6] C. Sasso, E. Zeno, M. Petit-Conil, D. Chaussy, M.N. Belgacem, S. Tapin-Lingua, D. Beneventi, Highly Conducting Polypyrrole/Cellulose Nanocomposite Films with Enhanced Mechanical Properties, Macromol. Mater. Eng. 295 (2010) 934–941. doi:10.1002/mame.201000148.

[7] D.O. Carlsson, G. Nyström, Q. Zhou, L.A. Berglund, L. Nyholm, M. Strømme, Electroactive nanofibrillated cellulose aerogel composites with tunable structural and electrochemical properties, J. Mater. Chem. 22 (2012) 19014–19024.

[8] J.K. Pandey, H. Takagi, A.N. Kakagaito, H. Kim, eds., Handbook of Polymer Nanocomposites. Processing, Performance and Application, first edit, Springer, New York, 2015. doi:10.1007/978-3-642-45232-1.

[9] W.K. Czaja, D.J. Young, M. Kawecki, R.M. Brown, The future prospects of microbial cellulose in biomedical applications, Biomacromolecules. 8 (2007) 1–12.

[10] M. Ul-Islam, W.A. Khattak, M. Kang, S.M. Kim, T. Khan, J.K. Park, Effect of post-synthetic processing conditions on structural variations and applications of bacterial cellulose, Cellulose. 20 (2013) 253–263. doi:10.1007/s10570-012-9799-9.

[11] J.M. Rajwade, K.M. Paknikar, J. V. Kumbhar, Applications of bacterial cellulose and its composites in biomedicine, Appl. Microbiol. Biotechnol. (2015) ASAP. doi:10.1007/s00253-015-6426-3.

[12] H. Wang, L. Bian, P. Zhou, J. Tang, W. Tang, Core–sheath structured bacterial cellulose/polypyrrole nanocomposites with excellent conductivity as

supercapacitors, J. Mater. Chem. A. 1 (2012) 578–584. doi:10.1039/C2TA00040G.

[13] J. Xu, L. Zhu, Z. Bai, G. Liang, L. Liu, D. Fang, W. Xu, Conductive polypyrrole-bacterial cellulose nanocomposite membranes as flexible supercapacitor electrode, Org. Electron. Physics, Mater. Appl. 14 (2013) 711–718. doi:10.1016/j.orgel.2013.09.042.

[14] D. Müller, C.R. Rambo, L.M. Porto, W.H. Schreiner, G.M.O. Barra, Structure and properties of polypyrrole/bacterial cellulose nanocomposites, Carbohydr. Polym. 94 (2013) 655–662. doi:10.1016/j.carbpol.2013.01.041.

[15] L. Tang, J. Han, Z. Jiang, S. Chen, H. Wang, Flexible conductive polypyrrole nanocomposite membranes based on bacterial cellulose with amphiphobicity, Carbohydr. Polym. 117 (2015) 230–235. doi:10.1016/j.carbpol.2014.09.049.

[16] J.A. Marins, B.G. Soares, K. Dahmouche, S.J.L. Ribeiro, H. Barud, D. Bonemer, Structure and properties of conducting bacterial cellulose-polyaniline nanocomposites, Cellulose. 18 (2011) 1285–1294. doi:10.1007/s10570-011-9565-4.

[17] W. Hu, S. Chen, Z. Yang, L. Liu, H. Wang, Flexible electrically conductive nanocomposite membrane based on bacterial cellulose and polyaniline, J. Phys. Chem. B. 115 (2011) 8453–8457. doi:10.1021/jp204422v.

[18] D. Müller, J.S. Mandelli, J.A. Marins, B.G. Soares, L.M. Porto, C.R. Rambo, G.M.O. Barra, Electrically conducting nanocomposites: Preparation and properties of polyaniline (PAni)-coated bacterial cellulose nanofibers (BC), Cellulose. 19 (2012) 1645–1654. doi:10.1007/s10570-012-9754-9.

[19] A.N. Aleshin, A.S. Berestennikov, P.S. Krylov, I.P. Shcherbakov, V.N. Petrov, I.N. Trapeznikova, R.I. Mamalimov, A.K. Khripunov, A.A. Tkachenko, Electrical and optical properties of bacterial cellulose films modified with conductive polymer PEDOT/PSS, Synth. Met. 199 (2015) 147–151.

[20] S. Khan, M. Ul-Islam, W.A. Khattak, M.W. Ullah, J.K. Park, Bacterial cellulose-poly(3,4-ethylenedioxythiophene)-poly(styrenesulfonate) composites for optoelectronic applications, Carbohydr. Polym. 127 (2015) 86–93. doi:10.1016/j.carbpol.2015.03.055.

[21] H. Wang, E. Zhu, J. Yang, P. Zhou, D. Sun, W. Tang, Bacterial Cellulose

Nanofiber-Supported Polyaniline Nanocomposites with Flake-Shaped Morphology as Supercapacitor Electrodes, J. Phys. Chem. C. 116 (2012) 13013–13019.

[22] B. Surma-Ślusarska, S. Presler, D. Danielewicz, Characteristics of bacterial cellulose obtained from Acetobacter Xylinum culture for application in papermaking, Fibres Text. East. Eur. 16 (2008) 108–111.

[23] T. Łojewski, K. Zieba, J. Łojewska, Size exclusion chromatography and viscometry in paper degradation studies. New Mark-Houwink coefficients for cellulose in cupri-ethylenediamine, J. Chromatogr. A. 1217 (2010) 6462–6468. doi:10.1016/j.chroma.2010.07.071.

[24] M. Lay, J.A. Méndez, M. Delgado-Aguilar, K.N. Bun, F. Vilaseca, Strong and electrically conductive nanopaper from cellulose nanofibers and polypyrrole, Carbohydr. Polym. (2016). doi:10.1016/j.carbpol.2016.06.102.

[25] M.M. Hamedi, A. Hajian, A.B. Fall, K. Hkansson, M. Salajkova, F. Lundell, L. Wgberg, L. a. Berglund, Highly conducting, strong nanocomposites based on nanocellulose-assisted aqueous dispersions of single-wall carbon nanotubes, ACS Nano. 8 (2014) 2467–2476. doi:10.1021/nn4060368.

[26] J.H. Johnston, F.M. Kelly, J. Moraes, T. Borrmann, D. Flynn, Conducting polymer composites with cellulose and protein fibres, Curr. Appl. Phys. 6 (2006) 587–590. doi:10.1016/j.cap.2005.11.067.

[27] S. Gea, F.G. Torres, O.P. Troncoso, C.T. Reynolds, F. Vilasecca, M. Iguchi, T. Peijs, Biocomposites based on bacterial cellulose and apple and radish pulp, Int. Polym. Process. 22 (2007) 497–501. doi:10.3139/217.2059.

[28] S. Gea, E. Bilotti, C.T. Reynolds, N. Soykeabkeaw, T. Peijs, Bacterial cellulose-poly(vinyl alcohol) nanocomposites prepared by an in-situ process, Mater. Lett. 64 (2010) 901–904. doi:10.1016/j.matlet.2010.01.042.

[29] C.R. Rambo, D.O.S. Recouvreux, C.A. Carminatti, A.K. Pitlovanciv, R. V. Antônio, L.M. Porto, Template assisted synthesis of porous nanofibrous cellulose membranes for tissue engineering, Mater. Sci. Eng. C. 28 (2008) 549–554. doi:10.1016/j.msec.2007.11.011.

[30] H. Koga, T. Saito, T. Kitaoka, M. Nogi, K. Suganuma, A. Isogai, Transparent, conductive, and printable composites consisting of TEMPO-oxidized

nanocellulose and carbon nanotube, Biomacromolecules. 14 (2013) 1160–1165.
doi:10.1021/bm400075f.